A THERMO-RESPONSIVE BUPRENORPHINE-NALOXONE SOLID LIPID NANOPARTICLE NASAL SPRAY FOR THE TREATMENT OF OPIOID ADDICTION

SARJAN PATEL

A dissertation submitted to the Faculty of Health Sciences, University of the Witwatersrand, in fulfilment of the requirements for the degree of Master of Pharmacy

Supervisor:

Professor Yahya E. Choonara

Department of Pharmacy and Pharmacology, Faculty of Health Sciences, University of the Witwatersrand, Johannesburg, South Africa

Co-Supervisors:

Doctor Mershen Govender

Department of Pharmacy and Pharmacology, Faculty of Health Sciences, University of the Witwatersrand, Johannesburg, South Africa

Associate Professor Neil Butkow

Department of Pharmacy and Pharmacology, Faculty of Health Sciences, University of the Witwatersrand, Johannesburg, South Africa

Johannesburg, 2025

DECLARATION

I, Sarjan Patel, declare that this dissertation is my own work. It has been submitted for the degree of Master of Pharmacy in the Faculty of Health Sciences at the University of Witwatersrand, Johannesburg, South Africa. It has not been submitted before for any degree or examination at this or any other University.

S. Patel

_____

This 23rd day of July 2025

DEDICATION

I, proudly and respectfully dedicate this dissertation to my parents as without their guidance, support and sacrifice this would not have been possible. It is only because of their upbringing and guidance that today I have reached this platform.

This work is also proudly dedicated to myself as it took me immense hard work, dedication and discipline to finish this project.

“Never limit your challenges, instead challenge your limitations”

-words to live by given to me by myself.

RESEARCH OUTPUTS

Publications

1. Sarjan Patel, Mershen Govender and Yahya E. Choonara. A Review of The Advanced Drug Delivery Strategies and Barriers to Treat Opioid Use Disorder. (To be submitted to AAPS PharmSciTech).

2. Sarjan Patel, Mershen Govender, Neil Butkow and Yahya E. Choonara. The Design of Sustained-Release Buprenorphine- and Naloxone- loaded Solid Lipid Nanoparticles for the Treatment of Opioid Use Disorder. (To be submitted to Pharmaceutics).

3. Sarjan Patel, Mershen Govender, Neil Butkow and Yahya E. Choonara. An *In Situ* Thermo-responsive Buprenorphine- and Naloxone- loaded Solid Lipid Nanoparticle Nasal Spray for the Treatment of Opioid Use Disorder. (To be submitted to the International Journal of Pharmaceutics).

Poster Representation

1. Sarjan Patel, Mershen Govender, Neil Butkow and Yahya E. Choonara. Formulation of a Thermo-responsive Naloxone-loaded Solid Lipid Nanoparticle Nasal Spray for the Treatment of Opioid Use Disorder. Annual Molecular Biosciences Research Thrust (MBRT) Postgraduate Research Day 2023, University of Witwatersrand, 7th December 2023.

ETHICS DECLARATION

I hereby confirm that the following study entitled “A Thermo-responsive Buprenorphine-Naloxone Solid Lipid Nanoparticle Nasal Spray for the Treatment of Opioid Addiction” had received approval from the Animal Ethics Research Committee (AERC) of the University of the Witwatersrand with ethics clearance number: Waiver 10-11-2023-O (Refer to Annex A).

I hereby confirm that the following study entitled “A Thermo-responsive Buprenorphine-Naloxone Solid Lipid Nanoparticle Nasal Spray for the Treatment of Opioid Addiction” had received approval from the Human Research Ethics Committee (HREC) of the University of the Witwatersrand with ethics clearance number: W-CBP-230405-03 (Refer to Annex B).

ACKNOWLEDGEMENTS

Throughout my journey of completing this dissertation, there have been several people who inspired, assisted and guided me. I would like to convey my sincerest appreciation, gratitude and acknowledgement to them for assisting me in achieving the goals that I had set for myself.

My sincerest thankfulness and everlasting appreciation are to the almighty God, without whom, nothing would have been possible. Thank you for always listening to my prayers and being there to guide me whenever I felt lost through this journey.

Endless love and appreciation to my parents for always being there for me and believing in me.

Respect and appreciation to my research supervisor Prof. Yahya E. Choonara, who believed and gave me the opportunity to conduct this research. I truly thank you for guiding and inspiring me through this journey.

My utmost appreciation, respect and thankfulness to Dr. Mershen Govender, my co-supervisor who has always been supportive, inspiring and a real mentor to me. Your supervision on this project is immeasurable and without your guidance, this journey would never have been a success.

My respect and appreciation to Prof. Neil Butkow, for helping me conceptualize and look at the bigger picture with regards to the project.

My immense respect to Prof. Pradeep Kumar, Dr. Poornima Ramburrun, Dr. Gillian Mahumane, Prof. Thashree Marimuthu, Prof. Lisa Du Toit and all the doctors and professors at the Wits Advanced Drug Delivery Platform (WADDP) for creating such an inspiring environment.

My humble thankfulness to Dr. Hillary Mndlovu, Mr. Bafana Temba, Ms. Tshidi Sekgotho, Dr. Mduduzi Sithole and all the technical support team at the Department of Pharmacy and Pharmacology for assisting and making sure that I received all my laboratory requirements.

I would like to thank and appreciate the National Research Foundation (NRF): South Africa's

Research Chair Initiative (SARChI), Wits: Postgraduate Merit Award (PMA), HETERO Pharmaceuticals Drugs and Faculty Research Committee (FRC) of the University of the Witwatersrand for all the financial support provided.

Lastly, to all my amazing friends and colleagues at WADDP for always supporting, encouraging and inspiring me throughout the journey.

ABSTRACT

In the treatment of chronic pain, the analgesic ladder protocol recommends an escalation to potent opioids, including morphine, fentanyl and related analogues, after reaching maximum dosing with NSAIDs and less potent opioids like codeine. When opioids are used on a regular basis, however, they lead to various side effects including dependence, addiction, tolerance, withdrawal, euphoria and severe respiratory depression, a condition known as opioid use disorder (OUD) or opioid addiction. OUD is a chronic and relapsing disorder of the brain caused by the repeated exposure to exogenous opioids.

At present, opioid antagonists like naltrexone and naloxone (NLX) are used as a treatment option which acts immediately but being antagonistic in nature, they lead to sudden withdrawal symptoms. To overcome this, a partial opioid agonist-antagonist such as buprenorphine (BUP) if used in combination can provide a more preferred treatment. Currently, this combination is available in the market as a sublingual tablet, but due to the effects of the Blood-Brain Barrier (BBB), a low bioavailability and residence time is experienced resulting in frequent dosing to have the required therapeutic effect, which is less patient compliant.

The application of nanotechnology in the therapeutic and diagnostic fields has proved to be effective in improving the physicochemical properties of the drugs and the delivery system including improve patient compliance. Solid lipid nanoparticles (SLNs) have emerged as a carrier system that can deliver APIs across the BBB with a novel controlled or sustained drug delivery approach, target specificity, higher bioavailability, enhanced efficacy and reduced toxicity. The presence of a biocompatible lipid or modified lipid core in the SLNs help in the encapsulation of both hydrophilic and lipophilic APIs and provides stability by prohibiting leakage and degradation of APIs. Additionally, the drug containing SLNs can easily enter the CNS through the olfactory region of the nasal cavity via trans and para cellular pathways and avoid undergoing first pass metabolism. Although the nasal route is advantageous, the mucociliary clearance mechanism plays a significant role as a barrier to the delivery mechanism and absorption of the therapeutic agents. However, with the addition of thermo-responsive and mucoadhesive polymers that increase the viscosity of the drug delivery system, the mucociliary clearance mechanism can be overcome.

Therefore, a mucoadhesive *in situ* thermo-responsive BUP and NLX loaded SLN nasal spray was developed in this study as a potential treatment for OUD.

The individual drug-loaded polymeric SLNs were formulated using the modified double emulsification technique, with each SLN optimized for particle size, entrapment efficiency and drug release using the Box-Behnken Design. The particle size, zeta potential and entrapment efficiency for NLX-loaded SLNs were found to be 142.2 nm, -18.2 mV and 78.7%, respectively, and for BUP-loaded SLNs were found to be 128.2 nm, -19.8 mV and 99.2%, respectively. The polymeric i.e. poly-caprolactone containing BUP- and NLX- loaded SLNs further allowed for the respective drugs to stay in the CNS and release over a period of week i.e. 7 days and as they were lipid i.e. glyceryl monostearate coated and in nano-size range, allowed an increased bioavailability of the drugs across the BBB. The quantification of NLX and BUP was done using a UV-Vis Spectrophotometer and HPLC, followed by the molecular structure

assessment for both the NLX- and BUP- loaded SLNs using a FTIR and thermal behaviour characterization using a DCS and TGA.

Thereafter, the optimized drug containing SLNs were loaded in an optimized mucoadhesive *in situ* thermo-responsive gel (ISTG) matrix formulated using the cold method composed of Pluronic F-127 and hydroxypropyl methylcellulose for nose-to-brain drug delivery. Through the characterization of the physicochemical properties, ISTG was found to be thermo-responsive at physiological nasal temperature i.e. 34 °C and mucoadhesive to overcome the mucociliary clearance rate of the nasal cavity. Additionally, *ex vivo* permeation studies were conducted where 72% of the drug containing SLNs were found to permeate across the porcine nasal membrane within 7 hours, indicating a good permeation rate. Lastly, the individual drug-loaded optimized SLNs i.e. NLX-loaded SLNs and BUP-loaded SLNs and the drug containing SLN-loaded ISTG were found to be biocompatible using HEK293 cells as 84.16%, 85.39% and 84.86% cell viability were observed after 72 hours, respectively. Therefore, from the results obtained it can be concluded that the drug containing SLN-loaded ISTG has the potential to become an effective and patient compliant treatment option for opioid use disorder.

TABLE OF CONTENTS

CHAPTER 1
INTRODUCTION

CHAPTER 2
A REVIEW OF THE ADVANCED DRUG DELIVERY STRATEGIES AND BARRIERS TO TREAT OPIOID USE DISORDER

CHAPTER 3
THE DESIGN OF SUSTAINED-RELEASE NALOXONE-LOADED SOLID LIPID NANOPARTICLES FOR THE TREATMENT OF OPIOID USE DISORDER

CHAPTER 4
BUPRENORPHINE-LOADED SOLID LIPID NANOPARTICLES AS A COMBINATIVE INTERVENTION FOR OPIOID USE DISORDER

CHAPTER 5
A THERMO-RESPONSIVE NASAL GEL SYSTEM FOR THE TARGETED, SUSTAINED RELEASE OF BUPRENORPHINE AND NALOXONE

CHAPTER 6
CONCLUSIONS, LIMITATIONS AND RECOMMENDATIONS

REFERENCES AND ANNEXES

LIST OF EQUATIONS

LIST OF FIGURES

LIST OF TABLES

LIST OF COMMONLY USED ABBREVIATIONS

%EE	Entrapment efficiency
%LC	Loading capacity
A2D2	Automatic antidote delivery device
Ag-Pd	Gold-palladium
APIs	Active pharmaceutical ingredients
AUC	Area under the curve
BBB	Blood brain barrier
BBD	Box behnken design
BUP	Buprenorphine
CDC	Centers for Disease Control and Prevention
CNS	Central nervous system
DCM	Dichloromethane
DDSs	Drug delivery systems
DLS	Dynamic light scattering
DMEM	Dulbecco's modified eagle medium
DMSO	Dimethyl sulfoxide
DPBS	Dulbecco's phosphate-buffered saline
DSC	Differential scanning calorimeter
DSLN-loaded ISTG	BUP and NLX containing solid lipid nanoparticle-loaded *in situ* thermo-responsive gel
EM	Emulsion
EVA	Ethylene vinyl acetate
FBS	Fetal bovine serum
FTIR	Fourier transform infrared spectroscopy
GABA	Gamma-aminobutyric acid
GMS	Glyceryl monostearate
HEK293	Human embryonic kidney
HPC	Hydroxypropyl cellulose
HPMC	Hydroxypropyl methylcellulose
ISFG	*In situ* forming gel
ISFI	*In situ* forming implant
ISFLLCG	*In situ* forming lipid-lipid crystal gel
ISTG	*In situ* thermo-responsive gel

LYO	Lyophilized
MMT	Methadone maintenance program
MTT	(3-[4,5-dimethylthiazol-2-yl]-2,5 diphenyl tetrazolium bromide)
NLX	Naloxone
NLX-cNPs	Naloxone-loaded covalent nanoparticles
NLX-MP	NLX loaded microsphere
NSAIDs	Non-steroidal anti-inflammatory drugs
ORP	Organic phase
OUD	Opioid use disorder
PAA	Poly(acrylic acid)
PBS	Phosphate buffer saline
PCL	Polycaprolactone
PDI	Polydispersity index
PDLLA	Poly (D,L-lactic acid)
Pen-Strep	Penicillin-streptomycin
Pf-127	Pluronic F-127
PLA	Poly(lactic acid)
PLGA	Poly(lactide-co-glycolide)
PLLA-b-PPAd	Poly(l-lactide)-block-poly (propylene adipate)
PVP	Polyvinyl pyrrolidone
RES	Reticuloendothelial system
RP-HPLC	Reverse Phase-High Performance Liquid Chromatography
SEM	Scanning electron microscopy
SLNs	Solid-lipid nanoparticles
TA	Texture analyzer
TGA	Thermogravimetric analysis
$T_{sol\text{-}gel}$	Sol-gel transition temperature
WHO	World Health Organization

CHAPTER 1
INTRODUCTION

1.1 Background to this study

In 1986, World Health Organization (WHO) in an effort to provide guidance on the use of analgesics, including paracetamol, non-steroidal anti-inflammatory drugs (NSAID's) and opioids, by acknowledging patient, professional and regulatory legal concerns, suggested a conventional stepwise approach for acute and chronic pain management, which widely became known as the WHO analgesic ladder protocol (Choudhury et al., 2024; Raffa and Pergolizzi, 2014). As per the WHO's analgesic ladder protocol, the addition of low or moderate potency opioids should only be done after the initiation of alternative analgesic agents at their maximum daily doses (McGuire and Slavin, 2020; Vargas-Schaffer, 2010). The concern with low to moderate potency opioids, such as codeine and tramadol, however, is their low maximal efficacy potential along with a significant adverse effect profile, including the risk of constipation, nausea, vomiting and possibly respiratory depression. In clinical cases where low to moderate potency opioids have been proven to be ineffective, the guidelines suggest the introduction of high potency opioids such as morphine, fentanyl, pethidine and oxycodone as part of the therapeutic intervention (Hagedorn, 2022; Vergne-Salle, 2016; Yang et al., 2020). Opioids, however, when used on a regular basis may lead to major drawbacks like dependence, addiction, tolerance, withdrawal, euphoria, severe respiratory depression and potentially death (Hanna and Senderovich, 2021).

According to the data reported by the United States Centers for Disease Control and Prevention (CDC) in 2022, 107,800 people died due to opioid overdose in the United States, increasing to 109,745 by 2023 (Ahmad et al., 2024; Nichols et al., 2023; Sharifi, 2021; Taylor and Samet, 2022). This follows the trend over the last 20 years, with the current number of deaths due to opioid overdoes expected to rise further over the coming years (Figure 1.1 shows a graphical representation of deaths per 100,000 that were caused due to opioid overdose from 1999 – 2021, as provided by the CDC). A similar situation of deaths attributed to opioid overdose can now be seen in South Africa and worldwide.

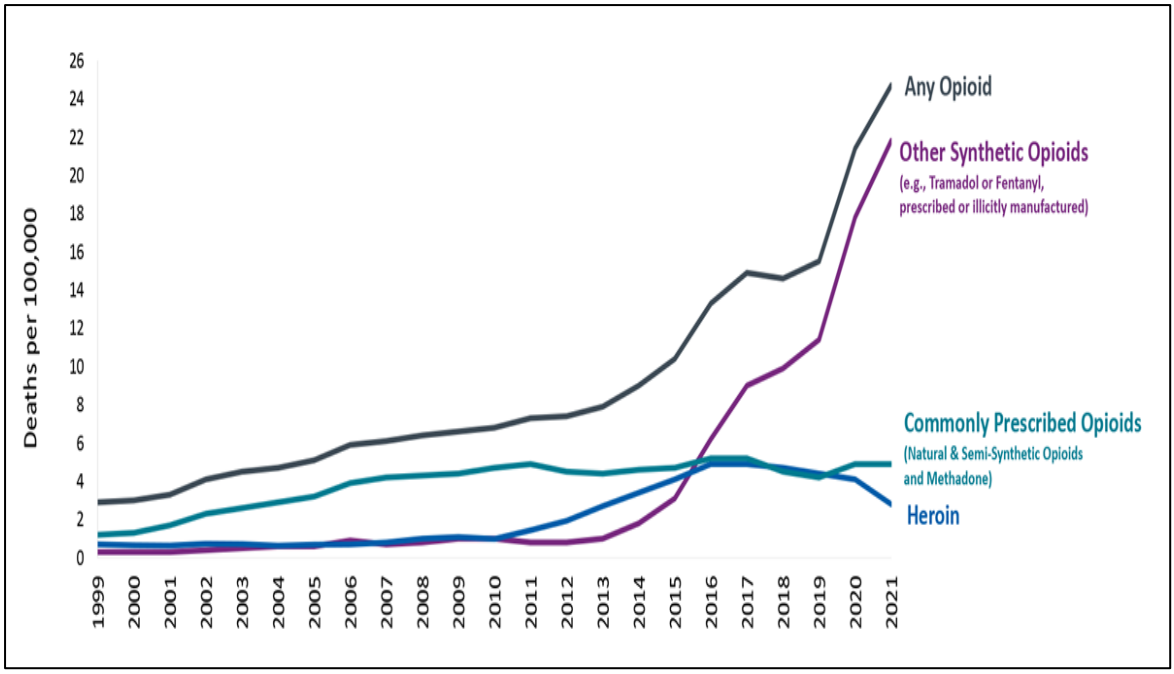

Figure 1.1. Graphical representation of the deaths reported by the CDC that occurred due to opioid overdose from 1999 – 2021 (Reproduced with permission from , © 2021 The Author(s)).

The majority of the patients that overdose or have been subjected to toxic levels of opioids, die from the complications associated with respiratory depression caused by the reduction of brain stem respiratory centre's responsiveness to carbon dioxide, as well as depressing the respiratory centres in the pons and medulla (Pathan and Williams, 2012). On a cellular level, opioids produce their effects via interaction on the opioid receptors i.e. mu (μ), delta (δ) and kappa (K) leading to analgesia, euphoria and respiratory depression (Palmer et al., 2022; Tripathi, 2010). These receptors are mainly situated in the spinal and supraspinal region i.e. medulla, midbrain, limbic and cortical area of the central nervous system (CNS). The main analgesic effect is produced by the activation of receptors that results in an increase in potassium (K^+) efflux, a blockade on sodium (Na^+) influx channels and a decreased conductance of calcium (Ca^{2+}) channels at presynaptic ascending spinal pathways. Therefore, opioids have a hyper polarisation effect on many terminals and prevent the ascending pathways from being activated by pain stimulation (Lambert, 2023; Paul et al., 2021; Plein and Rittner, 2018). Additionally, opioids have the potential to suppress the release of Gamma-aminobutyric acid (GABA), which in turn increases dopamine release, resulting in an euphoretic effect (Valentino and Volkow, 2018).

In the treatment of long-term opioid use disorder (OUD), most strategies involve the use of an opioid antagonist at the μ opioid receptor, such as naltrexone and naloxone (NLX) that occupies the receptors for a specific period and reduces the need of opioids. Additionally, a partial μ opioid receptor agonist and κ opioid receptor antagonist, such as buprenorphine

(BUP) is one of the most preferred drug used in the treatment of OUD (Chiang, 2003; Heidbreder et al., 2023). In the treatment of emergency situations resulting from both OUD and opioid overdose, NLX has also emerged as a powerful life-saving drug which reverses the respiratory depression caused by substances such as codeine, oxycodone, fentanyl and related drugs (Kassick et al., 2019). NLX as a sustained treatment is, however, limited by a rapid elimination rate with a short plasma half-life of approximately 1.5 - 2.0 hours and a high first-pass metabolism by the liver. Consequently, in order to maintain the antagonistic effect of NLX, in the emergency setting, it needs to be administered every 2 - 4 hours or frequently by constant infusion (Saari et al., 2024).

Conversely, BUP, which is a partial μ opioid receptor agonist and κ opioid receptor antagonist, at lower concentrations stimulates the μ opioid receptor causing analgesia and euphoria but at higher concentrations starts to block the μ opioid receptor. This dual action limits the higher doses of BUP that would normally be required in OUD treatment but may also lead to an increase in the risk of abuse or enhanced binding of BUP at the μ opioid receptor. As with NLX, BUP also has a rapid rate of elimination with a short plasma half-life approximately 6 – 7 hours and a high first-pass metabolism (Chiang, 2003; Compton et al., 2006; Mooney and Saxon, 2019).

The usual treatment of OUD is therefore the long-term use of opioid antagonists or partial opioid agonist-antagonist, in which frequent dosing is required. The formulations which currently exist on the market for the treatment of OUD and opioid overdose include sublingual tablets (e.g., Suboxone®), intravenous injections (e.g., Vivitrol®), transdermal patches (e.g., Butrans®) and nasal spray (e.g., Narcan®) (Sharifi, 2021). These products, as reported do have an immediate and potent effect, however, there is still room for growth in the pharmacokinetic and pharmacodynamic properties, such as the residence time for certain products, with some being approximately 2 - 4 hours, leads to a need for frequent dosing. Additionally, many products have a low bioavailability, in part due to the pharmacokinetic properties of the drug as well as their inability to cross the blood brain barrier (BBB) to where the active ingredient is required to function.

1.2 Rationale and Motivation

The oral route is usually considered over other routes of administration for the treatment of diseases or conditions due to its high patient compliance. However, in the case of OUD treatment, it is not efficient, as the administered drugs undergo profound first-pass metabolism and gastro-intestinal degradation. Additionally, the transdermal, vaginal and rectal routes are considered non-compliant, as they are inconsistent when it comes to drug absorption. The

implant or parenteral routes are therefore considered to be one of the most reliable options in long term treatment of OUD but is less patient compliant. The nasal route, however, can be considered as one of the potential preferred routes for OUD and opioid overdose treatment as it circumvents first-pass metabolism, while being anatomically closer to the required site of action and more patient compliant. The nasal route functions by delivering the drugs or drug delivery system using two major cranial nerves that regulates the blood to the nasal mucosa: the ophthalmic and trigeminal nerves (maxillary and mandibular), out of which the maxillary and ophthalmic nerves play an important role of supplying the drugs from the nose to the CNS crossing the BBB via the para-cellular and trans-cellular routes (Goonoo et al., 2014; Govender et al., 2023; Sharifi, 2021; Vitore et al., 2023). The mucociliary clearance rate of the nasal cavity may, however, cause problems for the administered drug due to the human body's natural defence mechanism (Kapoor et al., 2016). This can be overcome by increasing the muco-adhesive nature of the delivery system by adding muco-adhesive polymers and by decreasing the particulate/lipid components into the nano-size range.

This study therefore seeks to overcome the above-mentioned therapeutic concerns or barriers through the development of a mucoadhesive *in situ* thermo-responsive gelling (ISTG) nasal spray containing polymeric solid-lipid nanoparticles (SLNs) separately loaded with BUP and NLX, optimized based on their respective pharmacokinetic properties, for the site-specific and prolonged delivery to the brain for the treatment of OUD. SLNs have been used due to their ability to overcome the concern of high elimination rates for NLX and BUP by allowing the drugs to release in the CNS over a period of one week, while increasing the bioavailability of the drugs across the BBB, allowing for a longer dosing interval. To overcome the concern of mucociliary clearance prior to absorption, the drug-loaded SLNs developed in this study have been delivered via the nasal route in the form of a thermo-responsive nasal spray prepared using the "cold method", which upon change in temperature converts from sol to thin layer gel. This helps by increasing the muco-adhesive nature of the drug delivery system, resulting in an increased residence time on the nasal mucosa, prolonging the drugs duration of action. Through nasal spray dosage form, the drug-loaded SLNs can therefore easily enter the CNS through olfactory region of the nasal cavity via trans and para cellular pathways. A schematic representation of the site-specific delivery of BUP and NLX from the ISTG nasal spray is shown in Figure 1.2.

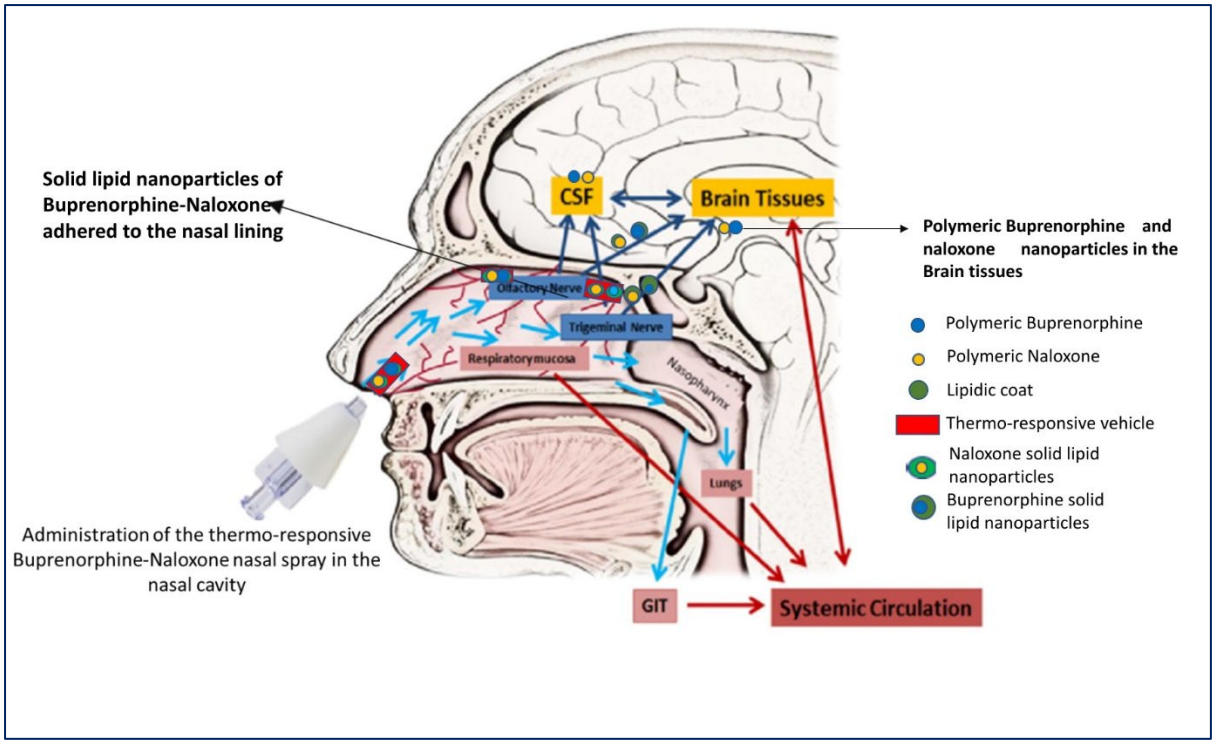

Figure 1.2. Schematic representation of nose to brain drug delivery of thermo-responsive gelling nasal spray containing SLNs of buprenorphine and naloxone (Adapted with permission from Kapoor et al. (2016), © 2016 Elsevier).

1.3 Novelty, Aim and Objectives

1.3.1 Novelty

The elimination rate of BUP and NLX is very high therefore, they were loaded into polymeric SLNs, allowing the drugs to release in the CNS over a period of one week. The SLNs were composed of polycaprolactone (PCL), allowing for prolonged release, and were lipid i.e. glyceryl monostearate (GMS) coated, which allowed for increased bioavailability of the drugs across the BBB. The nasal spray dosage form is advantageous as the drugs avoid undergoing first pass metabolism and is more patient compliant as the administration of drugs will be once a week via a nasal spray. The dosage form was furthermore formulated in the form of an ISTG to overcome the mucociliary clearance by increasing the muco-adhesive nature of the gel system allowing it to give more time for the complete uptake of SLNs. This extensive design provides a novel approach to OUD treatment and addresses many of the concerns associated with conventional OUD interventions.

1.3.2 Aim

The aim of this study was to develop an ISTG nasal spray containing SLNs for the site-specific delivery of BUP and NLX to the brain for treatment of long-term OUD.

1.3.3 Objectives

In order to achieve the above-mentioned aim, the following objectives were required to be achieved:

1. Formulation and statistical optimization of NLX- and BUP- loaded SLNs for the delivery to the brain via the nasal route.
2. Characterization of the developed SLNs using Zeta-Sizing, Fourier Transform Infrared Spectrometry and Scanning Electron Microscopy prior to the determination of the drug loading and entrapment efficiency using UV-Vis Spectrophotometry and *in vitro* drug release studies.
3. Formulation of an ISTG nasal gel, prior to the incorporation of the NLX- and BUP- loaded SLNs and characterization using the Thermo-Hake MARS Modular Advanced Rheometer and Texture Analyser.
4. Development of a High-performance Liquid Chromatography methodology for the separation of NLX and BUP prior to *in vitro* drug release studies on the ISTG with the NLX- and BUP- loaded SLNs.
5. Evaluation of the cytotoxicity of the ISTG containing NLX- and BUP- SLNs on human embryonic kidney (HEK293) cells using the (3-[4,5-dimethylthiazol-2-yl]-2,5 diphenyl tetrazolium bromide) (MTT) assay.
6. *Ex vivo* permeation studies of the ISTG containing NLX- and BUP- loaded SLNs using porcine nasal membrane.

1.4 Overview of the Dissertation

Chapter One of this dissertation provides a brief introduction and background to OUD and how the improvisation of drug delivery systems (DDSs) assists in OUD treatment. Additionally, the rationale and motivation as well as novelty, aim and objectives of this study are provided.

Chapter Two of this dissertation provides a detailed literature review on the DDSs available for the treatment of OUD. This review emphasizes how polymer-based DDSs and modified DDSs play an integral role in OUD treatment and the improvement of patient outcomes. Additionally, further in this review, the barriers related to DDSs for OUD treatment are mentioned, as well as the future outlook for OUD interventions, to which this study aims to address

Chapter Three of this dissertation provides the design and statistical optimization of the NLX-loaded SLNs utilizing the Box-Behnken experimental design, prior to the evaluation, characterization and cytotoxicity assessment of the optimized NLX-loaded SLNs.

Chapter Four of this dissertation provides the design and statistical optimization of the BUP-loaded SLNs utilizing the Box-Behnken experimental design. Additionally, the evaluation, characterization and cytotoxicity assessment of the optimized BUP-loaded SLNs is provided as a part of this chapter.

Chapter Five of this dissertation provides the detailed pre-formulation studies and optimization of the ISTG, as well as the loading of blank-, NLX- and BUP- loaded SLNs into the ISTG. Additionally, the evaluation, characterization and cytotoxicity assessment of the unloaded ISTG and blank-, NLX- and BUP- loaded SLNs into the ISTG has been presented in this chapter as well as the *ex vivo* permeation studies of the drug containing SLN-loaded ISTG using porcine nasal membrane.

Chapter Six of this dissertation provides the conclusion and limitations of this study and the future recommendations for advancing thermo-responsive nasal gelling systems as well as other advanced nose-to-brain DDSs for the treatment of OUD and other conditions involving the CNS.

CHAPTER 2
A REVIEW OF THE ADVANCED DRUG DELIEVRY STRATEGIES AND BARRIERS TO TREAT OPIOID USE DISORDER

2.1. Introduction

In the treatment of chronic pain, the analgesic ladder protocol recommends an escalation to potent opioids, including morphine and fentanyl (or their analogues), after reaching maximum dosing with NSAIDs or less potent opioids, such as codeine and tramadol (Choudhury et al., 2024; Raffa and Pergolizzi, 2014). Potent opioids when used regularly can, however, lead to drug dependence, addiction, tolerance, and withdrawal, a clinical impairment known as OUD (Kakko et al., 2019; Strang et al., 2020). Specifically, the United States CDC in 2021 reported that approximately 80,816 deaths in the United States could be attributed to natural or semi-synthetic opioid abuse, increasing to 109,745 by 2023 (Ahmad et al., 2024; Nichols et al., 2023; Skolnick, 2022; Taylor and Samet, 2022), while data obtained in 2022 determined that around 6.1 million people were affected globally by OUD, which also includes the use of non-food and drug administration (FDA) approved synthetic opioids, such as N-desethyl isotonitazene, which is 20 times stronger than fentanyl (Nataraj et al., 2024; Sharifi, 2021; Walton et al., 2023; Young et al., 2016). Further research has also shown that approximately 1 million patients with OUD remain untreated annually due to a lack of access to effective OUD treatment (Jones et al., 2015).

Opioids work on the mu (μ), delta (δ) and kappa (K) receptors of the brain by activating the potassium (K^+) efflux, blocking the sodium (Na^+) influx and decreasing the conductance of calcium (Ca^{+2}) channels of the presynaptic ascending spinal pathways (Palmer et al., 2022; Paul et al., 2021; Plein and Rittner, 2018; Tripathi, 2010). Opioids have a hyper polarization effect on these receptors, thereby preventing the ascending pathways from being activated by pain stimulation (Lambert, 2023). GABA interneurons additionally have a regulatory effect on the brain i.e., suppression on the dopamine producing neurons. Opioids block the inhibitory control exerted by the GABA neurons resulting in the reduction of GABA-mediated (GABAergic) presynaptic neurotransmitter release, which increases ventral tegmental area dopaminergic activity, thereby leading to an enhanced brain reward mechanism as well as an increased drug-consumption and possibly drug-craving behaviour (Bakare et al., 2024; Lambert, 2023; Valentino and Volkow, 2018). These pathways allow for possible intervention by drug molecules, allowing for the treatment of OUD. Figure 2.1 represents the mechanism of actions of opioids on the control mechanism of dopamine release and pain stimulation.

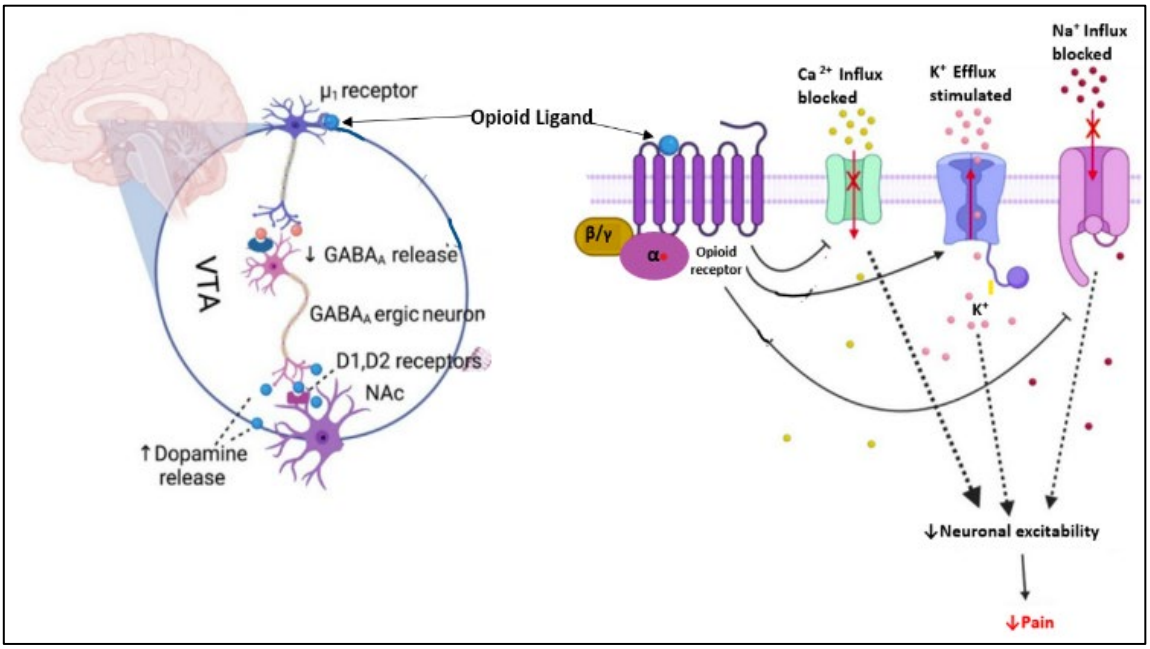

Figure 2.1. Schematic representation of the pharmacological actions of opioids on the control mechanism of dopamine release and pain stimulation (Adapted from Paul et al. (2021), © 2021 by the authors).

The current treatment approach for OUD constitutes the use of opioid agonists, partial opioid agonist-antagonists, and opioid antagonists. Of these agents, methadone, BUP, NLX, naltrexone, and nalmefene are the most commonly administered and although these agents are effective, they are often hindered by their pharmacokinetic profiles (Paul et al., 2021; Tripathi, 2010). Methadone was the first agonist developed and used in 1964 to manage heroin dependence and is currently used to treat OUD. It is rapidly absorbed with peak plasma effects reached after approximately 4 hours and has a mean half-life of 22 hours (Chalabianloo et al., 2024). Methadone can also develop cross-tolerance with other opioids and is therefore used as a replacement for opioid maintenance treatment. Specifically, studies have proven that 1 mg of methadone has the potency to replace 4 mg of morphine, resulting in the methadone maintenance program (MMT) being one of the most widely considered OUD treatment options (Hanna and Senderovich, 2021). It should, however, be noted that methadone has a gradual onset of action, is generally long-acting and can result in drug accumulation, unintended toxicity, and dependence in long term treatment interventions (Mooney and Saxon, 2019).

BUP, conversely, is a partial μ opioid receptor agonist and K opioid receptor antagonist with a rapid absorption, reaching peak plasma levels approximately 1 hour after ingestion. It, however, has a poor bioavailability of only 35% (Chiang, 2003; Compton et al., 2006; Mooney and Saxon, 2019; Strain et al., 2004). Additionally, to reduce the abuse liability of BUP without

affecting its efficacy, it is usually administered in combination with an opioid antagonist, such as NLX (Heidbreder et al., 2023). NLX, naltrexone and nalmefene are examples of opioid receptor antagonists that competitively bind to opioid receptors to stunt the physiological effects of opioids, heroin, and other abused drugs (Edinoff et al., 2021; Tripathi, 2010). NLX is rapidly absorbed reaching peak plasma levels within few minutes, when administered intravenously and sublingually. The half-life of NLX is 30 - 45 minutes with a bioavailability of 50% and can reverse the effects of exogenous opioids (Koyyalagunta, 2011; Saari et al., 2024). Naltrexone, on the other hand, requires approximately 1 hour to reach peak plasma levels with a half-life of 4 hours (Dunbar et al., 2006; Mooney and Saxon, 2019). Studies suggest that approximately 2.8 ng/mL and 2 ng/mL of serum naltrexone levels are effective to block the effects of 500 mg snorted pharmaceutical grade diamorphine and 25 mg intravenously administered heroin, respectively (Domnina et al., 2021; Goonoo et al., 2014).

In an effort to overcome the side-effects and drawbacks in the pharmacokinetic and pharmacodynamic properties of the opioid reversal agents and to potentiate their effects, various advanced DDSs have been developed employing diverse sustained- and controlled-release mechanisms (Al Ragib et al., 2022; Goonoo et al., 2014). These platforms have shown that the effects of first pass metabolism, the limited amount of drug reaching the brain due to BBB and the decreased residence time of the opioid reversal agents can prevail with the implementation of DDSs designed to the properties of the respective drug molecule and its functionality (Satapathy et al., 2021). This article therefore provides a concise incursion into the novel pharmaceutical strategies to treat OUD, with emphasis provided on the polymeric micro- and nano-systems that have been developed for this condition. The efficacy of these platforms along with the *in vivo* experimental and/or clinical trial data generated are further explored in tandem with the research gaps and future outlook for this important field of research.

2.2. Advanced drug delivery strategies for the treatment of OUD

The use of polymeric micro- and nano-particle-based DDSs, implantable devices and microencapsulation technologies is an emerging field with the potential to improve treatment outcomes for OUD. With the incorporation of advanced DDSs in treatment regimens, precise drug targeting, enhanced drug solubility, reduced drug dosages, mitigation of tolerance, combinational therapies and desired release profiles of the drugs administered can be achieved. Based on the release profile generated, these DDSs can be branched into immediate- and modified- release systems, with the modified-release systems subclassified further into delayed-, extended- and targeted- release systems, followed by extended-release systems being bifurcated into controlled- and sustained- release systems (Eleraky et al., 2020;

Goonoo et al., 2014; Gude and Varun, 2024; Khizar et al., 2023; Sultana et al., 2022; Tiwari et al., 2012).

The DDSs alongside the delivery route plays a vital role in overcoming the barriers to treat OUD. Of the various routes of administration used, the sublingual, parenteral, transdermal and nasal routes are the most preferred for the delivery of opioid reversal agents, as they circumvent the effect of first-pass metabolism (Sultana et al., 2022; Tiwari et al., 2012). Provided below are the various pharmaceutical systems that have been developed for OUD treatment, categorized based on their functionality and dosage forms.

2.2.1. Biomaterials used in the design of OUD therapeutics

Polymers have become an integral part of OUD DDS design due to their improved drug-release properties and superior circulation time, while allowing for predictable and effective site-specific targeting (Srivastava et al., 2016). Biodegradable and biocompatible polymers offer a safe passage for drug delivery and involves the cleavage of covalent bonds between the polymers and OUD reversal agents without any changes in the pharmacological and physicochemical properties of the drugs delivered (Kasina et al., 2022; Liechty et al., 2010). Additionally, polymers that respond to external stimulus such as change in pH or temperature results in alteration of properties such as hydrophobic/ hydrophilic balance, solubility and release of OUD reversal molecules (Schmaljohann, 2006; Srivastava et al., 2016). Recent advancements in polymer-based controlled- and sustained- drug release systems and encapsulations, have aided in regulating drug administration by preventing under or overdosing of the therapeutic molecules. Additionally, these advanced systems have helped in minimizing side effects, while improving the bioavailability, residence time and patient compliance of drugs used in OUD treatments (Kasina et al., 2022; Liechty et al., 2010). The various polymers that have been used to develop advanced drug delivery platforms for OUD treatment have been summarized in Table **2.1**.

Table 2.1. Summary of the currently developed polymer-based DDSs for OUD.

Polymer	Drug Molecules*	Route of administration	Drug Release Period	Reference
Poly(lactic acid) (PLA)	NLX	Injectable	4 days	(Averick et al., 2024; Kassick et al., 2019; Kaur, 2018; Kovaliov et al., 2017)

	Naltrexone	Injectable	7 days	(Karavelidis et al., 2015; Nanaki et al., 2020)
	Naltrexone (Naltrel®)	Injectable	28 days	(Galloway et al., 2005; Goonoo et al., 2014; Liu et al., 2006; Tijani et al., 2022)
	Naltrexone (O'Neil®)	Implant	95-145 days depending on the dosage strength	(Goonoo et al., 2014; Krupitsky et al., 2012; Kunoe et al., 2009; Ngo et al., 2008)
Poly(lactide-co-glycolide) (PLGA)	NLX	Injectable	7 days	(Benéitez García et al., 2023; Benéitez et al., 2014)
	BUP	Injectable	21 days	(Kamali et al., 2019, 2018)
	BUP	Injectable	3 days	(Guarnieri et al., 2018a; Schreiner et al., 2021)
	Naltrexone (Vivitrol®)	Injectable	30 days	(Andhariya et al., 2017; Goonoo et al., 2014; Krupitsky et al., 2017; Ndegwa et al., 2017)
	BUP (Sublocade®)	Injectable	28 days	(Laffont et al., 2016; Nasser et al., 2016,

				2014; Packhaeuser et al., 2004; Rosenthal and Goradia, 2017; Rosenthal, 2019)
	BUP (NORVEX®)	Injectable	6 weeks	(Rosenthal and Goradia, 2017; Sigmon et al., 2006, 2004)
Ethylene vinyl acetate (EVA)	BUP (Probuphine®)	Implant	6 months	(Ling et al., 2010; Rosenthal, 2019; Rosenthal et al., 2013)
Polyvinyl pyrrolidone (PVP)	NLX	Transdermal	4-40 days depending on the array size	(Guarnieri et al., 2018b; Tijani et al., 2023)
	BUP	Transdermal	3 days	(Rahmani et al., 2021)
Poly(acrylic acid) (PAA)	BUP (Transtec®)	Transdermal	4-7 days depending on the dosage strength	(Budd and Collett, 2003; Likar et al., 2007; Sittl, 2003)
Hydroxypropyl methylcellulose (HPMC)	BUP and NLX (Suboxone® Sublingual Film)	Sublingual	12-24 hours depending on the dosage strength	(Borges et al., 2015; Gupta et al., 2022; Silva et al., 2015; Sullivan and Webster, 2015)
Hydroxypropyl cellulose (HPC)	BUP (Butrans®)	Transdermal	3 days	(Lanier et al., 2008, 2007; Rosenthal

	and Goradia, 2017; Wiegand et al., 2016)

*Marketed product names included where relevant

2.2.1.1. DDSs for extended drug release

DDSs designed for the extended release of the therapeutic moieties have become a very useful tool in medical practice, as they offer a wide range of advantages. These include reducing the dosing frequency of therapeutic moieties, maintaining therapeutic concentrations over a prolonged period and reducing drug toxicity at the site of action by minimizing drug accumulation, with the further potential to increase patient compliance and convenience (Bhowmik et al., 2018; Shah et al., 2015). Several extended DDSs, delivered via different routes of administration, for OUD treatment have recently been developed and have been discussed herein.

2.2.1.1.1 Injectables

Extended-release injectable formulations can serve as a platform technology for a wide range of drugs, offering the benefits of first-pass metabolism avoidance, a direct systemic intervention resulting in an immediate and effective therapeutic efficacy, cost-effectiveness and the potential to attract and retain high-risk individuals with OUD, as adherence to daily medication may be a challenge (Jindal et al., 2023; Socías and Nolan, 2021).

The extended release of drug molecules is particularly advantageous in the treatment of OUD due to it circumventing many of the pharmacokinetic concerns with OUD drug interventions, while also decreasing treatment intervals and increasing patient compliance. Following this theme, Kassick et al. explored the use of PLA in designing a long-acting NLX delivery system utilizing covalent injectable nanoparticle technology (Kassick et al., 2019). PLA is a synthetic, high strength biodegradable aliphatic polyester which is degradable through hydrolysis, proving it to be beneficial in OUD DDS design (Borandeh et al., 2021; Farah et al., 2016; Ulery et al., 2011). In this study, NLX-loaded covalent nanoparticles (NLX-cNPs) were prepared via the NLX initiated, ring opening polymerization reaction of L-lactide, as represented in Figure 2.2, using an organocatalyst to precipitate the NLX-PLA polymer followed by the nano-precipitation technique to obtain NLX-cNPs (Kassick et al., 2019; Kaur, 2018; Kovaliov et al., 2017). The NLX-cNPs were found to have a particle size, PDI and drug loading capacity of ≈243 nm, 0.15 and 7% w/w, respectively. Additionally, *in vitro* analysis of the Nal-cNPs exhibited sustained release linear kinetics over a period of 7 weeks with a cumulative release of 65% NLX. The *in vitro* biocompatibility assay of NLX-cNPs further demonstrated excellent

biocompatibility, as the nanoparticles showed no significant influence on cell viability across the concentration range of 250 µg/mL to 3 mg/mL on HEK293 cells, murine embryonic fibroblasts (NIH-3T3), and human keratinocytes (HaCaT). A rodent model of neuropathic pain was further used for the assessment of the *in vivo* efficacy of the NLX-cNPs, where a blocking effect by the NLX-cNPs on high dose morphine (10 mg/kg) for up to 98 hours was reported, substantially improving the duration of action of NLX and supporting the use of this DDS for the treatment of OUD (Averick et al., 2024; Kassick et al., 2019).

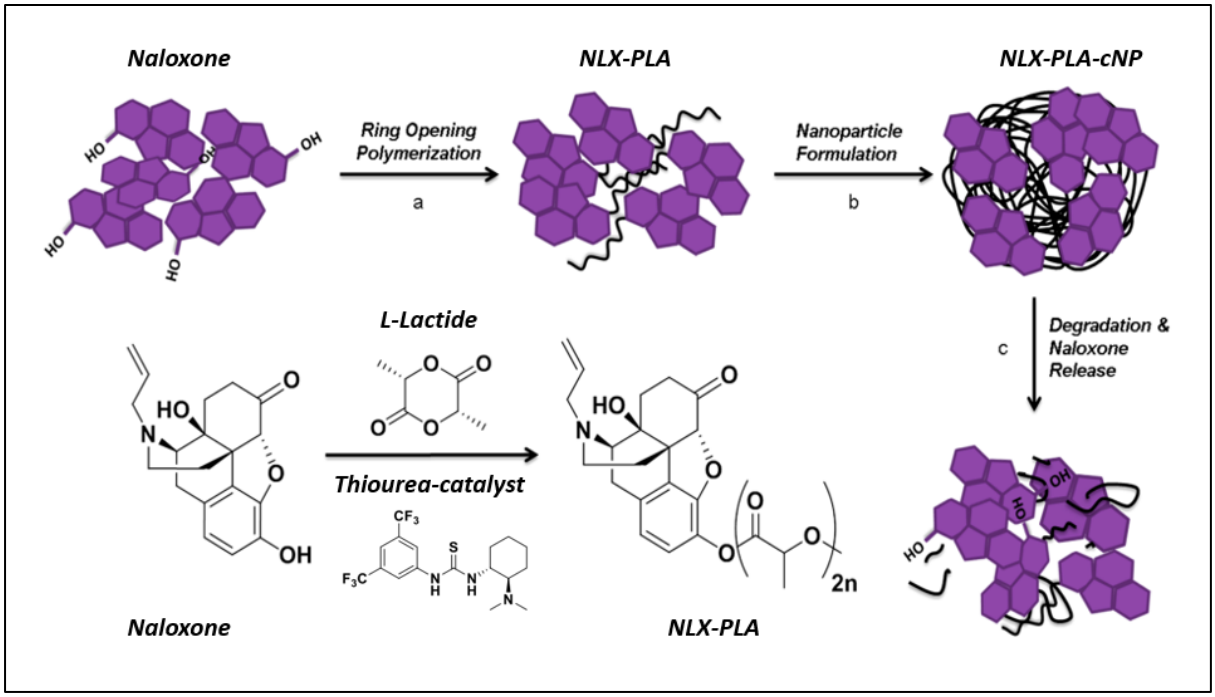

Figure 2.2. Schematic representation of the formulation of Covalent Naloxone-PLA Nanoparticles (NLX-PLA-cNPs): [a] Naloxone (NLX) initiated ring opening polymerization (ROP) of L-Lactide under thiourea-catalyst results in the formation of Naloxone-poly (L-lactide) polymer (NLX-PLA), [b] Nal-PLA is converted to Nal-PLA-cNPs using the nano-precipitation technique and [c] NLX is released from the nanoparticles because of the degradation of the bonds within NLX-PLA-cNPs due to ester hydrolysis (Adapted with permission from Kassick et al. (2019), © 2019, American Chemical Society).

In another study by Nanaki et al. (2020), a novel block copolymer of poly(l-lactide)-block-poly (propylene adipate) (PLLA-b-PPAd) was synthesized and used to encapsulate naltrexone forming a long-acting microparticle injectable formulation. The single emulsification method was used for the formulation of microparticles that ranged between 0.4 - 4.5 µm with a drug loading and entrapment efficiency of 8.30 ± 0.21% and 33.21 ± 1.62%, respectively. Additionally, through XRD and DSC analysis, it was found that naltrexone was present in the amorphous state in its microparticles. The study further noted that the *in vitro* drug release of the PLLA-b-PPAd-naltrexone microparticles was extended over a period of 7 days and that drug release of naltrexone was dependent on the copolymer composition. The model release

studies showed that the release of naltrexone from the microparticles was controlled by diffusion mechanism and with the extended release effect of this DDS, the duration of action of naltrexone was increased (Karavelidis et al., 2015; Nanaki et al., 2020).

Liu et al. (2006) and co-workers, have further described a naltrexone-loaded poly (D,L-lactic acid) (PDLLA) microsphere injectable formulation formulated using a microencapsulation technique based on the formation of a water-in-oil-in-water double emulsion. In this study, the particle size and encapsulation efficiency of the microspheres was found to be 200 μm and 82.73% respectively, with the injectable usually containing 300 mg of naltrexone releasing into the blood plasma at different stages, providing a sustained release. *In vitro* drug release of the naltrexone microspheres showed a cumulative release of 80% naltrexone at the end of 60 days. It should be noted that a similar drug delivery profile was observed for **'**Naltrel®**'** (DrugAbuse Sciences, Inc, Paris, France) which is a marketed naltrexone-containing injectable (Goonoo et al., 2014; Liu et al., 2006; Tijani et al., 2022). *In vivo* evaluation of these naltrexone-PDLLA microspheres using six-week-old Sprague Dawley rats weighing 200–220 g found that surface naltrexone released within 24 hours at the site of injection after which, within 48 hours the site of injection, the DDS underwent hydration, which lead to naltrexone-PDLLA polymer degradation at a slower rate, forming the monomer constituents. This resulted in a sustained naltrexone release phase over a period of 28 days which has the potential to substantially increase patient compliance (Galloway et al., 2005; Liu et al., 2006).

Kamali et al. (2018) further formulated an injectable *in situ* forming gel (ISFG) of buprenorphine using a PLGA-polyethylene glycol-PLGA (triblock) polymer and N-methyl-2-pyrrolidone as a solvent for decreasing the initial burst release of buprenorphine. PLGA is a biocompatible and biodegradable aliphatic polyester formed by the copolymerisation of lactic and glycolic acid monomers which, upon alteration in composition ratios can influence the solubility, degradation time and release profile of DDSs (Borandeh et al., 2021; Kapoor et al., 2015; Magill et al., 2023). In this study, a ring opening polymerization reaction using supercritical CO_2 ($ScCO_2$) method was used for the synthesis of the triblock polymer (Kamali et al., 2018). *In vitro, ex vivo, and in vivo* studies of the ISFG were compared by Kamali et al. (2019) to an *in situ* forming implant (ISFI) composed of copolymer PLGA 504H (like RBP-6000) and it was found that the initial burst release in *in vitro* media for the ISFG and ISFI were 6.19 ± 0.31% and 13.45 ± 1.14% respectively. ISFG was also found to have a significantly lower burst release than that for the ISFI because of the thermosensitive property of the triblock and hydrogen-bonding between the N-methyl-2-pyrrolidone molecules and that the polyethylene glycol of the triblock prevented the N-methyl-2-pyrrolidone from diffusing rapidly into the release medium. Further *in vivo* evaluation of the C_{max} of BUP in ISFG was found to be 6.95

± 0.98 ng/mL as compared to the 8.19 ± 1.02 ng/mL ISFI. The AUC and the serum concentration (C) range of BUP for the ISFG was further determined to be 2721.38 ± 69 and 1.87–7.12 respectively as compared to ISFI (AUC = 2727.36 ± 71, C = 1.75–10). This study additionally noted through *ex vivo* studies that the ISFG can be used as a new type of sustained-release injectable formulation as it released BUP over a period of 21 days with a smaller initial burst release than the ISFI and this is a potential benefit in therapeutic treatments (Kamali et al., 2019).

From a clinical trial perspective, Andhariya et al. (2017) and co-workers, have described a naltrexone containing PLGA (75:25) microsphere injectable formulation very similar to Vivitrol® (Alkermes, Inc, Cambridge, MA), a naltrexone containing marketed injectable formulation, in order to evaluate the properties of Vivitrol® (Andhariya et al., 2017). The injectable product usually contains 380 mg of naltrexone that releases into the blood plasma in different stages giving a sustain release. In the initial phase, the surface drug was released within 24 hours at the site of injection after which, within 48 hours the site of injection underwent hydration and the naltrexone-PLGA polymer degraded slowly to its monomer constituents and released naltrexone in sustained release phase over a period of 30 days. A similar mechanism of naltrexone release is observed in Vivitrol® (Andhariya et al., 2017; Goonoo et al., 2014; Krupitsky et al., 2017). Additionally, as per the clinical data obtained by Ndegwa et al. (2017) from the ALK21-013 randomized, placebo-controlled, double-blind trial, Vivitrol® was evaluated over a period of 24 weeks. A total of 250 patients were enrolled randomly with OUD out of which 126 received Vivitrol® and 124 received a placebo within one week of detoxification followed by every four weeks thereafter. Approximately 53.2% patients who received Vivitrol® completed the study as compared to 37.9% with the placebo. Additionally, Vivitrol® increased the proportion of opioid free weeks compared to the placebo group by 90% with Vivitrol® versus 35% with the placebo, proving the effectiveness of Vivitrol® (Ndegwa et al., 2017).

Using the double emulsion evaporation technique i.e. water-in-oil-in water (W1/O/W2) Benéitez et al. (Benéitez et al., 2014) formulated a subcutaneous NLX loaded microsphere (NLX-MP) injectable. In the study, naloxone hydrochloride (60 mg) was loaded in the formulation using sorbitan esters as emulsifiers to give the microspheres an entrapment efficiency of 70%. Additionally, sorbitan esters help in reducing the media acidification that is caused due to the degradation of PLGA. As per Benéitez et al. (2014), the PLGA present in the formulation provided a sustained release of naloxone hydrochloride over a period of 7 days (Benéitez et al., 2014). *In vitro* studies further demonstrated the antagonizing effect of NLX-MPs on morphine induced human neuroblastoma (SHSY5Y) cells and myenteric plexus-

longitudinal muscle tissue isolated from guinea-pig ileum over a period of 7 days. The *in vivo* evaluation of the NLX-MPs was carried out in morphine induced mice for testing the antagonism of the antinociceptive effect of morphine using the hot plate method. Results showed that subcutaneous administration of NLX-MPs blocked the morphine effect that was induced in mice. Additionally, the subcutaneous administration of the NLX-MPs enhanced NLX's therapeutic efficacy as a non-addictive medication, proving its potential as a suitable OUD intervention (Benéitez García et al., 2023).

Nasser et al. (2014), further described a subcutaneous microcapsule depot formulation that was designed to release BUP in a sustained manner over a period of 28 days (Nasser et al., 2014; Rosenthal and Goradia, 2017). The depot was formulated with a dose of 200 mg/ml of BUP, containing a biodegradable PLGA polymer and a biocompatible solvent i.e. N-methyl-pyrrolidone that worked on the precipitation technique. The formulation, when interacted with water, solidified at the surface of the subcutaneous space and provided the sustain release of BUP by increasing the residence time. The similar mechanism of drug release was observed in 'RBP-6000' (Indivior, Richmond, VA, USA) also known as Sublocade® which is a marketed BUP containing depot formulation (Nasser et al., 2014; Packhaeuser et al., 2004; Rosenthal and Goradia, 2017; Rosenthal, 2019). The clinical trials done by Nasser et al. (2016), suggested that a 300 mg RBP-6000 injection demonstrated rapid and sustained BUP exposure that blocked the agonistic effect of hydromorphone resulting in protection against the illicit opioids (Nasser et al., 2016). Additionally, RBP-6000 still maintained a ≥70% efficacy even though not being stimulated for a period of 2 weeks (Laffont et al., 2016). As per FDA briefing documents, a 24-week randomized, multisite and controlled safety efficacy study (n = 504) was done using 2 dosage regimens: RBP 6000 300 mg × 2 doses followed by 100 mg × 4 doses and RBP 6000 300 mg × 6 doses, against a placebo for treatment-seeking patients who were first induced with 8 - 24 mg of sublingual BUP over 2 weeks until clinically stable. The '300 mg × 6 doses' regimen showed more discontinuation as compared to the '300 mg × 2 doses' followed by '100 mg × 4 doses' regimen due to the adverse reaction at the site of injection, elevated liver enzymes, constipation and drug withdrawal syndrome concluding that the '300 mg × 2 doses' followed by '100 mg × 4 doses' regimen was safe and effective (Rosenthal and Goradia, 2017; Rosenthal, 2019).

Schreiner et al. (2021), also formulated a BUP containing microparticle depot formulation which was formulated through emulsification. The sustained release of BUP was achieved by polymerizing BUP with PLGA and formulating it into microparticle using polyvinyl alcohol (PVA). The microparticles had a particle size, drug loading and entrapment efficiency of 33.7 ± 10.9 µm, 4.1 ± 1.2% and 86.1% respectively. *In vitro* drug release studies further determined

that the polymeric BUP containing microparticles were found to have a cumulative sustained release of BUP over a period of 72 hours, which proves that the DDS helps in increasing the bioavailability and residence time of BUP at the site of action (Guarnieri et al., 2018; Schreiner et al., 2021).

Sigmon et al. (2004), described a BUP-loaded micro-capsule depot formulation 100-150 µm in size and formulated using the biodegradable PLGA polymer (65:35) and buprenorphine base functioning on the micro-capsule depot technology. A similar technology is used in NORVEX® (Biotek, Inc., Woburn, MA, USA) which is a BUP containing micro-capsule depot formulation. This technology helped to achieve the sustained release of BUP by increasing the residence time of BUP (Rosenthal and Goradia, 2017; Sigmon et al., 2004). Clinical data obtained by Sigmon et al., (2006). suggested that, once BUP micro-capsules were administered subcutaneously, BUP reached its maximum plasma peak levels on day 2 or 3, which gradually decreased to zero over a period of 6 weeks (Sigmon et al., 2006). In a 6-week controlled trial (n = 15) of a 58 mg BUP depot versus a placebo depot in opioid dependent participants, Sigmon et al. (2004) also found that the BUP micro-capsule depot was effective in suppressing the withdrawal symptoms from opioids and provided significant blockade of the opioid receptor as 86.6% recovery rate was observed in comparison to 13.4% recovery in placebo participants (Sigmon et al., 2004).

In a study conducted by Khodaverdi et al. (2023) and co-workers, a BUP containing sustained release *in situ* forming lipid-lipid crystal gel (ISFLLCG) formulation was prepared consisting of amphiphilic molecules, such as phosphatidylcholine (PC) and glycerol dioleate in the ratio of 50:50 (w/w%) in *N*-methyl-2-pyrrolidone solvent (Khodaverdi et al., 2023; Salikolimi et al., 2020). In this system when the ISFLLCG got into contact with interstitial aqueous fluid, it self-assembled into a reverse phase water-in-oil viscous liquid gel that eluted BUP at a predictable rate giving it a sustained release. A similar ISFLLCG system is seen in ‘CAM2038’ (FluidCrystal®; Camurus AB, Lund, Sweden), which is a BUP containing subcutaneous depot formulation (Rosenthal and Goradia, 2017; Tiberg et al., 2012; Tiberg and Johnsson, 2011). As per the *in vitro* drug release studies, the formulation was found to show a sustained release profile over a period of 30 days. The degradation rate and drug release profile were found to have the same linearity pattern and after a month, 42% of the formulation went under degradation indicating 42% of the drug was released through degradation and 58% via penetration mechanism. L929 skin fibroblasts were used for the assessment of *in vitro* cytotoxicity, where good biocompatibility of the formulation was found over 6, 12, 24 and 72 hours and 1, 2, 3 and 4 weeks. *In vivo* studies were further carried out on New Zealand rabbits for the assessment of gel formation after ISFLLCG administration, no gel formation was found

in the control and NMP-dissolved BUP groups, whereas the BUP-free ISFG and BUP ISFG displayed gel formation (Khodaverdi et al., 2023). In the evaluation of CAM2038, a randomized, double blind, multisite 24-week non-inferiority phase 3 trial was performed by Braeburn Pharmaceuticals on 428 participants with moderate to severe OUD. In the trial CAM2038 was tested against sublingual BUP at various sites and responders were defined as ≥ 33% (4 of 12) for Phase 1 urine toxicology tests and ≥ 67% (4 of 6) for Phase 2 urine toxicology tests being negative for illicit opioids. In another study by Braeburn Pharmaceuticals and Camurus (NASDAQ STO:CAMX), participants were induced with daily sublingual BUP with weekly subcutaneous placebo injection or weekly subcutaneous CAM2038 BUP injection with a daily sublingual placebo tablet. CAM2038 subcutaneous BUP injection was found to be superior compared to the sublingual BUP tablets due an increase in the percentage of urine samples negative for illicit opioids with this intervention (Lofwall et al., 2018; Rosenthal and Goradia, 2017; Rosenthal, 2019).

2.2.1.1.2 Implants

Implantable DDSs are surgically implanted medical devices designed to deliver therapeutic moieties in a controlled or sustained manner over a period of months to years at a specified target site and is one of the properties that can help to overcome the poor pharmacokinetics of opioid reversal agents. Additionally, with advancements made in implantable DDSs, several benefits like smart implants can monitor a patient's condition and administer drug as per requirement and due to its reduction in size is less invasive and easily localizable with more target specificity (Fayzullin et al., 2021; Huanbutta et al., 2024). In this section the various extended-release implantable DDSs that have been developed for OUD interventions have been discussed.

One such study who developed an implantable DDS for OUD explored the use of PDLLA (Ngo et al., 2008). This research developed an implant composed of naltrexone and poly(trans-3,6-dimethyl-1,4-dioxane-2,5-dione) (D,L) lactide microspheres, which were compressed into tablets (8 mm diameter, 5 mm thickness) followed by coating with PDLLA to achieve a sustained release of naltrexone. The platform which is marketed as **'**O'Neil®**'** (Go Medical Industries, Perth, Australia), is a naltrexone-containing implant which works on the same mechanism as described in this study (Goonoo et al., 2014; Ngo et al., 2008). As per data collected, 1 - 2 ng/mL of naltrexone was released for 3, 5 and 7 months from the 10, 20 and 30 pellet implants, respectively. The 1.1 g (10), 2.2 g (20) and 3.3 g (30) naltrexone implant treatment additionally maintained free blood naltrexone levels above 2 ng/mL for 95 days (95% CI 69-121), 136 days (95% CI 114-158) and 145 days (95% CI 125-167), respectively (Ngo et al., 2008). Further evaluating this type of platform, Krupitsky et al. (2012) evaluated O'Neil® in

a three-group, double-dummy design study carried out on 102 opioid dependent patients over a period of 6 months. This study noted that a larger proportion of urine samples were found to be opioid negative in the naltrexone implant group (52.9%), when compared to both the oral naltrexone (15.7%) and placebo (10.8%) groups, noting the benefits of using this implant over oral formulations (Krupitsky et al., 2012; Kunoe et al., 2009).

EVA is an FDA approved, transparent thermoplastic copolymer of ethylene and vinyl acetate monomers which are biocompatible for implants and parenteral applications in the treatment of OUD. The vinyl acetate content determines the crystallinity, melting point, stiffness and polarity of the EVA giving it an edge in developing various DDSs (Almeida et al., 2012, 2011; Repka et al., 2008; Schneider et al., 2017). One such platform was a BUP-containing subcutaneous implant developed by Rosenthal et al. (2013), for implantation in patients, who have shown sustained clinical stability on the transmucosal formulations of BUP (Rosenthal, 2019; Rosenthal et al., 2013). In this study, four 26 x 2.5 mm EVA polymer rods containing 80 mg of BUP hydrochloride were implanted via a single insertion point into the subdermal space of the inner upper forearm to achieve a controlled release of BUP. A similar mechanism of formulating BUP is observed in 'Probuphine®' (Titan Pharmaceuticals, San Francisco) which is a marketed BUP containing subcutaneous implant (Barnwal et al., 2017; Ling et al., 2010; Rosenthal, 2019; Rosenthal et al., 2013). The implant eluted BUP in a controlled way for over a period of 6 months.

Further, two randomized, double-blinded placebo-controlled multisite 24-week trials evaluating BUP implants were conducted by Ling et al. (2010) on participants with *DSM-IV* who were first clinically stabilized using 12 - 16 mg of sublingual BUP and did undergo standardized individual drug counselling. One hundred and sixty-two patients participated in the study where 108 participants received 4 BUP 80 mg implants, and 55 participants received 4 placebo implants. It was noted that those who received BUP implant had twice the study completion rate as compared to those who received placebo implants i.e. 65.7% vs 30.9%. Additionally, the BUP implant group showed more urine negative samples of illicit opioids compared to the placebo implants i.e. 40.4% vs 20.8% (Ling et al., 2010). A second study conducted by Rosenthal et al. (2013) was also a 24-week double-blind, placebo-controlled trial with the same parameters as first study with the addition of open-label sublingual BUP/NLX tablets, where the safety and efficacy study were taken into consideration. The BUP implant evaluated in this study was found to be non-inferior as compared to sublingual BUP/NLX tablets on the percentage of urine samples negative for opioids. The study results noted that 50.2% patients had urine samples negative for opioids in the BUP implant group as compared to 55.1% patients in the sublingual BUP/NLX group proving both had similar

treatment efficacy (Rosenthal et al., 2013).

Goonoo et al. (2014), has additionally described about **'**Prodetoxone®**'** (Fidelity Capital, Russia) and **'**Wedgewood®**'** (Wedgewood Pharmacy, America), naltrexone-containing hypodermic depot tablet implants which shows a sustained release drug profile because of their magnesium stearate matrix technology (Goonoo et al., 2014). Ramenskaya et al. (2005) has further reported a therapeutically significant naltrexone blood levels of 20 ng/mL from Prodetoxone® containing 1000 mg naltrexone over a period of 30 days via the high-performance liquid chromatography (HPLC) analysis on 60 opioid dependent patient's blood samples (Krupitsky et al., 2017; Ramenskaya et al., 2005). A 10-week randomized, double-blind, placebo-controlled trial of Prodetoxone® was also performed by Tiihonen and co-workers (Tiihonen et al., 2012) on 100 opioid dependent patients, where 50 patients received naltrexone implants and 50 patients received placebo. At the end of 10 weeks, the retention rate was 52% and 28% followed by 38% and 16% for drug free urine samples for the naltrexone group and placebo group respectively (Tiihonen et al., 2012). Furthermore, as described by Brewer (2002), the Wedgewood® implant showed blocking levels at 5 ng/mL for a period of 3 weeks after surgical insertion against a pure dose of 500 mg diamorphine (Brewer, 2002). Additionally, as per the clinical data obtained by Olsen et al. (2004) on 10 opioid dependent patients, the Wedgewood® implant maintained 1 ng/mL of blood plasma naltrexone levels for a period of 55 (range 30 - 80) days indicating that the DDS helped in improving the residence time of naltrexone and making it more patient compliant (Olsen et al., 2004).

In a study undertaken by Dhowan et al. (2019), a simple, low-cost, minimally invasive closed loop automatic antidote delivery device (A2D2) i.e. a NLX containing subcutaneous implant (SI) for the potential treatment of opioid overdoses was developed. This system functioned by detecting overdose-induced respiratory failure, in response to which a large dose of NLX was released to counteract the effect of the opioid. The A2D2 SI shown in Figure 2.3a is fabricated using four commercially available and biocompatible components: a high-density polyethylene (HDPE) tube, a polytetrafluoroethylene (PTFE) ball seal, a stainless steel (SS) tube heating element, and a phase change material (PCM) designed to melt at 42 °C. The subcutaneously placed device can be activated for releasing NLX using a time varying magnetic field which can be generated from a wearable magnetic field generator (Figure 2.3b). Due to the oscillating magnetic field, induction heating of the SS tubes occurs, which melts the PCM and diffuses NLX, as represented in Figure 2.3c. *In vitro* evaluation studies of the developed system showed that A2D2 can release 1.9 mg of NLX within 60 seconds and up to 8.8 mg in 600 seconds, displaying the effectiveness of the A2D2 DDS in administering NLX in opioid

overdose situations (Dhowan et al., 2019).

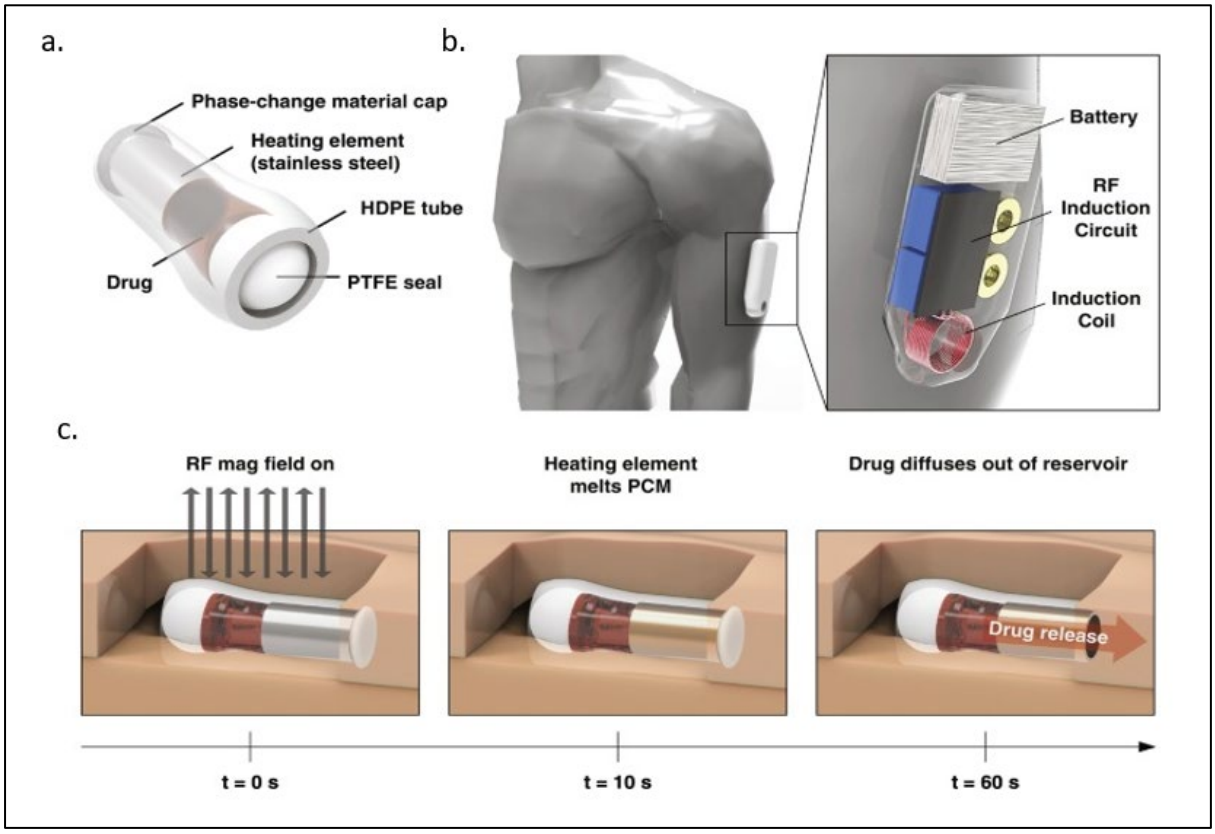

Figure 2.3. Schematic representation of [a] the automatic antidote delivery device (A2D2) with all its components, [b] the wearable magnetic field generator used to stimulate the release of drug from the A2D2 subcutaneous implant (SI) and [c] how the drug is diffused out from the A2D2 SI when, time varying magnetic field is applied to the SI which allows the heating element to reach the melting temperature of PCM and drug is diffused. (Reproduced with permission from Dhowan et al. (2019), © 2019 Elsevier).

2.2.1.1.3 Transdermal systems

Extended-release transdermal DDSs like adhesive patches, microneedle (MN) patches and molecularly imprinted polymeric patches can provide a safe, convenient, effective, non-invasive and patient compliant means of long-term direct systemic drug delivery via permeation across the layers of skin. Additionally, these transdermal DDSs have the benefit of bypassing first-pass metabolism, thus providing continuous delivery of drug over an extended period (Jeong et al., 2021; Karve et al., 2024). With the incorporation of these beneficial pharmacodynamic properties, the poor pharmacokinetics of opioid reversal agents can be overcome. In this section, the various extended-release transdermal DDSs for OUD treatment have been discussed.

One such study by Tijani et al. focused on the design of a transdermal polymeric MN patch derived from PVP with delivery and pharmacokinetic properties useful in eliminating NLX's

delivery limitations and making it comparable with the commercially marketed NLX products (Tijani et al., 2023). PVP is a biocompatible, non-toxic, temperature-resistant, chemically inert and water-soluble polymer, which in solution has good wetting properties providing excellent film forming properties for various DDSs including those for oral, topical, transdermal, and ocular administration (Borandeh et al., 2021; Kariduraganavar et al., 2014; Kurakula and Rao, 2020). In this study, the polymeric MN patches were composed of varying dimensions i.e. 500 µm; 100 array, 800 µm; 100 array and 600 µm; 225 array and loaded with NLX at a dosing strength of 17.89 ± 0.23 mg, 17.2 ± 0.77 mg, and 17.8 ± 1.01 mg, respectively. Using the thumb force technique and methylene blue dye on the porcine ear skin, the insertion efficiency of micro-needles was determined to be 94 ± 4.8%, 90.6 ± 1.69%, and 96 ± 1.29% for the 500 µm ,800 µm and 600 µm patches respectively. Drug permeation across the porcine ear skin was further found to be 2.4%, 10% and 23% after 24 hours and a sustained drug release of 40, 10 and 4 days was found for the 500, 800 and 600 µm MN formulations, respectively, which indicated the substantial enhancement in the release profile and residence time of NLX (Guarnieri et al., 2018; Tijani et al., 2023).

Rahmani et al. (2021), further formulated a BUP-loaded PVA/PVP (BUP/PVA/PVP) nanofiber-based transdermal DDS. The electrospinning technique was used for the fabrication of BUP/PVA/PVP nanofiber mats, with the average diameter and electrical conductivity of the nanofiber solution 104 nm and 1261 µsecond respectively. The viscosity, shear rate and contact angle of the nanofibers were found to be 119 Pa·second, 105 1/second and 70° respectively. *In vitro* drug release studies carried out on the BUP/PVA/PVP noted a cumulative sustained release of BUP over a period of 72 hours, which proved that this DDS helped in improvising the residence time and patient compliance of BUP (Rahmani et al., 2021).

Budd and Collett (2003), additionally described about a BUP-loaded transdermal patch **'**Transtec®**'**, first launched in Switzerland and Germany in 2001 and is now marketed all over Europe. The transdermal patch utilises the favourable pharmacokinetic properties of BUP and an adhesive matrix technology, where BUP was homogeneously incorporated in a solid polymer matrix of PAA-derived poly [acrylic acid-co-butyl-acrylate-co-(2-ethylhexyl) acrylate-co-vinyl acetate] (5:15:75:5). PAA is a high molecular weight water-soluble polymer derived from the polymerization of acrylic acid monomers. The hydrophilic nature and cross-linked structure of PAA allows it to readily absorb water (pH-responsive) to form hydrogels, which makes them suitable for various controlled DDSs (Mastropietro et al., 2017; Pandey et al., 2019; Ritthidej, 2011). In this study, the adhesive BUP patch was non-invasive and the polymer matrix along with the backing layer, which was made up of poly(ethylene-terephthalate), helped in providing slow and continuous release of BUP into systemic

circulation. This matrix patch structure further avoided the risk of 'dose-dumping', which was found in older reservoir patch systems (Budd and Collett, 2003). The patch is now available in three different dosage strengths with total loading doses of 20 mg, 30 mg, and 40 mg designed to release BUP at a steady controlled rate of 35 µg/hour, 52.5 µg/hour, and 70 µg/hour respectively, corresponding to a daily administered dose of 0.8 mg/day, 1.2 mg/day, and 1.6 mg/day, respectively (Likar, 2006).

In the evaluation of Transtec® by Sittl (2003), pharmacokinetic studies showed that after single application of the patch, plasma levels of BUP continuously increased and reached the minimum effective concentration (MEC) after 24 hours, when using the 20 mg patch, and 12 hours after using the 40 mg patch. The initial recommendation on dose maintenance was that each patch remains effective for 3 days (Sittl, 2003). However, as per an open, randomized cross-over-study in chronic pain patients, Likar et al. (2007) found that clinically effective plasma concentrations of all three i.e. 20 mg, 30 mg and 40 mg transdermal patches were reached after 24 hours and that these levels were maintained for 4 days throughout the application period, indicating that the patch can be used effectively over a period of 4 days (Likar et al., 2007). 'Butrans®' is also a BUP containing transdermal patch composed of 46.6 mg BUP and is designed to deliver 5, 7.5, 10, 15 or 20 µg/hour of BUP. An aqueous solution of ethanol and propylene glycol solution, with trace amount of lauric acid is used in the transdermal formulation, which acts as a penetration enhancer (Lanier et al., 2008). HPC is also bound in the adhesive matrix of the microporous membrane and provides sustained release of BUP via diffusion into the systemic circulation. HPC is water-soluble cellulose ether polymer manufactured by reacting alkali cellulose with propylene oxide yielding a highly substituted cellulose ether making it available in different average molecular weights, which makes it suitable for formulating DDSs with different release profiles (Dürig and Karan, 2019).

In another 10-day detoxification trial undertaken by Lanier et al. (2008), 9 opioid dependent patients were selected from whom blood samples were collected prior and after the application of transdermal patch for analysis of the levels and effectiveness of BUP. At the end of the study, it was concluded that the transdermal patch reduced the withdrawal symptoms within 24 hours of the patch application and continued to decline thereafter. The patch was found to be safe, well tolerated and delivered a mean of 1.9 mg/day BUP over a period of 3 days. Additionally, a significant suppression of craving was maintained for a period of 7 days after the patch was removed suggesting the effectiveness of the transdermal patch (Lanier et al., 2008, 2007).

2.2.1.2. DDSs for enhanced drug bioavailability

The incorporation of nanotechnology to DDSs has played a vital role in enhancing bioavailability of therapeutic moieties across the BBB. Maximum bioavailability leads to increased residence time and therapeutic efficacy. Factors responsible for helping opioid reversal agents cross BBB include molecular weight (≤ 400 Dalton), size (nano meter range), morphology (spherical), ionization (physiological pH) and lipophilicity which are all provided by advanced DDSs (Satapathy et al., 2021; Teleanu et al., 2022). In this section, the various DDSs responsible for enhancing drugs bioavailability across the BBB have been discussed.

2.2.1.2.1 Sublingual delivery

Sublingual DDSs are used when a rapid onset of action is required and is associated with a better treatment efficacy, as the therapeutic moieties delivered via this DDS bypass first-pass metabolism providing an increased bioavailability at the site of action (Saha et al., 2017). This beneficial pharmacodynamic property has therefore been used for the effective administration of opioid reversal agents. Specifically, Silva et al. (2015), described a BUP and NLX containing sublingual film that works on the Pharmfilm® technology, as represented in Figure 2.4 (Silva et al., 2015). Pharmfilm® is a polymeric matrix based on HPMC and polyethylene oxide, which is related to rapid drug absorption and has a loading capacity up to 80 mg. HPMC which belongs to the group of cellulose ether derivatives is a hydrophilic (water soluble), biodegradable, and biocompatible polymer used to enhance the efficacy of active pharmaceutical ingredients in the controlled/sustained release DDSs (Deshmukh et al., 2017).

A similar drug delivery mechanism of BUP and NLX is observed in 'Suboxone® Sublingual Film' (Reckitt Benckiser plc., England), which is a marketed sublingual film containing BUP and NLX. The film is available in four dosage strengths of BUP and NLX: 2/0.5 mg, 4/1 mg, 8/2 mg and 12/3 mg and has been extensively evaluated clinically for OUD efficacy (Borges et al., 2015; Gupta et al., 2022; Silva et al., 2015). In a 12-week open-label study conducted by Sullivan and Webster, (2015) on 249 opioid-dependent patients, who were stabilized by 8/2 to 32/8 mg/day of Suboxone® Sublingual tablets (SST) for approximately 30 days, the patients were converted to Suboxone® Sublingual Films (SSF) with 79.1% completing the 12-week study. The results of the study noted that rates of constipation reported at baseline declined from 41% to 13% after 12 weeks of SSF treatment, while the Clinical Opiate Withdrawal Scale total ranging from 10 to 25 (overall mean, 13.8) within 24 hours of taking their last SST dose reduced to 0 to 3 (overall mean, 0.7) at 3 hours after the initial dose of SSF. Treatment compliance was additionally high for SSF and <1% of urine samples were BUP-free including 92.4% of SSF-treated subjects not having urine samples tested positive for any non-prescribed opioid. A total of 91.3% and 82.5% subjects rated the taste of SSF as

pleasant or neutral and the ease of use as easy or neutral respectively, suggesting that SSF DDS is an effective and patient compliant way of delivering NLX and BUP (Sullivan and Webster, 2015).

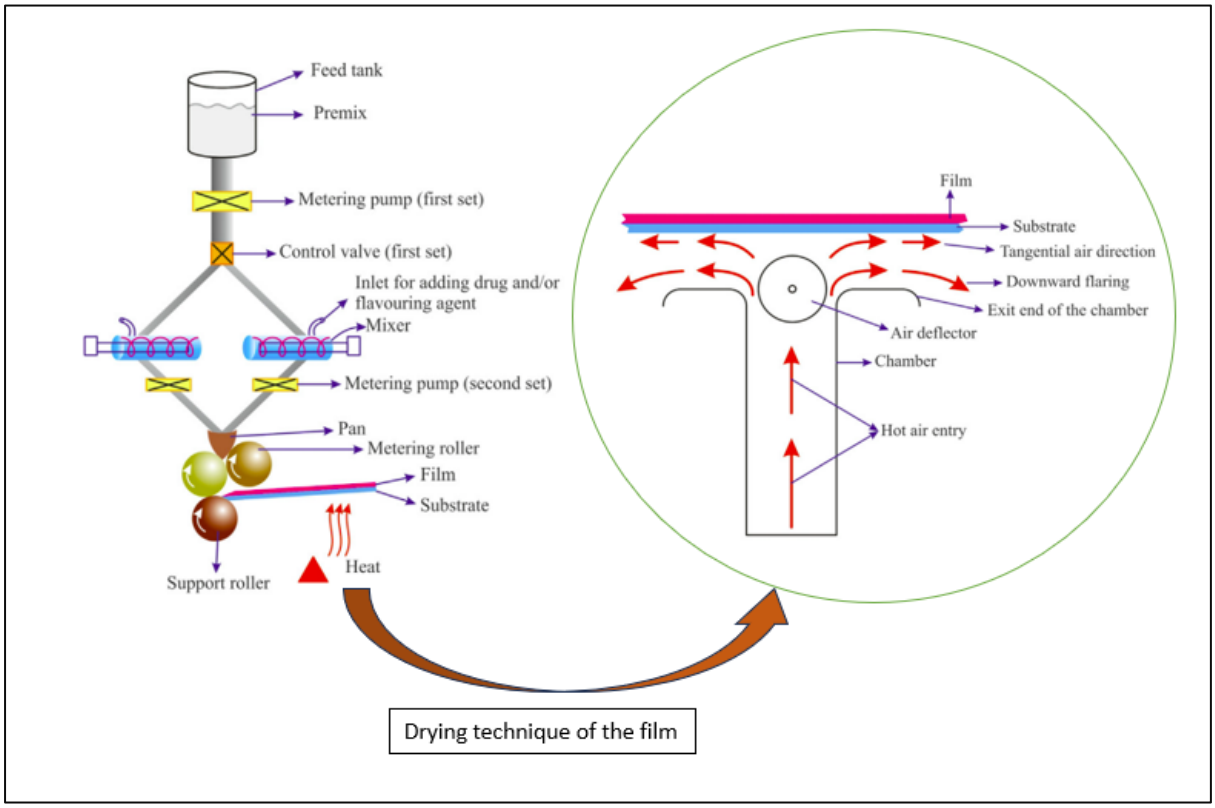

Figure 2.4. Schematic representation of the Pharmfilm® technology used in the manufacturing of Suboxone® sublingual film (Adapted with permission from Gupta et al. (2021), © 2021 Elsevier).

2.2.1.2.2 Intranasal formulations

The delivery of nanotechnology through the nasal delivery route is one of the most significant DDS interventions for treating OUD as it allows for maximum bioavailability across the BBB (Kisku et al., 2024). In the study by Voronkov et al. (2022) and co-workers, a bio-reversible derivative of NLX i.e. NX-90 was synthesized to be administered intranasally to yield a robust reversal of fentanyl induced overdose (OD) in rats. NX-90 was synthesized using the esterification reaction, as shown in Figure 2.5a, and by using the radioligand binding assays and Chemaxon software, the lipophilicity of NX-90 was found to be higher in comparison to NLX and similar to fentanyl (Figure 2.5b). *In vivo* evaluation of the system was conducted on 15 Wistar rats, where respiratory rate (RR), heart rate (HR) and body temperature (BT) were the primary parameters under observation along with secondary parameters like alertness (AN), astazia (AT), corneal reflex (CR), pinch reflex tail (PRT), pinch reflex toe (PRToe), righting reflex (Rref) and sternal recumbency (ST) were monitored. Doses of NLX 0.31 and

0.62 µmol/kg were administered in 2 groups and 0.31 and 0.62 µmol/kg of NX-90 in the other two groups of rats. As per the data represented in Figure 2.5c, all the monitored reflexes along with the heart rate (HR) and respiratory rate (RR) were completely restored faster in the NX-90 groups compared to NLX groups on equimolar bases when administered intranasally. Additionally, in rats treated with NX-90, the RR over the observed period (RR AUC) was found to be significantly higher across all doses without the occurrence of any re-narcotization (Voronkov et al., 2022).

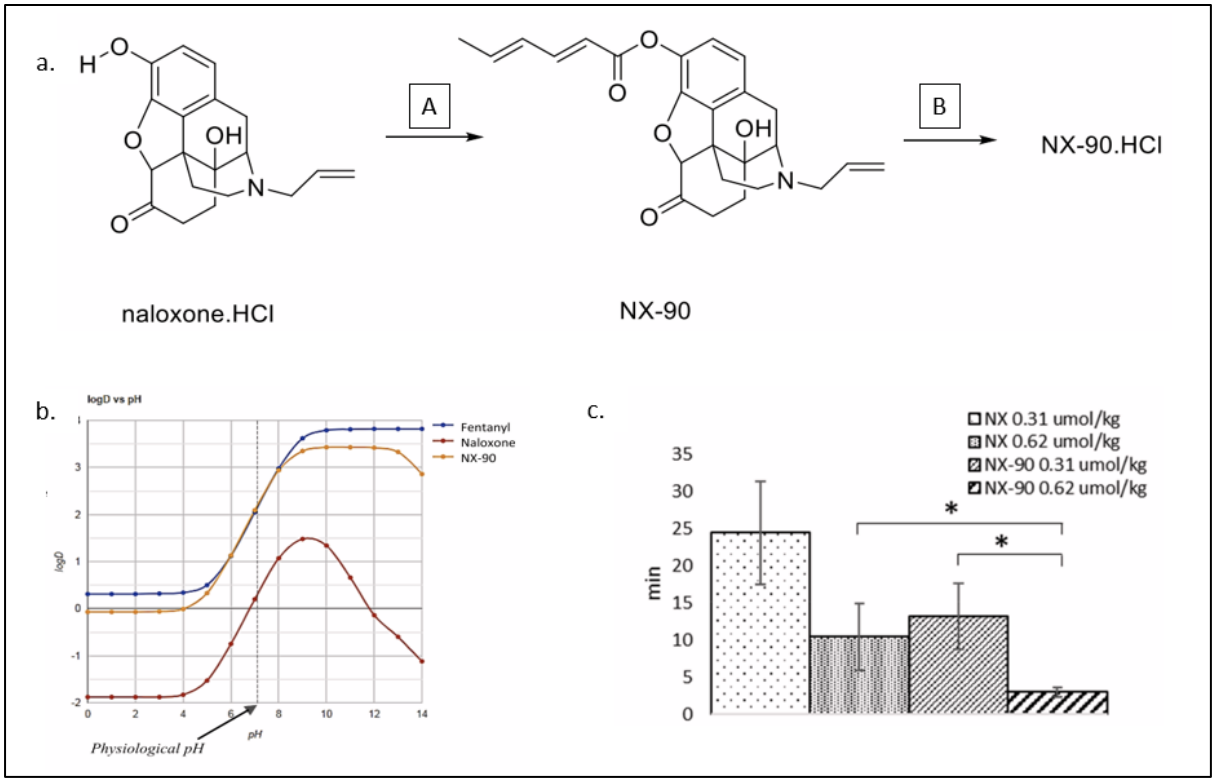

Figure 2.5. [a] Schematic representation of the synthesis of NX-90 and NX-90 HCl. The reagents and rection conditions: (A) 1-Ethyl-3-(3-dimethylaminopropyl) carbodiimide (EDCI), hexadienoic acid, 4-dimethylaminopyidine (DMAP), trimethylamine (Et3N), tetrahydrofuran (THF), 0 ºC; (B) Hydrochloric acid (HCl) gas, methyl tertiary-butyl ether (MTBE), 0 ºC. [b] Graphical representation of the comparison of lipophilicity between fentanyl, NLX (NX) and NX-90. [c] Graphical representation of the data obtained from the *in vivo* studies for the time consumed by NX (0.31 and 0.62 µmol/kg) and NX-90 (0.31 and 0.62 µmol/kg) to restore all the reflexes in rats. (Adapted with permission from Voronkov et al. (2022), © 2022 Elsevier).

In another study by Hasan et al. (2021) and co-workers, a NLX containing SLN intranasal system was formulated for the reversal of opioid overdose. The preparation of NLX-SLN was done using the solvent evaporation method where glyceryl monostearate served as the solid lipid, pluronic F127 as the surfactant and tween 80 as the co-surfactant. The particle size, zeta potential and PDI of NLX-SLN was found to be 190.2 nm, -16 mV and 0.082 respectively. Additionally, the entrapment and loading efficiency of NLX-SLN was found to be 95 ± 0.53% and 19.08 ± 0.11% respectively. As per the *in vitro* and *ex vivo* studies carried out, an initial

burst release of NLX was found within 15 minutes followed by a sustained release of NLX over a period of 6 hours. Both the *in vitro* and *ex vivo* drug release profiles were found to follow the Higuchi model for drug release meaning NLX showed maximum entrapment and release via the diffusion mechanism from the SLN matrix. Additionally, the *in vivo* studies using Sprague Dawley rats were carried out where the pharmacokinetic properties i.e. T_{max}, C_{max}, $AUC_{0-\infty}$, $T_{1/2}$ and K_e were found to be 240 ± 2.1 minutes, 163.95 ± 2.64 ng/mL, 17.75 ± 1.08 ng·hour/mL, 18.82 ± 2.51 ng·hour/mL, 70.71 ± 0.11 minutes and 0.098 ± 0.01 $hour^{-1}$ respectively suggesting the effectiveness and potential of this DDS (Hasan et al., 2021).

Various marketed products also exist for the treatment of opioid overdoses. Vitore et al. (2023) in their review described KLOXXADO®, NARCAN® and NYXOID® NLX-containing nasal sprays that are used in the emergency treatment of opioid overdose (Vitore et al., 2023). In Table 2.2, the pharmaceutical formulation and pharmacokinetic properties of all three nasal formulations have been described.

Table 2.2. Pharmaceutical and pharmacokinetic properties of intranasal formulations of naloxone used in the clinical practice. (Adapted with permission from Vitore et al. (2023), © 2023 Elsevier).

Brand name	**KLOXXADO®**	**NARCAN®**	**NYXOID®**
Active ingredient	NLX HCl	NLX HCl $2H_2O$	NLX HCl $2H_2O$
Excipients	Dehydrated alcohol, Disodium ethylenediaminetetraacetate, Propylene glycol, Sodium hydroxide and Hydrochloric acid, Purified water.	Benzalkonium chloride, Disodium ethylenediaminetetraacetate, Sodium chloride, Hydrochloric acid, Purified water.	Trisodium citrate dihydrate, Sodium chloride, Sodium hydroxide and Hydrochloric acid, Purified water.
T_{max} (h)	0.25	0.50	0.50
Dose	Single dose container-one spray delivers 0.1 mL solution containing 8 mg of NLX HCl.	Single dose container-one spray delivers 0.1 mL solution containing 4 mg NLX HCl $2H_2O$.	Single dose container - one spray delivers 0.1 mL solution

	containing 2 mg naloxone HCl $2H_2O$.

From the above-mentioned extended-release and enhanced bioavailability DDSs for the treatment of OUD, it is clear that polymeric micro- and nano-particle-based DDSs, implantable devices and microencapsulation technologies play an important role in overcoming the poor pharmacokinetic properties of the drugs used for treating OUD i.e. residence time, combinational therapy, release profile and bioavailability. Additionally, advanced DDSs help in controlling the release of drugs, improving treatment efficacy, target specificity, minimizing side effects and enhancing patient compliance.

2.3. Barriers to OUD treatment and future perspective

The efficacy of the therapeutic agents used in the treatment of OUD, are impacted by their poor bioavailability, the effects of first-pass metabolism, limited amounts of drug reaching the brain due to the BBB and a decreased residence time (Bell and Strang, 2020; Cao et al., 2023). The mentioned barriers can be overcome by the incorporation of advanced DDSs to enhance the effectiveness and patient compliance of opioid reversal agents. The polymer-based DDSs provide excellent targeting properties, biocompatibility and biodegradability with low toxicity. It also helps with designing novel biomaterial-mediated DDSs, which provide increased stability, higher drug-encapsulation with a better loading efficiency and a lower leakage of drugs. Additionally, numerous polymers because of their flexible physicochemical and pharmacokinetic properties play an integral part in enhancing the pharmacokinetic nature of drugs, including the residence and release rate of the drugs (Iravani and Varma, 2022; Sharma, 2024; Shi et al., 2024).

The route of administration i.e. implants, and injectables/depots are routes feasible for overcoming the lack in pharmacokinetic properties i.e. first pass metabolism and poor bioavailability of drugs that are used in OUD treatment and opioid overdose but in certain emergency situations, they are not patient compliant. On the other hand, the intranasal and transdermal routes along with the polymeric systems are an attractive approach for systemic drug delivery in the treatment of medical emergencies and long-term treatment options including being more patient compliant. The intranasal route acts as a feasible alternative to other modes of administration but, on the other hand, may also have challenges including rapid mucociliary clearance rate, non-uniform drug deposition at the targeted absorption site and volume limitation are encountered during intranasal formulation development. With the incorporation of novel excipients and polymers, all the above-mentioned challenges can be

overcome and made available in clinical practices. In addition, with the availability of modified intranasal DDSs, the pharmacokinetic properties i.e. release, residence time and bioavailability profiles of the drugs can be improvised as well as enhanced patient compliance and adherence to treatment (Chen et al., 2024; Garg, 2024; Ghosh et al., 2024; Govender et al., 2023; Qianqian Huang et al., 2024; Karve et al., 2024).

2.4. Conclusions

In this review various DDSs have been described for the target delivery of drugs to treat OUD in this rapidly evolving field. The poor bioavailability, effects of first-pass metabolism, limited amounts of drug reaching the brain due to the BBB and a decreased residence time are some of the poor pharmacokinetic properties of the therapeutic moieties which are a barrier to effective treatment outcomes. The current research demonstrates that novel DDSs give a positive enhancement to these drugs pharmacokinetic properties with minimum side effects. However, when it comes to the pharmacokinetic and pharmacodynamic properties of the drugs along with patients' compliance there is still some room for improvement, which can be achieved by integrating the pharmacological advancements with novel pharmaceutical strategies and innovative ideas.

CHAPTER 3
THE DEDIGN OF SUSTAINED-RELEASE NALOXONE-LOADED SOLID LIPID NANOPARTICLES FOR THE TREATMENT OF OPIOID USE DISORDER

3.1 Introduction

The application of nanotechnology in both the therapeutic and diagnostic fields has emerged as a promising tool to improve the outcomes for many unaccommodating cardiovascular, cancerous, neurodegenerative and respiratory diseases and disorders (Kim et al., 2010; Omer et al., 2020). This is due to the relatively smaller volumes and higher surface area of nanosystems which have enabled it to provide reticuloendothelial system (RES) bypass and targeted delivery along with increased bioavailability of active pharmaceutical ingredients (APIs) at the site of action (Albanese et al., 2012; Alexis et al., 2008; Omer et al., 2020).

The BBB is responsible for protecting and maintaining homeostasis of the brain and is a significant barrier to the targeted delivery of majority of the APIs (Govender et al., 2023; Satapathy et al., 2021). Factors responsible for helping APIs cross the BBB include molecular weight (≤ 400 Dalton), size (nanometer range), morphology (spherical), ionization (physiological pH) and lipophilicity (Huang et al., 2024; Jeong et al., 2023; Satapathy et al., 2021). Therefore, the emergence of nanotechnology has played a significant role in delivering drugs across the BBB for several neuropathological conditions (Garg, 2024).

As per Herlinger et al., OUD is a chronic and relapsing disorder of the brain caused by the repeated exposure of exogenous opioids (Herlinger and Lingford-Hughes, 2022). NLX, an opioid antagonist primarily administered intravenously (IV), intramuscularly (IM), subcutaneously (SC) and intranasally (IN) is a breakthrough therapeutic agent in the treatment of OUD and opioid overdose (Tijani et al., 2022). NLX when administered IV provides an immediate mode of action within 2 minutes but has a rapid clearance rate and short plasma half-life of approximately 30-81 minutes (Gupta et al., 2016; Papich and Narayan, 2022). Furthermore, a study conducted by Hussain et al., evidenced that when NLX is administered IN it showed a 101% more bioavailability, when compared to IV administration (Hussain et al., 1984; Vitore et al., 2023). Thereby, with the incorporation of nanotechnology and alternation in delivery routes, the pharmacokinetic and pharmacodynamic properties of NLX can be enhanced.

Nanoencapsulation of APIs in envelopes of biodegradable polymer has become a well-established technology for sustained or controlled release drug delivery, which has been given marketing approval by the FDA (Benéitez et al., 2014; De Oliveira Junior et al., 2019). Polycaprolactone (PCL) is an example of such polymer and is a FDA approved non-toxic, hydrophobic aliphatic polyester which undergoes biodegradation by hydrolysis. PCL is available in different molecular weights; thus, providing diverse degradation rates resulting in varying release profiles (Dash and Konkimalla, 2012; Pawar et al., 2023). Specifically, the successful entrapment of numerous APIs such as anti-cancer drugs, anti-inflammatories, anti-infective agents, proteins and psychotropic agents in PCL-based nanotechnology has led to improved therapeutic efficacy of these APIs (Govender et al., 2015; Pawar et al., 2023). Thus, the incorporation of PCL in a NLX-loaded DDS has the potential to improve the pharmacokinetic properties of NLX.

SLNs introduced in 1991 have emerged as a carrier system that can deliver APIs across the BBB with a novel controlled or sustained drug delivery approach, target specificity, higher bioavailability, enhanced efficacy and reduced toxicity (Bukke et al., 2024; Schwarz et al., 1994; Yasir and Sara, 2014). The presence of a biocompatible lipid or modified lipid (triglycerides, fatty acids, or waxes) core helps in the encapsulation of both hydrophilic and lipophilic APIs and provides stability by prohibiting leakage and degradation (chemical, oxidative, and photochemical degradation) of APIs (Kaur et al., 2008; Mishra et al., 2018; Satapathy et al., 2021). Additionally, SLNs can bypass the RES and provide an easy and cost-effective scale up, as represented in Figure 3.1 (Pardridge, 2012; Reddy et al., 2014; Satapathy et al., 2021). This chapter provides for the design, synthesis and optimization of sustained-release NLX-loaded polymeric SLNs for the management of OUD with the aim of providing better therapeutic efficacy through reduced dosing frequency, reduced dosage strength and improved bioavailability. This system is envisioned to release NLX at the target site for a longer duration thereby improving therapeutic outcomes and patient compliance. Additionally provided in this chapter is a Box Behnken Design (BBD) experiment aided in optimizing the critical material attributes (CMA) and critical process parameters (CPP) mainly related to the material and process respectively, which were a part of the critical quality attributes (CQA) that are important for the performance of the NLX-loaded SLNs (Hasan et al., 2021). Thereafter, the optimized NLX-loaded SLNs were characterized for their physicochemical properties such as particle size, potential, PDI, surface morphology, %encapsulation, release profile, thermal behavior and lastly biocompatibility studies using the HEK293 cell line.

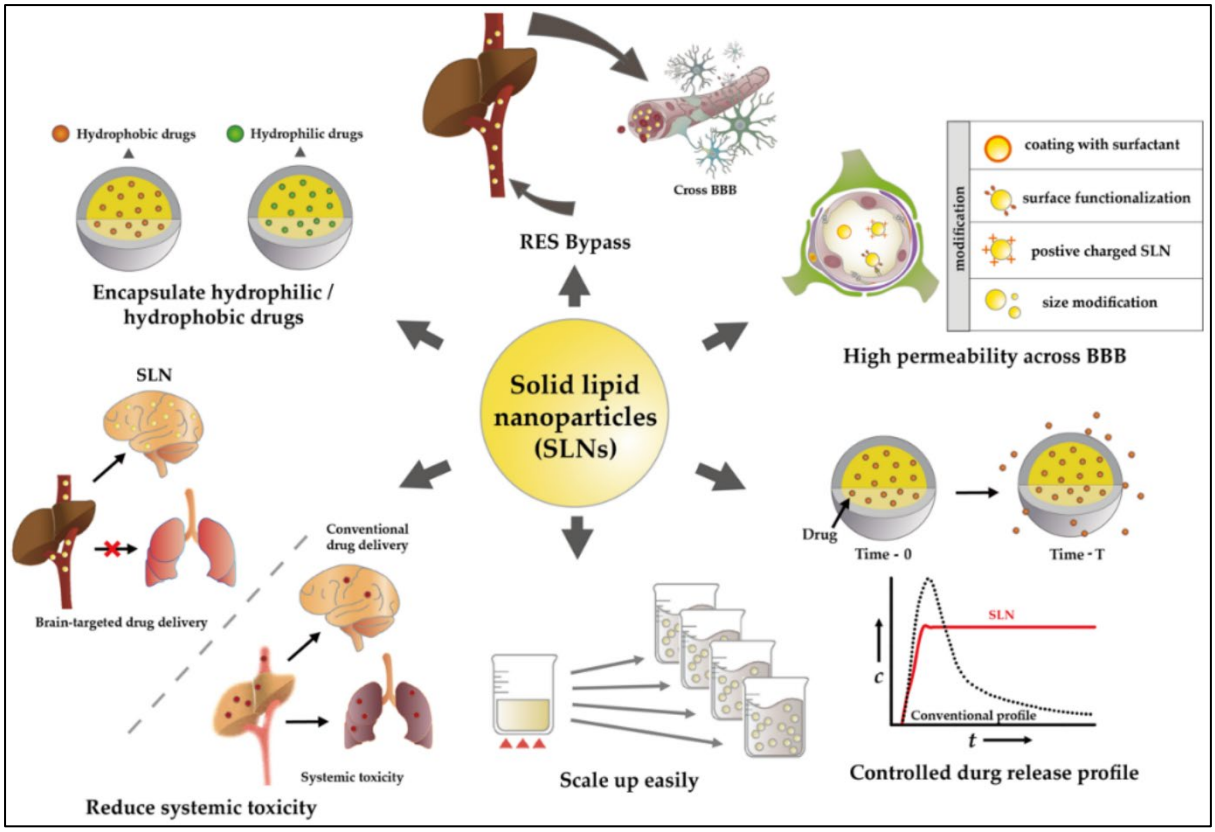

Figure 3.1. Representation of the several advantages offered by modified or polymeric SLNs such as compatibility in encapsulating both hydrophilic and hydrophobic drugs, bypassing the RES system, improving bioavailability across BBB, achieving the desired controlled drug release profile, possessing easy and cost-effective scale up properties and reducing systemic toxicity by enhancing target specificity (Reproduced with permission from Satapathy et al. (2021), © 2021 by the authors).

3.2 Materials and methods

3.2.1 Materials

Glyceryl Monostearate (GMS), Tween 80, Pluronic F-127 (Pf-127), polycaprolactone (Avg. Mw = 14 000) (PCL), dichloromethane (DCM), ethanol (99%), dimethyl sulfoxide (DMSO) and the (3-[4,5-dimethylthiazol-2-yl]-2,5 diphenyl tetrazolium bromide) (MTT) assay kit were purchased from Sigma-Aldrich (St. Louis, Missouri, USA), Naloxone hydrochloride dihydrate (NLX) from Leap Chem (Hangzhou, China), Dulbecco's Modified Eagle Medium (DMEM), Fetal Bovine Serum (FBS), penicillin-streptomycin (Pen-Strep) antibiotic solution and Dulbecco's phosphate-buffered saline (DPBS) from ThermoFisher Scientific (Randburg, South Africa) and Human embryonic kidney (HEK293) cells from American Type Culture Collection (ATCC, LGC-Standards, South Africa). All other chemicals were of analytical grade and used as received.

3.2.2 Preparation of the NLX-loaded SLNs

The NLX-loaded SLNs were formulated using the modified double emulsification technique as represented in Figure 3.2. Briefly, NLX was dissolved in ethanol using a bath sonicator (Beijing Ultrasonic Co., Ltd., Mainland, China) for 2 minutes at 40 °C, followed by the dissolution of PCL in DCM. The PCL solution was then added to the NLX solution under probe sonication (Sonics, Ultrasonic Processor, VCX130, Newtown, CT, USA), at 40% amplitude, 1.5 million joules and 1 minute, forming organic phase 1 (ORP1), with Pf-127 as a surfactant and tween 80 as co-surfactant added to water, forming the aqueous phase. ORP1 was then added to the aqueous phase under probe sonication (40% amplitude, 1.5 million joules and 8.5 minutes) to form emulsion 1 (EM1), with GMS dissolved in DCM to form organic phase 2 (ORP2). ORP2 was then added to EM1 and rotary evaporated (175 mbar, 30 minutes) to remove all the organic solvents and form EM2 containing the SLNs. The SLNs were thereafter separated from EM2 by centrifugation (Eppendorf AG, Barkhausenweg 1, 22339 Hamburg, Germany) at 10,000 RPM for 35 minutes at 4 °C, followed by the re-dispersion of the collected SLNs in Milli-Q distilled water (Merck Chemicals GmbH, Darmstadt, Germany). The SLNs were subsequently freeze dried using a lyophilizer (Labconco FreeZone 12 Console Freeze Dry, Kansas City, USA) for 17 hours to obtain dry SLNs powder.

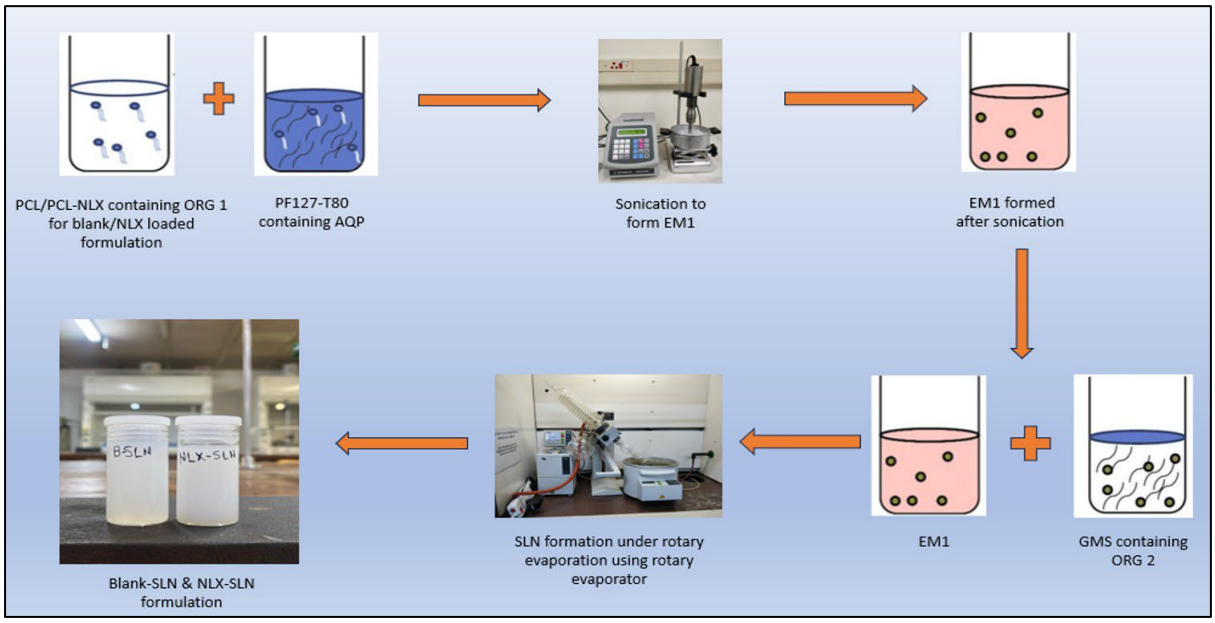

Figure 3.2. Representation of the preparation of unloaded and NLX-loaded SLNs using the modified double emulsification technique.

3.2.3 Statistical Optimization of the NLX-loaded SLNs

3.2.3.1 Construction of the BBD

A BBD (MINITAB®, V15, Minitab, USA) was used for the optimization of the formulated NLX-loaded SLNs as it allowed for quality predictions over a wide range of factors and is highly

time saving, as well as cost effective, and requires a smaller number of experimental trials to produce a higher order of response (Hasan et al., 2021). For the NLX-loaded SLNs, the independent variables were selected as: Lipid (GMS) concentration, Polymer (PCL) concentration and Surfactant/co-surfactant (Pf-127:Tween 80 = 5:1) concentration, whereas the dependent responses included particle size, entrapment efficacy and maximum drug release time.

3.2.3.2 Determination of BBD lower and upper limits of independent variables

Higher value (+1) and lower value (-1) of the independent variables were selected based on the particle size, zeta potential, PDI, entrapment efficiency (%EE) and maximum drug release during preliminary studies (Table 3.1) after which, the software automatically selected the middle value (0) and generated different combinations with the higher value (+1), middle value (0) and lower value (-1), as represented in Table 3.2. The ranges identified were based on the optimum size for the SLNs to cross the BBB ranges (between 40-200 nm), a zeta potential ranging between -15 to -30 mV for preventing the SLNs undergoing agglomeration, an entrapment efficiency of >70% for maximum NLX to reach the site of action and a maximum drug release for increased residence time along with a greater potential for patient compliance (Neves et al., 2015; Xinchen et al., 2023).

Table 3.1. The lower and upper limits of NLX-loaded SLNs independent variables are tabulated as Lipid (GMS) concentration, Polymer (PCL) concentration and Surfactant (Pf-127:Tween 80) concentration.

Factor	Coded level		
Independent variables	-1	0	+1
F1: Lipid concentration (GMS) (mg/mL)	4	7.5	11
F2: Polymer concentration (PCL) (mg/mL)	6	13	20
F3: Surfactant concentration (mg/mL)	5	12.5	20

Table 3.2. The 15- NLX-loaded SLNs formulations generated using the BBD.

Run	F1: GMS (mg/10mL)	F2: PCL (mg/5mL)	F3: Surfactant (mg/10mL)
1	110	100	125
2	75	65	125
3	110	65	200
4	40	65	200

5	110	30	125
6	75	30	200
7	110	65	50
8	75	65	125
9	75	30	50
10	75	100	50
11	40	65	50
12	40	30	125
13	75	65	125
14	75	100	200
15	40	100	125

3.2.3.3 Preparation of the BBD formulations

Using the modified double emulsification technique, as represented in 3.2.2, the formulations mentioned in Table 3.2 were formulated and analyzed for particle size, %EE and maximum drug release.

3.2.3.3.1 Determination of particle size for the generated BBD formulations

The dynamic light scattering (DLS) technique of the Zeta-Sizer Nano-ZS (Malvern Instruments, Malvern, UK) was used for the determination of particle size of the NLX-loaded SLNs at a set instrumental temperature of 25 ± 1 °C (n = 3). The freeze dried NLX-loaded SLNs were redispersed using Milli-Q distilled water prior to screening for their particle size ranging between 40-200 nm (Xinchen et al., 2023).

3.2.3.3.2 Determination of %EE for the generated BBD formulations

Prior to the evaluation of the %EE for the generated BBD formulations, a UV/Vis-spectrophotometer (Lambda 25, PerkinElmer, MA, USA) was used for the construction of a calibration curve i.e. a relation between concentration and absorbance of NLX (Figure 3.3) in phosphate buffer saline (PBS) solution. The lambda-max (λ-max) for NLX was confirmed at 280 nm by employing a full UV/Vis-spectrophotometry analysis, which falls in line with the findings by Hasan et al. (2021). Various concentrations of NLX i.e. 0 - 100 µg/mL were analyzed on the UV/Vis-spectrophotometer at 280 nm to obtain the absorbance values of the respective concentrations for the quantification of NLX.

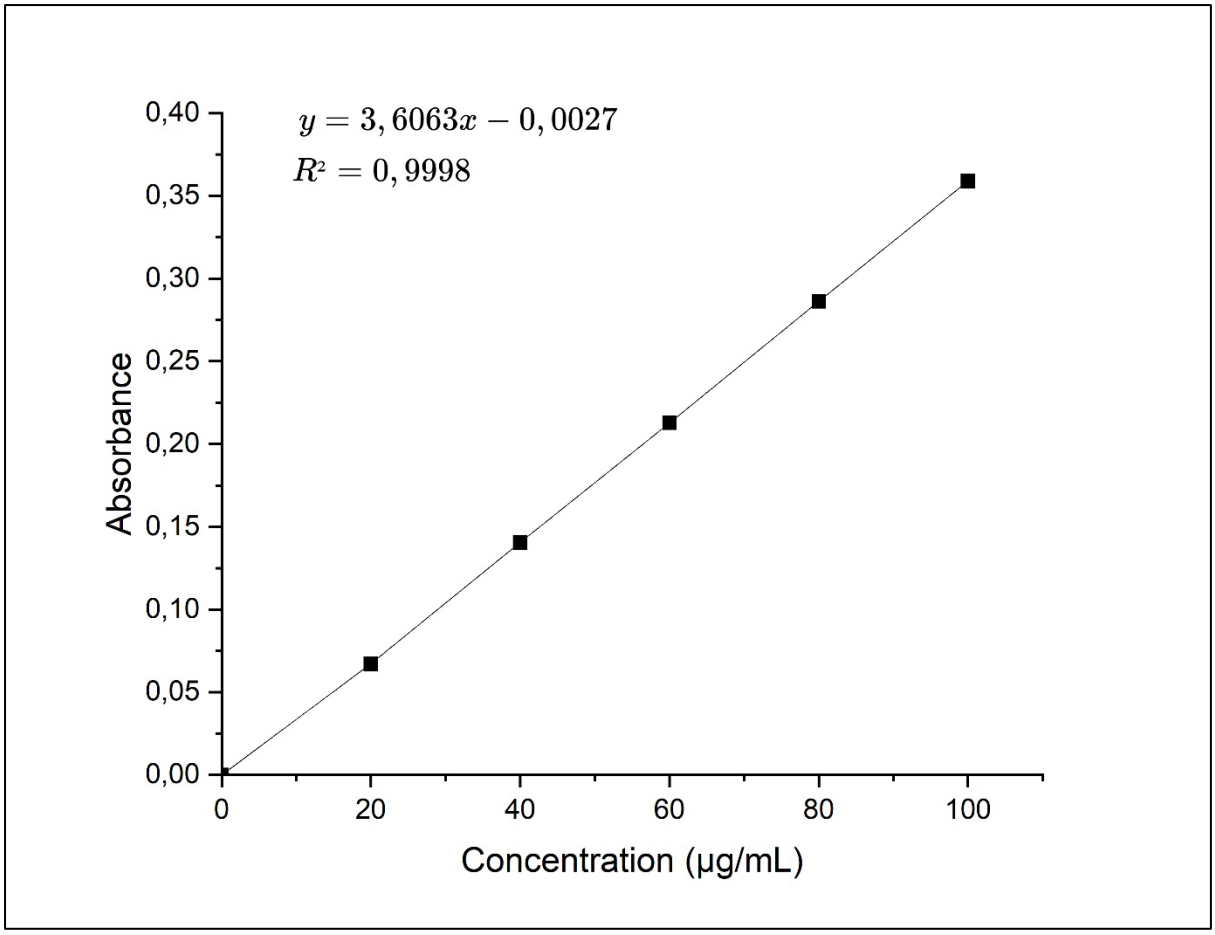

Figure 3.3. Representation of the calibration curve obtained for NLX.

The indirect method (n = 3) was used for the determination of %EE of NLX in the BBD NLX-loaded SLNs formulations as outlined by Joshi et al. (2012). The concentration of unentrapped NLX in aqueous phase of prepared NLX-loaded SLNs dispersion was calculated by separating the prepared NLX-loaded SLNs from the dispersion by ultracentrifugation. After centrifugation, the supernatant of the NLX-loaded SLNs dispersion was collected and the free NLX present in the supernatant was determined at 280 nm using the UV/Vis-spectrophotometer. The %EE was calculated using Equation 3.1:

$$\%EE = \frac{Initial\ drug\ (mg) - Free\ drug\ (mg)}{Initial\ drug\ (mg)} \times 100 \qquad \text{(Equation 3.1)}$$

Where, initial weight means the amount of NLX used to prepare the NLX-loaded SLNs and free drug means the amount of free NLX detected in the supernatant of NLX-loaded SLNs dispersion after centrifugation.

3.2.3.3.3 Determination of maximum drug release for the generated BBD formulations

Drug release studies (n = 3) on NLX-loaded SLNs was undertaken using the dialysis bag diffusion method as described by Onugwu et al. (2022). Briefly, NLX-loaded SLNs equivalent to 2.5 mg NLX was re-dispersed in 4 mL PBS (pH 7.2 - 7.4, simulating the pH of cerebrospinal fluid) solution and placed inside a dialysis membrane bag (molecular weight: 12,000 Dalton). The filled dialysis bag was then immersed into PBS (pH 7.2 - 7.4, 100 mL) solution and kept in an orbital shaker maintained at 25 rpm (37 ± 0.5 °C). Samples (3 mL) were withdrawn at predetermined time intervals i.e. 0, 1, 3, 6, 12, 24 hours followed by 2, 3, 4, 5, 6, 7, 8, 9, 10 days respectively, with 3 mL of freshly prepared PBS solution added to the release media after each sampling point to maintain sink conditions. The concentration of NLX released from the formulated NLX-loaded SLNs was thereafter calculated using the constructed calibration curve after analysis of the drug release samples at 280 nm using the UV/Vis spectrophotometer.

3.2.3.4 Optimization process of the dependent variables

Based on the BBD formulation results, the desired particle size, %EE and maximum drug release criteria were selected to optimize the SLNs for intranasal delivery of NLX which are represented in Table 3.3.

Table 3.3. The desired particle size, %EE and maximum drug release for the optimized NLX-loaded SLNs.

Dependent variables	Constraints
R1: Particle Size (nm)	150 nm
R2: EE (%)	Maximum
R3: Maximum Drug Release (days)	7 days

3.2.3.5 Characterization of the optimized NLX-loaded SLNs

3.2.3.5.1 Evaluation of the particle size, polydispersity index, zeta potential and surface morphology

The DLS technique of the Zeta-Sizer Nano-ZS as mentioned in 3.2.3.3.1 was used for the determination of particle size and polydispersity index (PDI) of the unloaded and NLX-loaded SLNs (n = 3). The zeta potential was determined using the Zeta-Sizer Nano-ZS instrument at a set temperature of 25 ± 1 °C. The SLNs were screened for particle size ranging between 40-200 nm, a PDI of ≤ 0.3 and a zeta potential of -15 to -30 mV (Xinchen et al., 2023). The particle shape and surface morphology of the formulated unloaded and NLX-loaded SLNs were further determined using a Scanning Electron Microscope (SEM) (Zeiss, Jena,

Germany). For the analysis, both the freeze-dried unloaded and NLX-loaded SLNs were redispersed using the Milli-Q distilled water followed by placing droplets of both the SLNs dispersion on individual aluminum stubs and allowing to dry overnight. Prior to capturing the SEM images for surface morphology, both SLNs were double-coated with gold-palladium (Ag-Pd) under vacuum using a sputter coater in order to induce induction.

3.2.3.5.2 Determination of the %EE and loading capacity

The indirect method (n = 3) as mentioned in 3.2.3.3.2 was used for the determination of %EE and loading capacity (%LC) of NLX in the optimized NLX-loaded SLNs formulation. The %EE and %LC were calculated using Equations 3.1 and 3.2 respectively.

$$\%LC = \frac{Initial\ drug\ (mg) - Free\ drug\ (mg)}{Nanoparticles\ weight\ (mg)} \times 100 \qquad \text{(Equation 3.2)}$$

Where, nanoparticles weight is the weight of NLX-loaded SLNs obtained after freeze drying.

3.2.3.5.3 *In vitro* drug release of the formulated SLNs

In vitro drug release studies (n = 3) on the optimized NLX-loaded SLNs was undertaken using the dialysis bag diffusion method as mentioned in 3.2.3.3.3. Additionally, several kinetic models such as Zero order, First order, Higuchi, Korsmeyer-Peppas and Hixson-Crowel models were employed to analyze the NLX release kinetic pattern from the optimized NLX-loaded SLNs using the DDSolver (Version 1.0) software.

3.2.3.5.4 Molecular structure assessment

All the starting materials used for formulating the SLNs including for both the freeze-dried unloaded and NLX-loaded SLNs were analyzed for the molecular transitions and interactions using a PerkinElmer ATR-FTIR (Spectrum 2000, Waltham, MA, USA) fitted with a single reflection diamond MIRTGS detector. A constant pressure of 110 psi, wavelength range of 4000-650 cm^{-1} and a resolution of 4 cm^{-1} were used to obtain the FTIR spectra.

3.2.3.5.5 Determination of thermal characteristics

All starting materials used for formulating the SLNs including for both the freeze-dried unloaded and NLX-loaded SLNs were analyzed for their thermal properties using a Differential Scanning Calorimeter (DSC) (Mettler Toledo DSC, STARe system, Schwerzenback, Switzerland). For the analysis, approx. 3 - 8 mg of solid/lyophilized samples are weighed into the aluminum crucibles and sealed. While sealing the crucible a small hole was pierced using a needle for the dissipation of pressure. An inert atmosphere was thereafter created in the

DSC using nitrogen gas i.e. 20 mL/minute with the samples heated over a range of 0-400 °C at a rate of 5 °C/minute. Evaluation of the thermally induced phase transitions of the samples involved plotting of thermograms as a function of heat flow against temperature.

3.2.3.5.6 Determination of the SLNs degradation rate

The thermal degradation temperatures of all the starting materials used for formulating the SLNs including for both the freeze-dried unloaded and NLX-loaded SLNs were determined using a Thermogravimetric Analyzer (TGA) (PerkinElmer, TGA 4000, Llantrisant, Wales, UK). The analysis process used included an inert atmosphere being created in the TGA using nitrogen gas i.e. 20 mL/minute, with the samples heated over a range of 30-600 °C at a rate of 5 °C/minute. Thermograms were plotted as percentage weight against temperature for analyzing the thermal degradation of the samples.

3.2.4 Cell culture and cytotoxicity studies

3.2.4.1 Cell culture

The HEK293 cells used for the cytotoxicity studies were maintained in a supplemented medium consisting of DMEM, 10% heat-inactivated FBS and 1% Pen-Strep antibiotic solution, with all cultures seeded into flasks containing supplemented medium and maintained at 37 °C in a humidified atmosphere of 5% CO_2 and 95% air. For the assays, HEK293 cells were sub-cultured in 96-well plates at a seeding density of 1 x 10^4 cells per well (90 µL). The treatments, i.e. NLX, unloaded SLNs and NLX-loaded SLNs were thereafter prepared in serial dilutions using DPBS.

3.2.4.2 Cytotoxicity studies using MTT assay kit

Cell viability, through the determination of mitochondrial activity of living cells, was measured by quantitative colorimetric assay (n = 3) using MTT. Briefly, 10 µL of the MTT labelling reagent was added to each well of the treated cell culture and incubated at 37 °C with 5% CO_2 and 95% air for a period of 4 hours where, metabolically active cells convert the yellow MTT tetrazolium crystals to a purple formazan crystal. Thereafter, 90 µL of solubilizing buffer reagent was added to each well and incubated overnight for further dissolution of formazan crystals. The supplemented media containing untreated seeded cells were used as positive control with DMSO treated cells serving as the negative control. A multimodal micro plate reader (Victor X3, manufactured by Perkin Elmer in Waltham, MA, USA) at 570 nm was used to quantify the absorbance values of the treated plates, with all samples evaluated in triplicate. Using the absorbance values obtained, the relative cell viability was calculated using Equation 3.3.

$$Percentage\ Cell\ Viability = \frac{\frac{Absorbance\ value\ of\ sample\ or\ treated\ cells}{Absorbance\ value\ of\ control\ or\ untreated\ cells}}{} \times 100 \qquad \text{(Equation 3.3)}$$

3.2.5 Statistical analysis

All the above-mentioned analyses were conducted in triplicate (n = 3) with Microsoft Excel used to express the mean and standard deviation of the obtained results. *p*-values of less than 0.05 ($p < 0.05$) were considered as an indication of statistically significant differences. OriginPro 2025 was used for the graphical representation of all results obtained.

3.3 Results and discussion

3.3.1 Statistical optimization using BBD

3.3.1.1 Determination of the lower and upper limits of the independent variable

The preliminary concentrations of GMS and Surfactant were taken into consideration as reported by Hasan et al. and the concentrations of PCL as reported by Omer et al (Hasan et al., 2021; Omer et al., 2020). From the results obtained by formulating the preliminary formulations, as mentioned in Table 3.4, the lower and upper limits of the independent variables were selected.

From the preliminary analysis of the results obtained, it was determined that when GMS concentration was below 4 mg/mL the particle size, PDI and zeta potential were not within the desired target. Similarly, the concentrations above 11 mg/mL the PDI, zeta potential and %EE were not within the desired range. Thus, concluding the lower and upper limits of GMS to be 4 and 11 mg/mL, respectively, as the concentration of GMS affected the PDI, zeta potential and %EE of the SLNs. In the case of the Surfactant, the concentrations below 5 mg/mL and above 20 mg/mL affected the particle size as the SLNs were not close to the target range. Thus, the lower and upper limits of Surfactant were selected as 5 and 20 mg/mL, respectively. PCL, similarly, had a major effect on the release profile of NLX from the NLX-loaded SLNs. The lower and upper limits of PCL were selected to be 6 and 20 mg/mL respectively, as the release profile for combinations below 6 mg/mL and above 20 mg/mL were not within the target range.

Table 3.4. Preliminary formulations determining the lower and upper limits of the independent variable for NLX-loaded SLN (n = 3).

	Independent Variables			Dependent Variables/Responses				
RUN	**GMS (mg/10mL)**	**PCL (mg/5mL)**	**Surfactant (mg/10mL)**	**Particle Size**	**PDI**	**Zeta Potential**	**%EE**	**Maximum Drug Release**
1	60	50	110	169.3 ± 4.87	0.192 ± 0.007	-17.2 ± 0.82	42.1 ± 0.62	5
2	40	50	110	170.4 ± 2.82	0.167 ± 0.005	-14.2 ± 1.11	48 ± 1.38	5
3	20	50	110	201.3 ± 3.49	0.276 ± 0.007	-10.1 ± 1.00	49 ± 1.11	5
4	110	50	110	97.4 ± 1.88	0.350 ± 0.006	-29.4 ± 0.65	34 ± 1.35	5
5	130	50	110	104.8 ± 2.15	0.391 ± 0.004	-35.33 ± 0.94	33 ± 1.60	6
6	60	30	110	138.2 ± 1.76	0.211 ± 0.005	-15.57 ± 1.16	41 ± 1.21	3
7	60	20	110	124.8 ± 1.76	0.244 ± 0.008	-11 ± 0.6	42 ± 0.91	2
8	60	100	110	170.1 ± 1.75	0.291 ± 0.006	-19.27 ± 0.74	40 ± 0.79	9
9	60	120	110	190.2 ± 2.06	0.365 ± 0.009	-20 ± 0.4	42 ± 1.56	10
10	60	50	50	109.2 ± 1.3	0.180 ± 0.006	-17.27 ± 1.12	55 ± 0.4	5
11	60	50	30	75.8 ± 2.12	0.172 ± 0.005	-18.1 ± 0.75	57 ± 0.49	5
12	60	50	200	199.2	0.264	-18.87	58	5

				± 3.47	± 0.006	± 0.91	± 0.58	
13	60	50	220	265.1 ± 3.37	0.283 ± 0.007	-18.17 ± 1.06	57 ± 1.06	5

3.3.1.2 Formulation optimization using BBD strategy

With the incorporation of the lower and upper limits of independent variables into the BBD software, a total of 15 experimental runs were generated for the determination of effects of the varying concentrations of lipids, polymers and surfactants on particle size, %EE and maximum drug release. Therefore, these generated runs (Table 3.5) were formulated and analyzed in triplicate.

Table 3.5. Summary of the responses observed from the formulations generated by the BBD for the optimization of the NLX-loaded SLNs (n = 3).

Run	R1: Particle Size (nm)	R2: EE (%)	R3: Maximum Drug Release (Days)
1	107,1 ± 3.22	36.00 ± 1.32	9
2	118.7 ± 2.97	35.24 ± 1.36	7
3	108.9 ± 2.23	68.96 ± 1.93	7
4	142.2 ± 2.28	33.97 ± 1.4	7
5	156.7 ± 5.64	58.00 ± 1.99	5
6	111.5 ± 1.65	44.19 ± 1.35	6
7	105.1 ± 2.16	39.32 ± 2.43	7
8	116.0 ± 2.35	33.43 ± 2.27	7
9	110.2 ± 1.13	62.85 ± 1.89	6
10	88.94 ± 2.54	60.59 ± 1.84	8
11	106.9 ± 1.9	78.73 ± 1.16	7
12	151.9 ± 1.21	59.09 ± 1.28	6
13	128.4 ± 1.47	30.16 ± 1.78	7
14	123.9 ± 2.86	28.13 ± 2.11	9
15	234.2 ± 0.69	60.74 ± 1.49	8

3.3.1.2.1 Effect of independent variables on dependent variable particle size

The particle size ranging between 40-200 nm for nanocarriers is considered to be the optimum size for crossing the BBB, especially for nose-to-brain DDSs (Xinchen et al., 2023). The Equation 3.4 obtained from the BBD for particle size showed both positive and negative effects of independent variables on dependent variables which are graphically represented in Figure

3.4. Additionally, the R^2 and R^2 (adj) had a difference of 12.9% (0.12) which is less than 20% (0.2) indicating that the adopted model was significant (Takalani et al., 2024).

$$Particle\ size = +96.4073 - 1.38639\ GMS - 0{,}134184\ PCL + 1{,}46595\ Surfactant + 0{,}0196939\ GMS * GMS + 0{,}0141837\ PCL * PCL - 0{,}00526667\ Sufactant * Surfactant - 0{,}0269388\ GMS * PCL - 0{,}00304762\ GMS * Surfactant + 0{,}00314286\ PCL * Surfactant \quad \text{(Equation 3.4)}$$

The negative values of GMS (-1.38639), PCL (-0.134184) and interaction between GMS*PCL (-0.0269388) showed the negative effect on particle size. The higher value of coefficient variable of Surfactant (+1.46595) as compared to GMS and PCL, showed that Surfactant had a more prominent and positive effect on particle size. Initially, with the increase in Surfactant concentration, particle size increased but after reaching a certain concentration, the size started decreasing which can be observed from the contour plots represented in Figure 3.4. Resultantly, the particle sizes ranged from 88.94 to 234.2 nm for the 15 formulations obtained from the BBD which is represented in Figure 3.5.

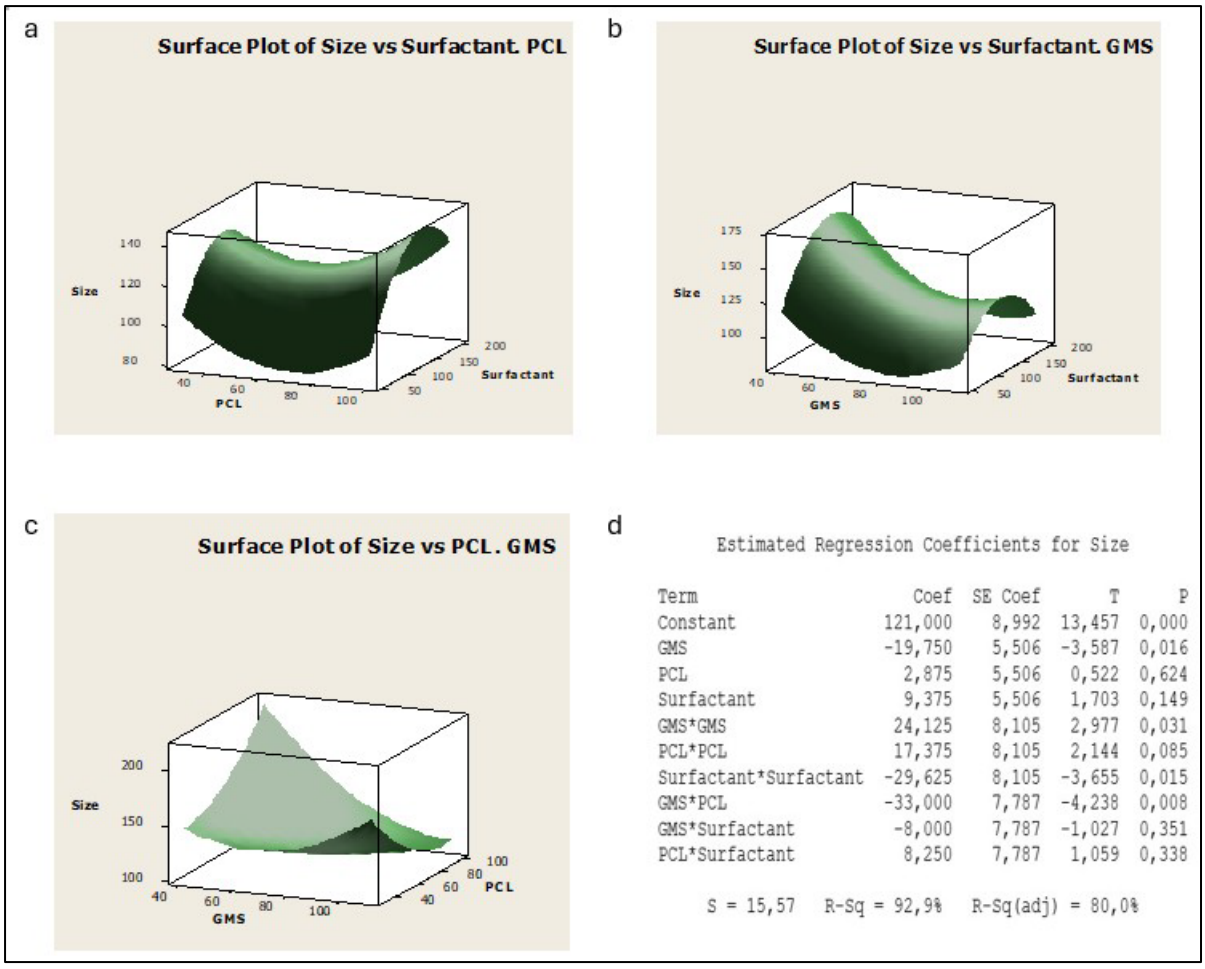

Figure 3.4. Effect of independent variables i.e. GMS, PCL and Surfactant on dependent

variable i.e. particle size represented in (a), (b) and (c) whereas the estimated regression coefficients for particle size is represented in (d).

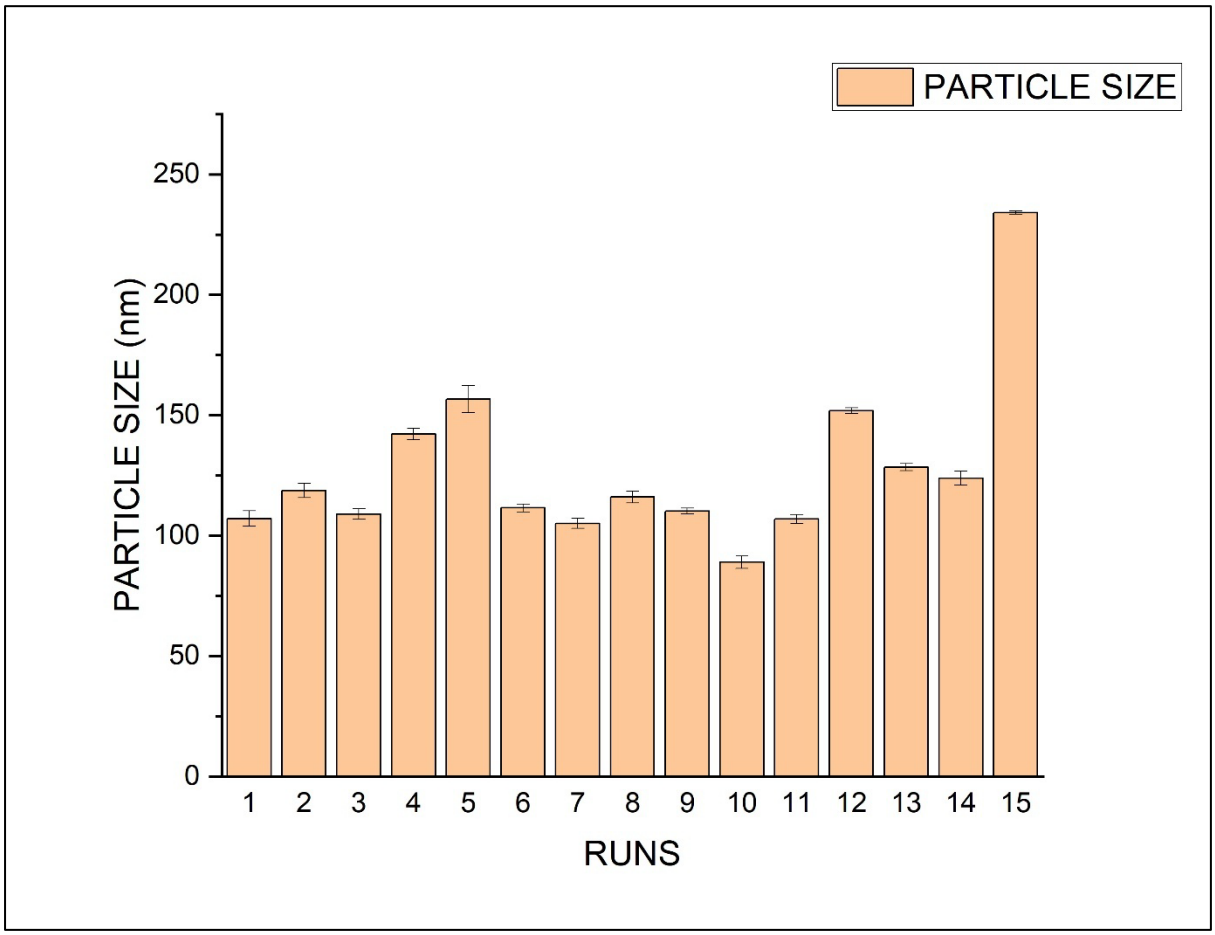

Figure 3.5. Representation of various particle sizes obtained from the BBD formulations (n = 3).

3.3.1.2.2 Effect of independent variables on dependent variable %EE

The maximum %EE of NLX nanocarriers is considered optimum as the maximum amount of NLX concentration is required at the site of action for therapeutic efficacy. Equation 3.5 obtained from the BBD for %EE showed both positive and negative effects of the independent variables on the dependent variables, which are graphically represented in Figure 3.6. Additionally, the R^2 and R^2 (adj) had a difference of 11.5% (0.115) which is less than 20% (0.2) indicating that the adopted model was significant (Takalani et al., 2024).

$$\%EE = +207{,}987 - 2{,}34320\,GMS - 0{,}362245\,PCL - 0{,}962646\,Surfactant + 0{,}0111565\,GMS * GMS + 0{,}00585034\,PCL * PCL + 0{,}00162963\,Surfactant * Surfactant - 0{,}00489796\,GMS * PCL + 0{,}00704762\,GMS * Surfactant - 0{,}00133333\,PCL * Surfactant \quad \text{(Equation 3.5)}$$

The negative values of GMS (-2.34320), PCL (-0.362245) and Surfactant (-0.962646) showed negative effect on %EE indicating lower the concentrations of independent variables higher will be the %EE. As GMS has a higher coefficient variable compared to PCL and Surfactant, it has more prominent effect. Additionally, from the contour plots observed in Figure 3.6, it can be stated that with the decreasing concentration of GMS, the %EE of NLX-loaded SLNs can be increased. Therefore, %EE ranged between 28.13 to 78.73% for the 15 formulations obtained from the BBD, which is represented in Figure 3.7.

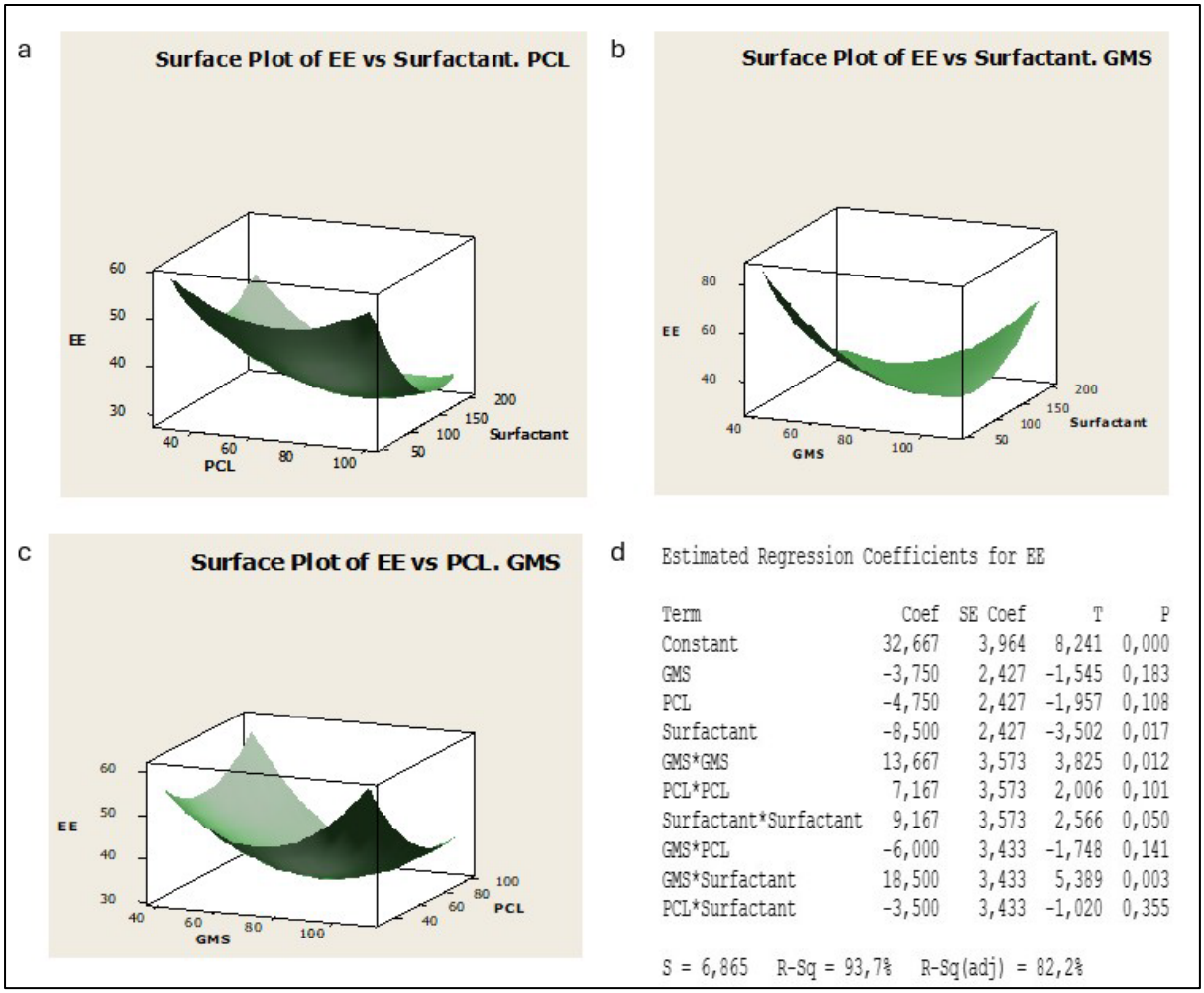

Figure 3.6. Effect of independent variables i.e. GMS, PCL and Surfactant on dependent variable i.e. %EE represented in (a), (b) and (c) whereas the estimated regression coefficients for %EE is represented in (d).

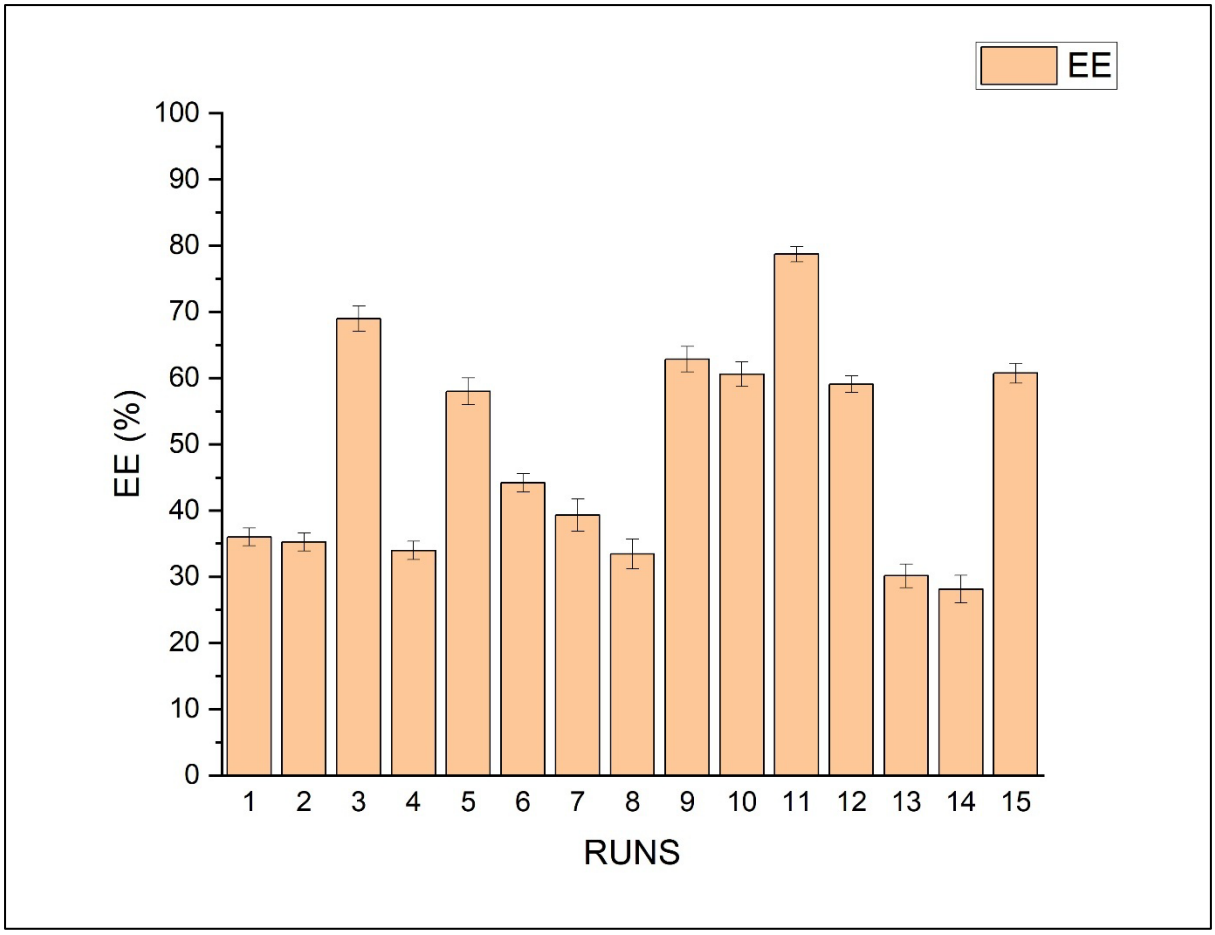

Figure 3.7. Representation of various %EE obtained from the BBD formulations (n = 3).

3.3.1.2.3 Effect of independent variables on dependent variable drug release

The prolonged drug release of NLX is considered optimum in this NLX-loaded SLNs system as prolonged release of NLX at the site of action would help to overcome the rapid clearance rate and short half-life of NLX, thus giving maximum therapeutic efficacy. Equation 3.6 obtained from the BBD for drug release showed both positive and negative effects of independent variables on dependent variables, which are graphically represented in Figure 3.8. Additionally, the R^2 and R^2 (adj) had a difference of 2.6% (0.026) which is less than 20% (0.2), indicating that the adopted model was significant (Takalani et al., 2024).

$$Drug\ Release = +7{,}20607 - 0{,}0112245\ GMS - 0{,}0164966\ PCL - 0{,}0100794\ Surfactant - 1{,}02041E-04\ GMS * GMS + 0{,}000102041\ PCL * PCL + 2{,}22222E-05\ Surfactant * Surfactant + 0{,}000408163\ GMS * PCL + 8{,}53954E-20\ GMS * Surfactant + 9{,}52381E-05\ PCL * Surfactant \quad \text{(Equation 3.6)}$$

PCL (-0.0164966) has the higher coefficient variable as compared to GMS (-0.0112245) and Surfactant (-0.0100794) indicating that PCL has more prominent effect. The negative value of PCL indicates a negative effect but the interactions between PCL*PCL (+0.000102041),

PCL*GMS (+0.000408163) and PCL*Surfactant (+9.52381E-05) are all positive, indicating with the increase in PCL concentration, a prolonged drug release is observed. Additionally, from the contour plots observed in Figure 3.8, it can be stated that with the increasing concentration of PCL, the prolonged release of NLX from NLX-loaded SLNs can be obtained. Therefore, drug release ranged between 5 to 9 days for the 15 formulations obtained from the BBD, which is represented in Figure 3.9.

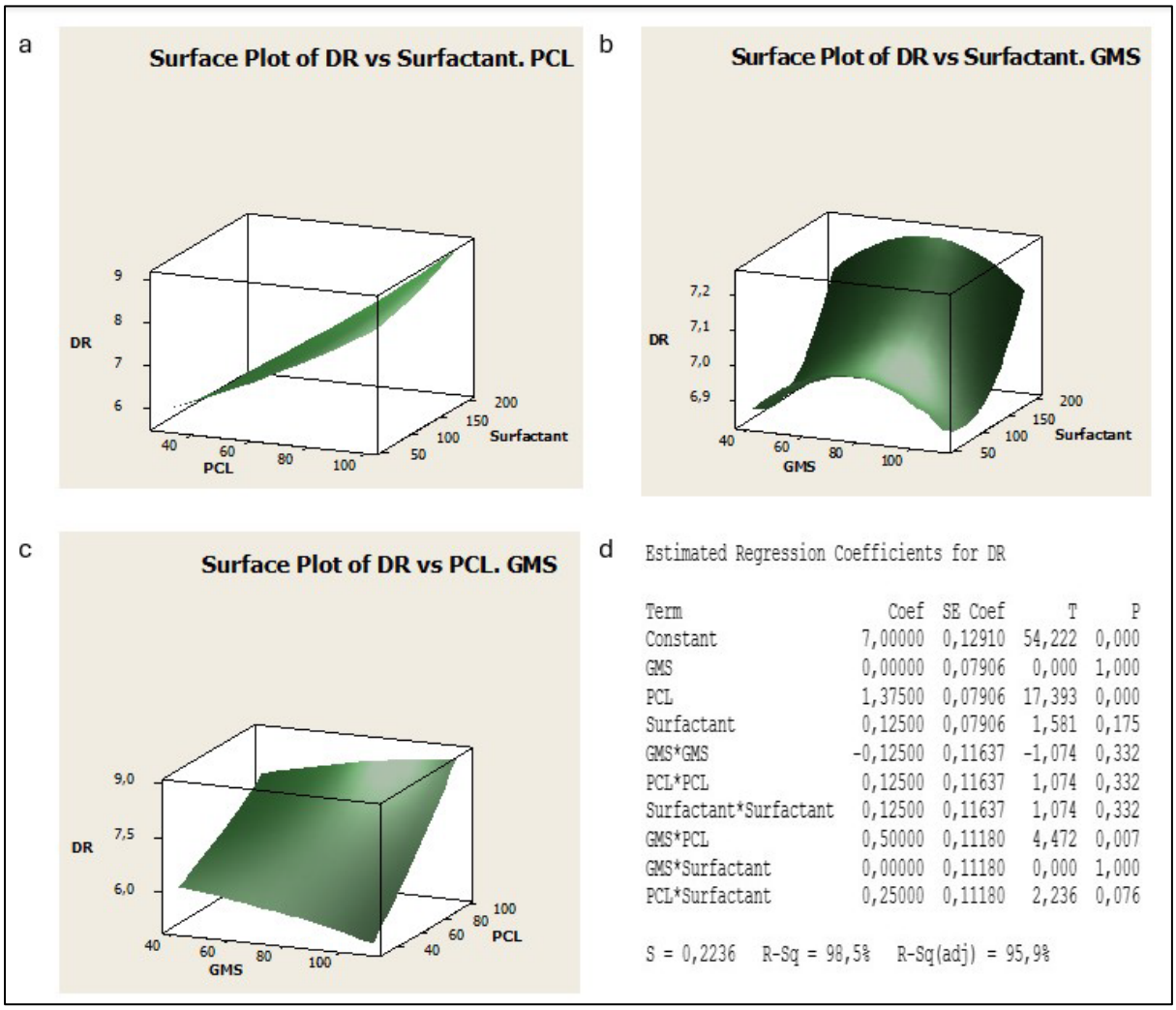

Figure 3.8. Effect of independent variables i.e. GMS, PCL and Surfactant on dependent variable i.e. drug release represented in (a), (b) and (c) whereas the estimated regression coefficients for drug release is represented in (d).

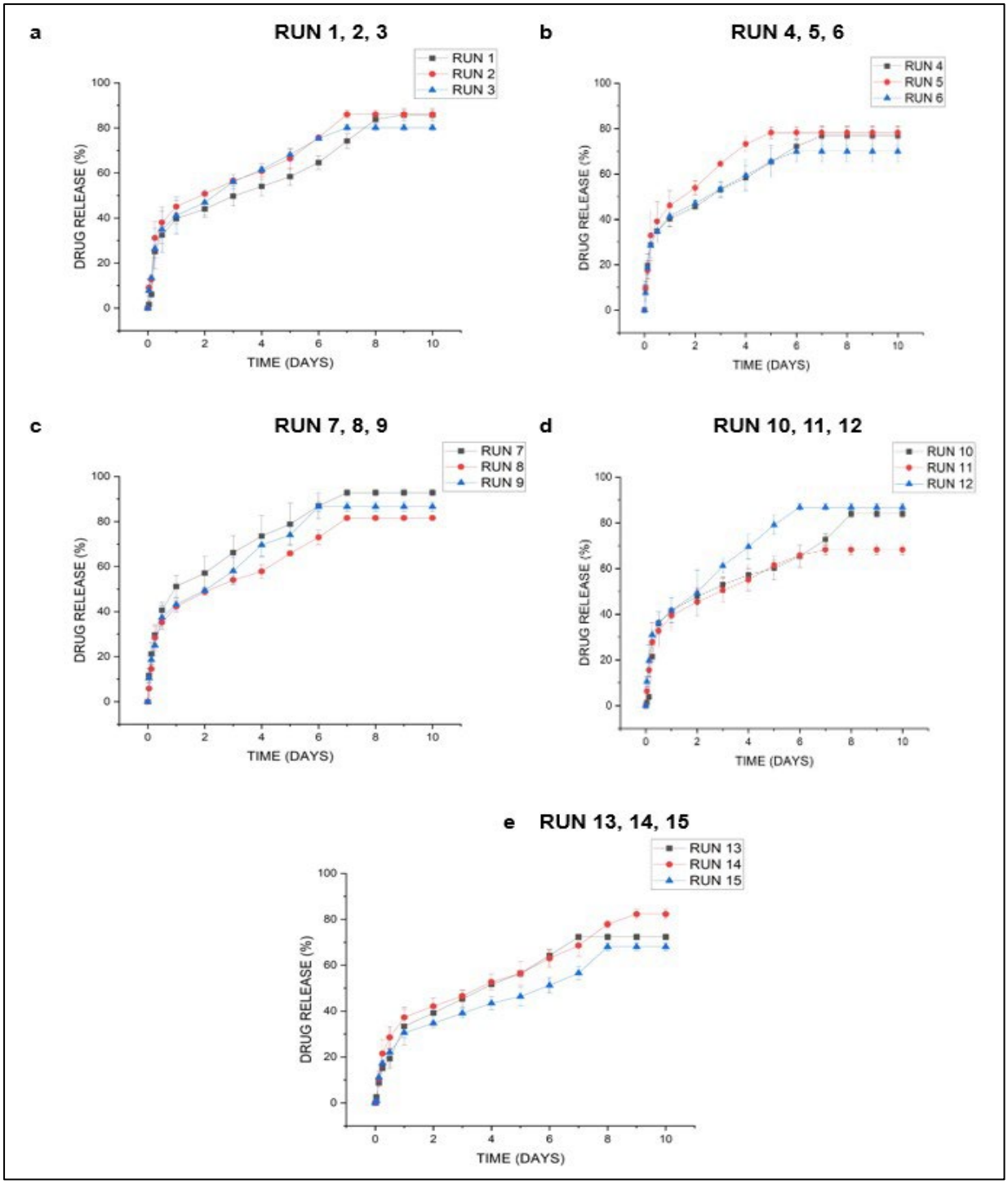

Figure 3.9. Representation of the cumulative *in vitro* drug release profiles of the formulations obtained from the BBD (n = 3).

3.3.2 Generation of the optimized NLX-loaded SLNs formulation

Using the master formula (Figure 3.10) obtained from the BBD, the NLX-loaded SLNs were prepared using the modified double emulsification technique, as provided in 3.2.2. NLX (4 mg) was dissolved in ethanol (5 mL) using the bath sonicator followed by the dissolution of PCL (72.5 mg) in DCM (5 mL). The PCL solution was then added to the NLX solution under probe

sonication to form ORP1. Pf-127 (76.4 mg) as surfactant and tween 80 (15.3 µL) as co-surfactant i.e. 5:1 was thereafter added to water (10 mL), forming the aqueous phase. ORP1 was subsequently added to the aqueous phase under probe sonication to form EM1. GMS (40 mg) was then dissolved in DCM (10 mL) to form ORP2. ORP2 was thereafter added to EM1 and rotary evaporated to remove all the organic solvents and form EM2 containing the SLNs. The SLNs were then separated from EM2 by centrifugation followed by the re-dispersion of the collected SLNs in Milli-Q distilled water (10 mL) and freeze drying to obtain dry SLNs powder. In Table 3.6, a comparison between the predicted and experimental values of particle size, %EE and maximum drug release are represented for the optimized NLX-loaded SLNs.

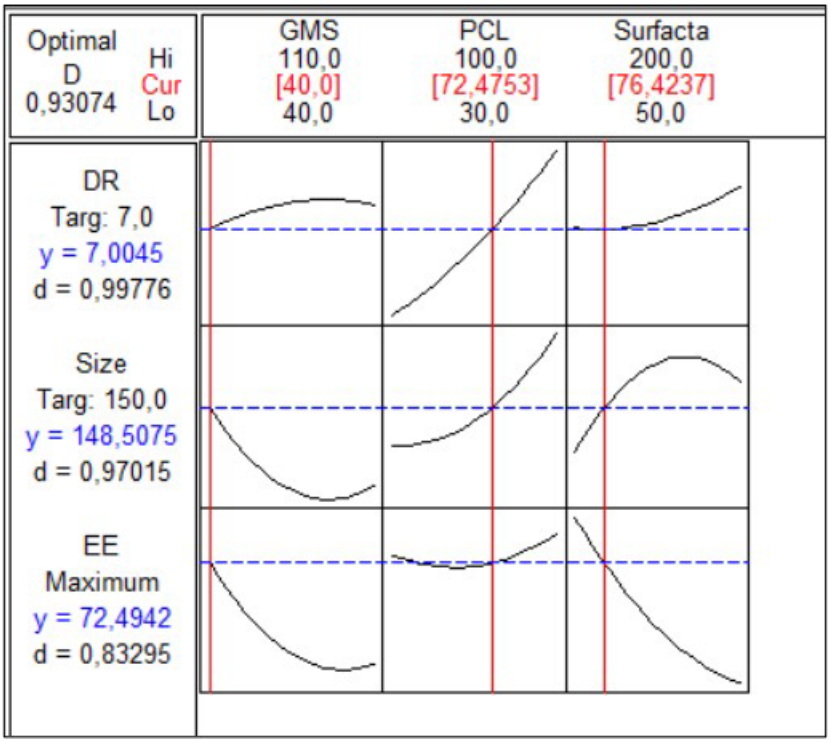

Figure 3.10. Representation of the master formula obtained for the preparation of optimized NLX-loaded SLNs with desired values of dependent variables using BBD.

Table 3.6. Predicted, experimental and desirability values of particle size, %EE and maximum drug release of NLX-loaded SLNs.

Dependent Variables	Predicted Values	Experimental Values	Desirability Values
Particle Size (nm)	148.5	142.2 ± 2.46	95.75%
EE (%)	72.49	78.7 ± 1.17	91.44%
Maximum Drug Release (Days)	7	7 ± 0	100%

3.3.3 Characterization of the optimized NLX-loaded SLNs

3.3.3.1 Evaluation of the particle size, PDI, zeta potential and surface morphology

As per the results obtained in the study conducted by Bazargani et al., SLNs within the range of 40-200 nm are preferable for easy bypass across the BBB (Bazargani et al., 2025). The mean particle size (Figure 3.11. a and c) of the unloaded and NLX-loaded SLNs were found to be 141.6 ± 6.42 and 142.2 ± 2.46 nm, respectively, suggesting that the SLNs could easily cross the BBB as they were within the acceptable range. The PDI (Figure 3.11. a and c) of the unloaded and NLX-loaded SLNs were found to be 0.210 ± 0.04 and 0.112 ± 0.02, respectively. The lower values of PDI ≤ 0.3 suggest the uniform distribution of the SLNs across the dispersion (Danaei et al., 2018). The zeta potential (Figure 3.11. b and d) of the unloaded and NLX-loaded SLNs were found to be -19.2 ± 3.74 and -18.2 ± 1.85 mV suggesting that the SLNs are stable and less prone to form aggregates (Pandya et al., 2018). The results obtained from the Zeta-Sizer Nano-ZS instrument were further verified by SEM for particle size and surface morphology. The unloaded and NLX-loaded SLNs were found to be under 200 nm and with a spherical shape when observed using the SEM, as represented in Figure 3.12 (a) and (c) which were found to be similar with the results obtained by Yasir et al. (2021). A comparison between Figure 3.12 (a) and (b) and Figure 3.12 (c) and (d), indicated that the in-lens images of both the unloaded and NLX-loaded SLNs i.e. Figure 3.12 (b) and (d) showed the inner polymer matrix being surrounded by the solid lipid layer i.e. GMS. Additionally, Figure 3.12 (c) showed no crystals of NLX being present in the surrounding or on the surface of the imaged NLX-loaded SLNs, indicating the complete encapsulation of NLX and suggesting no burst release of NLX would occur, which was displayed in a similar study conducted by Naik et al. (2024).

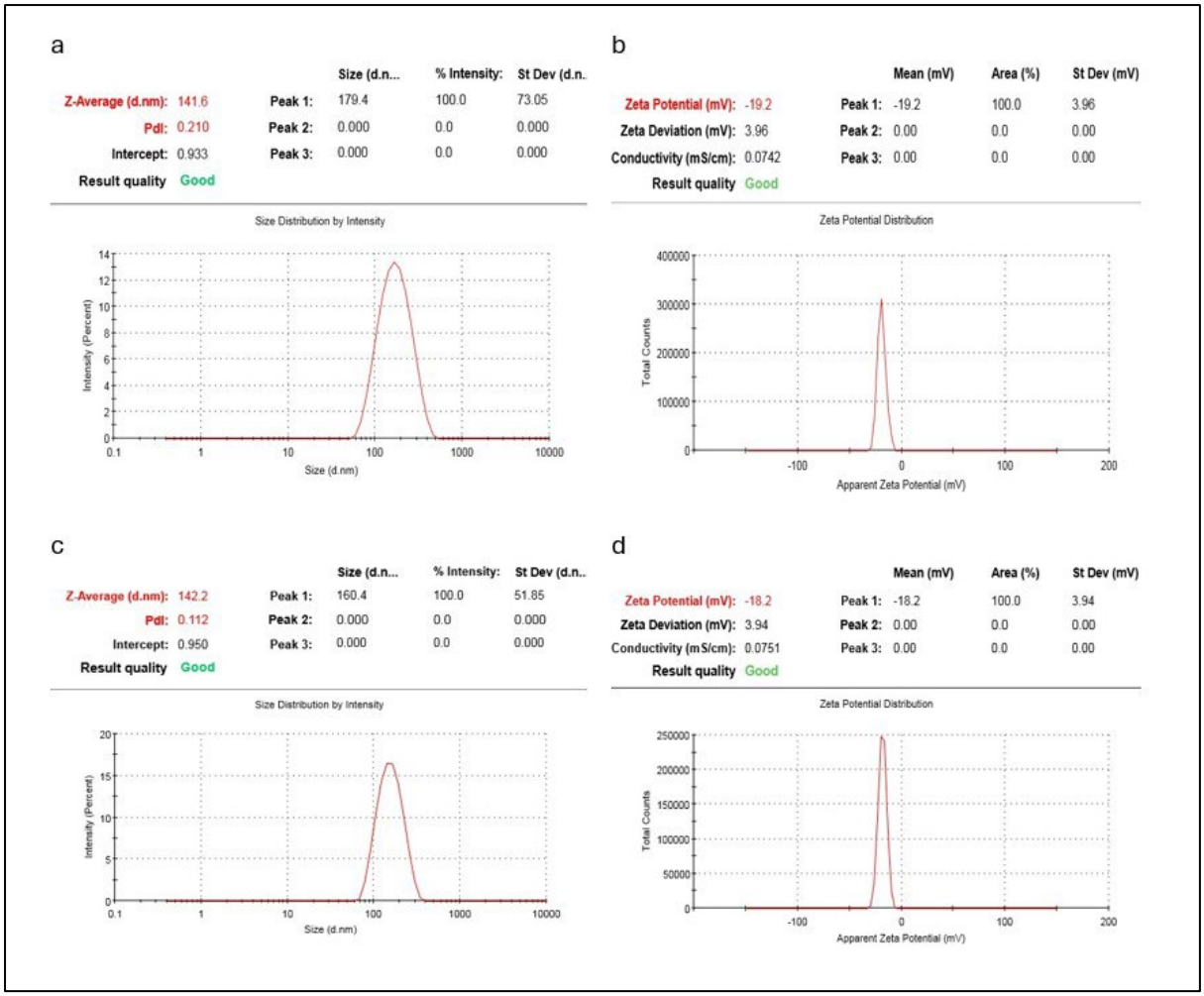

Figure 3.11. Profiles of (a) the particle size and PDI of the unloaded SLNs, (b) the zeta potential of the unloaded SLNs, (c) the particle size and PDI of the optimized NLX-loaded SLNs and (d) the zeta potential of the optimized NLX-loaded SLNs.

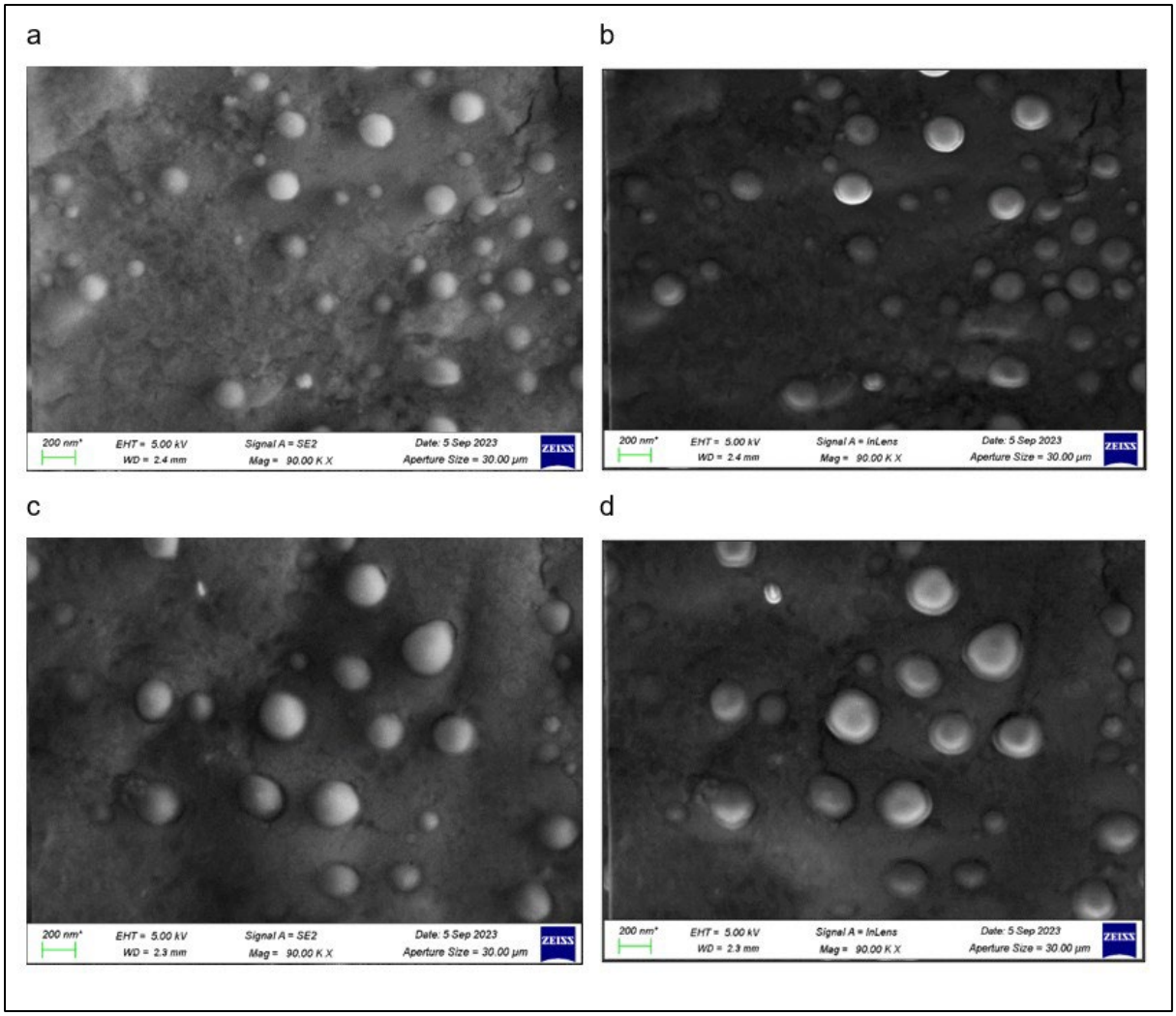

Figure 3.12. SEM micrographs of (a) the secondary lens imaging of the unloaded SLNs, (b) the in-lens imaging of the unloaded SLNs, (c) the secondary lens imaging of the optimized NLX-loaded SLNs and (d) the in-lens imaging of the optimized NLX-loaded SLNs.

3.3.3.2 Determination of %LC and %EE

The %LC and %EE of the optimized NLX-loaded SLNs were found to be 3.5 ± 0.13% and 78.7 ± 1.17%, respectively, representing a stable PCL and Surfactant polymer matrix within the GMS-coated SLNs to encapsulate higher percentage of NLX.

3.3.3.3 *In vitro* drug release of the NLX-loaded SLNs

In vitro drug release studies (n = 3) were conducted to determine the release profile of NLX from the optimized NLX-loaded SLNs. Approximately 50% of NLX was released from the NLX-loaded SLNs by the end of 2 days (48 hours) and the remaining 50% NLX was released over a period of the next 5 days (120 hours) indicating a release profile of NLX from NLX-loaded SLNs over a period of 7 days (168 hours), as represented in Figure 3.13. With the achievement of this release profile of NLX, it can be confirmed that the residence time of NLX at the site of action may be increased with the incorporation of NLX in the polymeric SLNs. Additionally, the

co-efficient of correlation (R^2) values were found to be 0.6979, 0.8933, 0.9724, 0.9883 and 0.8593 for Zero order, First order, Higuchi, Korsmeyer-Peppas and Hixson-Crowell models, respectively, as represented in Figure 3.14. As the R^2 value 0.9883 is closest to 1, it is considered as best fitting, indicating that NLX release from the NLX-loaded SLNs follow the Korsmeyer-Peppas model of release kinetics. The obtained release exponent n from the Korsmeyer–Peppas model was 0.405 which further confirms that the mechanism of NLX release exhibited a Fickian transport, implying that the release of NLX was controlled by diffusion, where NLX move through the polymer matrix. Additionally, the high value of Korsmeyer–Peppas kKP parameter (11.001) suggested that a burst release occurred during the initial phase of the release (Abdelgader et al., 2024; Danyuo et al., 2019).

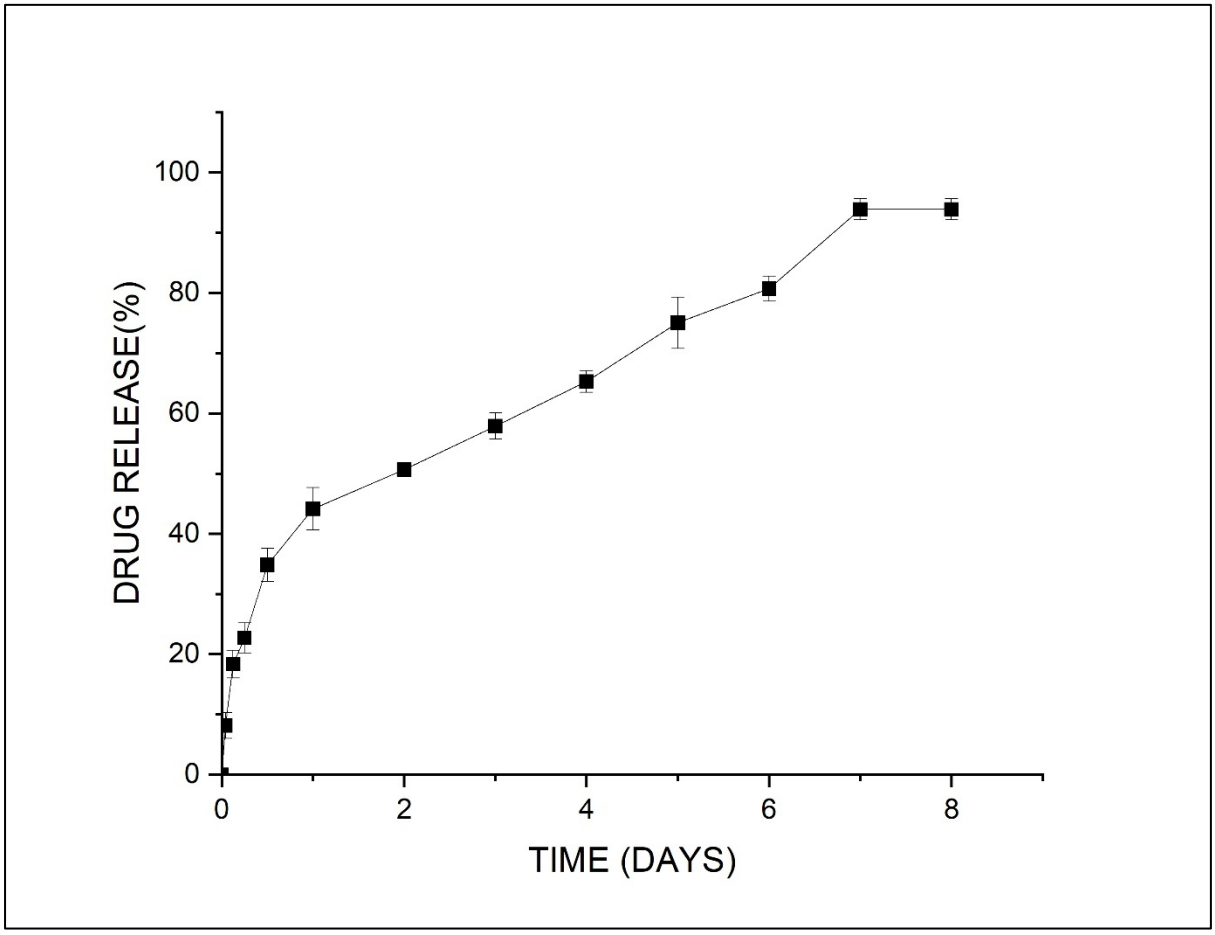

Figure 3.13. Representation of the *in vitro* drug release profile of NLX from NLX-loaded SLNs at 37 °C (n = 3).

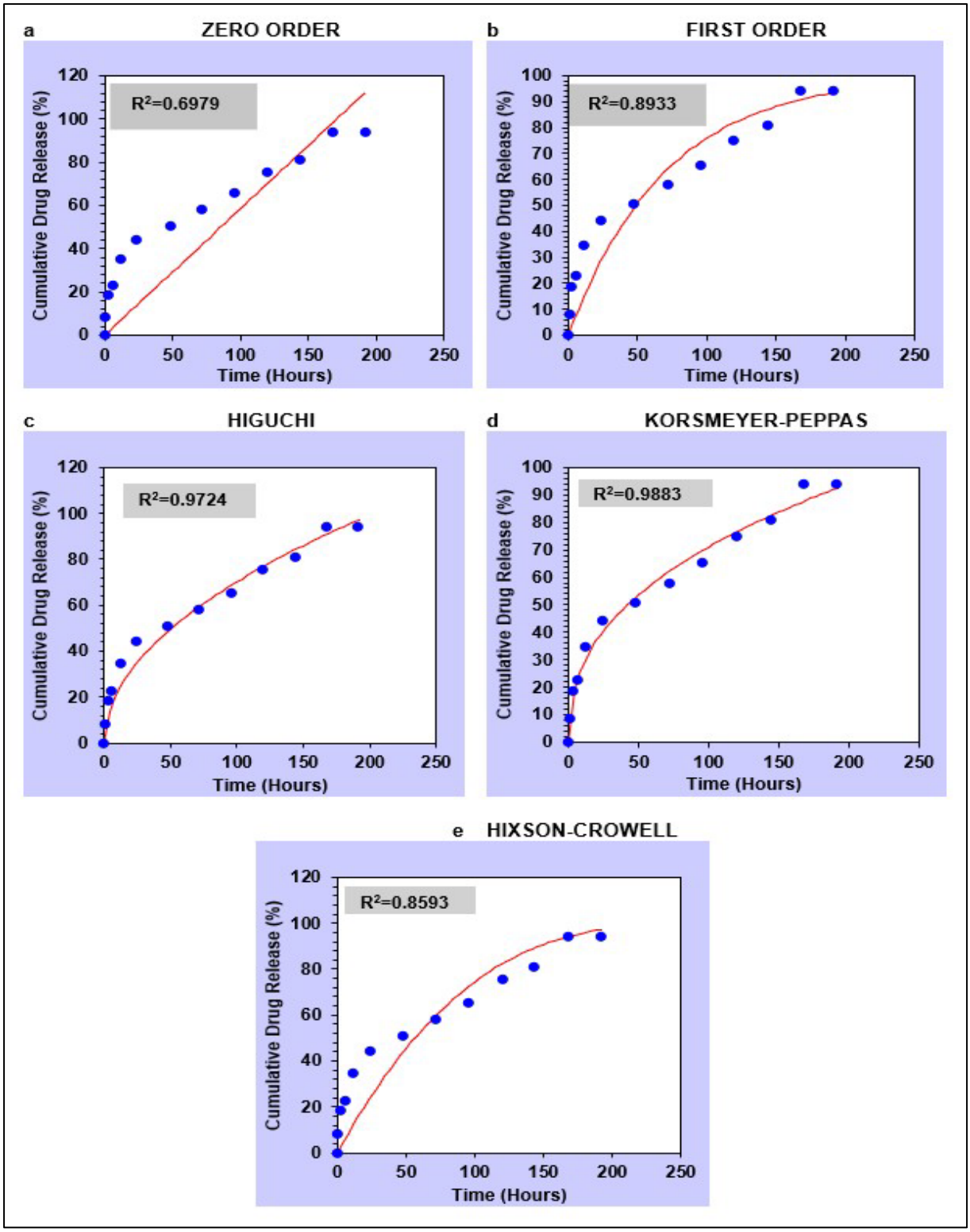

Figure 3.14. Representation of the *in vitro* NLX release profile data fitted to various kinetic models.

3.3.3.4 Molecular structure assessment

The FTIR spectra of all the starting materials, including the optimized unloaded and NLX-loaded SLNs, are represented in Figure 3.15. The characteristic FTIR peaks of NLX: 3511 cm^{-1} (free O-H), 3421 cm^{-1} (bonded O-H), 2974 cm^{-1} (N-H), 1715 cm^{-1} (C=O) and 1470 cm^{-1}

(aromatic) were present, which were similar to that described in previous research (Hasan et al., 2021). Evaluation of the GMS spectrum revealed 3299 cm^{-1} (O-H), 1729 cm^{-1} (C=O) and 1179 cm^{-1} (C-O) peaks were present, consistent with the study by Ng et al. (2018). PCL additionally displayed peaks at 2943 and 2866 cm^{-1} (asymmetric CH_2), 1720 cm^{-1} (C=O) and 1236 cm^{-1} (C-O-C) in line with the results obtained by Ali et al. (2014). Analysis of the FTIR spectra of the unloaded SLNs showed peaks at 3303 cm^{-1} (O-H), 2916 and 2850 cm^{-1} (C-H alkane), 1723 cm^{-1} (C=O) and 1174 cm^{-1} (C-O). The NLX-loaded SLNs showed the same characteristic peaks at 3299 cm^{-1} (O-H), 2916 and 2850 cm^{-1} (C-H alkane), 1723 cm^{-1} (C=O) and 1172 cm^{-1} (C-O) indicating the synthesis of SLNs, as the characteristic peaks of unloaded and NLX-loaded SLNs were found to be the same as GMS, indicating the outer layer of SLNs were made of GMS, consistent with the SEM images represented in Figure 3.12. This results can also be compared with the results obtained by Ebrahimi et al. (2015), where the characteristic peaks of NLX: 3511 cm^{-1} (N-H) and 1470 cm^{-1} (aromatic) were absent in the NLX-loaded SLNs, indicating the complete encapsulation of NLX within the polymeric core (Ebrahimi et al., 2015).

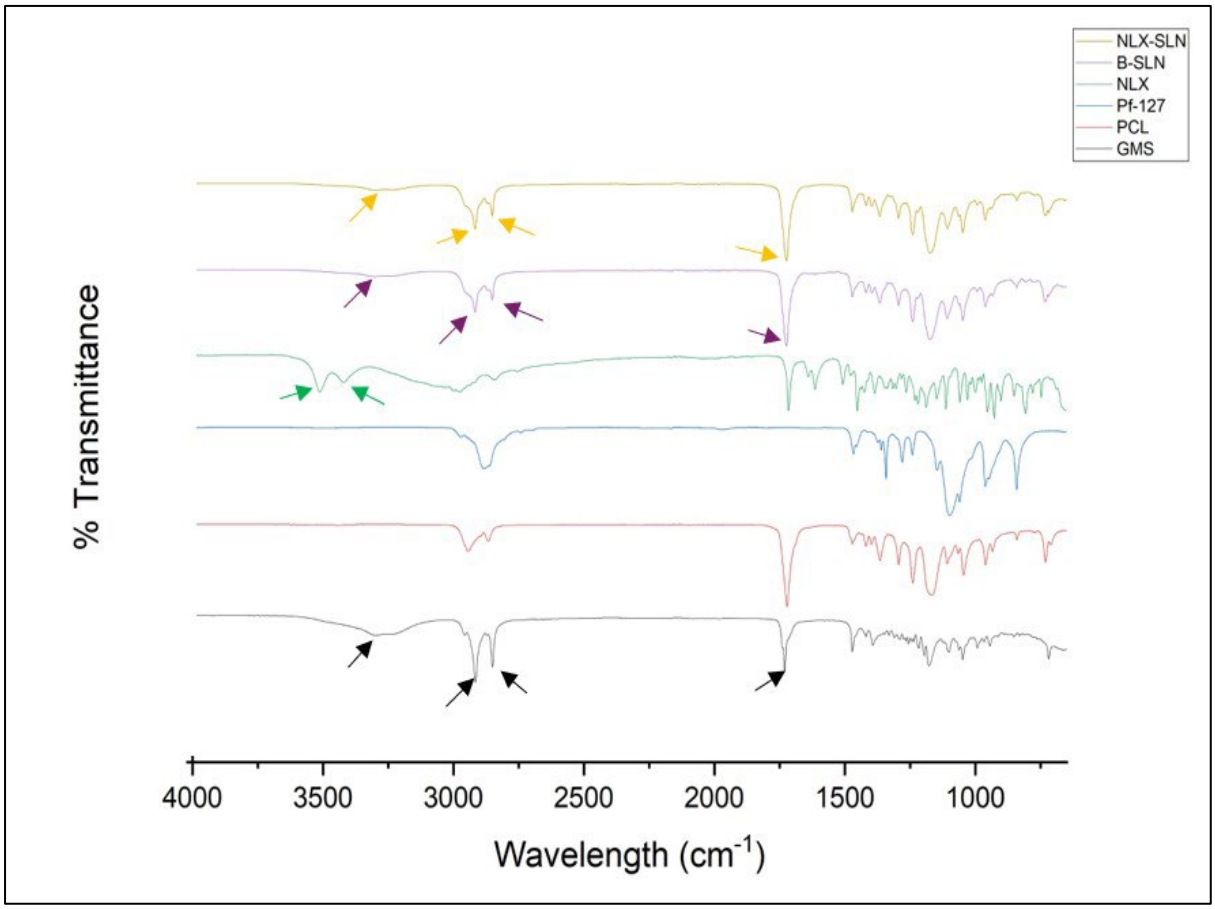

Figure 3.15. FTIR spectra of the NLX-loaded SLNs, unloaded SLNs (B-SLN), NLX, Pf-127, PCL and GMS.

3.3.3.5 Determination of the thermal characteristics

DCS analysis was performed on all the starting materials as well as on the unloaded and optimized NLX-loaded SLNs for the determination of their thermal behaviors, as represented in Figure 3.16. Pf-127 and GMS showed endothermic peaks at 58 °C and 65.8 °C whereas, PCL showed endothermic peaks at 68.2 °C and 385 °C, which falls in line with previous studies (Karolewicz et al., 2014; Kerman et al., 2005; Ng et al., 2018). NLX showed characteristic endothermic peaks at 127.5 °C and 194.3 °C, including an exothermic peak at 266.2 °C, which can be further verified by the results obtained in the study by Guguta et al. (2009). The unloaded SLNs showed endothermic peaks at 55.3 °C, 62.7 °C and initiation of one at 387 °C. NLX-loaded SLNs further showed endothermic peaks at 55.5 °C, 67.5 °C and initiation of one at 390 °C. The endothermic peaks of both the unloaded and NLX-loaded SLNs are similar and lied within the range of Pf-127, PCL and GMS indicating the formation of SLNs (Yasir and Sara, 2014). Additionally, NLX-loaded SLNs showed a characteristic endothermic peak at 186.2 °C and an exothermic peak at 263.8 °C, which were similar peaks to NLX indicating the encapsulation of NLX within the SLNs.

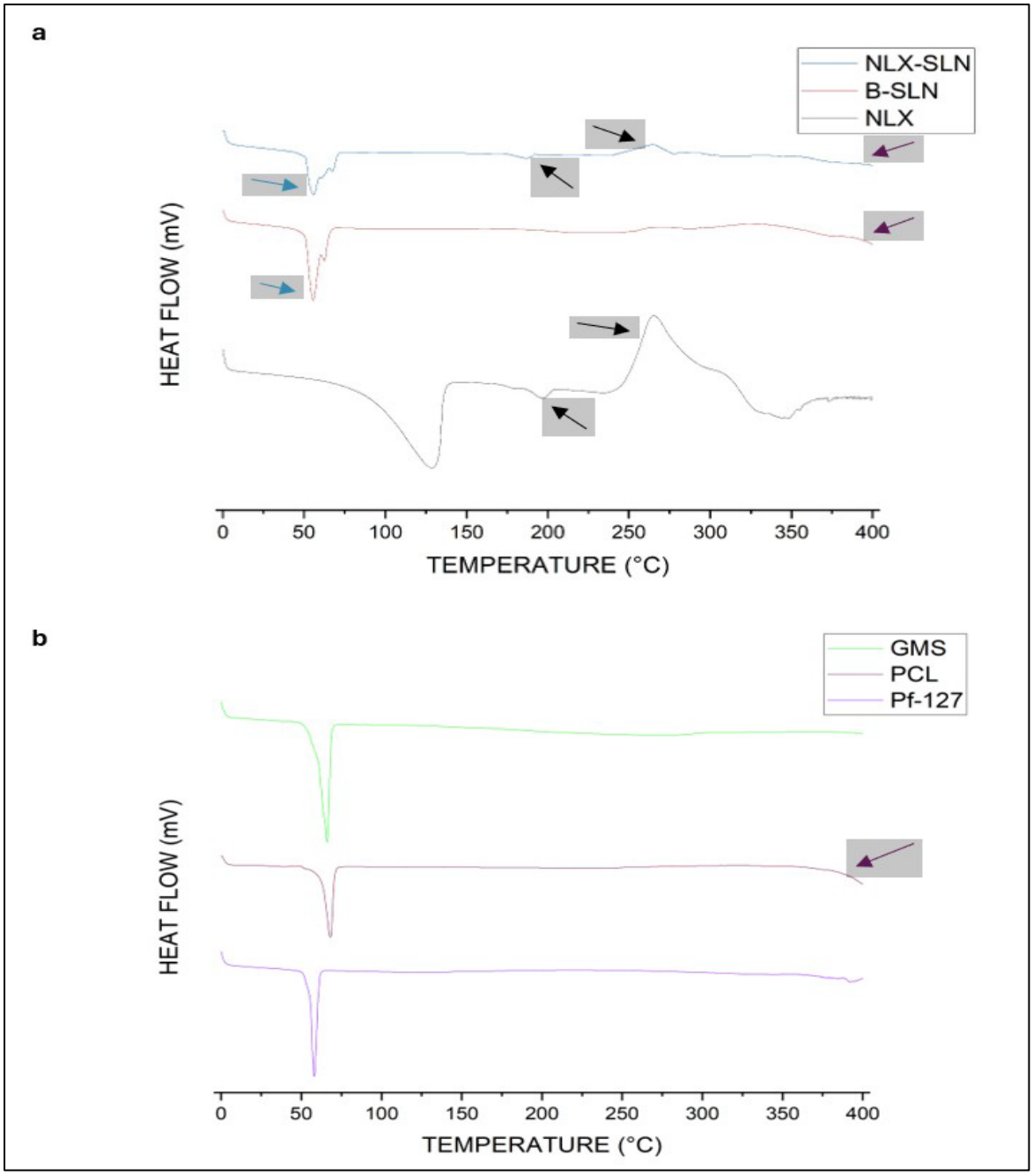

Figure 3.16. DSC thermograms of (a) NLX, unloaded (B-SLN) and optimized NLX-loaded SLNs and (b) Pf-127, PCL and GMS used for the synthesis of both the SLNs.

3.3.3.6 Determination of the degradation rate

TGA analysis was done on all the starting materials, as well as on unloaded and NLX-loaded SLNs, as represented in Figure 3.17, to determine their degradation rates. The % weight loss of the unloaded SLNs and NLX-loaded SLNs started at 221 °C and 205 °C, respectively. By the end i.e. 600 °C, 4.9% and 8.9% of the unloaded and optimized NLX-loaded SLNs still remained indicating the formation of GMS-coated SLNs, as 15.3% of GMS remained undegraded at 600 °C, consistent with the study carried out by Tian et al. (2018). Additionally, 4% more of the NLX-loaded SLNs were found ,compared to the unloaded SLNs, which

indicated the presence of NLX as, 40.85% of NLX remained un-degraded at 600 °C (Guguta et al., 2009; Tian et al., 2018).

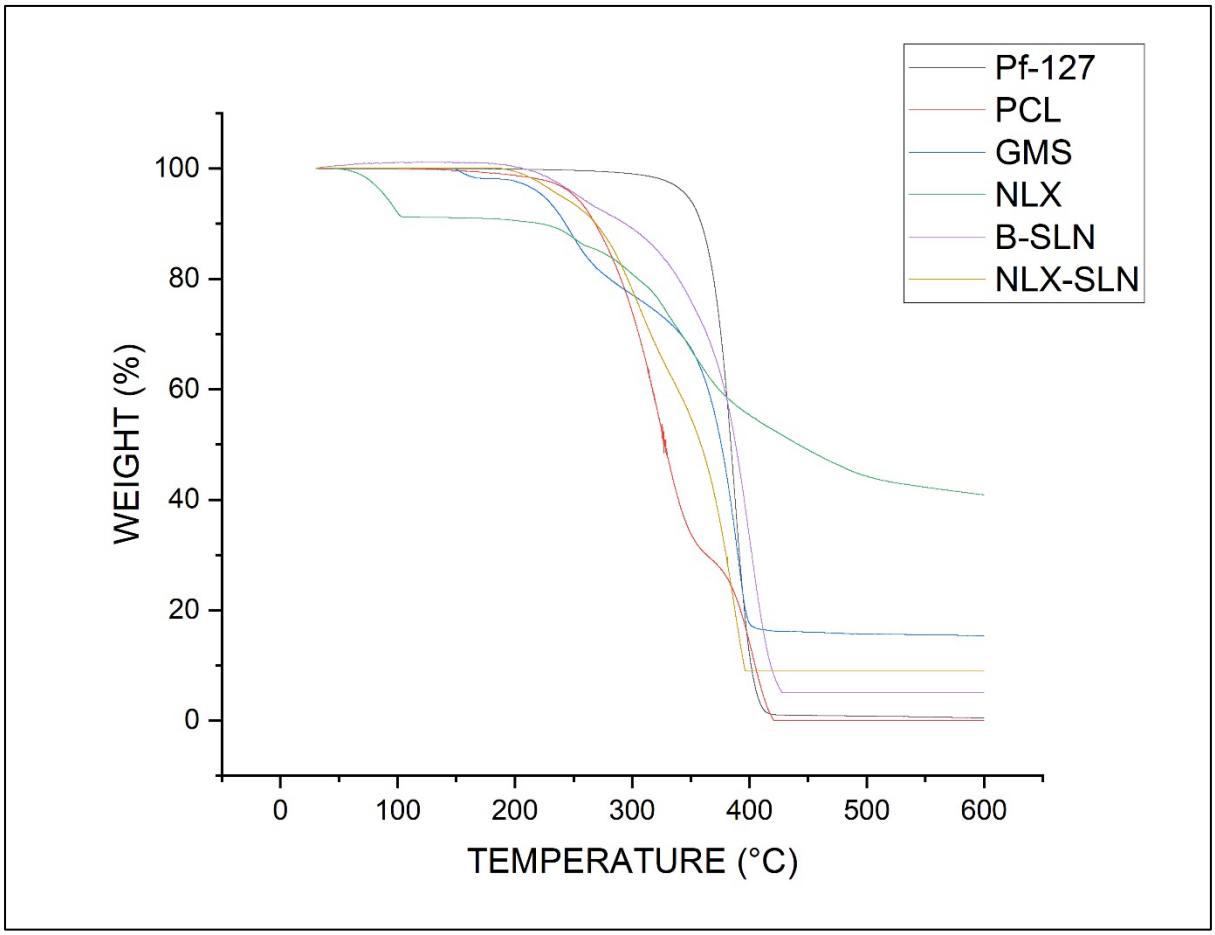

Figure 3.17. TGA thermograms of the unloaded (B-SLN) and optimized NLX-loaded SLNs including all the materials used for the synthesis of the SLNs.

3.3.4 Cell culture and cytotoxicity studies

The assessment for potential cytotoxicity of NLX-loaded SLNs on HEK293 cells is represented in Figure 3.18. To determine biocompatibility, cell treatment groups were incubated for 24, 48 and 72 hours in the presence of various concentrations of NLX (0.625-80 µg/mL), NLX-loaded SLNs (equivalent to 0.625-80 µg/mL) and SLNs without NLX where, they were compared to the positive control or untreated cells. Figure 3.19 represents the microscopic imaging of positive control, negative control, NLX, unloaded SLNs and NLX-loaded SLNs treated cells taken after 48 hours using an inverted microscope at 4X magnification. After 24 hours, the maximum concentration of NLX, unloaded SLNs and NLX-loaded SLNs showed cell viability of 89.91 ± 9.4%, 92.54 ± 2.9% and 91.11 ± 2.9%, respectively, whereas the minimum concentrations showed 94.45 ± 3.5%, 95.11 ± 3.7% and 95.99 ± 4.1% cell viability. At 48 hours, the maximum concentration of NLX, unloaded SLNs and NLX-loaded SLNs showed cell viability of 85.34 ± 6.8%, 88.11 ± 2.4% and 88.81 ± 3.1%, respectively, whereas the

minimum concentrations showed 89.29 ± 2.6%, 93.25 ± 2.8% and 90.19 ± 3.5% cell viability. After 72 hours, the maximum concentration of NLX, unloaded SLNs and NLX-loaded SLNs showed cell viability of 83.55 ± 1.3%, 84.77 ± 2.6% and 84.16 ± 2.0%, respectively, while the minimum concentrations showed 86.78 ± 2.1%, 89.31 ± 1.8% and 88.60 ± 2.2% cell viability. Statistical evaluation of the data noted statistical significance at all time points and concentrations ($p < 0.01$), when compared to the positive control, due to the low variability between samples and the consistent values across sample runs. However, as per ISO 10993-5, a %cell viability above 80% is considered non-cytotoxic; with 80%–60% weakly; 60%–40% moderately and a viability below 40% strongly cytotoxic (López-García et al., 2014). Thus, from the data obtained it can be concluded that NLX, unloaded SLNs and NLX-loaded SLNs showed good cell biocompatibility as even after 72 hours, none of the %cell viability dropped below 80% indicating no cytotoxic effect was observed. Additionally, as observed from the data obtained, it can be concluded that NLX-loaded SLNs had equivalent or more viable cells compared to NLX and the unloaded SLNs indicating that the incorporation of NLX within SLNs helped in improving the cell biocompatibility properties of NLX.

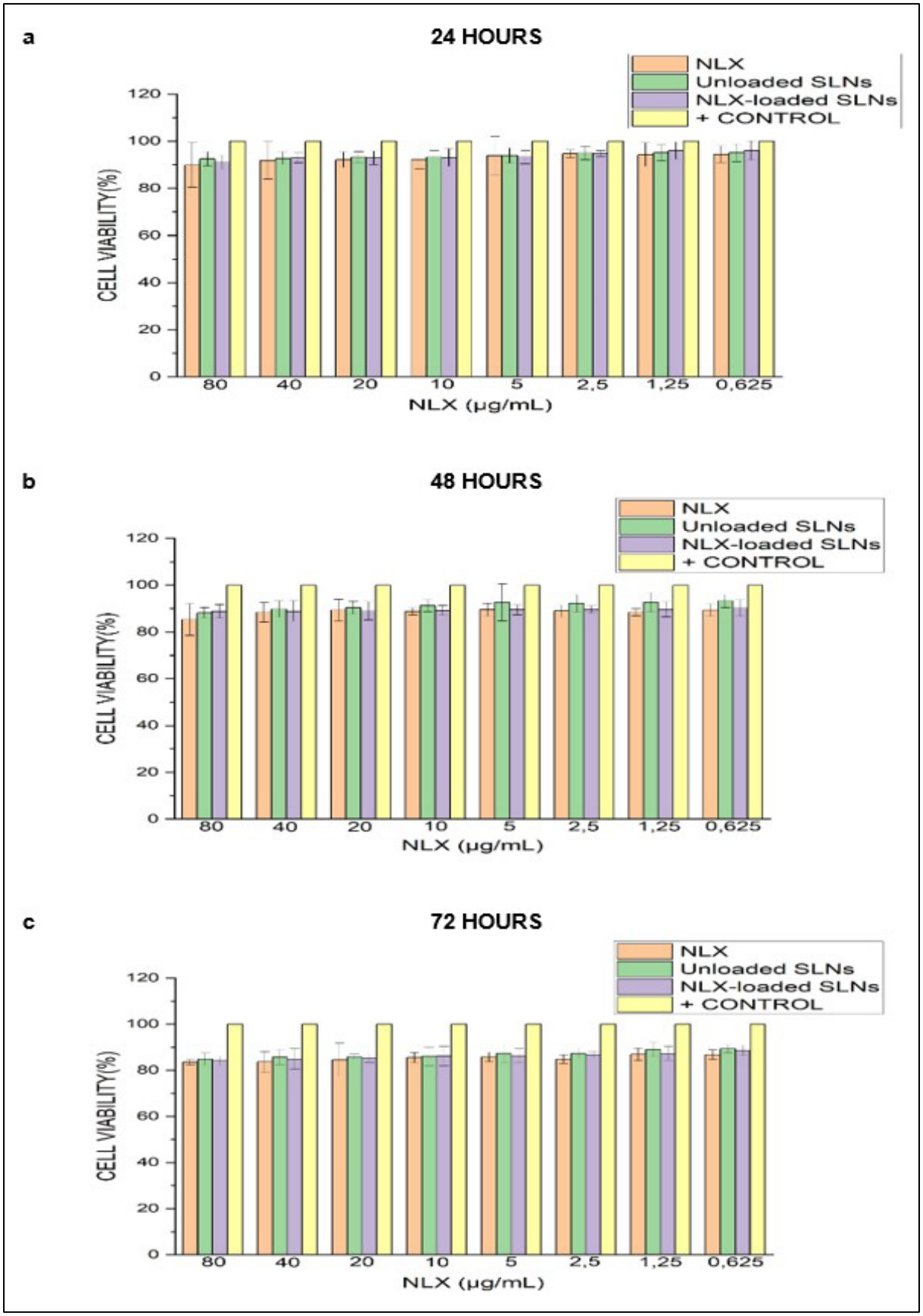

Figure 3.18. HEK293 cells biocompatibility with various concentrations of NLX, unloaded SLNs and NLX-loaded SLNs (a) after 24 hours (b) after 48 hours and (c) after 72 hours (n = 3 with a $p \leq 0.01$ for all cases).

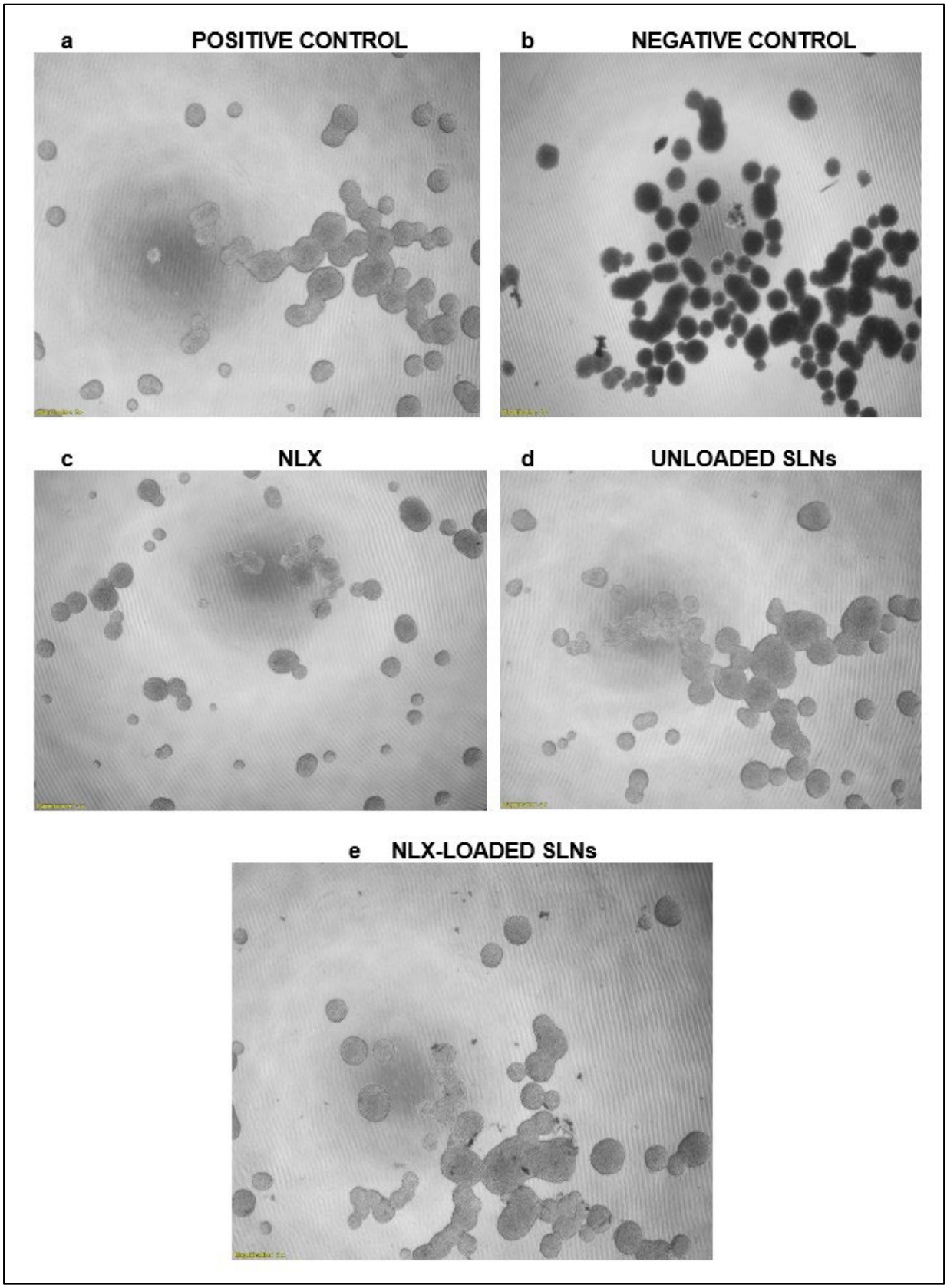

Figure 3.19. Representation of the microscopic imaging of (a) positive control, (b) negative control, (c) NLX, (d) unloaded SLNs and (e) the optimized NLX-loaded SLNs treated cells. All images were taken after 48 hours at 4X magnification.

3.4 Conclusion

In this chapter, polymeric NLX-loaded SLNs were synthesized for the sustained release of NLX, overcoming its poor pharmacokinetic properties. The polymeric NLX-loaded SLNs were successfully formulated using the modified double emulsification technique, where the desired particle size, PDI and zeta potential were obtained. Additionally, further verification of the particle size and shape was done using SEM imaging ensuring that the SLNs would cross the BBB with ease. The desired physicochemical properties of the NLX-loaded SLNs were obtained and confirmed using FTIR, DSC and TGA to ensure their desired molecular transition and stable thermal behavior. The maximum %EE and %LC of NLX within the SLNs was further obtained and *in vitro* release of NLX from the SLNs was observed over a period of one week, which suggested a potential increased bioavailability of NLX across the BBB and increased residence time at the site of action. The NLX-loaded SLNs additionally showed no significant signs of *in vitro* cytotoxicity against HEK293 cells, indicating their excellent biocompatibility. Therefore, with the achievement of the desired properties from the NLX-loaded SLNs, it can be an effective potential treatment for OUD.

CHAPTER 4
BUPRENORPHINE-LOADED SOLID LIPID NANOPARTICLES AS A COMBINATIVE INTERVENTION FOR OPIOID USE DISORDER

4.1 Introduction

BUP is a partial μ opioid receptor agonist and K opioid receptor antagonist used in the treatment of OUD as well as in pain management due to its mixed agonistic-antagonistic effect (De Aquino et al., 2021; Lutfy and Cowan, 2004). It is one of the most preferred drugs in the treatment of OUD because of its mixed agonistic-antagonistic effect, as it reduces cravings for opioids and prevents opioid-dependent patients from undergoing withdrawal symptoms (Nasser et al., 2016). However, BUP undergoes extensive first-pass metabolism and therefore has a low oral bioavailability of 35% (Elkader and Sproule, 2005). Additionally, a bioavailability of 49-63% has been reported by Nath et al. for BUP when delivered sublingually (Nath et al., 1999). Therefore, with the incorporation of advanced DDSs and through the use of alternate delivery routes, the pharmacokinetic and pharmacodynamic properties of BUP can be improved.

DDSs which sustain/control the release of drugs loaded in formulations is considered to be a modern tool to achieve a prolonged and consistent drug release at the site of action, thereby leading to peak plasma exposure, reduced side effects and reduced application intervals (Schreiner et al., 2021). Specifically, polymeric SLNs due to their beneficial physicochemical properties, as mentioned in Chapter 3 (3.1) for the delivery of NLX, have the potential to improve the pharmacodynamic and pharmacokinetic properties of drugs such as BUP. Therefore, this chapter provides for the design, synthesis and optimization of sustained-release BUP-loaded polymeric SLNs for the management of OUD with the aim of providing better therapeutic efficacy through reduced dosing frequency, reduced dosage strength and improved bioavailability. This system is envisioned to release BUP at the target site for a longer duration thereby improving therapeutic outcomes and patient compliance, similar to that of the NLX-loaded SLNs developed in Chapter 3. Additionally provided in this chapter is the construction and evaluation of BBD experiment, which aided in the optimizing of the material composition and formulation processes, which are important factors for the performance of the BUP-loaded SLNs (Hasan et al., 2021). Thereafter, the optimized BUP-loaded SLNs were characterized for their physicochemical properties such as particle size, zeta potential, PDI, surface morphology, %EE, release profile, thermal behaviour and lastly biocompatibility studies using the HEK293 cell line.

4.2 Materials and methods

4.2.1 Materials

Buprenorphine Hydrochloride (BUP), GMS, Tween 80, Pf-127, PCL (Avg Mw = 14 000), DCM, Ethanol (99%), DMSO and MTT assay kit were purchased from Sigma-Aldrich (St. Louis, Missouri, USA), DMEM, FBS, Pen-Strep antibiotic solution and DPBS from ThermoFisher Scientific (Randburg, South Africa) and HEK293 cells from ATCC (LGC-Standards, South Africa). All other chemicals were of analytical grade and used as received.

4.2.2 Preparation of the BUP-loaded SLNs

The BUP-loaded SLNs were formulated using the modified double emulsification technique, as described in Chapter 3 (3.2.2). Briefly, BUP was dissolved in ethanol followed by the dissolution of PCL in DCM in a separate vessel. The PCL solution was then added to the BUP solution under probe sonication, at 40% amplitude, 1.5 million joules and 1 minute, forming ORP1, with Pf-127 as a surfactant and tween 80 as co-surfactant added to water, forming the aqueous phase. ORP1 was then added to the aqueous phase under probe sonication (40% amplitude, 1.5 million joules and 8.5 minutes) to form EM1, with GMS dissolved in DCM to form ORP2. ORP2 was then added to EM1 and rotary evaporated (175 mbar, 30 minutes) to remove all the organic solvents and form EM2 containing the BUP-loaded SLNs. The SLNs were thereafter separated from EM2 by centrifugation at 10,000 RPM for 35 minutes at 4 °C, followed by the re-dispersion of the collected BUP-loaded SLNs in Milli-Q distilled water. The SLNs were subsequently freeze dried using a lyophilizer for 17 hours to obtain a dry SLN powder.

4.2.3 Statistical optimization of the BUP-loaded SLNs

4.2.3.1 Construction of the BBD

A BBD (MINITAB®, V15, Minitab, USA) was used for the optimization of the formulated BUP-loaded SLNs as mentioned in Chapter 3 (3.2.3.1). For the BUP-loaded SLNs, the independent variables were selected as: Lipid (GMS) concentration, Polymer (PCL) concentration and Surfactant/Co-surfactant (Pf-127:Tween 80 = 5:1) concentration whereas, the dependent responses included the particle size, %EE and maximum drug release time.

4.2.3.2 Determination of BBD lower and upper limits of independent variables

The same lower and upper limits as mentioned in Chapter 3 (3.2.3.2 and 3.3.1.1) for the NLX-loaded SLNs were used for BUP-loaded SLNs due to the similarity between the physicochemical properties of the two drugs (Jönsson et al., 2018). Table 4.1 represents the lower and upper limits of BUP-loaded SLNs independent variables and Table 4.2 represents the 15-formulations generated utilizing the BBD.

Table 4.1. The lower and upper limits of BUP-loaded SLNs independent variables are tabulated as Lipid (GMS) concentration, Polymer (PCL) concentration and Surfactant (Pf-127:Tween 80) concentration.

Factor	Coded level		
Independent variables	-1	0	+1
F1: Lipid concentration (GMS) (mg/mL)	4	7.5	11
F2: Polymer concentration (PCL) (mg/mL)	6	13	20
F3: Surfactant concentration (mg/mL)	5	12.5	20

Table 4.2. The 15 formulations generated for the statistical optimization of the BUP-SLNs using the BBD.

Run	F1: GMS (mg/5mL)	F2: PCL (mg/2.5mL)	F3: Surfactant (mg/5mL)
1	37.5	32.5	62.5
2	55	15	62.5
3	37.5	32.5	62.5
4	37.5	15	25
5	55	32.5	100
6	55	32.5	25
7	20	50	62.5
8	20	15	62.5
9	37.5	32.5	62.5
10	20	32.5	100
11	55	50	62.5
12	20	32.5	25
13	37.5	15	100
14	37.5	50	25
15	37.5	50	100

4.2.3.3 Preparation of the BBD formulations

Using the modified double emulsification technique, as represented in 4.2.2, the formulations mentioned in Table 4.2 were formulated and analysed for particle size, %EE and maximum drug release.

4.2.3.3.1 Determination of particle size for the generated BBD formulations

The DLS technique of the Zeta-Sizer Nano-ZS, as mentioned in Chapter 3 (3.2.3.3.1) (n = 3), was used for the determination of the particle size of the BUP-loaded SLNs. For the analysis, the freeze-dried BUP-loaded SLNs were screened for a particle size ranging between 40 - 200 nm (Xinchen et al., 2023).

4.2.3.3.2 Determination of %EE for the generated BBD formulations

Prior to the evaluation of the %EE for the BBD formulations, a UV/Vis-spectrophotometer was used for the construction of a calibration curve i.e. a relation between concentration and absorbance of BUP (Figure 4.1) in PBS. The lambda-max (λ-max) for BUP was confirmed at 285 nm by employing a full UV/Vis-spectrophotometry analysis, which falls in line with the findings by Mundhey et al. (2016). Various concentrations of BUP i.e. 0-88 µg/mL were analysed on the UV/Vis-spectrophotometer at 285 nm to obtain the absorbance values of the respective concentrations for the quantification of BUP.

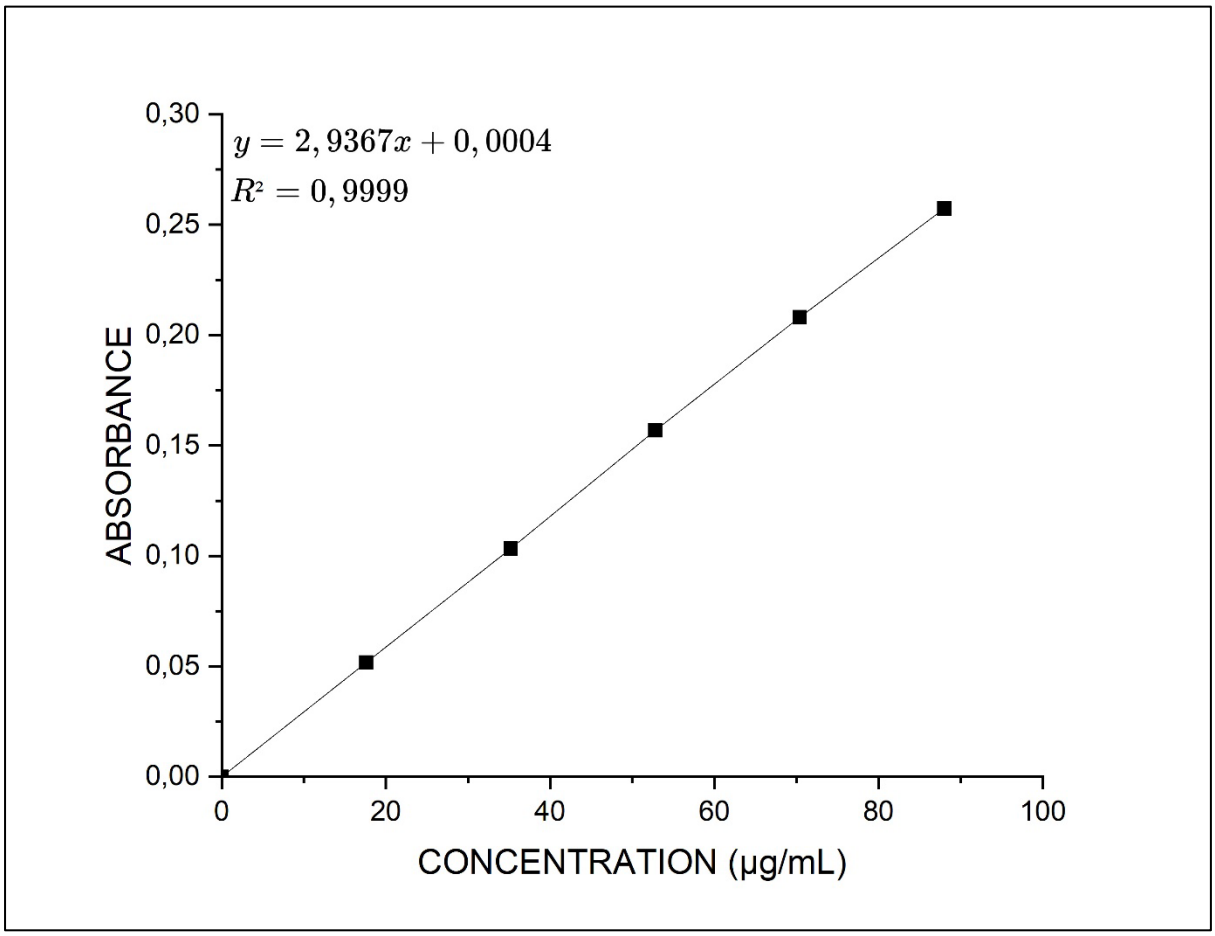

Figure 4.1. The constructed calibration curve for BUP.

The indirect method as discussed in Chapter 3 (3.2.3.3.2) was used for the determination of %EE (Equation 3.1) of BUP in the BUP-loaded SLNs formulations at 285 nm using a UV/Vis-spectrophotometer.

4.2.3.3.3 Determination of maximum drug release for the generated BBD formulations

Drug release studies (n = 3) on the BUP-loaded SLNs was done using the dialysis bag diffusion method as discussed in Chapter 3 (3.2.3.3.3), where the concentration of BUP

released from the formulated BUP-loaded SLNs to PBS was analysed and measured at 285 nm by UV/Vis spectroscopy.

4.2.3.4 Optimization process of the dependent variables

Based on the BBD formulation results, the desired particle size, %EE and maximum drug release criteria were selected to optimize the SLNs for the intranasal delivery of BUP, which is represented in Table 4.3.

Table 4.3. The desired particle size, %EE and maximum drug release for the optimized BUP-loaded SLNs.

Dependent variables	Constraints
R1: Particle Size (nm)	125 nm
R2: EE (%)	Maximum
R3: Maximum Drug Release (days)	7 days

4.2.3.5 Characterization of the optimized BUP-loaded SLNs

4.2.3.5.1 Evaluation of the particle size, PDI, zeta potential and surface morphology

As described in Chapter 3 (3.2.3.3.1), DLS measurements through a Zeta-Sizer Nano-ZS (n = 3) was used for the determination of particle size, PDI and zeta potential of the unloaded and BUP-loaded SLNs. The SLNs were screened for a particle size ranging between 40-200 nm, a PDI of ≤ 0.3 and a zeta potential of -15 to -30 mV (Neves, 2015; Xinchen et al., 2023). Additionally, the particle shape and surface morphology of the formulated unloaded and BUP-loaded SLNs were determined using a SEM, with the sample preparation for SEM undertaken as stated in Chapter 3 (3.2.3.5.1).

4.2.3.5.2 Determination of the %EE and %LC

The indirect method as described in Chapter 3 (3.2.3.3.2 and 3.2.3.5.2) (n = 3) was used for the determination of %EE (Equation 3.1) and %LC (Equation 3.2) of BUP in the optimized BUP-loaded SLNs formulation at 285 nm using a UV/Vis-spectrophotometer.

4.2.3.5.3 *In vitro* drug release of the formulated SLNs

In vitro drug release studies (n = 3) on the optimized BUP-loaded SLNs were done using the dialysis bag diffusion method as discussed in Chapter 3 (3.2.3.3.3), where the concentration of BUP released from the optimized BUP-loaded SLNs to PBS was analysed and measured at 285 nm. Additionally, several kinetic models such as the Zero order, First order, Higuchi, Korsmeyer-Peppas and Hixson-Crowel models were employed to analyse the BUP release

kinetic pattern from the optimized BUP-loaded SLNs using DDSolver software.

4.2.3.5.4 Molecular structure assessment

All starting materials used for formulating the SLNs including both the freeze-dried unloaded and BUP-loaded SLNs, were analysed for their molecular transitions and interactions using a PerkinElmer ATR-FTIR. The instrumental parameters for the analysis were as described in Chapter 3 (3.2.3.5.4) to obtain the FTIR spectra.

4.2.3.5.5 Determination of thermal characteristics

All starting materials used for formulating the SLNs including for both the freeze-dried unloaded and BUP-loaded SLNs were analysed as discussed in Chapter 3 (3.2.3.5.5) for their thermal properties using a DSC.

4.2.3.5.6 Determination of the SLNs degradation rate

The thermal degradation temperatures of all the starting materials used for formulating the SLNs including for both the freeze-dried unloaded and BUP-loaded SLNs were determined using a TGA, as discussed in Chapter 3 (3.2.3.5.6).

4.2.4 Cell culture and cytotoxicity studies

4.2.4.1 Cell culture

The HEK293 cells were maintained, cultured and seeded as discussed in Chapter 3 (3.2.4.1) with the treatments i.e. BUP, unloaded SLNs and BUP-loaded SLNs thereafter prepared in serial dilutions using DPBS (2.5 - 320 µg/mL).

4.2.4.2 Cytotoxicity studies using MTT assay kit

Cell viability, through the determination of mitochondrial activity of living cells was measured by quantitative colorimetric assay (n = 3) using MTT over 72 hours, as discussed in Chapter 3 (3.2.4.2), and through the absorbance values obtained, the relative cell viability was calculated using Equation 3.3.

4.2.5 Statistical analysis

All analyses were conducted in triplicate (n = 3) with Microsoft Excel used to express the mean and standard deviation of the obtained results. P values of less than 0.05 ($p < 0.05$) were considered to be an indication of statistical significance. OriginPro 2025 was additionally used for the graphical representation of all results obtained.

4.3 Results and discussion

4.3.1 Statistical optimization using BBD

4.3.1.1 Formulation optimization using BBD strategy

With the incorporation of the lower and upper limits of independent variables into the BBD software, a total of 15 experimental runs were generated for the determination of effects of the varying concentrations of lipid, polymer and surfactant on particle size, %EE and maximum drug release. Table 4.4 provides the response results of the BBD design with all studies undertaken in triplicate.

Table 4.4. Summary of the responses observed from the formulations generated by the BBD for the optimization of the BUP-loaded SLNs (n = 3).

Run	R1: Particle Size (nm)	R2: EE (%)	R3: Maximum Drug Release (Days)
1	122.3 ± 1.97	98.9 ± 0.95	7
2	116.7 ± 2.41	98.6 ± 0.76	6
3	115.5 ± 4.5	98.8 ± 0.76	7
4	124.8 ± 2.18	99.1 ± 0.71	6
5	118.5 ± 1.38	98.5 ± 0.5	7
6	125.8 ± 3.86	99.5 ± 0.45	7
7	123.5 ± 2.51	98.8 ± 0.98	9
8	126.5 ± 3.05	98.8 ± 0.98	5
9	127.4 ± 1.15	98.5 ± 0.5	7
10	128.2 ± 2.38	99.3 ± 0.29	7
11	175.4 ± 3.42	99.5 ± 0.45	9
12	117.7 ± 2.82	98.8 ± 0.76	7
13	91.84 ± 3.35	99.3 ± 0.29	5
14	128.1 ± 2.23	99.1 ± 1.00	9
15	119.8 ± 3.97	99.5 ± 0.45	9

4.3.1.1.1 Effect of independent variables on dependent variable particle size

The particle size ranging between 40 - 200 nm for nanocarriers is considered to be the optimum size for crossing the BBB, especially for nose-to-brain DDSs (Xinchen et al., 2023). Equation 4.1 obtained from the BBD for particle size showed both positive and negative effects of the independent variables on the dependent variables, which are graphically represented in Figure 4.2. Additionally, the R^2 and R^2 (adj) had a difference of 19% (0.19) which is less than 20% (0.2) indicating that the adopted model was significant (Takalani et al., 2024).

$$Particle\ size = +198.517 - 3.44830\ GMS - 2.65306\ \text{PCL} + 0.625185\ \text{Surfactant} + 0.0336054\ \text{GMS} * \text{GMS} + 0.0123810\ \text{PCL} * \text{PCL} - 0.00654815\ \text{Sufactant} * \text{Surfactant} + 0.0497959\ \text{GMS} * \text{PCL} - 0.00647619\ \text{GMS} * \text{Surfactant} + 0.00952381\ \text{PCL} * \text{Surfactant} \quad \text{(Equation 4.1)}$$

The higher value of coefficient variable of GMS (-3.44830), as compared to PCL (-2.65306) and Surfactant (+0.625185), showed that GMS had a more prominent effect on particle size. Initially, with the increase in GMS concentration, the particle size decreased, but after a certain concentration GMS showed a positive effect, i.e. with the increase in GMS concentration, the particle size increased. Additionally, with the increase in PCL concentration, the particle size increased which can be stated from the positive values obtained in Equation 4.1 from the interactions between PCL*PCL, PCL*GMS and PCL*Surfactant. The mentioned effects of both GMS and PCL can be evidenced from the contour plots represented in Figure 4.2. Resultantly, the particle sizes ranged from 91.84 to 175.4 nm for the 15 formulations obtained from the BBD, which is represented in Figure 4.3.

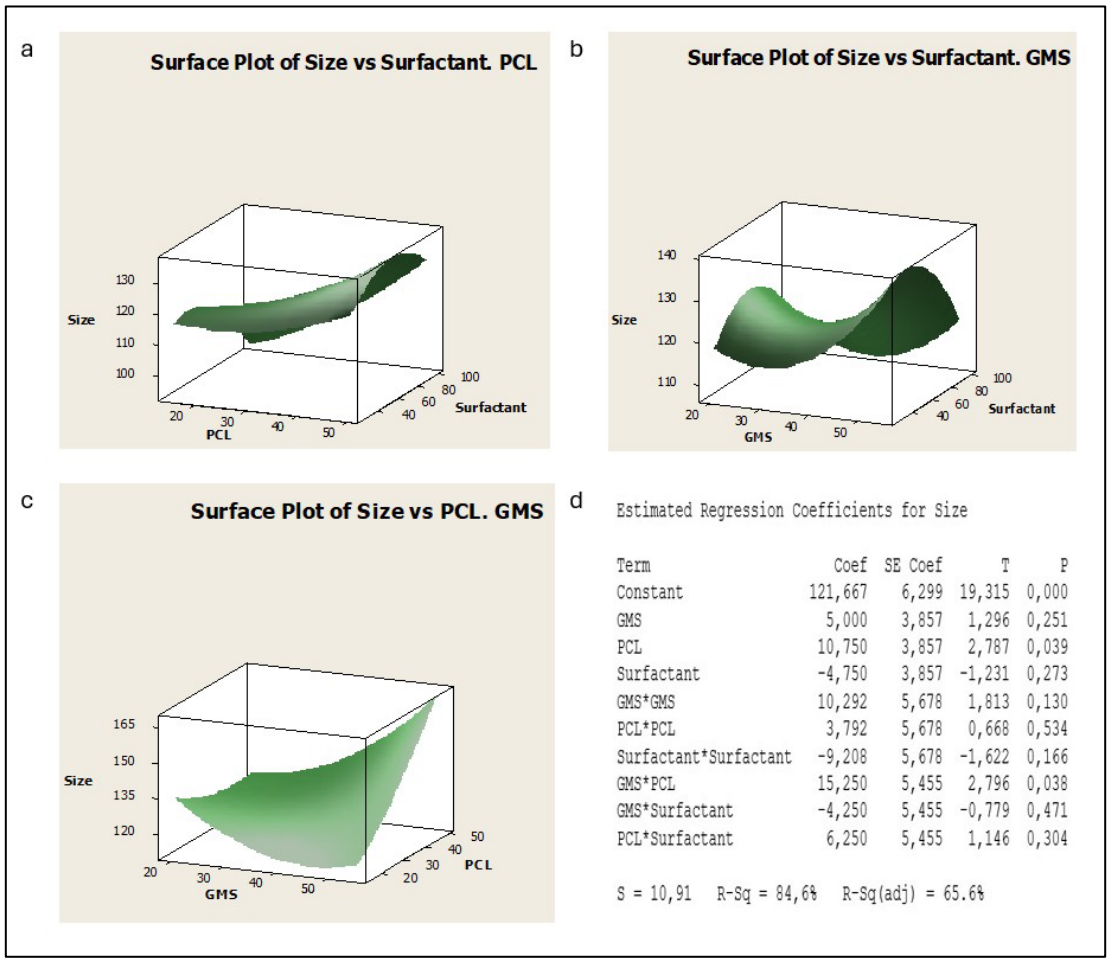

Figure 4.2. Effect of the independent variables i.e. GMS, PCL and Surfactant on the dependent variable i.e. particle size, as represented in (a), (b) and (c), whereas the estimated regression coefficients for particle size is represented in (d).

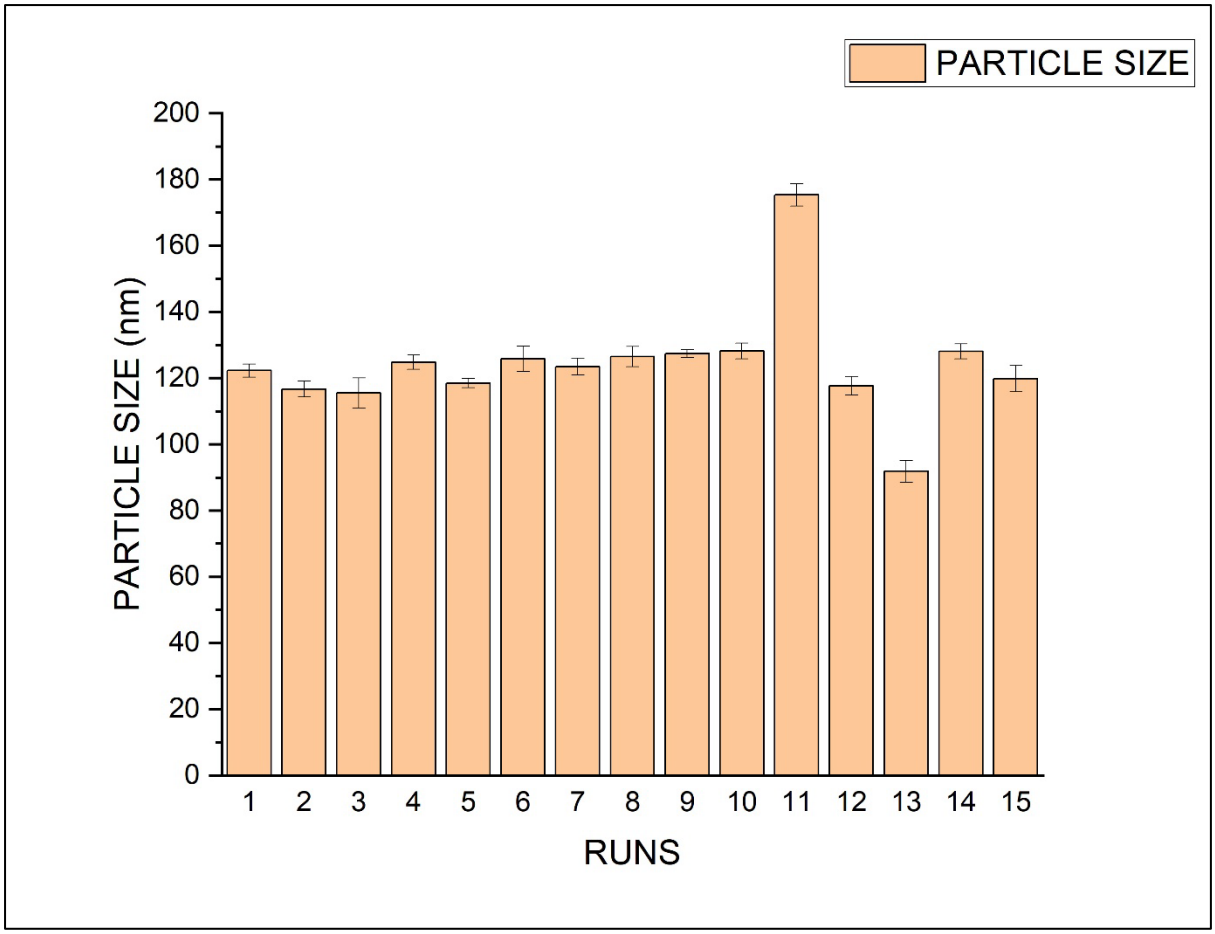

Figure 4.3. Representation of various particle sizes obtained for the BBD formulations (n = 3).

4.3.1.1.2 Effect of independent variables on dependent variable %EE

The maximum %EE of BUP nanocarriers is considered optimum, as this decreases the amount of SLNs required at the site of action for therapeutic efficacy. Equation 4.2 obtained from the BBD for %EE showed no effects of the independent variables on dependent variables, which are graphically represented in Figure 4.4, indicating none of the independent variables are responsible for the variation in %EE. Figure 4.5 represents the %EE ranging between 98.5 - 99.5% for the 15 formulations obtained from the BBD.

$$\%EE = +99.00 + 0.000\ \mathrm{GMS} + 0.000\ \mathrm{PCL} + 0.000\ \mathrm{Surfactant} + 0.000\ \mathrm{GMS} * \mathrm{GMS} + 0.000\ \mathrm{PCL} * \mathrm{PCL} + 0.000\ \mathrm{Surfactant} * \mathrm{Surfactant} + 0.000\ \mathrm{GMS} * \mathrm{PCL} + 0.000\ \mathrm{GMS} * \mathrm{Surfactant} + 0.000\ \mathrm{PCL} * \mathrm{Surfactant} \quad \text{(Equation 4.2)}$$

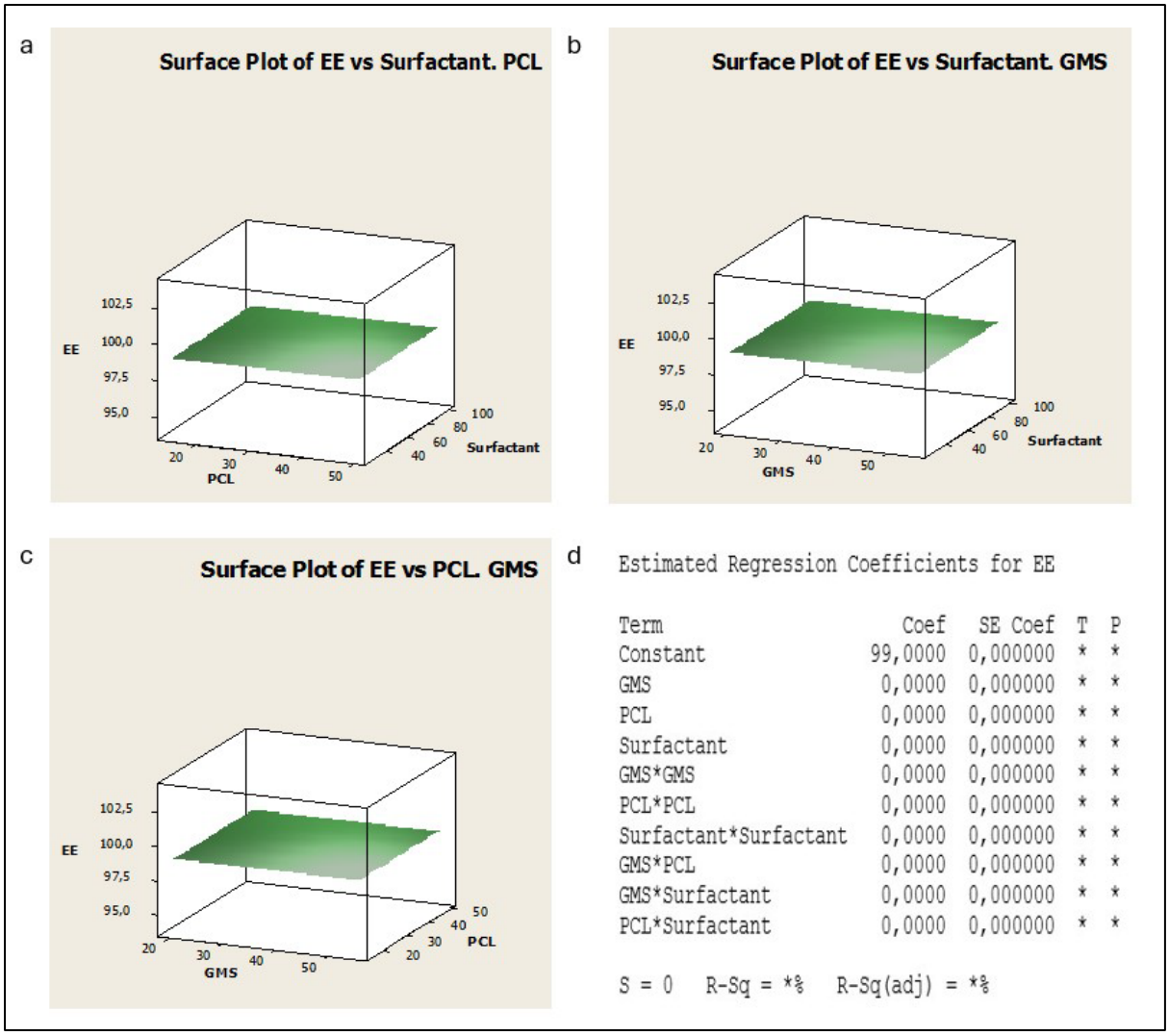

Figure 4.4. Effect of the independent variables i.e. GMS, PCL and Surfactant on the dependent variable i.e. %EE, as represented in (a), (b) and (c), whereas the estimated regression coefficients for %EE is represented in (d).

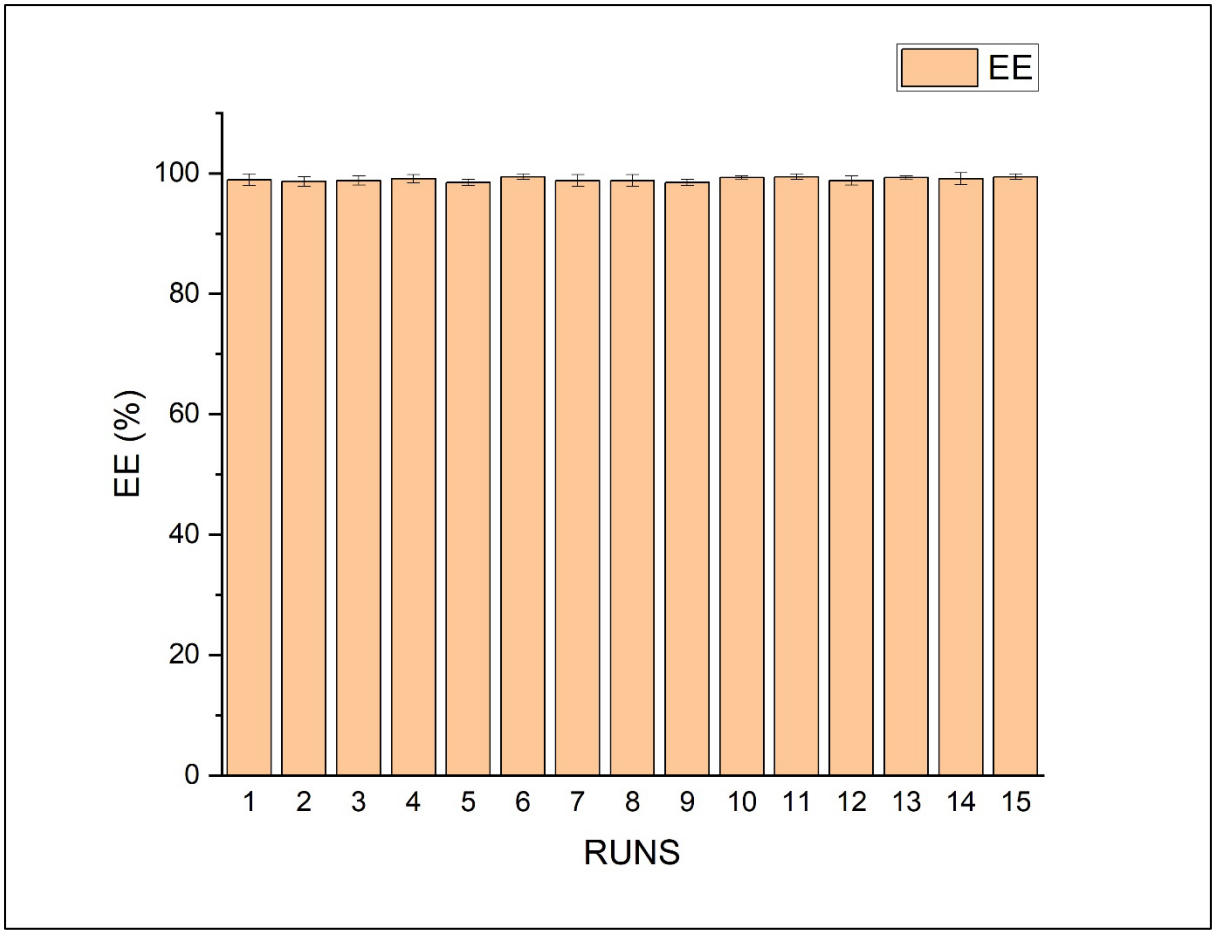

Figure 4.5. Representation of various %EE obtained for the BBD formulations (n = 3).

4.3.1.1.3 Effect of independent variables on dependent variable drug release

The prolonged drug release of BUP is considered optimum in this BUP-loaded SLNs system, as prolonged release of BUP at the site of action would help to overcome the rapid clearance rate and short half-life of BUP, thus giving maximum therapeutic efficacy and a decreased dosing interval. Equation 4.3 obtained from the BBD for drug release showed both positive and negative effects of independent variables on dependent variables, which are graphically represented in Figure 4.6. Additionally, the R^2 and R^2 (adj) had a difference of 1.7% (0.017) which is less than 20% (0.2), indicating that the adopted model was significant (Takalani et al., 2024).

$$Drug\ Release = +4.33163 + 0.0336735\ \mathrm{GMS} + 0.0537415\ \mathrm{PCL} - 0.0157143\ \mathrm{Surfactant} + 5.64388\mathrm{E} - 19\ \mathrm{GMS} * \mathrm{GMS} + 0.000816327\ \mathrm{PCL} * \mathrm{PCL} - 8.08024\mathrm{E} - 20\ \mathrm{Surfactant} * \mathrm{Surfactant} - 8.16327\mathrm{E} - 04\ \mathrm{GMS} * \mathrm{PCL} + 9.79394\mathrm{E} - 21\ \mathrm{GMS} * \mathrm{Surfactant} + 0.000380952\ \mathrm{PCL} * \mathrm{Surfactant} \quad \text{(Equation 4.3)}$$

PCL (+0.0537415) has the higher coefficient variable as compared to GMS (+0.0336735) and Surfactant (-0.0157143) indicating that PCL has a more prominent effect. The positive value

of PCL, including the positive values of interactions between PCL*PCL and PCL*Surfactant, indicates that with the increase in concentration of PCL, a prolonged BUP release from BUP-loaded SLNs can be obtained. Additionally, from the contour plots observed in Figure 4.6, it can be stated that with the increasing concentration of PCL, the prolonged drug release from BUP-loaded SLNs can be obtained. Therefore, drug release ranged between 5 to 9 days for the 15 formulations obtained from the BBD, which is represented in Figure 4.7.

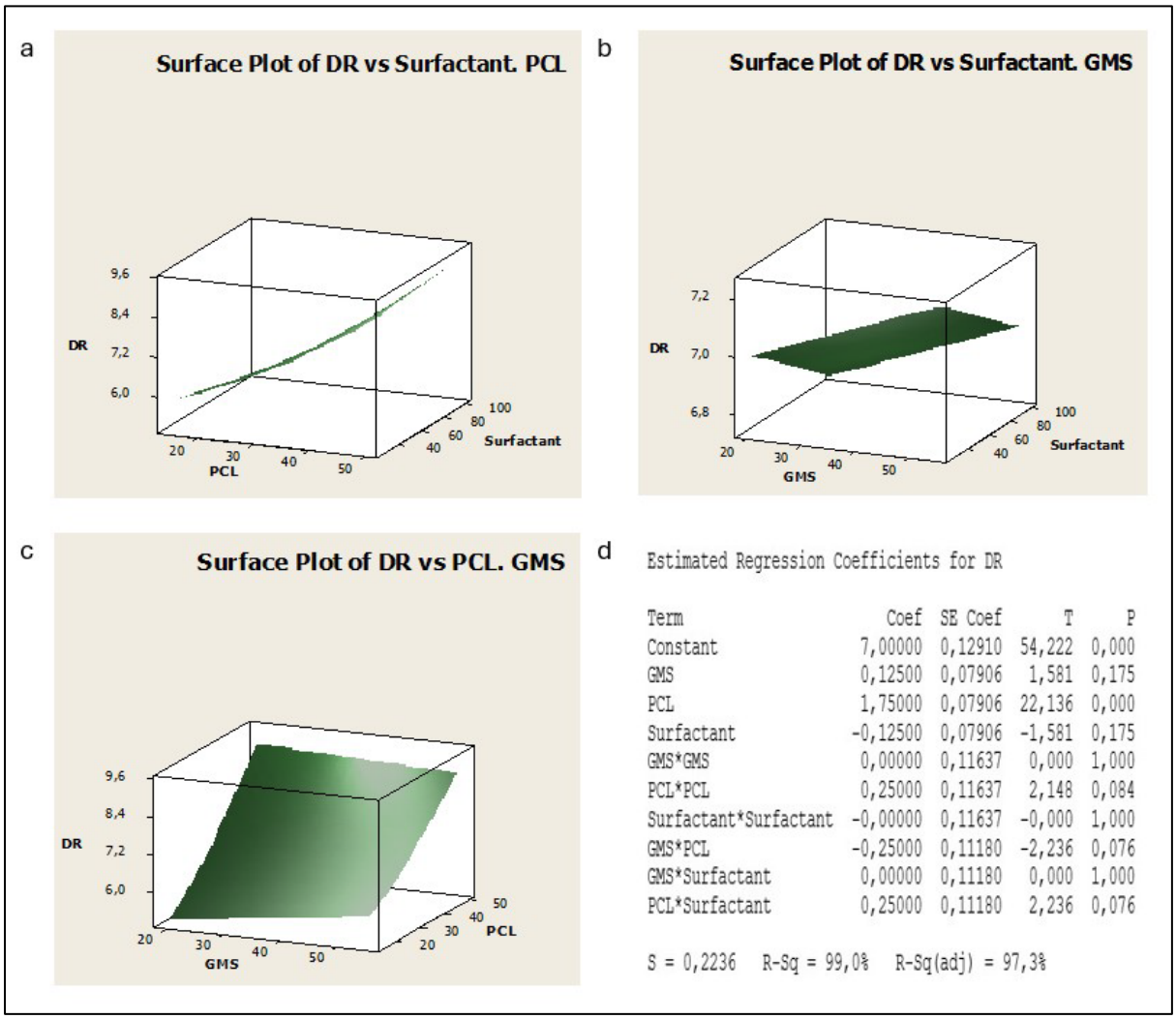

Figure 4.6. Effect of the independent variables i.e. GMS, PCL and Surfactant on the dependent variable i.e. drug release, as represented in (a), (b) and (c), whereas the estimated regression coefficients for drug release is represented in (d).

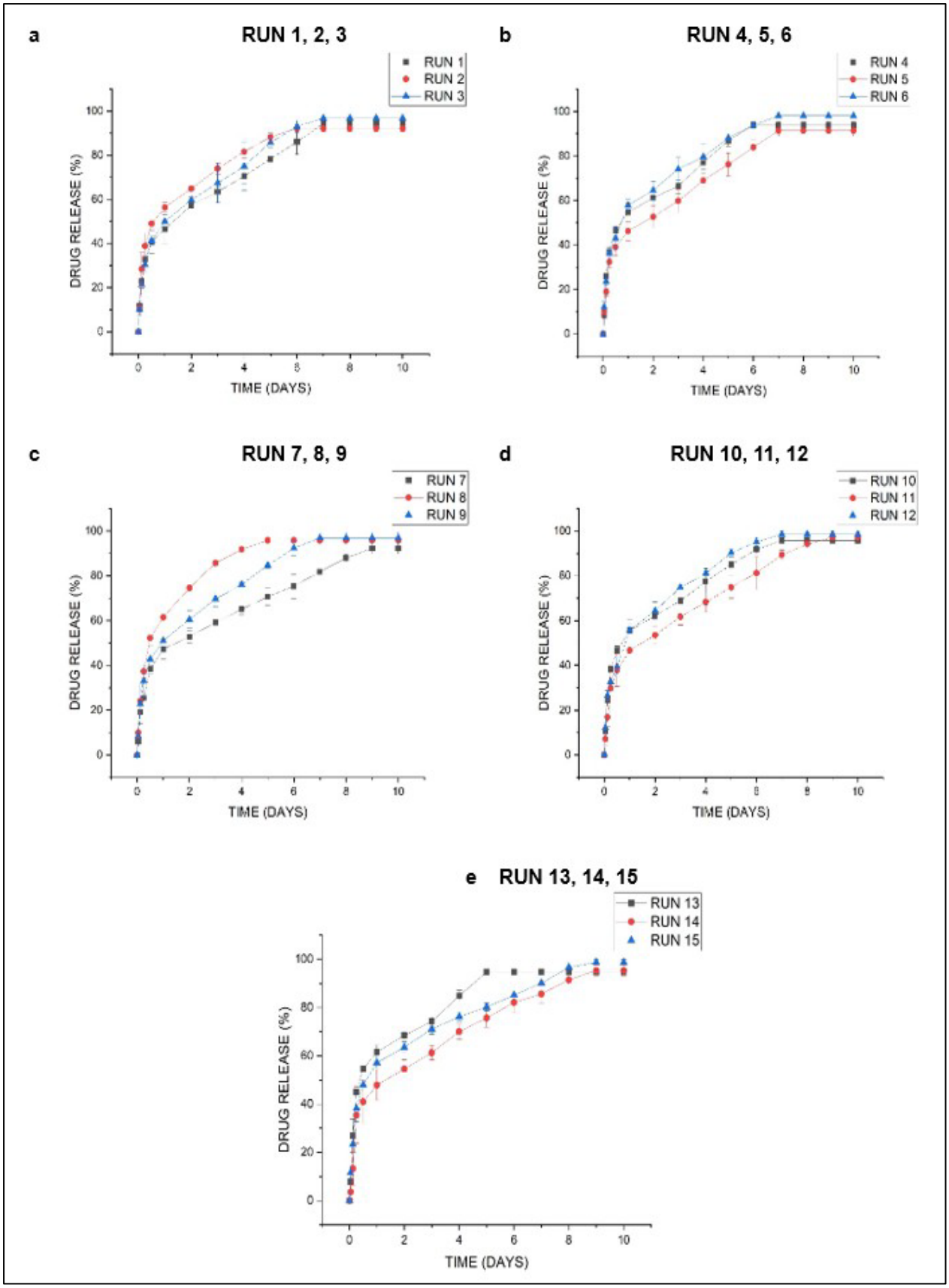

Figure 4.7. Representation of the cumulative *in vitro* drug release profiles of the BUP-SLN formulations obtained from the BBD (n = 3).

4.3.2 Generation of the optimized BUP-loaded SLNs formulation

Using the optimized composition obtained from the BBD (Figure 4.8), the BUP-loaded SLNs were prepared using the modified double emulsification technique, as provided in Chapter 3 (3.2.2). The optimized formulation composition included BUP (2 mg), PCL (32.13 mg), Pf-127 (80.38 mg), tween 80 (16.07 µL) and GMS (50.82 mg). Table 4.5 provided a comparison between the predicted and experimental values of particle size, %EE and maximum drug release for the optimized BUP-loaded SLNs.

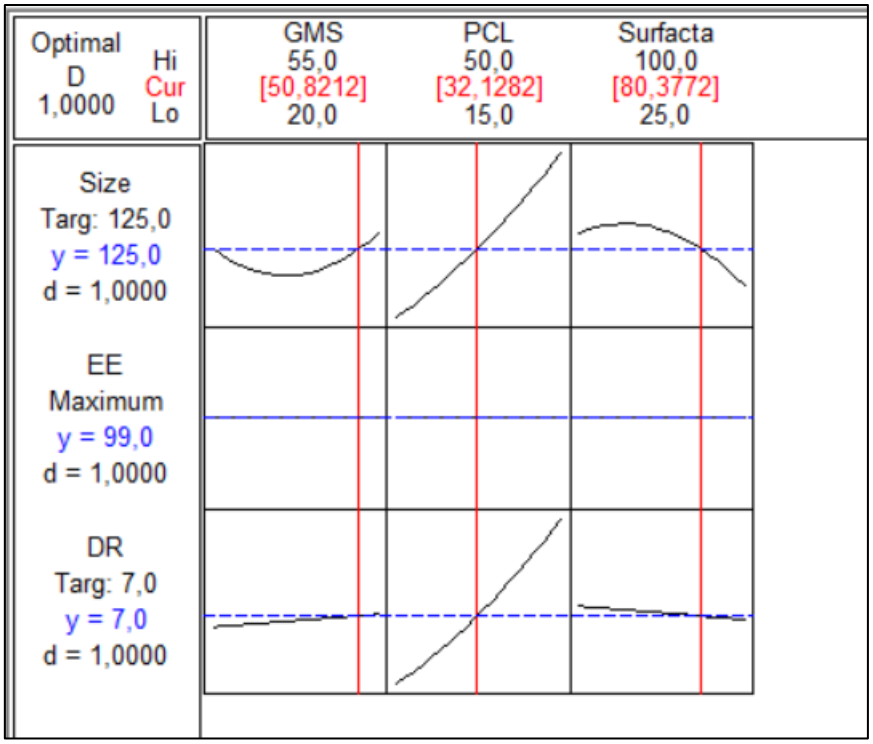

Figure 4.8. Representation of the formulation composition obtained for the preparation of the optimized BUP-loaded SLNs, including the desired values of dependent variables using the BBD.

Table 4.5. Predicted, experimental and desirability values of particle size, %EE and maximum drug release of the optimized BUP-loaded SLNs.

Dependent Variables	Predicted Values	Experimental Values	Desirability Values
Particle Size (nm)	125	128.2 ± 2.03	97.44%
EE (%)	99	99.2 ± 0.70	99.80%
Maximum Drug Release (Days)	7	7 ± 0	100%

4.3.3 Characterization of the optimized BUP-loaded SLNs

4.3.3.1 Evaluation of the particle size, PDI, zeta potential and surface morphology

As per the results obtained in the study conducted by Bazargani et al., SLNs within the range of 40-200 nm are preferable for easy bypass across the BBB (Bazargani et al., 2025). The mean particle size (Figure 4.9 a and c) of the unloaded and BUP-loaded SLNs were found to be 135.5 ± 3.79 and 128.2 ± 2.03 nm, respectively, suggesting that the SLNs could easily cross the BBB, as they were within the acceptable range. The PDI (Figure 4.9 a and c) of the unloaded and BUP-loaded SLNs were found to be 0.165 ± 0.02 and 0.154 ± 0.01, respectively. The lower values of PDI ≤ 0.3 suggest the uniform distribution of the SLNs across the dispersion (Danaei et al., 2018). The zeta potential (Figure 4.9 b and d) of the unloaded and BUP-loaded SLNs were found to be -18.2 ± 2.71 and -19.8 ± 1.55 mV suggesting that the SLNs are stable and less prone to form aggregates (Pandya et al., 2018). The results obtained from the Zeta-Sizer Nano-ZS instrument were further verified by SEM for particle size and surface morphology. The unloaded and BUP-loaded SLNs were found to be under 200 nm and with a spherical shape when observed using the SEM, as represented in Figure 4.10 (a) and (c), which were found to be similar with the results obtained by Yasir et al. (2021). A comparison between Figure 4.10 (a) and (b) and Figure 4.10 (c) and (d), indicated that the in-lens images of both the unloaded and BUP-loaded SLNs i.e. Figure 4.10 (b) and (d) showed the inner polymer matrix being surrounded by the solid lipid layer i.e. GMS. Additionally, Figure 4.10 (c) showed no crystals of BUP being present in the surrounding, or on the surface of the imaged BUP-loaded SLNs, indicating the complete encapsulation of BUP, suggesting no burst release of BUP would occur, similar to the study conducted by Naik et al. (2024).

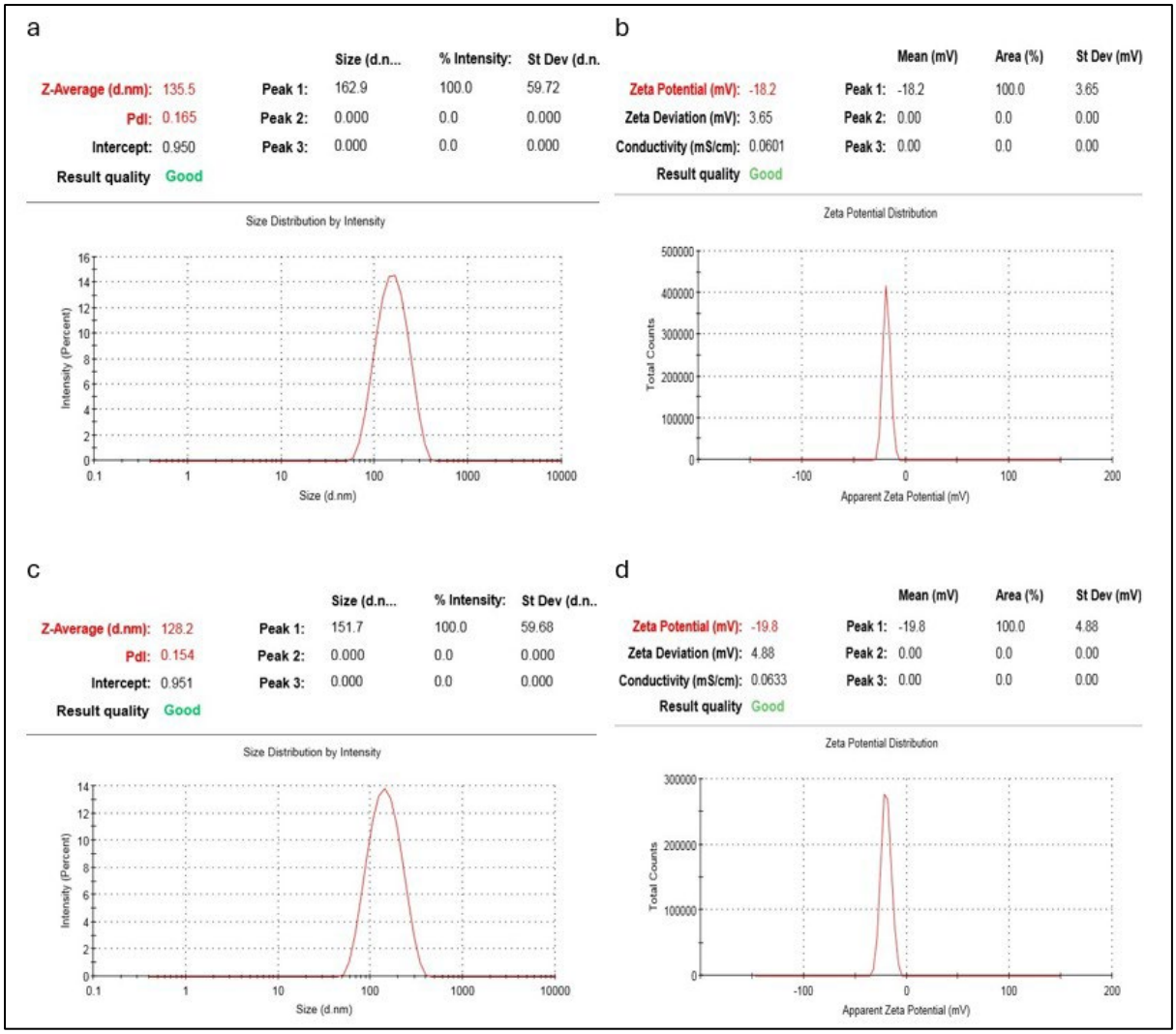

Figure 4.9. Profiles of (a) the particle size and PDI of the unloaded SLNs, (b) the zeta potential of the unloaded SLNs, (c) the particle size and PDI of the optimized BUP-loaded SLNs and (d) the zeta potential of the optimized BUP-loaded SLNs.

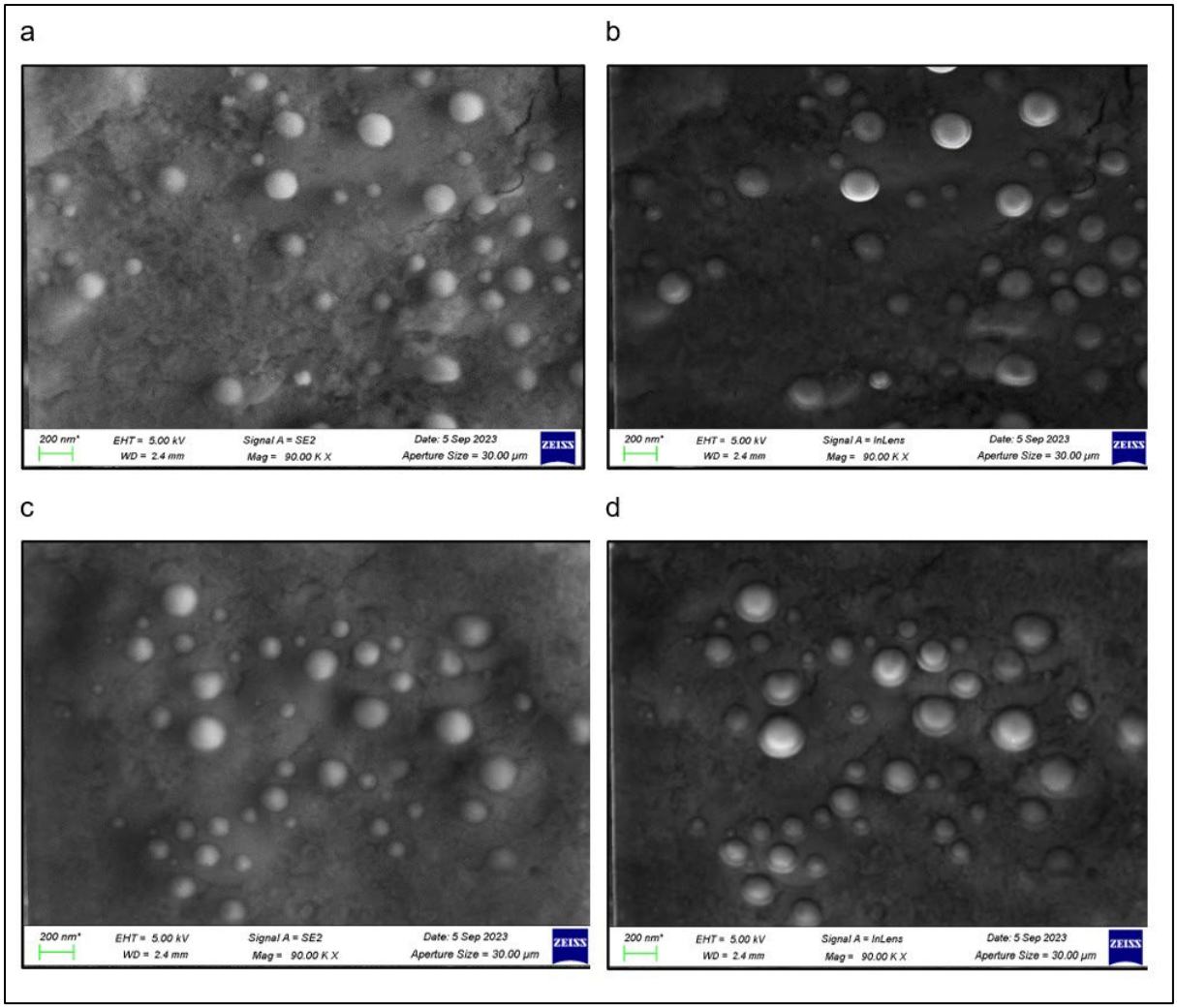

Figure 4.10. SEM micrographs of (a) the secondary lens imaging of the unloaded SLNs, (b) the in-lens imaging of the unloaded SLNs, (c) the secondary lens imaging of the optimized BUP-loaded SLNs and (d) the in-lens imaging of the optimized BUP-loaded SLNs.

4.3.3.2 Determination of the %LC and %EE

The %LC and %EE of the optimized BUP-loaded SLNs were found to be 4.5 ± 0.40% and 99.2 ± 0.71% respectively, representing a stable PCL and Surfactant polymer matrix within the GMS-coated SLNs to encapsulate higher percentage of BUP.

4.3.3.3 *In vitro* drug release of the BUP-loaded SLNs

In vitro drug release studies (n = 3) were conducted to determine the release profile of BUP from the optimized BUP-loaded SLNs. Approximately 50% of BUP was released from the BUP-loaded SLNs by the end of day 1 (24 hours) and the remaining 50% BUP was released over a period of next 6 days (144 hours), indicating a release profile of BUP from BUP-loaded SLNs over a period of 7 days (168 hours), as represented in Figure 4.11. With the achievement of this release profile of BUP, it can be confirmed that the residence time of BUP at the site of action may be increased with the incorporation of BUP in the polymeric SLNs. Additionally,

the co-efficient of correlation (R^2) values were found to be 0.3479, 0.8251, 0.8684, 0.9852 and 0.7561 for Zero order, First order, Higuchi, Korsmeyer-Peppas and Hixson-Crowell models, respectively, as represented in Figure 4.12. As the R^2 value 0.9852 is closest to 1, it is considered as best fitting, indicating that BUP release from the BUP-loaded SLNs follow the Korsmeyer-Peppas model of release kinetics. The obtained release exponent n from the Korsmeyer–Peppas model was 0.299 which further confirms that the mechanism of BUP release exhibited a Fickian transport, implying that the release of BUP was controlled by diffusion, where BUP move through the polymer matrix. Additionally, the high value of Korsmeyer–Peppas kKP parameter (20.721) suggested that a burst release occurred during the initial phase of the release (Abdelgader et al., 2024; Danyuo et al., 2019).

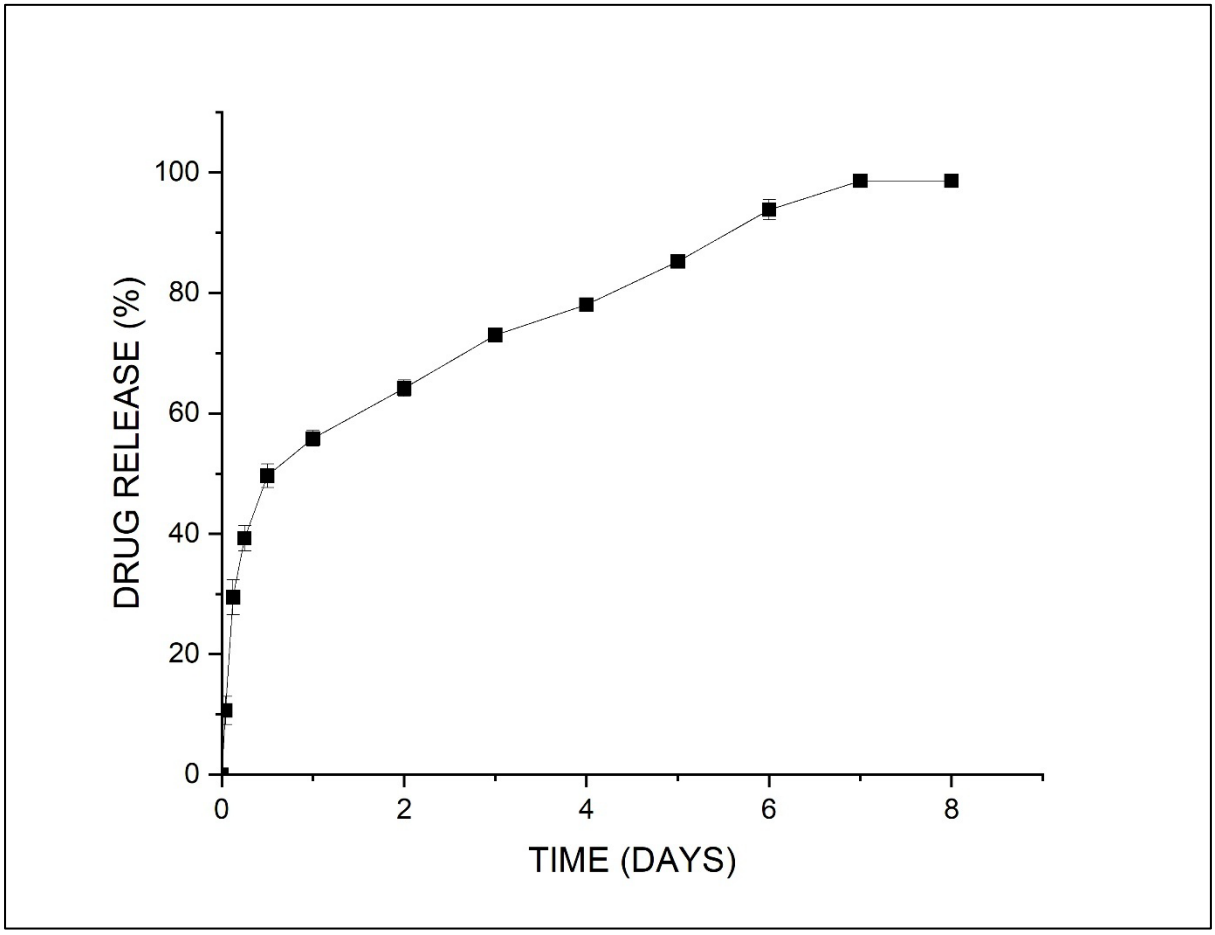

Figure 4.11. Representation of the *in vitro* drug release profile of BUP from the optimized BUP-loaded SLNs (n = 3).

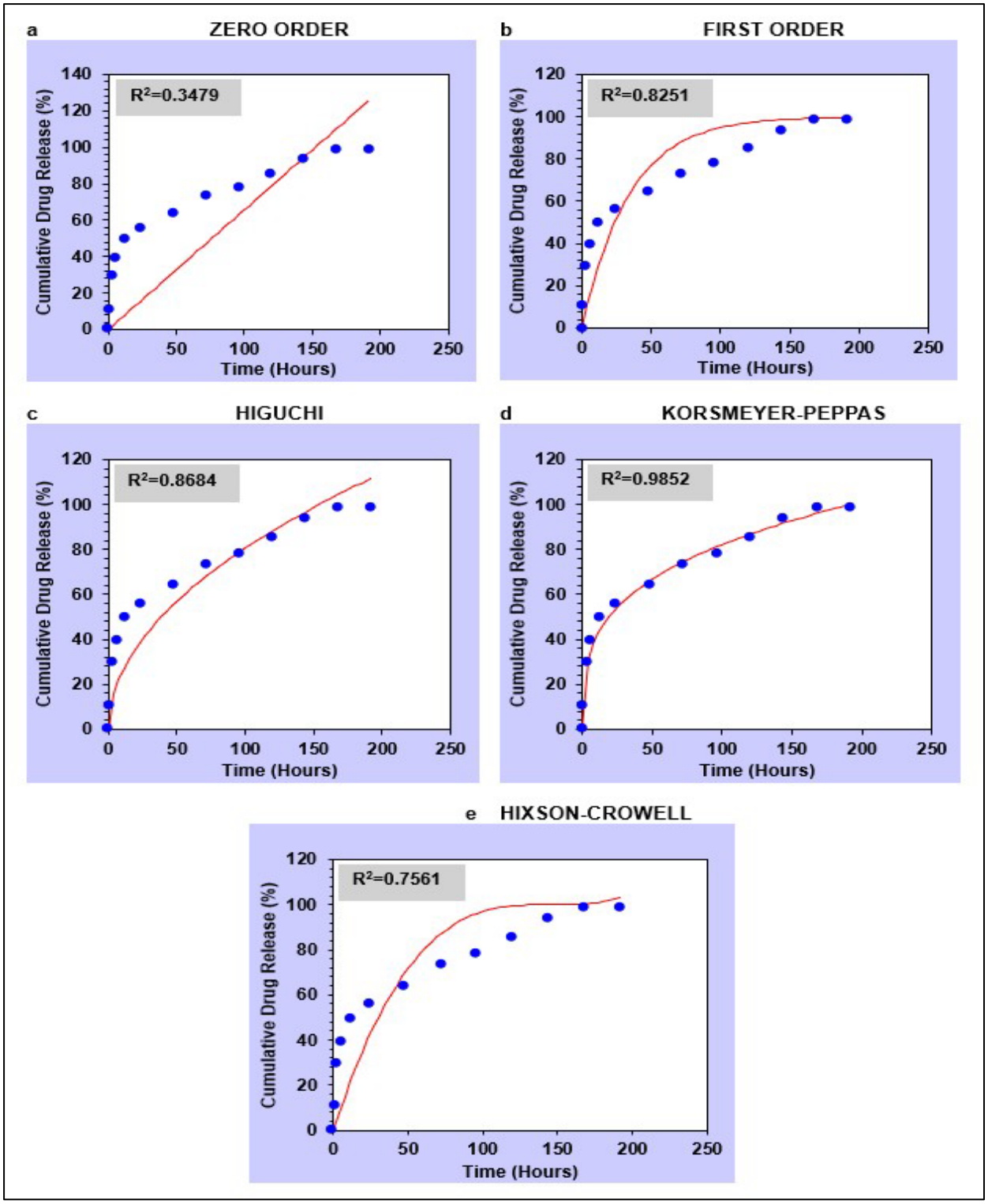

Figure 4.12. Representation of the *in vitro* BUP release profile data fitted to various kinetic models.

4.3.3.4 Molecular structure assessment

The FTIR spectra of all the starting materials, including the optimized unloaded and BUP-loaded SLNs, are represented in Figure 4.13. The characteristic FTIR peaks of BUP: 3545 cm^{-1} (O-H), 3136 cm^{-1} (N-H), 1470 cm^{-1} (aromatic) and 1112 cm^{-1} (C-O-C) were present,

which were similar to that described in previous research (Alizadeh et al., 2019; Mohammadi et al., 2020). Evaluation of the GMS spectrum revealed peaks at 3299 cm^{-1} (O-H), 1729 cm^{-1} (C=O) and 1179 cm^{-1} (C-O) were present, consistent with the study by Ng et al. (2018). PCL additionally displayed peaks at 2943 and 2866 cm^{-1} (asymmetric CH_2), 1720 cm^{-1} (C=O) and 1236 cm^{-1} (C-O-C), in line with the results obtained by Ali et al. (2014). Analysis of the FTIR spectra of the unloaded SLNs showed peaks at 3299 cm^{-1} (O-H), 2919 and 2850 cm^{-1} (C-H alkane), 1724 cm^{-1} (C=O) and 1180 cm^{-1} (C-O). The BUP-loaded SLNs showed the same or similar characteristic peaks at 3298 cm^{-1} (O-H), 2917 and 2853 cm^{-1} (C-H alkane), 1730 cm^{-1} (C=O) and 1181 cm^{-1} (C-O) validating the synthesis of SLNs, as the characteristic peaks of unloaded and BUP-loaded SLNs were found to be the same as GMS, indicating the outer layer of SLNs were made of GMS, consistent with the SEM images represented in Figure 4.10. This results can also be compared with the results obtained by Ebrahimi et al. (2015), where the characteristic peaks of BUP: 3136 cm^{-1} (N-H) and 1470 cm^{-1} (aromatic) were absent in the BUP-loaded SLNs, representing the complete encapsulation of BUP within the polymeric core (Ebrahimi et al., 2015).

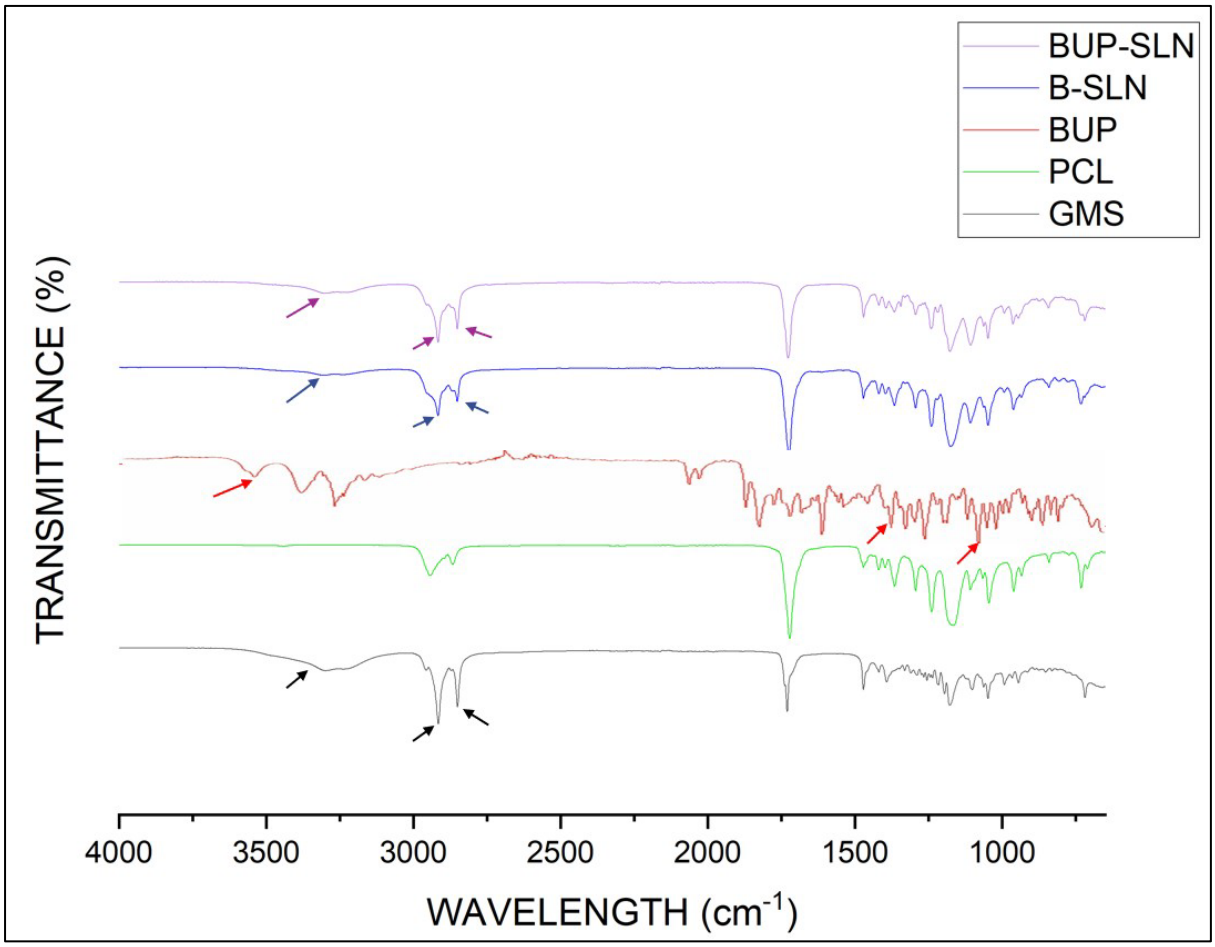

Figure 4.13. FTIR spectra of the BUP-loaded SLNs, unloaded SLNs (B-SLNs), BUP, PCL and GMS.

4.3.3.5 Determination of the thermal characteristics

DCS analysis was performed on all the starting materials, as well as on the unloaded and optimized BUP-loaded SLNs, for the determination of their thermal behaviours, as represented in Figure 4.14. Pf-127 and GMS showed endothermic peaks at 58 °C and 65.8 °C, whereas PCL showed endothermic peaks at 68.2 °C and 385 °C, comparative to previous studies (Karolewicz et al., 2014; Kerman et al., 2005; Ng et al., 2018). BUP showed a characteristic endothermic peak at 289.5 °C, which can be further verified by the results obtained in the study by Yeola et al. (2014). The unloaded SLNs showed endothermic peaks at 55.3 °C, 62.7 °C and initiation of one at 387 °C. BUP-loaded SLNs further showed endothermic peaks at 54.8 °C, 61.2 °C and initiation of one at 387 °C. The endothermic peaks of both the unloaded and BUP-loaded SLNs are similar and lied within the range of Pf-127, PCL and GMS indicating the formation of SLNs (Yasir and Sara, 2014). Additionally, the BUP-loaded SLNs showed a characteristic endothermic peak at 281 °C, which is a similar peak to BUP indicating the encapsulation of BUP within the SLNs.

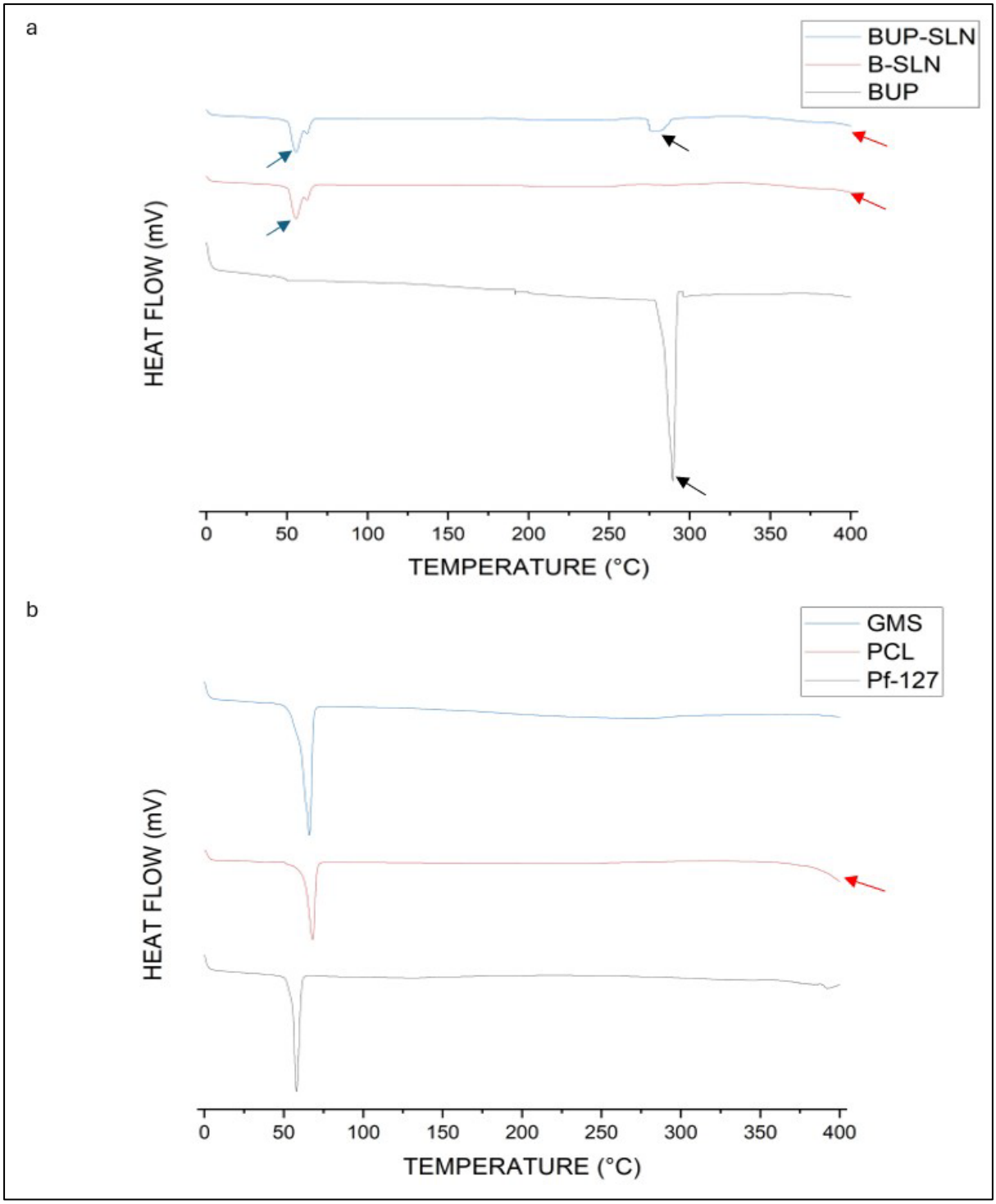

Figure 4.14. DSC thermograms of (a) BUP, unloaded (B-SLN) and optimized BUP-loaded SLNs and (b) Pf-127, PCL and GMS used for the synthesis of both the SLNs.

4.3.3.6 Determination of the degradation rate

TGA analysis was done on all the starting materials, as well as on the optimized unloaded and BUP-loaded SLNs, as represented in Figure 4.15 to determine their degradation rates. The % weight loss of the unloaded SLNs and BUP-loaded SLNs started at 221 °C and 193.7 °C respectively. By the end i.e. 600 °C, 4.9% and 6.8% of unloaded and BUP-loaded SLNs still

remained, indicating the formation of GMS-coated SLNs, as 15.3% of GMS remained undegraded at 600 °C, consistent with the study carried out by Tian et al. (2018). Additionally, 1.9% more of the BUP-loaded SLNs were detected, compared to the unloaded SLNs, which indicated the presence of BUP, as 14.9% of BUP remained undegraded at 600 °C (Guguta et al., 2009; Tian et al., 2018).

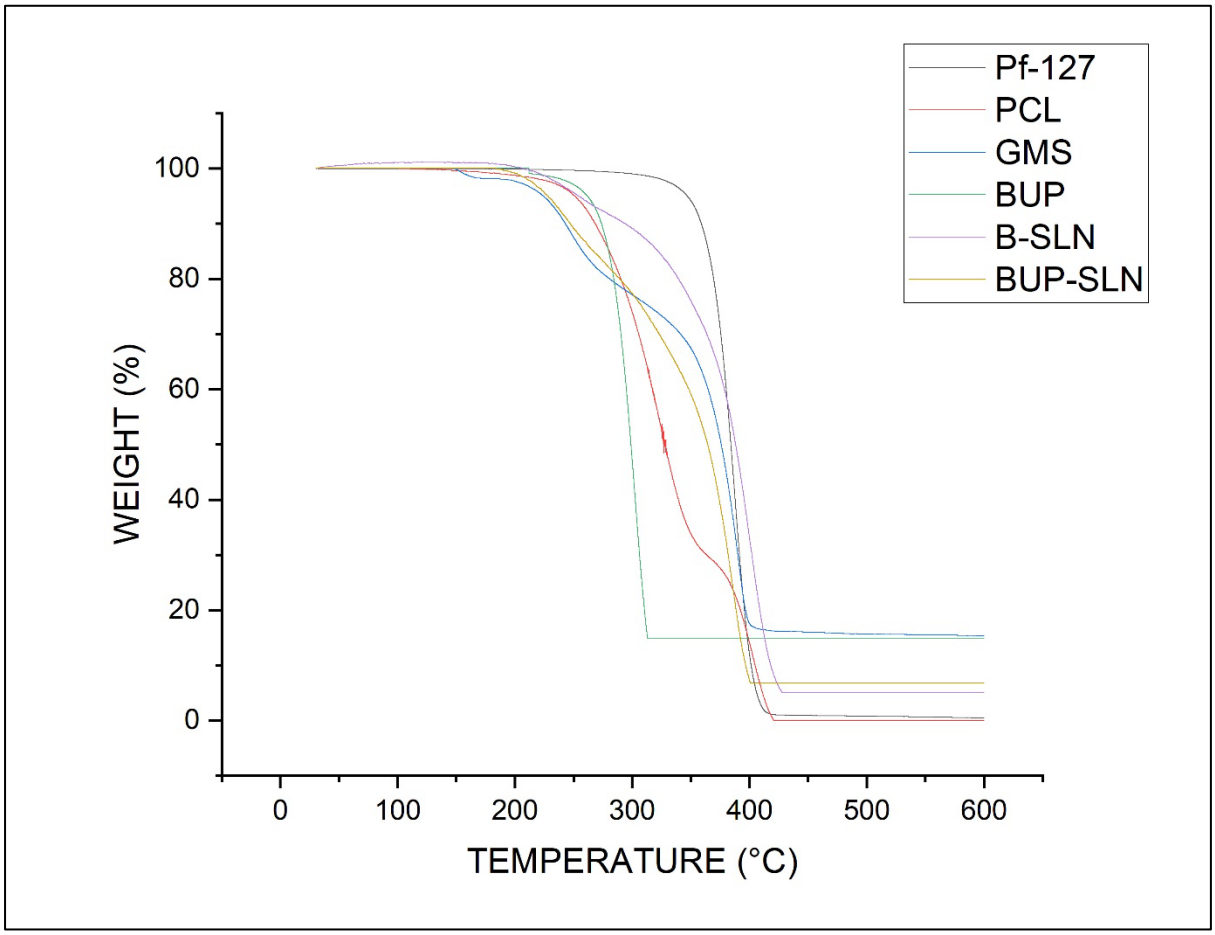

Figure 4.15. TGA thermograms of the unloaded (B-SLN) and optimized BUP-loaded SLNs including all the materials used for the synthesis of SLNs.

4.3.4 Cell culture and cytotoxicity studies

The assessment for potential cytotoxicity of the BUP-loaded SLNs on HEK293 cells is represented in Figure 4.16. To determine cytocompatibility, cell treatment groups were incubated for 24, 48 and 72 hours in the presence of various concentrations of BUP (2.5 - 320 µg/mL), BUP-loaded SLNs (equivalent to 2.5 - 320 µg/mL) and SLNs without BUP and compared to a positive control or untreated cells. Figure 4.17 represents the microscopic imaging of positive control, negative control, BUP, unloaded SLNs and BUP-loaded SLNs treated cells taken after 48 hours using an inverted microscope with 4× magnification. After 24 hours, the maximum concentration of BUP, unloaded SLNs and BUP-loaded SLNs showed a cell viability of 89.29 ± 0.02%, 92.54 ± 2.98% and 90.72 ± 0.03%, respectively, whereas the

minimum concentrations showed 94.11 ± 0.01%, 95.09 ± 3.70% and 95.61 ± 0.02% cell viability. At 48 hours, the maximum concentration of BUP, unloaded SLNs and BUP-loaded SLNs showed cell viability of 84.69 ± 0.02%, 88.09 ± 2.37% and 88.54 ± 0.02%, respectively, whereas the minimum concentrations showed 88.74 ± 0.05%, 93.25 ± 2.79% and 92.06 ± 0.08% cell viability, while after 72 hours, the maximum concentration of BUP, unloaded SLNs and BUP-loaded SLNs showed cell viability of 81.54 ± 0.05%, 84.77 ± 2.62% and 85.39 ± 0.04%, respectively, while the minimum concentrations showed 85.01 ± 0.02%, 89.31 ± 1.82% and 88.61 ± 0.03% cell viability. Statistical evaluation of the data noted a statistical significance at all time points and concentrations ($p < 0.01$), when compared to the positive control, due to the low variability between samples and the consistent values across sample runs. However, as per ISO 10993-5, a %cell viability above 80% is considered non-cytotoxic; within 80% - 60% weakly; 60% - 40% moderately and below 40% strongly cytotoxic (López-García et al., 2014). Thus, from the data obtained it can be concluded that BUP, unloaded SLNs and BUP-loaded SLNs showed good cytocompatibility, as even after 72 hours, none of the %cell viability dropped below 80%, indicating no cytotoxic effect was observed. Additionally, as determined from the data obtained, it can be concluded that the BUP-loaded SLNs had equivalent or greater cell viability when compared to pure BUP and the unloaded SLNs, indicating that the incorporation of BUP within SLNs helped in improving the cytocompatibility properties of BUP.

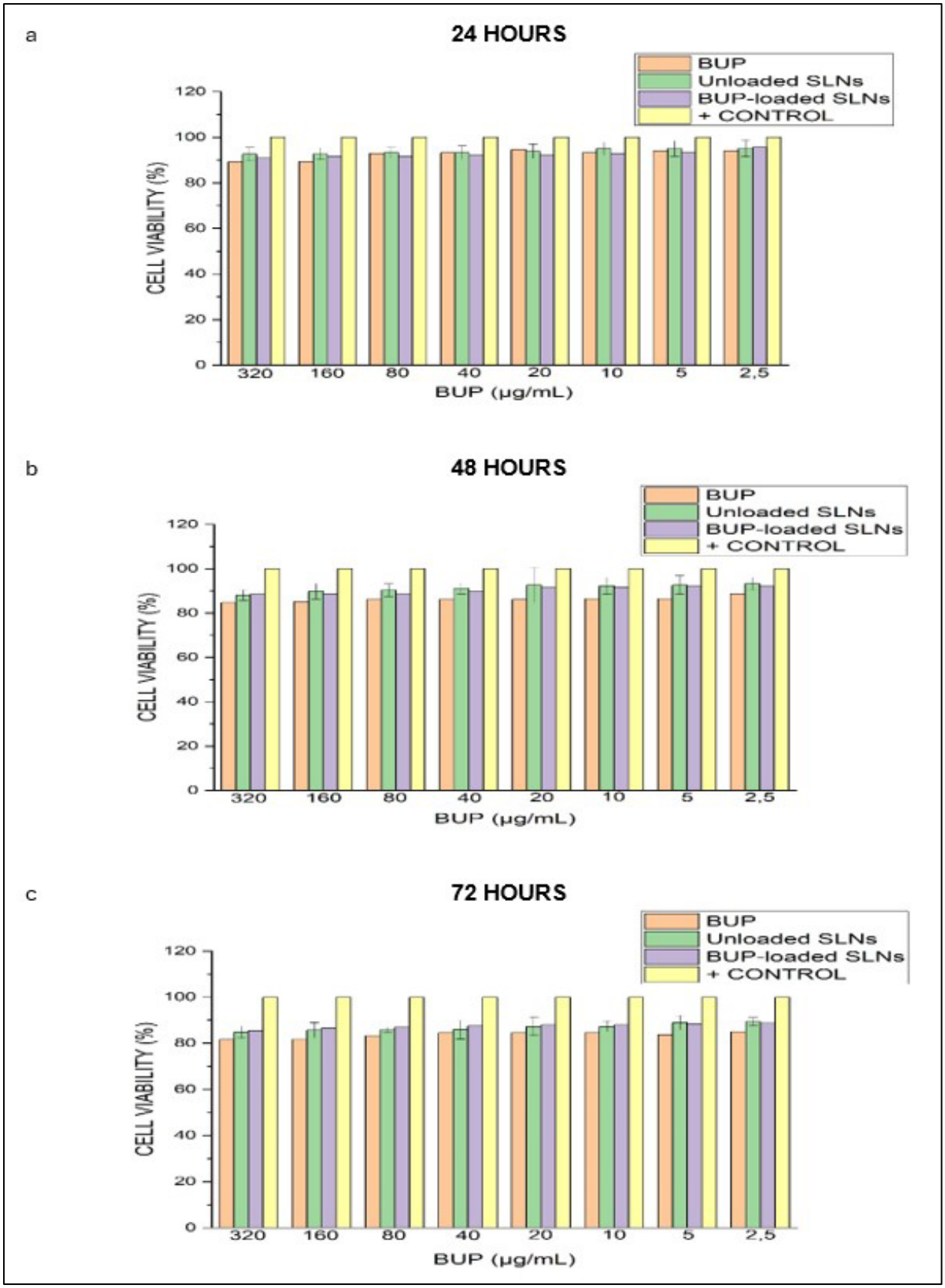

Figure 4.16. HEK293 cell cytocompatibility after treatment with various concentrations of BUP, unloaded SLNs and BUP-loaded SLNs for (a) 24 hours (b) 48 hours and (c) 72 hours ($n = 3$ and $p \leq 0.01$ at all cases).

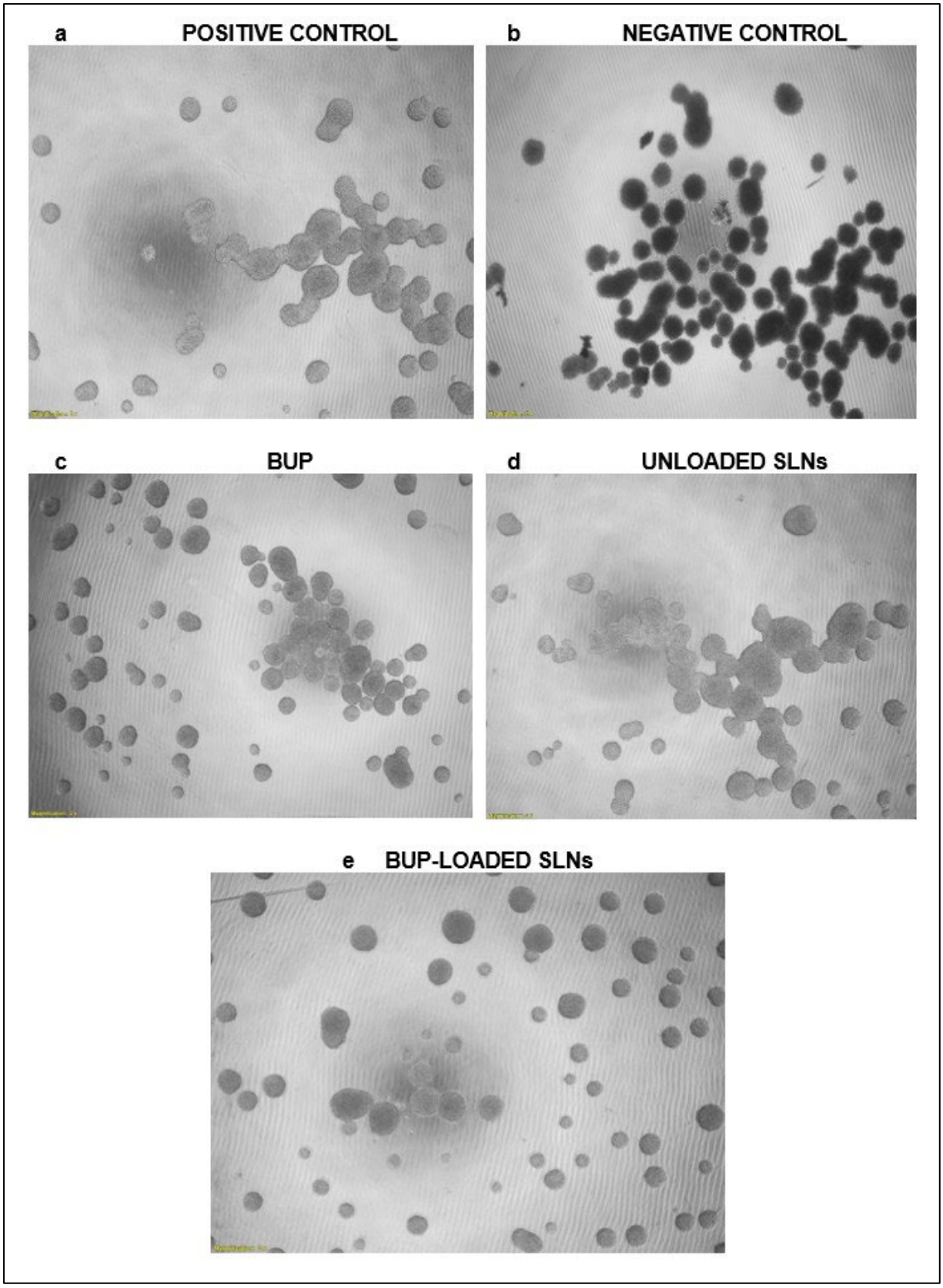

Figure 4.17. Representation of the microscopic imaging of (a) the positive control, (b) the negative control, (c) BUP, (d) unloaded SLNs and (e) the optimized BUP-loaded SLNs treated cells All images were taken after 48 hours at 4X magnification.

4.4 Conclusion

In this chapter, polymeric BUP-loaded SLNs were synthesized for the sustained release of BUP, potentially overcoming its poor pharmacokinetic properties. The polymeric BUP-loaded SLNs were successfully formulated using the modified double emulsification technique, where the desired particle size, PDI and zeta potential were obtained. Additionally, further verification of the particle size and shape was undertaken using SEM imaging ensuring that the SLNs would cross the BBB. The desired physicochemical properties of the BUP-loaded SLNs were obtained and confirmed using FTIR, DSC and TGA, ensuring their desired molecular transition and stable thermal behaviour. The maximum %EE and %LC of BUP within the SLNs was further obtained and *in vitro* release of BUP from the SLNs was observed over a period of one week (7 days), which suggested potential increased bioavailability of BUP across the BBB and an increased residence time at the site of action. The BUP-loaded SLNs additionally showed no significant signs of *in vitro* cytotoxicity against HEK293 cells, indicating their excellent cytocompatibility. Therefore, with the achievement of the desired properties from the BUP-loaded SLNs, it can be an effective potential treatment for OUD alone and in combination with other synergistic interventions, such as the NLX-loaded SLNs developed in Chapter 3. The following chapter therefore explores the potential to incorporate the optimized NLX-loaded SLNs developed in Chapter 3 and the optimized BUP-loaded SLNs in this chapter within a intranasally administered drug delivery system for the treatment of OUD.

CHAPTER 5
A THERMO-RESPONSIVE NASAL GEL SYSTEM FOR THE TARGETED, SUSTAINED RELEASE OF BUPRENORPHINE AND NALOXONE

5.1 Introduction

CNS diseases and disorders like Parkinson's, Alzheimer's, stroke and epilepsy are currently among the major global health concerns and are second only to cardiovascular diseases, as per Lancet Neurology and the Global Burden of Diseases (Agrawal et al., 2018; Wang et al., 2024). Approximately, 805 million people worldwide are affected due to CNS diseases and disorders and among them, OUD affects a significant proportion (Wang et al., 2024). BUP and NLX are one of the most preferred drugs in the treatment of OUD, but due to their plasma half-life and oral bioavailability, they have major drawbacks (Mooney and Saxon, 2019; Saari et al., 2024). However, through the combination of enhancements in pharmacology and advanced DDSs, the poor pharmacokinetic and pharmacodynamic properties of BUP and NLX can be resolved.

As compared to the other drug delivery routes available, the nasal route is one of the most preferred routes for the delivery of therapeutic agents to the CNS because of the direct passage between the nasal mucosa and CNS (Chaturvedi et al., 2011). Additionally, the nasal route contributes to therapeutic efficacy by avoiding the first-pass metabolism, allowing for increased bioavailability by avoiding systemic exposure, overcoming disadvantages of BBB and by providing a more patient compliant alternative, when compared to other delivery routes (Cunha et al., 2021). Figure 5.1 represents the intranasal route and key components involved in nose-to-brain drug delivery.

Although the nasal route is advantageous, the mucociliary clearance mechanism plays a significant role as a barrier to the delivery mechanism and absorption of the therapeutic agents (Giunchedi et al., 2020; Gupta and Kumar, 2019). However, with the addition of thermo-responsive and mucoadhesive polymers that increase the viscosity of the DDSs, the mucociliary clearance mechanism can be overcome. This mucoadhesive ISTG formulation establishes an electrostatic interaction between the formulation and the mucin present within the nasal mucosa, resulting in an increase in the residence time within the nasal cavity (Martins et al., 2019).

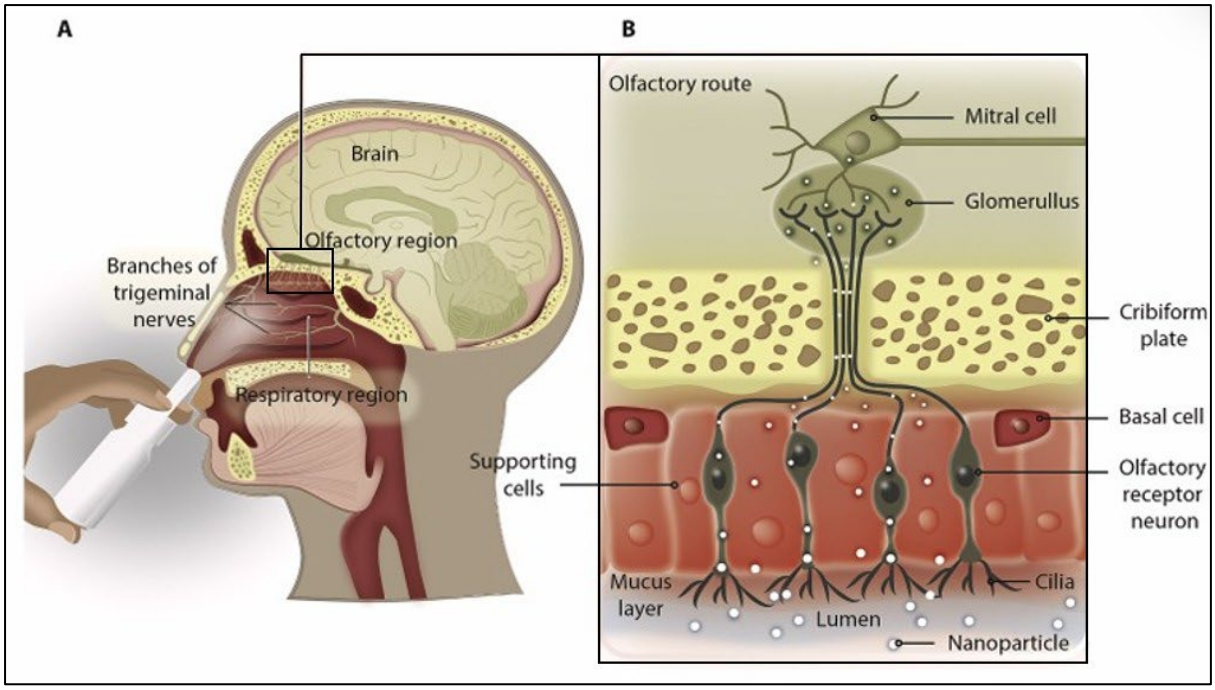

Figure 5.1. Schematic representation of (A) the anatomical features of intranasal route and (B) key components involved in delivering nanosystems from the nose to brain (Reproduced with permission from Formica et al. (2022), © 2022 The Author(s)).

Poloxamer, also known as Pluronic (Pf-127) is one of the most preferred thermo-responsive polymers for nose-to-brain DDSs. It is a non-ionic, hydrophilic triblock copolymer of polyoxyethylene-polyoxypropylene-polyoxyethylene (POE-POP-POE) exhibiting thermo-reversible properties where, it remains as a liquid dosage form at lower or normal room temperature and forms a gel at physiological body temperature depending on the concentration of Pf-127 used (Paavola et al., 2016; Wang et al., 2024). As per Cunha et al., Pf-127 on its own, however, has very less or no mucoadhesive properties therefore, the addition of mucoadhesive agent like HPMC is necessary to increase the residence time of the formulation within the nasal cavity (Cunha et al., 2022). HPMC is a non-ionic, non-toxic, biodegradable and biocompatible polymer with emulsifying, suspending, viscosity-enhancing and mucoadhesive properties (Fahmy, 2012; Patel and Bummer, 2017). Therefore, the combination of Pf-127 and HPMC is majorly used for the preparation of nose-to-brain mucoadhesive ISTG DDS. Additionally, the incorporation of nanosystems within the ISTG matrix is considered as an effective way to deliver drugs to the CNS, as it acts as a protective barrier against enzymatic degradation and mucociliary clearance of the therapeutic nanosystem in the nasal passage (Akilo et al., 2019; Cunha et al., 2022; Wu et al., 2007).

The NLX- and BUP- loaded SLNs dispersion as formulated in Chapter 3 and 4, respectively, possesses low viscosity and low mucoadhesiveness which can potentially hinder their nasal residence time, leading to decreased nasal systemic absorption and decreased nose-to-brain

drug delivery. Therefore, both BUP- and NLX- loaded SLNs dispersion were formulated in the form of ISTG, which remains as a liquid dosage form at normal room temperature and undergoes sol-gel transition when comes in contact with the physiological intranasal temperature i.e. 34 °C, allowing for maximal drug delivery to the CNS. This chapter provides for the design and optimization of a sustained-release BUP and NLX containing SLN-loaded ISTG (DSLN-loaded ISTG) for the management of OUD with the aim of providing better therapeutic efficacy through reduced dosing frequency, reduced dosage, improved bioavailability and increased patient compliance. The optimized DSLN-loaded ISTG was characterized for its physicochemical properties such as molecular transition, sol-gel transition temperature ($T_{sol-gel}$), viscosity and thermal behaviour followed by the *in vitro* drug release studies of BUP and NLX. Through *ex vivo* permeation studies the permeability of BUP- and NLX- loaded SLNs from the DSLN-loaded ISTG across the nasal membrane was assessed in addition to the drug release from the SLNs after permeation. Lastly, biocompatibility studies of the DSLN-loaded ISTG were undertaken using the HEK293 cell line.

5.2 Materials and methods

5.2.1 Materials

BUP, GMS, Tween 80, Pf-127, PCL (Avg Mw = 14 000), HPMC, DCM, Ethanol (99%), DMSO, Mucin from porcine stomach type II and MTT assay kit were purchased from Sigma-Aldrich (St. Louis, Missouri, USA), NLX from Leap Chem (Hangzhou, China), DMEM, FBS, Pen-Strep antibiotic solution and DPBS from ThermoFisher Scientific (Randburg, South Africa) and HEK293 cells from ATCC (LGC-Standards, South Africa). All other chemicals were of analytical grade and used as received.

5.2.2 Preparation and optimization of the ISTG

The cold method as described by Schmolka et al., was used for the preparation of the ISTG (Fatouh et al., 2017; Schmolka, 1972). Briefly, HPMC was added slowly to chilled Milli-Q distilled water maintained at 4 °C followed by the slow addition of Pf-127 under constant stirring. This mixture was thereafter refrigerated overnight for the complete dissolution of HPMC and Pf-127 to form the ISTG and freeze-dried using a lyophilizer to obtain dry powder. The solution form of ISTG were used for the primary screening of $T_{sol-gel}$, viscosity and mucoadhesion. The freeze-dried ISTG were formulated to increase the shelf-life of the formulation and avoid the premature release of the loaded drugs from the SLNs into the ISTG. For the optimization of ISTG, various formulations comprising of different concentrations of Pf-127 and lyophilized (LYO) Pf-127 along with HPMC were formulated which are represented in Table 5.1. and the optimized ISTG was determined based on their $T_{sol-gel}$, viscosity and mucoadhesion.

Table 5.1. Formulations comprising of different concentrations of Pf-127 and HPMC along with Pf-127.

Formulations
17% Pf-127
19% Pf-127
21% Pf-127
17% Pf-127 LYO
17% Pf-127+0.1% HPMC LYO
17% Pf-127+0.2% HPMC LYO
17% Pf-127+0.3% HPMC LYO

5.2.2.1 Determination of the ISTG $T_{sol-gel}$

5.2.2.1.1 Stirring magnetic bar method

The stirring magnetic bar method (n = 3), as described by Dorraj and Moghimi was used for the determination of the $T_{sol-gel}$ of all ISTGs (Dorraj and Moghimi, 2015). Briefly, for this analysis, 10 mL of each formulation was placed in a 50 mL beaker and observed over 10 to 40 °C, while stirring at 200 rpm using a magnetic bar over a magnetic stirrer, as represented in Figure 5.2. The temperature at which the magnetic bar stopped motion was considered as $T_{sol-gel}$.

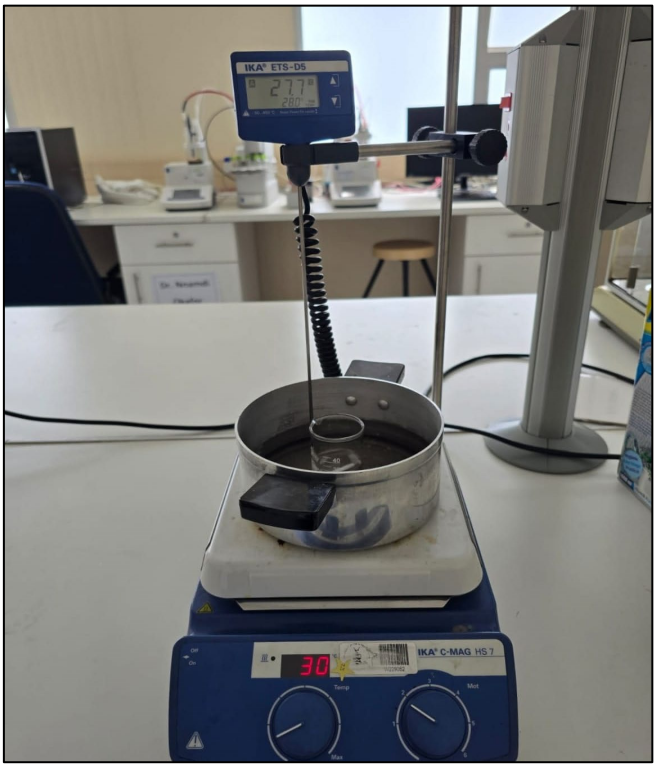

Figure 5.2. Representation of the magnetic stirrer assembly used for the stirring magnetic bar method.

5.2.2.1.2 Temperature ramp method

The $T_{sol-gel}$ i.e. temperature ramp measurements of all formulated ISTGs was undertaken using the ThermoHaake MARS Modular Advanced Rheometer (Thermo Fischer Scientific, Karlsruhe, Germany) fitted with a cone and plate, having geometrical parameters of 3.5 cm diameter and cone angle of 1° (Akilo et al., 2019). All formulations were analysed over a range of 15 to 40 °C and at a constant frequency of 1 Hz with the $T_{sol-gel}$ assessed using the generated temperature-ramp graph.

5.2.2.2 Analysis of the ISTG viscosity

The ThermoHaake MARS Modular Advanced Rheometer was used for the determination of gel viscosity. The temperature-ramp method used for the determination of $T_{sol-gel}$ was further utilized to determine the viscosity of the formulations at each temperature point. The viscosity at 34 °C for all the formulated ISTGs was considered in this analysis due to the physiological temperature of the nasal cavity being 34 °C (Cunha et al., 2022).

5.2.2.3 Determination the gel strength and mucoadhesion

Simulated nasal mucus, used for the physical property assessments of all the ISTGs, was prepared by dissolving 8% mucin from porcine stomach type II, 7.5 mg/mL NaCl, 1.3 mg/mL KCl and 0.3 mg/mL $CaCl_2$ $2H_2O$. A TA-XT2 Texture Analyser (TA) (Stable Micro Systems, Surrey, UK) (n = 3) was used for the assessment of gel strength and mucoadhesion of the formulations (Cunha et al., 2022; Masiuk et al., 2016). For the experiment, the temperature control chamber was maintained at 34 °C, a 0.5 mm diameter cylindrical probe to which the pig nasal membrane dipped in simulated nasal mucus was attached, with a load cell of 5 kg, trigger force of 0.5 N and test speed of 3 mm/second used. The porcine nasal membrane was sourced from the Wits Research Animal Facility (WRAF), University of the Witwatersrand under ethics waiver number 10-11-2023-O. The graph of force versus time obtained from the TA was used for the determination of gel strength and mucoadhesion.

5.2.3 Preparation of the DSLN-loaded ISTG

The NLX- and BUP- loaded SLNs equivalent to 1 mg NLX and 4 mg BUP, respectively, were added to the optimized ISTG (17% Pf-127+0.3% HPMC) and stirred for 2 minutes for the complete dispersion of both SLNs in the optimized ISTG. The DSLN-loaded ISTG was thereafter freeze dried in a lyophilizer to obtain a dry powder.

5.2.4 Characterization of the DSLN-loaded ISTG

5.2.4.1 Molecular structure assessment

All the starting materials used for formulating the DSLN-loaded ISTG including for both the freeze-dried drug-free SLN-loaded ISTG (SLNs with no drug loaded) and DSLN-loaded ISTG were analysed for the molecular transitions and interactions using a PerkinElmer ATR-FTIR. The instrumental parameters for analysis were as described in Chapter 3 (3.2.3.5.4) to obtain the FTIR spectra.

5.2.4.2 Determination of the $T_{sol-gel}$

5.2.4.2.1 Stirring magnetic bar method

The stirring magnetic bar method (n = 3) as described by Dorraj et al., discussed in 5.2.2.1.1 was used for the determination of $T_{sol-gel}$ of the drug-free SLN-loaded ISTG and DSLN-loaded ISTG (Dorraj and Moghimi, 2015).

5.2.4.2.2 Temperature ramp method

The $T_{sol-gel}$ i.e. temperature ramp measurements of the drug-free SLN-loaded ISTG and DSLN-loaded ISTG was done using the ThermoHaake MARS Modular Advanced Rheometer, as discussed in 5.2.2.1.2 (Akilo et al., 2019).

5.2.4.3 Analysis of the ISTG viscosity

The ThermoHaake MARS Modular Advanced Rheometer was used for the determination of gel viscosity (n = 3) as discussed in 5.2.2.2 for the drug-free SLN-loaded ISTG and DSLN-loaded ISTG.

5.2.4.4 Determination of gel strength and mucoadhesion

A TA was used for the assessment of gel strength (n = 3) and mucoadhesion (n = 3) as discussed in 5.2.2.3 for drug-free SLN-loaded ISTG and DSLN-loaded ISTG.

5.2.4.5 Assessment of the freeze-dried DSLN-loaded ISTG dispersion time and sol-gel transition time

The freeze-dried DSLN-loaded ISTG was added to Milli Q-distilled water and observed manually under time control until complete dispersion had occurred. The time taken (n = 3) for the complete dispersion of the formulation was considered to be the dispersion time of the freeze-dried DSLN-loaded ISTG.

As represented in Figure 5.2, the magnetic stirrer assembly was used for the determination of the sol-gel transition time (n = 3). The formulation-containing beaker along with a magnetic

stirrer bar was placed in a water bath maintained at 34 °C. The time taken for the magnetic stirrer bar to stop its motion is considered to be the sol-gel transition time.

5.2.4.6 Determination of the thermal characteristics

5.2.4.6.1 DSC analysis

All the starting materials used for formulating the DSLN-loaded ISTG including for both the freeze-dried drug-free SLN-loaded ISTG and DSLN-loaded ISTG were analysed as discussed in Chapter 3 (3.2.3.5.5) for their thermal properties using a DSC.

5.2.4.6.2 TGA analysis

The thermal degradation temperatures of all the starting materials used for formulating the DSLN-loaded ISTG including for both the freeze-dried drug-free SLN-loaded ISTG and DSLN-loaded ISTG were determined using a TGA, as discussed in Chapter 3 (3.2.3.5.6).

5.2.4.7 *In vitro* drug release studies

In vitro drug release studies (n = 3) of the DSLN-loaded ISTG were done using the dialysis bag diffusion method as discussed in Chapter 3 (3.2.3.3.3) where, the concentration of BUP and NLX released from the DSLN-loaded ISTG to PBS was analysed and measured using Reverse Phase-High Performance Liquid Chromatography (RP-HPLC) analysis.

5.2.4.7.1 High Performance Liquid Chromatography analysis

The RP-HPLC method developed and validated by Mundhey et al. was used for the simultaneous detection and quantification of BUP and NLX (Mundhey et al., 2016). A Waters C18 column (250 x 4.6 mm, 5 µm) and mobile phase comprised of acetonitrile and 0.05 M KH_2PO_4 buffer (1 mL orthophosphoric acid and pH adjusted to 6 using triethylamine) in the ratio of 75:25, degassed under sonication, was used for the analysis. Additionally, a flow rate of 1 mL/min and a detection wavelength of 285 nm was used. The retention times of BUP and NLX were 12.270 minutes and 3.210 minutes, respectively. A typical HPLC chromatogram for the quantification of BUP and NLX is provided in Figure 5.3.

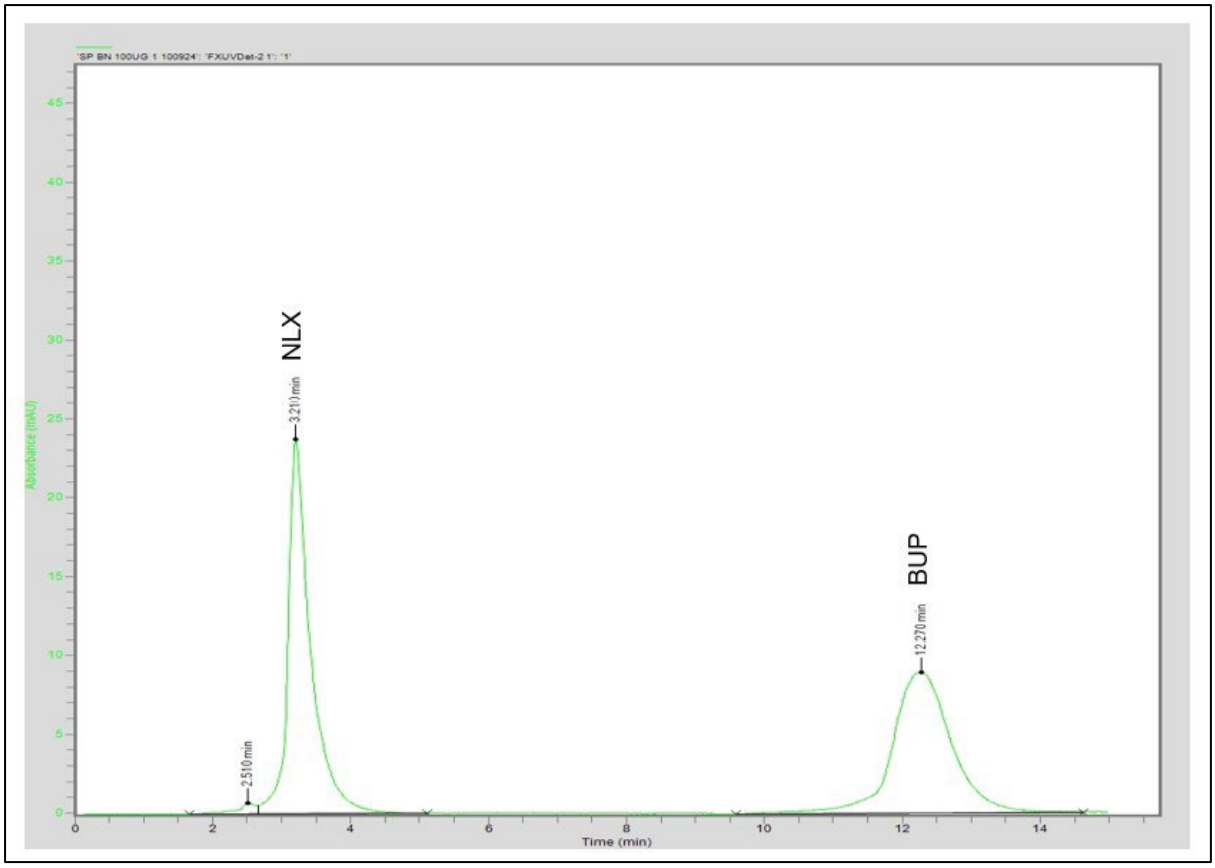

Figure 5.3. Representation of the chromatograms of standard solution of BUP (100 µg/mL) and NLX (100 µg/mL).

For the simultaneous quantification of BUP and NLX a calibration curve (Figure 5.4) i.e. a relation between concentration and area under the curve (AUC) was constructed using the HPLC. Various concentrations of NLX (0 - 200 µg/mL) and BUP (0 - 200 µg/mL) were analysed at 285 nm to obtain the AUC values of the respective concentrations for the quantification of NLX and BUP.

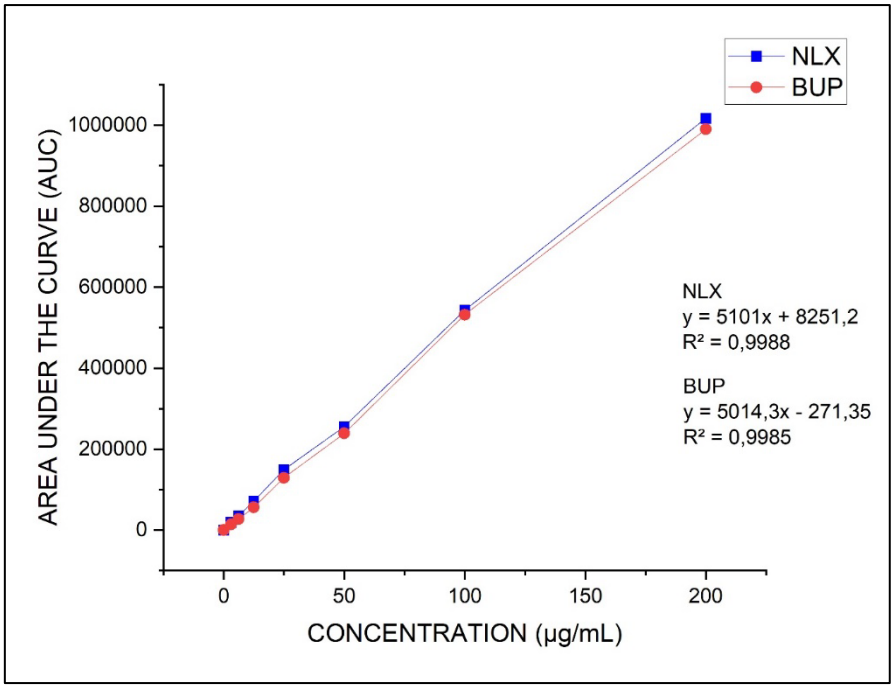

Figure 5.4. The constructed calibration curve for simultaneous quantification of BUP and NLX.

5.2.4.8 *Ex vivo* permeability studies

Ex vivo permeation studies (n = 3) were conducted on pig nasal mucosa membrane using a Franz diffusion cell to determine the permeability of the SLNs across the nasal membrane prior to the release of the loaded BUP and NLX. The porcine nasal mucosal tissue was stored in PBS solution (pH 7.4) at -80 °C. The nasal mucosa was mounted and stabilized on a Franz diffusion cell assembly, which contained 12 mL PBS solution (pH 6.8, simulating the nasal fluid pH condition) in the receptor compartment, as represented in Figure 5.5. The DSLN-loaded ISTG equivalent to 4 mg BUP and 1 mg NLX was re-dispersed in 3 mL PBS (pH 6.8) solution and placed in the donor compartment of capacity 3 mL. Samples from donor compartment i.e. 0.3 mL were withdrawn at predetermined time intervals i.e. 0, 0.25, 0.5, 1, 2, 3, 4, 5, 6, 7 and 8 hours, respectively and to maintain the sink conditions equal volume (0.3 mL) of PBS solution was added to the receptor compartment. The concentration of BUP and NLX permeated from the DSLN-loaded ISTG through nasal mucosa to the receptor compartment was analysed and measured after 7 days of incubation at 37 °C using HPLC analysis as the complete release of BUP and NLX from the SLNs take 7 days (proved in Chapter 3, Section 3.3.3.3 and Chapter 4, Section 4.3.3.3). As a control, all release samples were placed at 37 °C for 7 days to ensure that no SLNs were extracted during the sample withdrawal process.

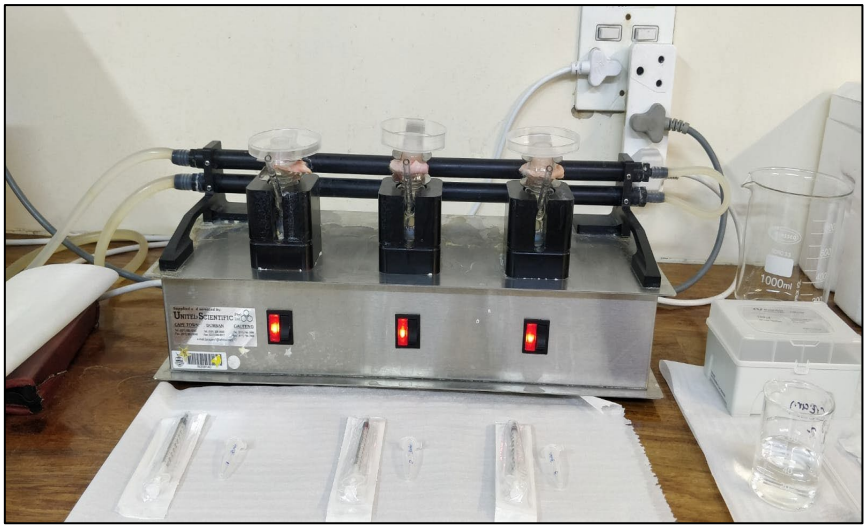

Figure 5.5. Representation of the franz diffusion assembly used for the *ex vivo* permeation studies of DSLN-loaded ISTG.

5.2.5 Cell culture and cytotoxicity studies

5.2.5.1 Cell culture

The HEK293 cells were maintained, cultured and seeded as discussed in Chapter 3 (3.2.4.1) and the treatments i.e. ISTG and DSLN-loaded ISTG both equivalent to 2.5:0.625 - 320:80 µg/mL concentration of BUP:NLX were thereafter prepared in serial dilutions using DPBS.

5.2.5.2 Cytotoxicity studies using MTT assay kit

Cell viability, through the determination of mitochondrial activity of living cells was measured by quantitative colorimetric assay using MTT (n = 3), as discussed in Chapter 3 (3.2.4.2), and using the absorbance values obtained, the relative cell viability was calculated using Equation 3.3.

5.2.6 Statistical analysis

All analyses were conducted in triplicate (n = 3) with Microsoft Excel used to express the mean and standard deviation of the obtained results. P values of less than 0.05 ($p < 0.05$) were considered to be an indication of statistical significance. OriginPro 2025 was additionally used for the graphical representation of all results obtained.

5.3 Results and discussion

5.3.1 Preparation, characterization and optimization of ISTG

5.3.1.1 Determination of the $T_{sol\text{-}gel}$

5.3.1.1.1 Stirring magnetic bar method

As per Bayanati et al., the acceptable temperature range of ISTG for nose to brain drug delivery is within 25 to 37 °C (Bayanati et al., 2021). Table 5.2 represents the $T_{sol\text{-}gel}$ results

obtained for all the pre-formulated ISTG. ISTG consisting of 17%, 19% and 21% Pf-127 was formulated and from the results obtained, 17% Pf-127 (28 ± 0.3 °C) was within the acceptable range and consistent with the study by Akilo et al. (2019). Additionally, from the results obtained for 17% Pf-172 and 17% Pf-127 LYO (30.1 ± 0.4 °C) it can be stated that after lyophilization, the $T_{sol-gel}$ was increased and more compatible for nose-to-brain drug delivery.

HPMC was added to the Pf-127 solution to increase the mucoadhesive strength of the formulation. From the results obtained for the lyophilized 0.1%, 0.2% and 0.3% HPMC added to 17% Pf-127 it can be noted that with the increase in HPMC concentration, the $T_{sol-gel}$ decreases, which falls in line with previous studies and 17% Pf-127+0.3% HPMC LYO formulation was considered as the optimized gel formulation for nose-to-brain drug delivery based on the $T_{sol-gel}$ (Rao et al., 2017).

Table 5.2. The $T_{sol-gel}$ results (n = 3) obtained for all the formulated ISTGs using the magnetic stirrer bar method.

Formulations	$T_{sol-gel}$ (°C)
17% Pf-172	28 ± 0.3
19% Pf-127	26.1 ± 0.4
21% Pf-127	24.1 ± 0.3
17% Pf-127 LYO	30.1 ± 0.4
17% Pf-127+0.1% HPMC LYO	33.11 ± 0.4
17% Pf-127+0.2% HPMC LYO	31.8 ± 0.3
17% Pf-127+0.3% HPMC LYO	30.9 ± 0.2

5.3.1.1.2 Temperature ramp method

In the temperature ramp method, the storage modulus (G') and loss modulus (G") of the formulations are taken into consideration which are plotted against temperature as represented in Figure 5.6 for the $T_{sol-gel}$. When the G" value is greater than G', the formulation is considered to be in the liquid phase but when the G' value is greater than G", the formulation is found to be in the gel phase (Ramli et al., 2022). The $T_{sol-gel}$ results of the formulated ISTG iterations obtained using the temperature ramp method are represented in Table 5.3. From the results obtained, it was concluded that 17% Pf-127+0.3% HPMC formulation is considered to be the optimized ISTG, aligning to the stirrer-bar method results, as it was within the acceptable $T_{sol-gel}$ for nose-to-brain DDS.

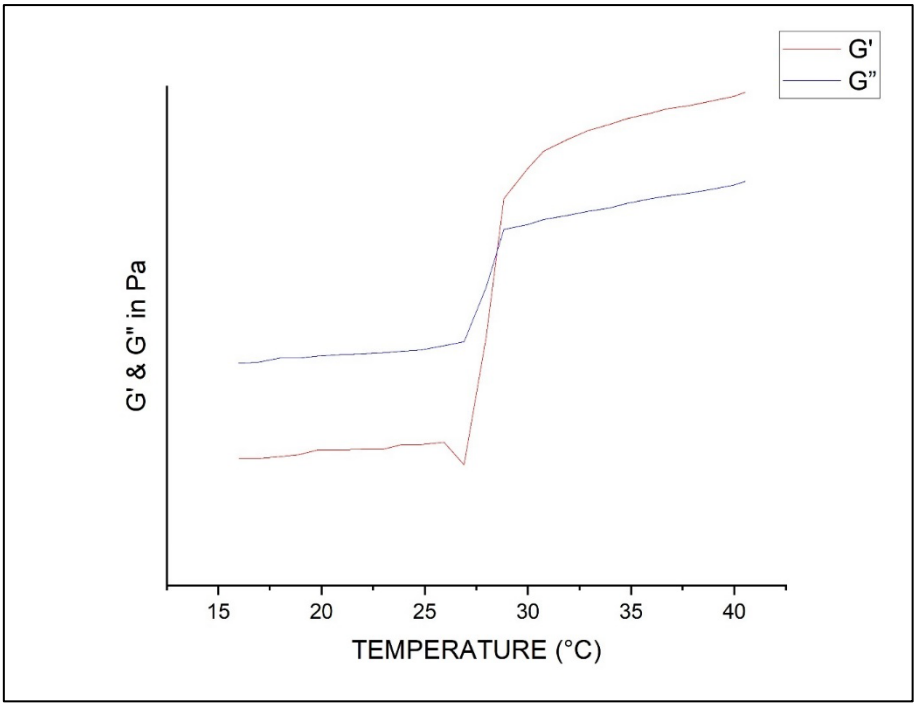

Figure 5.6. Representation of the temperature ramp graph for the $T_{sol-gel}$ of the optimized ISTG (17% Pf-127+0.3% HPMC LYO).

Table 5.3. The $T_{sol-gel}$ (n = 3) results obtained for the formulated ISTG iterations using the temperature ramp method.

Formulation	$T_{sol-gel}$ (°C)
17% Pf-172	24.67 ± 0.61
19% Pf-127	22.29 ± 0.59
21% Pf-127	20.71 ± 0.62
17% Pf-127 LYO	25.99 ± 0.11
17% Pf-127+0.1% HPMC LYO	30.65 ± 0.57
17% Pf-127+0.2% HPMC LYO	29.63 ± 0.55
17% Pf-127+0.3% HPMC LYO	28.66 ± 0.58

5.3.1.2 Analysis of the ISTG viscosity

The viscosity results of all the formulated ISTG iterations obtained using the temperature ramp method are represented in Table 5.4. The obtained results were consistent with the study by Sridhar et al. (2018) and further validate the use of the 17% Pf-127+0.3% HPMC formulation composition as the optimized ISTG due to its high viscosity and therefore resistance to mucociliary clearance resulting in longer residence time within the nasal passage.

Table 5.4. The ISTG viscosity (n = 3) results obtained for the formulated ISTG iterations.

Formulation	Viscosity (Pa second)
17% Pf-127 LYO	10.56 ± 0.52
17% Pf-127+0.1% HPMC LYO	11.82 ± 0.23
17% Pf-127+0.2% HPMC LYO	13.48 ± 0.25
17% Pf-127+0.3% HPMC LYO	14.12 ± 0.28

5.3.1.3 Determination of gel strength and mucoadhesion

The time taken by the probe to which the pig nasal membrane dipped in simulated nasal mucus to attach and thereafter detach itself from the formulations is considered to be the gel strength of all the ISTGs. The gel strength of all the ISTGs are represented in Figure 5.7, where the time taken for the detachment of the probe for freeze dried 17% Pf-127, 0.1%, 0.2% and 0.3% HPMC added to 17% Pf-127 were found to be 0.06 ± 0.053, 1.13 ± 0.025, 1.91 ± 0.036 and 2.85 ± 0.035 minutes, respectively, and comparable with the results obtained by Salatin et al. (2018). Additionally, from the results obtained it can be stated that with the increasing concentration of HPMC, the gel strength increased which is considered suitable for holding the SLNs within the gel matrix.

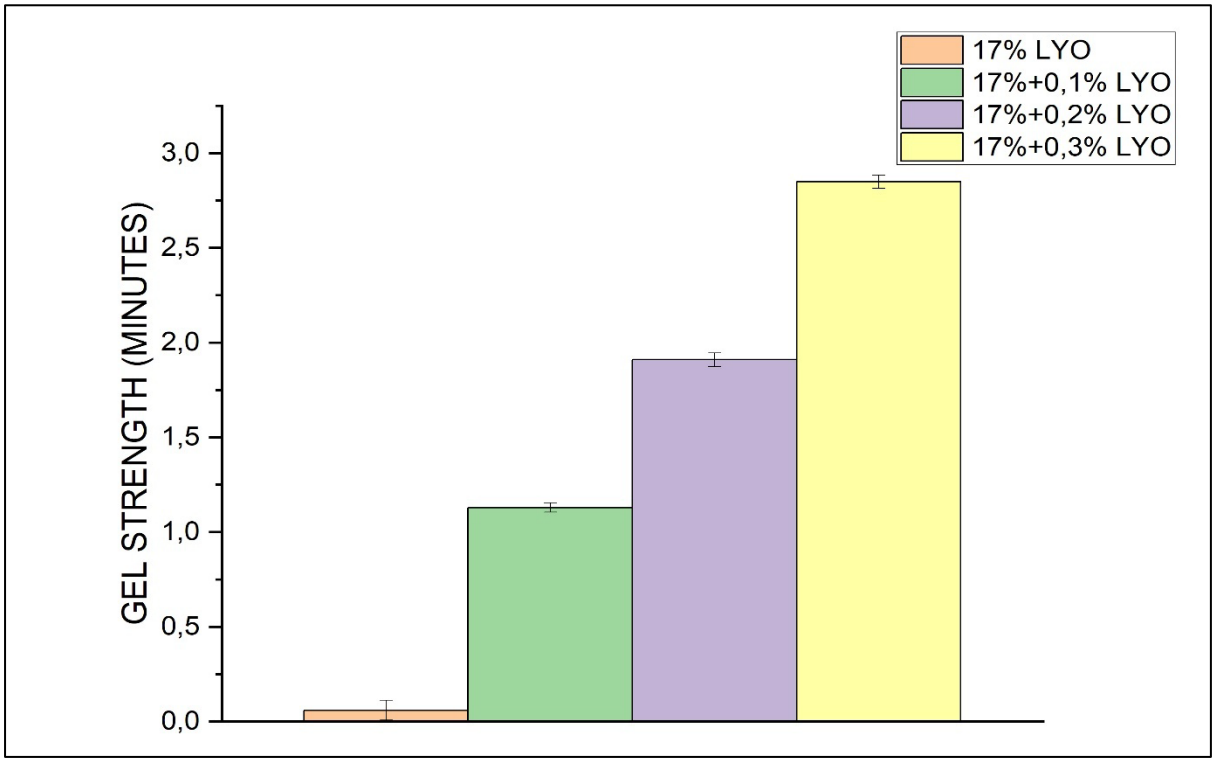

Figure 5.7. Representation of the gel strength (n = 3) of freeze dried 17% Pf-127, 17% Pf-127+0.1% HPMC, 17% Pf-127+0.2% HPMC and 17% Pf-127+0.3% HPMC.

The force required for the probe to which the pig nasal membrane dipped in simulated nasal mucus was attached to detach itself from the formulations is considered to be the mucoadhesion of all the ISTGs. The higher the force required for the detachment of the probe, higher will be the mucoadhesion. The mucoadhesive strength of all the ISTGs are represented in Figure 5.8, where the force required for the detachment of the probe for freeze dried 17% Pf-127, 0.1%, 0.2% and 0.3% HPMC added to 17% Pf-127 were found to be 0.012 ± 0.0005, 0.030 ± 0.0002, 0.048 ± 0.0004 and 0.069 ± 0.0004 N, respectively, and consistent with the results obtained by Wang et al. (2017). Additionally, from the results obtained it can be stated that with the increasing concentration of HPMC, the mucoadhesion increased which helps to overcome the mucociliary clearance rate.

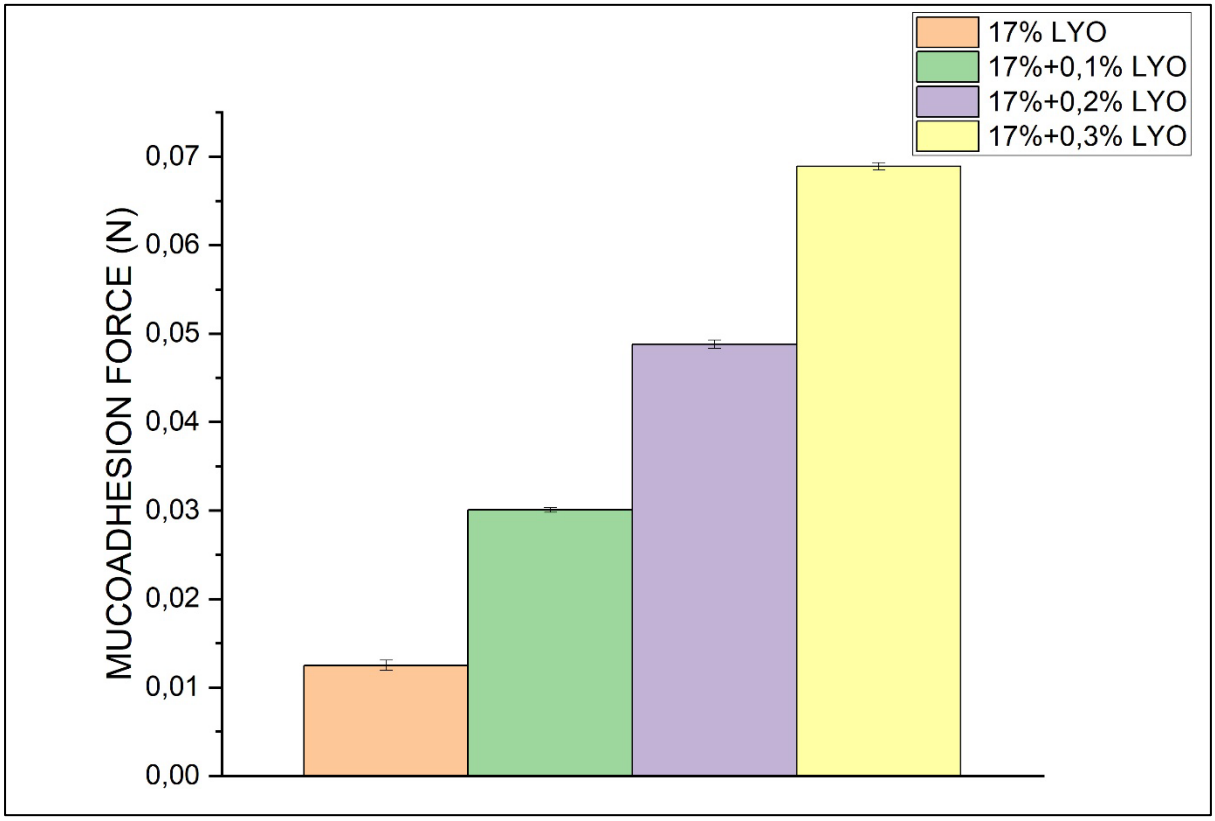

Figure 5.8. Representation of the gel mucoadhesion (n = 3) of freeze dried 17% Pf-127, 17% Pf-127+0.1% HPMC, 17% Pf-127+0.2% HPMC and 17% Pf-127+0.3 HPMC.

5.3.2 Characterization of the DSLN-loaded ISTG

5.3.2.1 Molecular structure assessment

The FTIR spectra of all the starting materials, including the optimized drug-free SLN-loaded ISTG and DSLN-loaded ISTG, are represented in Figure 5.9. The characteristic FTIR peaks of GMS, PCL, NLX, unloaded SLNs and NLX-loaded SLNs are discussed in Chapter 3 (3.3.3.4) and for BUP and BUP-loaded SLNs in Chapter 4 (4.3.3.4). The characteristic FTIR peaks of Pf-127: 2883 cm^{-1} (C-H stretching), 1343 cm^{-1} (O-H bending) and 1104 cm^{-1} (C-O-C

stretching) were present, which were similar to that described in previous research (Karolewicz et al., 2014). FTIR peaks of HPMC: 3447 cm^{-1} (O-H stretching), 2890 cm^{-1} (C-H stretching), 1342 cm^{-1} (O-H bonding) and 1064 cm^{-1} (C-O) were present and consistent with the study by Iqbal et al. (2017). The optimized freeze-dried ISTG revealed peaks at 2877 cm^{-1} (C-H stretching), 1341 cm^{-1} (O-H bending) and 1100 cm^{-1} (C-O-C stretching). Analysis of the FTIR spectra of the optimized freeze-dried drug-free SLN-loaded ISTG showed peaks at 2887 cm^{-1} (C-H stretching), 1342 cm^{-1} (O-H bending) and 1099 cm^{-1} (C-O-C stretching). The optimized DSLN-loaded ISTG showed the same or similar characteristic peaks as ISTG and drug-free SLN-loaded ISTG at 2882 cm^{-1} (C-H stretching), 1342 cm^{-1} (O-H bending) and 1097 cm^{-1} (C-O-C stretching) validating the synthesis of ISTG and consistent with the results obtained by Alves et al. (2018). The characteristics peaks of SLNs, BUP-loaded SLNs and NLX-loaded SLNs were absent, indicating the complete encapsulation of them within the ISTG.

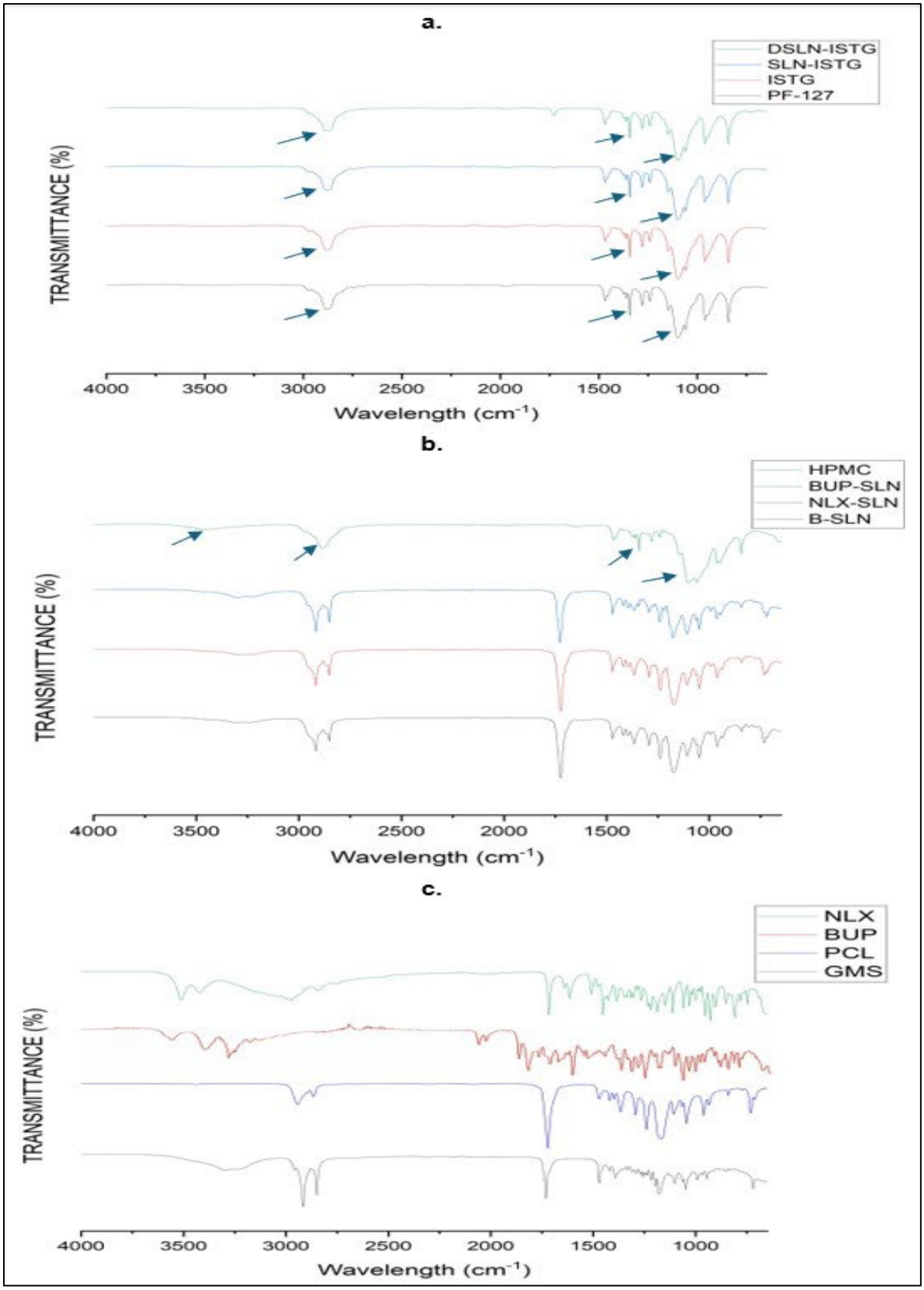

Figure 5.9. FTIR spectra of (a) Pf-127, ISTG, drug-free SLN-loaded ISTG (SLN-ISTG) and DSLN-loaded ISTG (DSLN-ISTG), (b) unloaded SLNs (B-SLN), NLX-loaded SLN (NLX-SLN), BUP-loaded SLNs (BUP-SLN) and HPMC and (c) GMS, PCL, BUP and NLX.

5.3.2.2 Determination of the $T_{sol-gel}$

5.3.2.2.1 Stirring magnetic bar method

The $T_{sol-gel}$ for drug-free SLN-loaded ISTG and DSLN-loaded ISTG was found to be 32.5 ± 0.5 °C and 34.7 ± 0.2 °C, respectively, which were within the acceptable range for nose-to-brain DDS and consistent with the previous studies (Cunha et al., 2022). Additionally, with the incorporation of SLNs and drug containing SLNs, the $T_{sol-gel}$ of the optimized ISTG was increased. The results obtained using this method were further verified using the temperature ramp method (5.3.3.1.2).

5.3.2.2.2 Temperature ramp method

The $T_{sol-gel}$ of the optimized drug-free SLN-loaded ISTG and DSLN-loaded ISTG were found to be 30.92 ± 0.98 °C and 32.91 ± 0.94 °C, respectively, which are graphically represented in Figure 5.10 and were found to be within the acceptable range for nose-to-brain DDS.

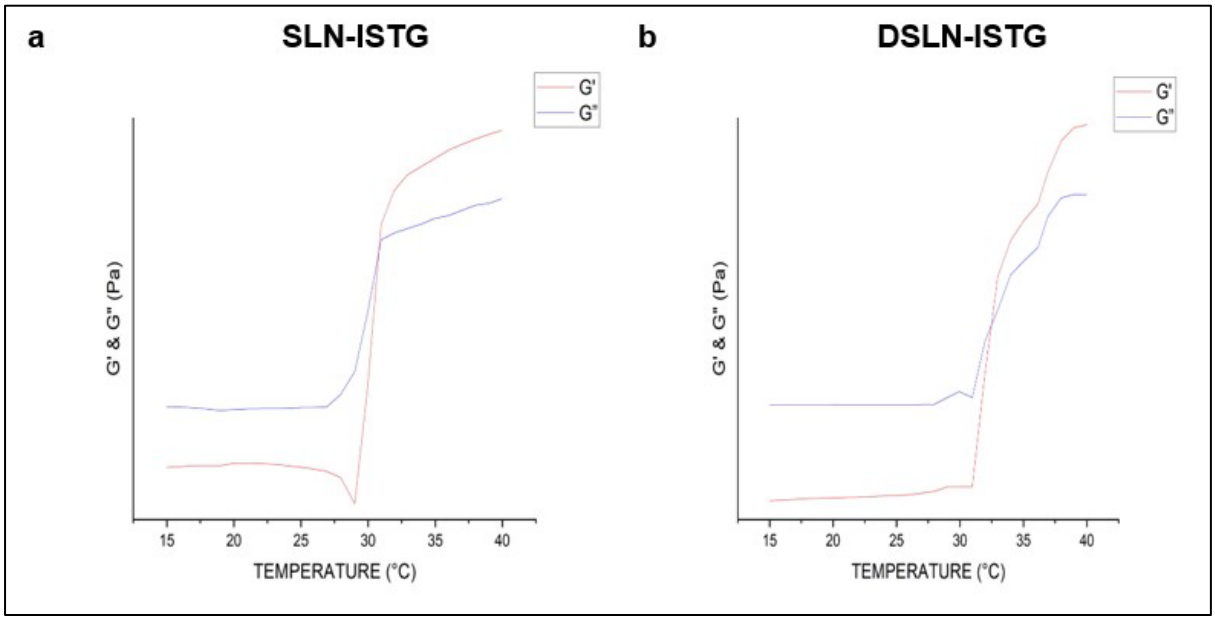

Figure 5.10. Representation of the temperature ramp graphs for the $T_{sol-gel}$ of the optimized (a) drug-free SLN-loaded ISTG (SLN-ISTG) and (b) DSLN-loaded ISTG (DSLN-ISTG).

5.3.2.3 Analysis of the DSLN-loaded ISTG viscosity

The viscosity of the optimized drug-free SLN-loaded ISTG and DSLN-loaded ISTG were found to be 16.47 ± 0.36 and 17.17 ± 0.26 Pa second, respectively, which were found to be acceptable for the nose-to-brain drug delivery, as it helps to overcome the mucociliary clearance rate and increase the residence time of the formulation within the nasal cavity, providing enough time for the complete uptake of drug-loaded SLN into the CNS. The obtained results were found consistent with the study by Sridhar et al. (2018).

5.3.2.4 Determination of gel strength and mucoadhesion

Gel strength helps in determining the capacity of the gel to withstand external force and the capacity of the gel to entrap SLNs within the gel matrix. As discussed in 5.3.1.3, the higher the time taken for the detachment of the probe, the higher the gel strength will be. The gel strength of the drug-free SLN-loaded ISTG and DSLN-loaded ISTG were found to be 2.42 ± 0.036 and 2.32 ± 0.035 minutes, respectively, and comparable with the results obtained by Salatin et al. (2018). From the results obtained it can be stated that with the increasing concentration of other excipients such as SLNs and drug-loaded SLNs, the gel strength decreased but capable of delivering drug-loaded SLNs in the form of ISTG via nose-to-brain DDS.

As discussed in 5.3.1.3, the higher the force required for the detachment of the probe, the higher the mucoadhesion will be. The mucoadhesive strength of the drug-free SLN-loaded ISTG and DSLN-loaded ISTG were found to be 0.049 ± 0.0006 and 0.046 ± 0.0006 N, respectively, and consistent with the results obtained by Wang et al. (2017). From the results obtained it can be stated that with the increasing concentration of other excipients such as SLNs and drug-loaded SLNs, the mucoadhesion decreased, but both the formulations were noted to be still capable to overcome the mucociliary clearance rate and increase the residence time of the formulation within the nasal cavity for the complete uptake of the drug-loaded SLNs into the CNS.

5.3.2.5 Assessment of the freeze-dried DSLN-loaded ISTG dispersion time and sol-gel transition time

The dispersion time of the optimized freeze-dried drug-free SLN-loaded ISTG and DSLN-loaded ISTG were found to be 30.17 ± 1.75 and 32.83 ± 2.25 minutes, respectively, indicating a decrease in dispersion time of the optimized ISTG which makes the formulations more patient compliant, as the initial dissolution time of Pf-127 and HPMC was observed to be overnight in the synthesis phase. Additionally, Figure 5.11 represents the transition of the freeze-dried DSLN-loaded ISTG after complete dispersion. The time taken for the sol-gel transition at 34 °C of the freeze-dried drug-free SLN-loaded ISTG and DSLN-loaded ISTG were found to be 1.08 ± 0.14 and 1.25 ± 0.25 minutes, respectively, indicating an immediate sol-gel phase transition, leading to an increased residence time of the formulations within the nasal cavity. The results achieved are comparable with the results obtained by El Taweel et al. (2021) and Rao et al. (2017).

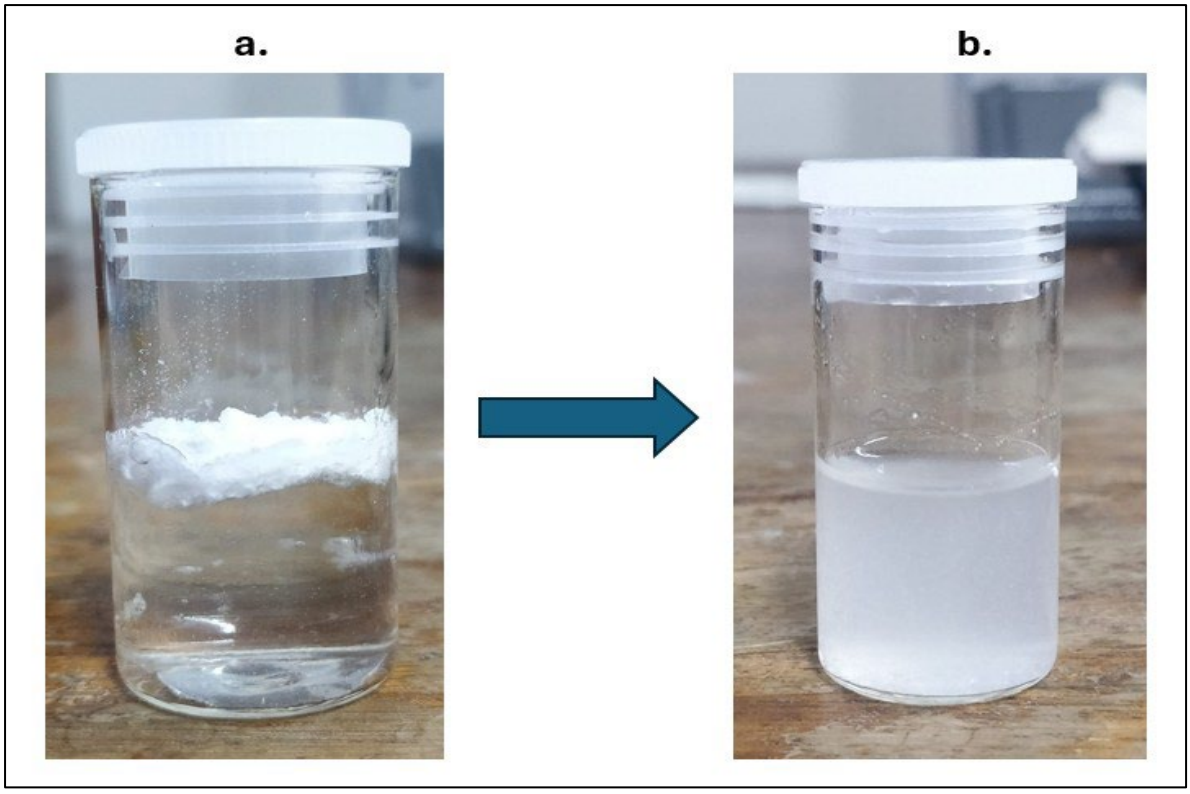

Figure 5.11. Representation of the complete dissolution of (a) freeze dried DSLN-loaded ISTG powder to form a (b) uniform liquid dispersion.

5.3.2.6 Determination of thermal characteristics

5.3.2.6.1 DSC analysis

DSC analysis was performed on all the starting materials, as well as on the optimized ISTG, drug-free SLN-loaded ISTG and DSLN-loaded ISTG, for the determination of their thermal behaviours, as represented in Figure 5.12. The DSC analysis of GMS, PCL, NLX, unloaded SLNs and NLX-loaded SLNs are discussed in Chapter 3 (3.3.3.5) and for BUP and BUP-loaded SLNs in Chapter 4 (4.3.3.5). Pf-127 showed an endothermic peak at 58 °C and HPMC showed an endothermic peak at 72.17 °C and an exothermic peak at 380.33 °C, which are comparative to previous studies (Karolewicz et al., 2014; Rani et al., 2015). The optimized freeze-dried ISTG showed an endothermic peak at 57.83 °C and characteristic exothermic peaks at 140.17 °C and 380.83 °C. The optimized drug-free SLN-loaded ISTG showed an endothermic peak at 56.83 °C and exothermic peaks at 148.83 °C and 383.5 °C. Furthermore, the optimized DSLN-loaded ISTG showed the same or similar endothermic peak at 56.68 °C and exothermic peaks at 154.17 °C and 379 °C to ISTG and drug-free SLN-loaded ISTG, indicating the synthesis of ISTG. Additionally, it can be verified that all three optimized formulations were composed of Pf-127 and HPMC as, the formulations had the characteristic endothermic peak of Pf-127 (58 °C) and the characteristic exothermic peak of HPMC (380.33 °C), which are comparative to the results obtained in previous study (Parhi, 2016). The

absence of all the characteristic peaks of SLNs, BUP-loaded SLNs and NLX-loaded SLNs indicate the complete encapsulation of them with the gel matrix of ISTG.

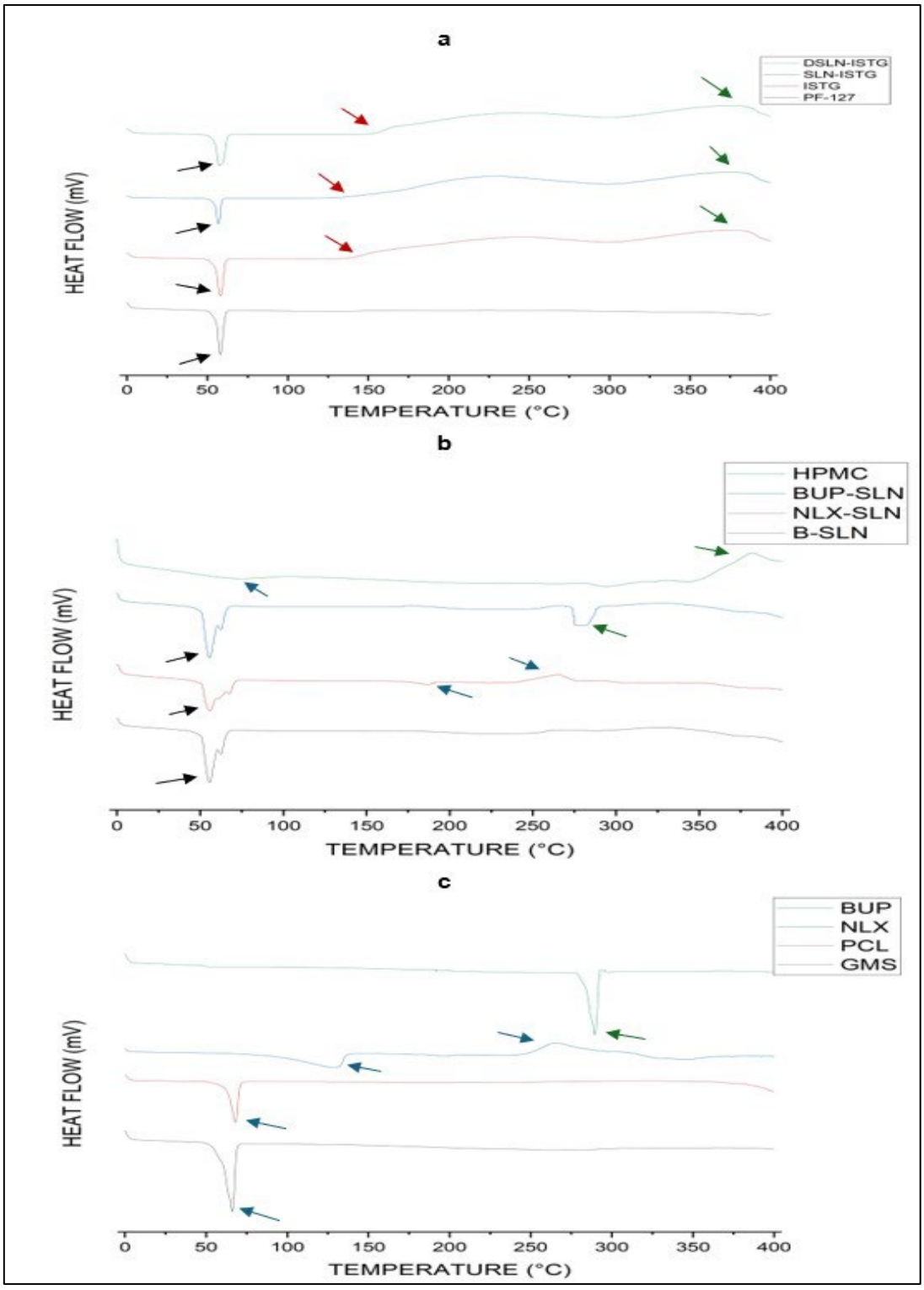

Figure 5.12. DSC thermograms of (a) DSLN-loaded ISTG (DSLN-ISTG), drug-free SLN-loaded ISTG (SLN-ISTG), ISTG and Pf-127, (b) HPMC, BUP-loaded SLNs (BUP-SLN), NLX-loaded SLNs (NLX-SLN) and unloaded-SLNs (B-SLN) and (c) BUP, NLX, PCL and GMS used for the synthesis of optimized DSLN-loaded ISTG.

5.3.2.6.2 Thermogravimetric analysis

TGA analysis was done on all the starting materials, as well as on the optimized ISTG, drug-free SLN-loaded ISTG and DSLN-loaded ISTG, as represented in Figure 5.13 to determine their degradation rates. The %weight loss of GMS, PCL and unloaded SLNs are discussed in Chapter 3 (3.3.3.6) and for BUP in Chapter 4 (4.3.3.6). The %weight loss of the optimized ISTG, drug-free SLN-loaded ISTG and DSLN-loaded ISTG started at 314.6 °C, 334.3 °C and 328.6 °C, respectively. By the end i.e. 600 °C, 2.01% of ISTG remained undegraded indicating the presence of HPMC in the formulation composition, as 9.55% of HPMC remained undegraded. Furthermore, 7.57% and 9.59% of drug-free SLN-loaded ISTG and DSLN-loaded ISTG, respectively remained undegraded at end of 600 °C, indicating the presence of HPMC and SLN within the formulation, as 9.55% of HPMC and 4.99% of SLN remained undegraded at 600 °C, which is comparative with the results obtained by Hassan et al. (2022) in his study. Additionally, 2.02% of DSLN-loaded ISTG was found more as compared to drug-free SLN-loaded ISTG indicating the presence of BUP (14.88%) and NLX (40.84%) within the formulation.

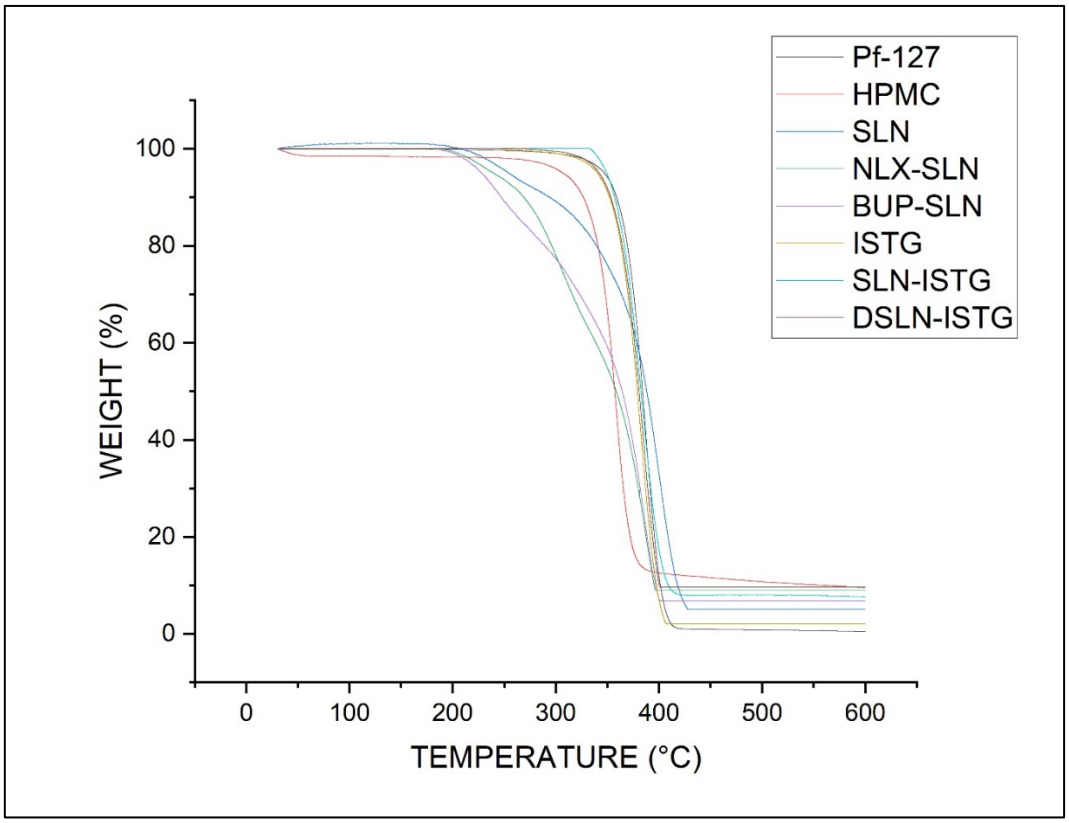

Figure 5.13. TGA thermograms of the ISTG, drug-free SLN-loaded ISTG (SLN-ISTG) and optimized DSLN-loaded ISTG (DSLN-ISTG) including all the materials used for the synthesis of DSLN-loaded ISTG.

5.3.2.7 *In vitro* drug release studies

In vitro drug release studies were conducted to determine the release profile of BUP and NLX from the optimized DSLN-loaded ISTG. Approximately 50% of BUP and NLX were released from the DSLN-loaded ISTG by the end of day 3 (72 hours) and the remaining 50% of BUP and NLX were released over a period of the next 4 days (96 hours), indicating a release profile of BUP and NLX over a period of 7 days (168 hours), as represented in Figure 5.14. With the achievement of this release profile of BUP and NLX, it can be confirmed that the release profile of BUP and NLX from the SLNs were not affected by the ISTG as both NLX-loaded SLNs (Chapter 3, Section 3.3.3.3) and BUP-loaded SLNs (Chapter 4, Section 4.3.3.3) had a release profile over 7 days which is the same for DSLN-loaded ISTG.

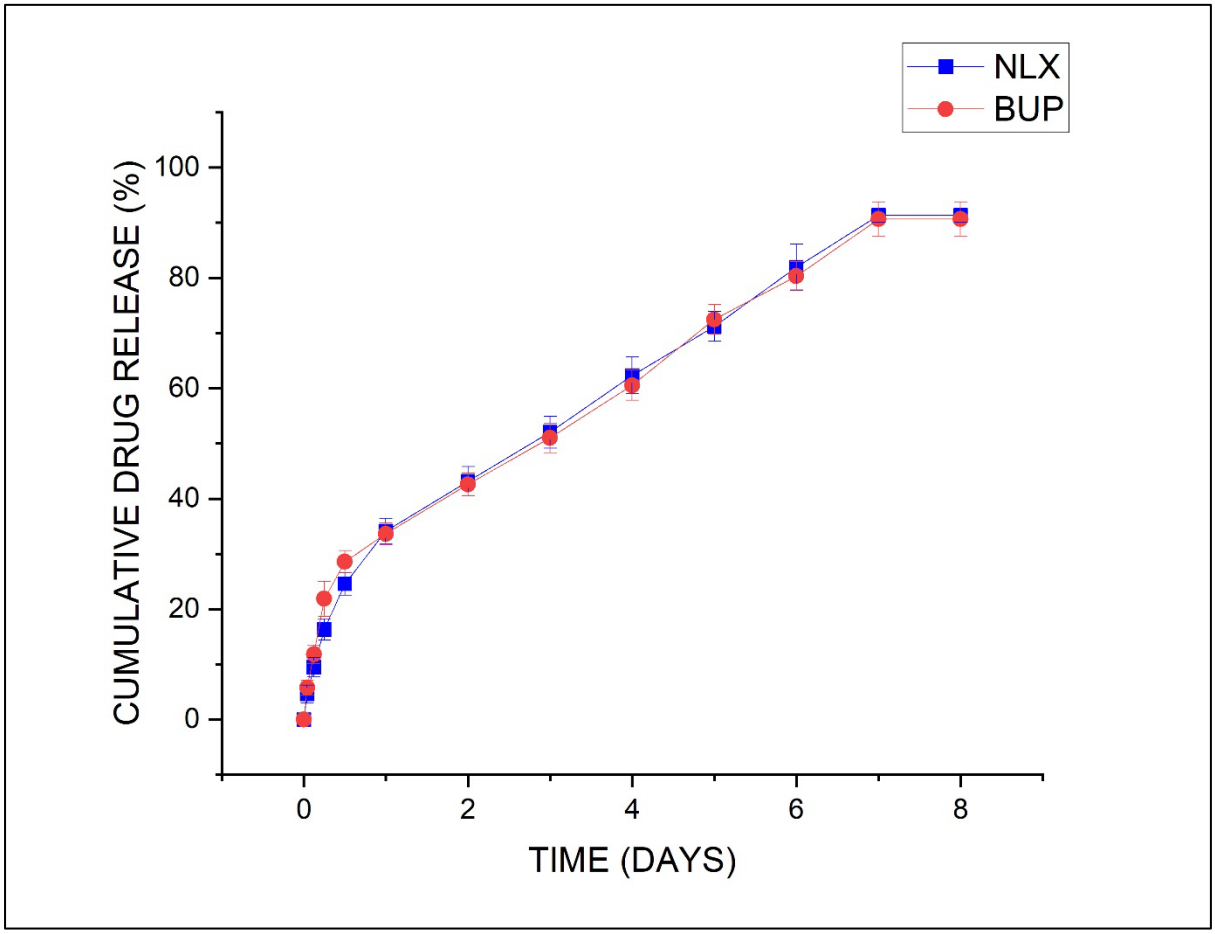

Figure 5.14. Representation of the *in vitro* drug release profile of BUP and NLX from the optimized DSLN-loaded ISTG (n = 3).

5.3.2.8 *Ex vivo* permeability studies

Ex vivo SLNs permeability studies were conducted to determine the permeation rate of BUP-loaded SLNs and NLX-loaded SLNs from the optimized DSLN-loaded ISTG across the pig nasal membrane. This study was done to mimic the permeation of drug-loaded SLNs from the optimized DSLN-ISTG across the human nasal membrane into the CNS. Using the HPLC

analysis, approximately 50% of BUP-loaded SLNs and NLX-loaded SLNs were found to be permeated from the DSLN-loaded ISTG by the end of 5 hours and the remaining, approximately 22% over a period of next 2 hours, indicating that the permeation rate of BUP-loaded SLNs and NLX-loaded SLNs was over a period of 7 hours, as represented in Figure 5.15. The HPLC analysis of the collected samples when done after 4 hours (i.e. at 12 hours) of sample collection a cumulative release of BUP and NLX was found to be 40% and when the same samples were analysed after 7 days of incubation in an orbital shaker maintained at 37 °C, showed a cumulative release of 72%. When both the results of HPLC analysis i.e. 12 hours and 7 days were compared, it can be stated that the drug-loaded SLNs had permeated across the nasal membrane and that the premature release of NLX and BUP from the DSLN-ISTG did not occur. From this study it was concluded that drug-loaded SLN equivalent to 72% of BUP and NLX permeated across the nasal membrane from the DSLN-ISTG without affecting the release profile of BUP- and NLX- loaded SLNs.

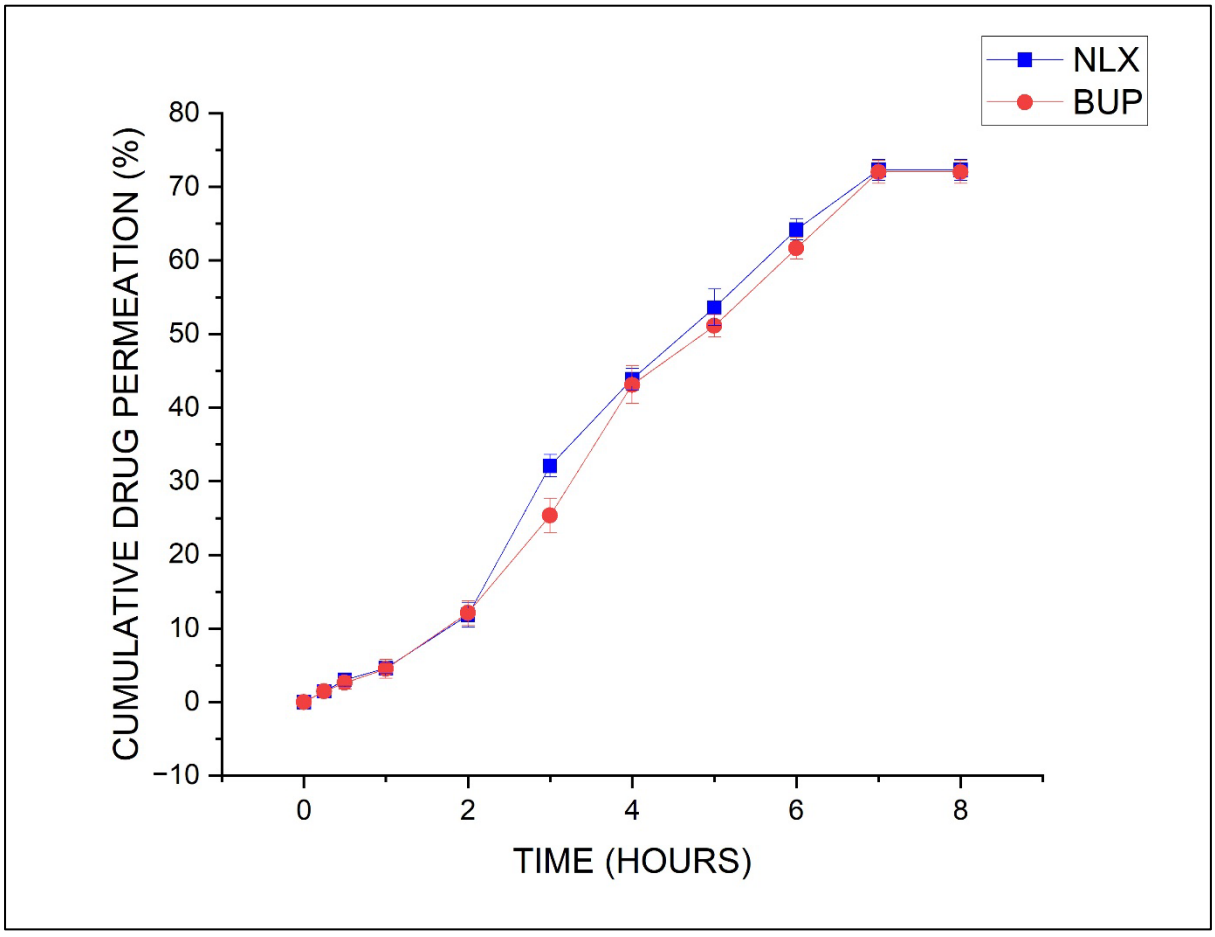

Figure 5.15. Representation of the *ex vivo* drug permeation profile of BUP and NLX from the optimized DSLN-loaded ISTG (n = 3).

5.3.3 Cell culture and cytotoxicity studies

The assessment for potential cytotoxicity (n = 3 and p ≤ 0.001 indicating the results are

statistically significant) of the DSLN-loaded ISTG on HEK293 cells is represented in Figure 5.16. The cytocompatibility of NLX, unloaded SLNs and NLX-loaded SLNs are discussed in Chapter 3 (3.3.3.7) and for BUP and BUP-loaded SLNs in Chapter 4 (4.3.3.7). Additionally, to determine the cytocompatibility of various concentrations of ISTG (equivalent to 2.5:0.625-320:80 µg/mL concentration of BUP:NLX) and DSLN-loaded ISTG (equivalent to 2.5:0.625-320:80 µg/mL concentration of BUP:NLX) were incubated for 24, 48 and 72 hours and compared to a positive control or untreated cells. Figure 5.17 represents the microscopic imaging of positive control, negative control, BUP-loaded SLNs, NLX-loaded SLNs, ISTG and DSLN-loaded ISTG treated cells taken after 48 hours using an inverted microscope with a 4× magnification. After 24 hours, the maximum concentration of ISTG and DSLN-loaded ISTG showed a cell viability of 94.26 ± 0.014% and 92.63 ± 0.032%, respectively, whereas the minimum concentrations showed 97.5 ± 0.053% and 96.02 ± 0.044% cell viability. At 48 hours, the maximum concentration of ISTG and DSLN-loaded ISTG showed cell viability of 88.38 ± 0.045% and 86.41 ± 0.035%, respectively, whereas the minimum concentrations showed 93.49 ± 0.048% and 91.40 ± 0.037% cell viability, while after 72 hours, the maximum concentration of ISTG and DSLN-loaded ISTG showed cell viability of 86.96 ± 0.113% and 84.86 ± 0.039%, respectively, while the minimum concentrations showed 91.99 ± 0.034% and 87.74 ± 0.039% cell viability. Statistical evaluation of the data noted a statistical significance at all time points and concentrations ($p < 0.01$), when compared to the positive control, due to the low variability between samples and the consistent values across sample runs. However, as per ISO 10993-5, %cell viability above 80% are considered non-cytotoxic; within 80% - 60% weakly; 60% - 40% moderately and below 40% strongly cytotoxic (López-García et al., 2014). Thus, from the data obtained it can be concluded that the ISTG and DSLN-loaded ISTG showed good cytocompatibility, as even after 72 hours, none of the %cell viability dropped below 80%, indicating no cytotoxic effect was observed.

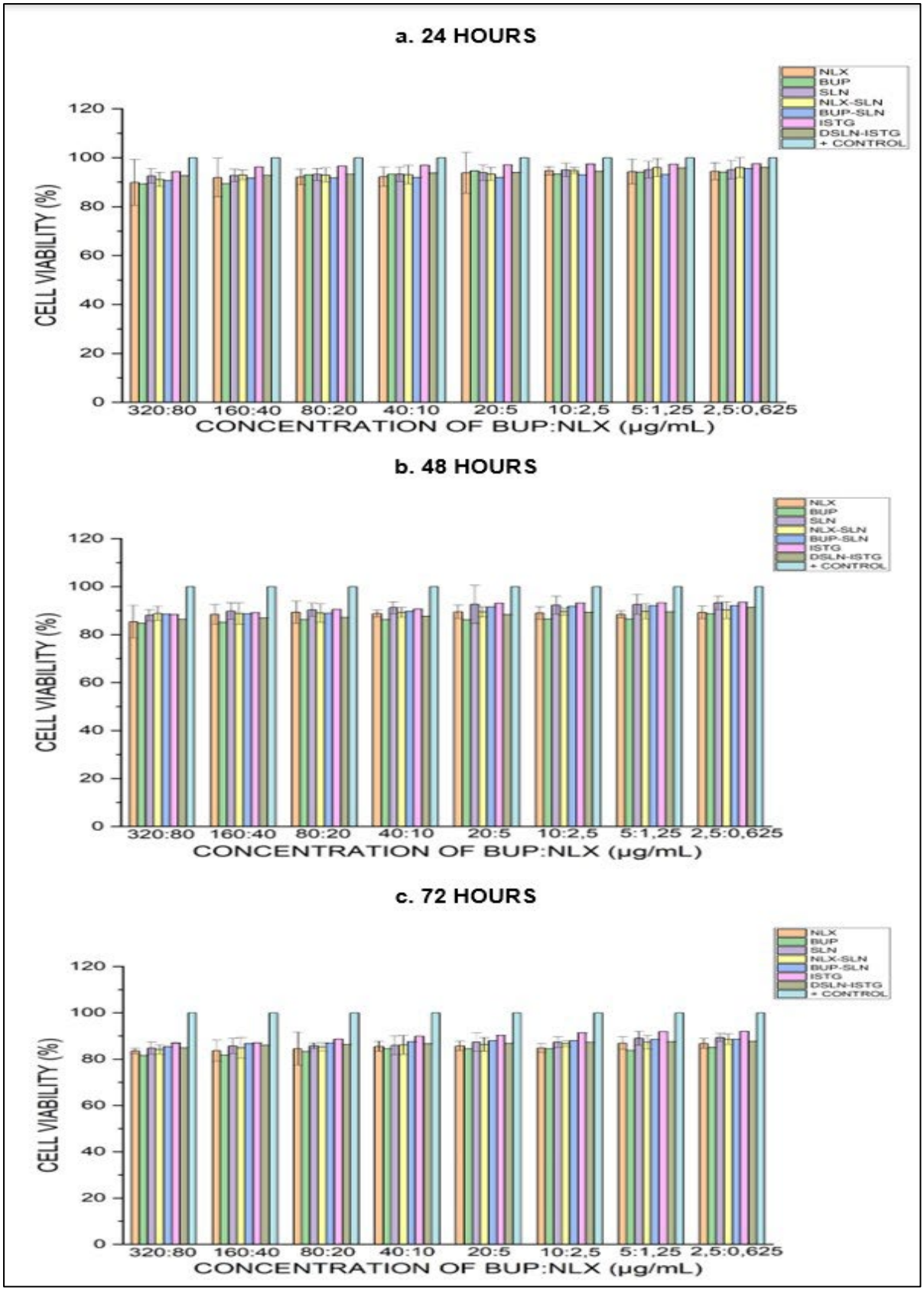

Figure 5.16. HEK293 cell cytocompatibility after treatment with various concentrations of NLX, BUP, unloaded SLNs (SLN), NLX-loaded SLN (NLX-SLN), BUP-loaded SLNs (BUP-SLN), ISTG and DSLN-loaded ISTG (DSLN-ISTG) for (a) 24 hours (b) 48 hours and (c) 72 hours ($n = 3$ and $p \leq 0.01$ at all cases).

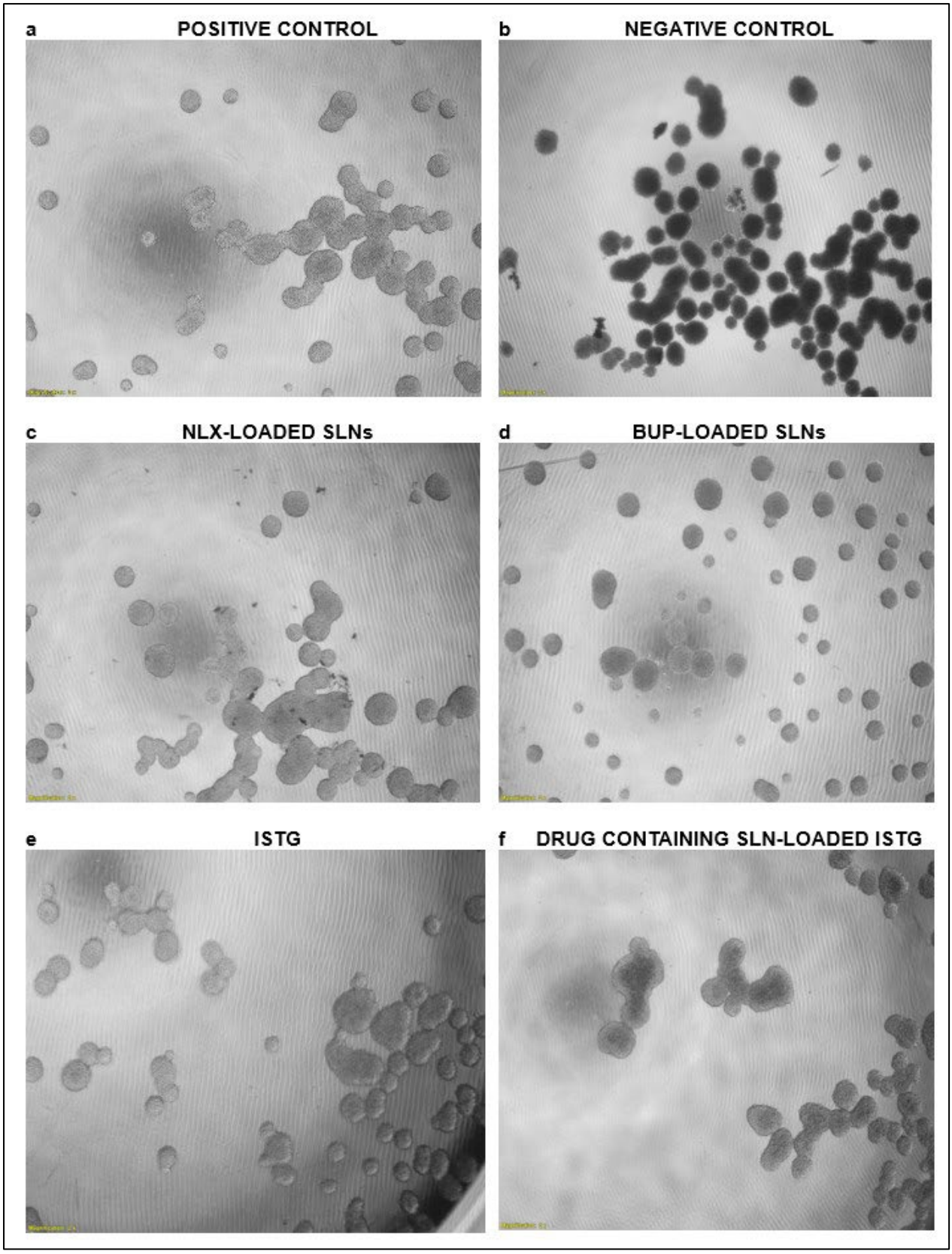

Figure 5.17. Representation of the microscopic imaging of (a) the positive control, (b) the negative control, (c) the optimized NLX-loaded SLNs, (d) the optimized BUP-loaded SLNs, (e) the ISTG and (f) the optimized DSLN-loaded ISTG treated cells. All images were taken after 48 hours at 4X magnification.

5.4 Conclusion

In this chapter, a DSLN-loaded ISTG was synthesized for the sustained release of BUP and NLX, potentially helping in overcoming the poor pharmacokinetic and pharmacodynamic properties of BUP and NLX. The DSLN-loaded ISTG was formulated using the cold method, where the desired $T_{sol\text{-}gel}$, viscosity and mucoadhesion were obtained for nose-to-brain DDS. The desired physicochemical properties of the DSLN-loaded ISTG were obtained and confirmed using FTIR, DSC and TGA, ensuring their desired molecular transition and stable thermal behaviour. The maximum entrapment of BUP- and NLX- loaded SLNs were found within the ISTG, as *in vitro* release of BUP and NLX from the DSLN-loaded ISTG was observed over a period of one week (7 days), which suggested potential increased bioavailability of BUP and NLX across the BBB and an increased residence time at the site of action. Additionally, from the *ex vivo* permeability studies it was concluded that the desired therapeutic dose of BUP and NLX permeated across the nasal membrane within 8 hours. The DSLN-loaded ISTG additionally showed no significant signs of *in vitro* cytotoxicity against HEK293 cells, indicating their excellent cytocompatibility. Therefore, with the incorporation of NLX-loaded SLNs developed in Chapter 3 and BUP-loaded SLNs in Chapter 4 within the optimized ISTG, the DSLN-loaded ISTG can be an effective and patient compliant potential treatment option for OUD. The sustained release of NLX will give an antagonistic effect and the simultaneous sustained release of BUP will provide a partial agonistic as well as partial antagonistic effect by helping avoid the opioid-dependent patients from undergoing sudden withdrawal symptoms.

CHAPTER 6
CONCLUSIONS, LIMITATIONS and RECOMMENDATIONS

6.1. Conclusions

The efficacy of the therapeutic agents used in the treatment of OUD, are impacted by their poor bioavailability, the effects of first-pass metabolism, limited amounts of drug reaching the brain due to the BBB and a decreased residence time at the site of action. Additionally, the route of administration for the DDSs employed plays a vital role in the effectiveness of the therapeutic agents. However, the mentioned barriers can be overcome by the incorporation of advanced DDSs to enhance the effectiveness and patient compliance of opioid reversal agents.

The review discussed in this research in Chapter 2 extensively mentions the current DDSs available and their effectiveness in the treatment of OUD. Using this review as a guide, a thermo-responsive, sustained-release BUP- and NLX- loaded SLN nasal spray was considered as a potential therapeutic treatment option for OUD. The sustained release of NLX was chosen to give an antagonistic effect, while the simultaneous sustained release of BUP provides partial agonistic, as well as partial antagonistic effects by helping avoid opioid-dependent patients from undergoing sudden withdrawal symptoms.

In this study, the polymeric BUP- and NLX- loaded SLNs were synthesized for the sustained release of BUP and NLX, overcoming their poor pharmacokinetic properties. The polymeric BUP- and NLX- loaded SLNs were successfully formulated using the modified double emulsification technique, where the targeted particle size, PDI and zeta potential were obtained. Additionally, further verification of the particle size and shape was undertaken using SEM imaging ensuring that the SLNs would cross the BBB with ease. The desired physicochemical properties of the BUP- and NLX- loaded SLNs were achieved and confirmed using FTIR, DSC and TGA ensuring their desired molecular transition and stable thermal behaviour. The maximum %EE and %LC of BUP and NLX within the SLNs was further obtained and the *in vitro* release of BUP and NLX from the SLNs was observed over a period of one week (7 days), which suggested potential increased bioavailability of BUP and NLX across the BBB and increased residence time at the site of action. The BUP- and NLX- loaded SLNs additionally showed no significant signs of *in vitro* cytotoxicity against HEK293 cells, indicating their excellent biocompatibility.

The formulated BUP- and NLX -loaded SLNs dispersion possessed low viscosity and low mucoadhesiveness which can potentially hinder their nasal residence time, leading to decreased nasal systemic absorption and decreased nose-to-brain drug delivery. Therefore, both BUP- and NLX- loaded SLNs dispersion were formulated in the form of an ISTG, which remained as a liquid dosage form at normal room temperature and undergoes sol-gel phase transition when encountered the physiological intranasal temperature i.e. 34 °C, allowing for maximal adhesion and increased drug delivery to the CNS. The optimized DSLN-loaded ISTG was characterized for its physicochemical properties such as molecular transition, $T_{sol\text{-}gel}$, viscosity and thermal behaviour followed by the *in vitro* drug release studies of BUP and NLX where, drug release was observed over a period of 7 days indicating that there was no change in the SLNs properties and maintained a sustained release of BUP and NLX. Through *ex vivo* permeation studies the permeability of BUP- and NLX- loaded SLNs from the DSLN-loaded ISTG across the pig nasal membrane was assessed where 72% of BUP- and NLX- loaded SLNs were found to be permeated within 7 hours indicating an effective uptake of drug loaded SLNs into the CNS. Lastly, the biocompatibility studies of DSLN-loaded ISTG were done using the HEK293 cell line where the formulation was not found to be cytotoxic. Therefore, it can be concluded that with the incorporation of BUP- and NLX- loaded SLNs within the optimized ISTG, the DSLN-loaded ISTG can be a potential effective and patient compliant treatment option for OUD.

6.2. Limitations and Recommendations

The current dissertation focuses on the design, formulation and characterization of DSLN-loaded ISTG as a potential treatment option for OUD. The majority of the preliminary characterizations were covered in this study but in terms of sprayability characterization i.e. evaluation of mucociliary clearance and nasal residence time, cellular autoimmune responses and cytotoxic assessment on nasal endothelial cells can be further conducted. The pre-clinical *in vivo* pharmacokinetic and tolerability assessments using animal studies and a comparative study with commercially available OUD treatment regimen in terms of release kinetics and delivery efficiency can be carried out for further characterization and validation of the formulation as the claims of sustain release and permeation in this research are based on *in vitro* and *ex vivo* studies. Additionally, a β-arrestin recruitment assay could be carried out to determine and analyse the competitive nature of BUP and NLX at the receptor site against various opioids. Given the therapeutic application and the presence of burst release in the initial phase of drug release, long-term and accelerated stability studies assessing changes in particle size, zeta potential, drug content and physical appearance over time can be taken into consideration.

In terms of novel recommendations, nanoemulsions in place of SLNs is one of the potential nanocarriers which could overcome the difficulties that were faced during the study. In terms of uniform dispersion and stability, nanoemulsions if modified as per necessity could be more beneficial as compared to SLNs. Additionally, in terms of sprayability nanoemulsions could have an upper hand as compared to SLNs. The delivery media for the SLNs were also designed to be thermo-responsive in this study, but a pH responsive gelling system could be one of the potential DDSs that could prove to be advantageous over thermo-responsive DDS, as the DDS would have more control over the sol-gel phase transition when compared to a thermo-responsive DDS. Furthermore, the current DSLN-loaded ISTG was designed as a once off weekly dose, which must be dispersed in distilled water before use. However, with the incorporation of advanced DDS concepts more effective modifications can be applied to this particular part of the study where the formulation can be dispensed in the form of a dispersion without affecting the release profile of BUP and NLX.

The formulated SLN-loaded ISTG in this study can therefore serve as a nose-to-brain DDS not only for opioid reversal drugs but also for majority of the drugs acting on the CNS with minor adjustments. The developed DDS in this study can open doors to new potential treatment options to any disease or disorder related to CNS and provide important concepts and methodologies that can facilitate various novel pharmaceutical DDSs and other relevant fields of research.

REFERENCES

Abdelgader, A., Govender, M., Kumar, P., Choonara, Y.E., 2024. A Novel Intrauterine Device for the Spatio-Temporal Release of Norethindrone Acetate as a Counter-Estrogenic Intervention in the Genitourinary Syndrome of Menopause. Pharmaceutics 16, 587. https://doi.org/10.3390/pharmaceutics16050587

Agrawal, M., Saraf, Swarnlata, Saraf, Shailendra, Antimisiaris, S.G., Hamano, N., Li, S.-D., Chougule, M., Shoyele, S.A., Gupta, U., Ajazuddin, Alexander, A., 2018. Recent advancements in the field of nanotechnology for the delivery of anti-Alzheimer drug in the brain region. Expert Opin. Drug Deliv. 15, 589–617. https://doi.org/10.1080/17425247.2018.1471058

Ahmad, F., Cisewski, J., Rossen, L., Sutton, P., 2024. Products - Vital Statistics Rapid Release - Provisional Drug Overdose Data. Natl. Cent. Health Stat. 1–10. https://www.cdc.gov/nchs/nvss/vsrr/drug-overdose-data.htm#print

Akilo, O.D., Kumar, P., Choonara, Y.E., Du Toit, L.C., Pradeep, P., Modi, G., Pillay, V., 2019. In situ thermo-co-electroresponsive mucogel for controlled release of bioactive agent. Int. J. Pharm. 559, 255–270. https://doi.org/10.1016/j.ijpharm.2019.01.044

Al Ragib, A., Chakma, R., Dewan, K., Islam, T., Kormoker, T., Idris, A.M., 2022. Current advanced drug delivery systems: Challenges and potentialities. J. Drug Deliv. Sci. Technol. 76, 103727. https://doi.org/10.1016/j.jddst.2022.103727

Albanese, A., Tang, P.S., Chan, W.C.W., 2012. The Effect of Nanoparticle Size, Shape, and Surface Chemistry on Biological Systems. Annu. Rev. Biomed. Eng. 14, 1–16. https://doi.org/10.1146/annurev-bioeng-071811-150124

Alexis, F., Pridgen, E., Molnar, L.K., Farokhzad, O.C., 2008. Factors Affecting the Clearance and Biodistribution of Polymeric Nanoparticles. Mol. Pharm. 5, 505–515. https://doi.org/10.1021/mp800051m

Ali, S., Khatri, Z., Oh, K.W., Kim, I.-S., Kim, S.H., 2014. Preparation and characterization of hybrid polycaprolactone/cellulose ultrafine fibers via electrospinning. Macromol. Res. 22, 562–568. https://doi.org/10.1007/s13233-014-2078-x

Alizadeh, T., Atashi, F., Akhoundian, M., Ganjali, M.R., 2019. Highly selective extraction and

voltammetric determination of the opioid drug buprenorphine via a carbon paste electrode impregnated with nano-sized molecularly imprinted polymer. Microchim. Acta 186, 654. https://doi.org/10.1007/s00604-019-3736-7

Almeida, A., Claeys, B., Remon, J.P., Vervaet, C., 2012. Hot-Melt Extrusion Developments in the Pharmaceutical Industry, in: Douroumis, D. (Ed.), Hot-Melt Extrusion: Pharmaceutical Applications. Wiley, pp. 43–69. https://doi.org/10.1002/9780470711415.ch3

Almeida, A., Possemiers, S., Boone, M.N., De Beer, T., Quinten, T., Van Hoorebeke, L., Remon, J.P., Vervaet, C., 2011. Ethylene vinyl acetate as matrix for oral sustained release dosage forms produced via hot-melt extrusion. Eur. J. Pharm. Biopharm. 77, 297–305. https://doi.org/10.1016/j.ejpb.2010.12.004

Alves, T., Souza, J., Rebelo, M., Pontes, K., Santos, C., Lima, R., Jozala, A., Grotto, D., Severino, P., Rai, M., Chaud, M., 2018. Formulation and evaluation of thermoresponsive polymeric blend as a vaginal controlled delivery system. J. Sol-Gel Sci. Technol. 86, 536–552. https://doi.org/10.1007/s10971-018-4662-6

Andhariya, J.V., Shen, J., Choi, S., Wang, Y., Zou, Y., Burgess, D.J., 2017. Development of in vitro-in vivo correlation of parenteral naltrexone loaded polymeric microspheres. J Control Release 255, 27–35. https://doi.org/10.1016/j.jconrel.2017.03.396

Averick, S.E., Kassick, A.J., Song, D., Zhang, B., Vigliaturo, J., Luengas, D., Silva-Ortiz, P., Pravetoni, M., Raleigh, M.D., 2024. Evaluating the rate of reversal of fentanyl-induced respiratory depression using a novel long-acting naloxone nanoparticle, cNLX-NP. Front. Psychiatry 15, 1366186. https://doi.org/10.3389/fpsyt.2024.1366186

Bakare, T.T., Uzoeto, H.O., Gonlepa, L.N., Cosmas, S., Ajima, J.N., Arazu, A.V., Ezechukwu, S.P., Didiugwu, C.M., Ibiang, G.O., Osotuyi, A.G., Durojaye, O.A., 2024. Evolution and challenges of opioids in pain management: Understanding mechanisms and exploring strategies for safer analgesics. Med. Chem. Res. 33, 563–579. https://doi.org/10.1007/s00044-024-03207-1

Barnwal, P., Das, S., Mondal, S., Ramasamy, A., Maiti, T., Saha, A., 2017. Probuphine® (buprenorphine implant): a promising candidate in opioid dependence. Ther. Adv. Psychopharmacol. 7, 119–134. https://doi.org/10.1177/2045125316681984

Bayanati, M., Khosroshahi, A.G., Alvandi, M., Mahboobian, M.M., 2021. Fabrication of a

Thermosensitive In Situ Gel Nanoemulsion for Nose to Brain Delivery of Temozolomide. J. Nanomater. 2021, 1–11. https://doi.org/10.1155/2021/1546798

Bazargani, A., Hejazi, M., Fernandez, M., Cordeiro, A., Tsala Ebode, J., Lewinski, N., Da Rocha, S., Golshahi, L., 2025. PEGylated solid lipid nanoparticles for the intranasal delivery of combination antiretroviral therapy composed of Atazanavir and Elvitegravir to treat NeuroAIDS. Int. J. Pharm. 670, 125166. https://doi.org/10.1016/j.ijpharm.2025.125166

Bell, J., Strang, J., 2020. Medication Treatment of Opioid Use Disorder. Biol. Psychiatry 87, 82–88. https://doi.org/10.1016/j.biopsych.2019.06.020

Benéitez García, M.C., Girón Moreno, R., Colmena Crespo, I., Díez-Orejas, R.M., Martín Fontelles, M.I., Goicoechea García, C., Sánchez-Robles, E.M., Gil-Alegre, M.E., 2023. Promising biomedical subcutaneous delivery system in opioid disaccustom process: In vitro/in vivo evaluation of naloxone microparticles on antagonist effect of morphine. Int. J. Pharm. 635, 122766. https://doi.org/10.1016/j.ijpharm.2023.122766

Benéitez, M.C., Espada, J.I., Fernandes, D., De La Ossa, D.H.P., Gil-Alegre, M.E., 2014. Influence of Surfactant on the Characteristics of $W_1/O/W_2$ -Microparticles. J. Surfactants Deterg. 17, 11–18. https://doi.org/10.1007/s11743-013-1505-x

Bhowmik, D., Bhanot, R., Kumar, K.P.S., 2018. Extended Release Drug Delivery-An Effective Way of Novel Drug Delivery System. Res. J. Pharm. Dos. Forms Technol. 10, 233. https://doi.org/10.5958/0975-4377.2018.00035.6

Borandeh, S., Van Bochove, B., Teotia, A., Seppälä, J., 2021. Polymeric drug delivery systems by additive manufacturing. Adv. Drug Deliv. Rev. 173, 349–373. https://doi.org/10.1016/j.addr.2021.03.022

Borges, A.F., Silva, C., Coelho, J.F.J., Simões, S., 2015. Oral films: Current status and future perspectives II — Intellectual property, technologies and market needs. J Control Release 206, 108–121. https://doi.org/10.1016/j.jconrel.2015.03.012

Brewer, C., 2002. Serum naltrexone and 6-beta-naltrexol levels from naltrexone implants can block very large amounts of heroin: a report of two cases. Addict. Biol. 7, 321–323. https://doi.org/10.1080/13556210220139541

Budd, K., Collett, B.J., 2003. III. Old dog'new (ma)trix † †Declaration of interest. Dr Collett was a member of the Transtec Advisory Board (two Meetings) organised by Napp

Pharmaceuticals and has been in receipt of three travel grants from that company over the last 5 years. Dr Budd was a member of the Transtec Advisory Boards of Napp Pharmaceuticals and Grunenthal GmbH and has received lecture and travel expenses from both companies. Br. J. Anaesth. 90, 722–724. https://doi.org/10.1093/bja/aeg133

Bukke, S.P.N., Venkatesh, C., Bandenahalli Rajanna, S., Saraswathi, T.S., Kusuma, P.K., Goruntla, N., Balasuramanyam, N., Munishamireddy, S., 2024. Solid lipid nanocarriers for drug delivery: design innovations and characterization strategies—a comprehensive review. Discov. Appl. Sci. 6, 279. https://doi.org/10.1007/s42452-024-05897-z

Cao, D., Li, F., Wu, N., Li, J., 2023. Insights into the mechanisms underlying opioid use disorder and potential treatment strategies. Br. J. Pharmacol. 180, 862–878. https://doi.org/10.1111/bph.15592

Chalabianloo, F., Fadnes, L.T., Johansson, K.A., Hoiseth, G., Vold, J.H., Kringen, M.K., Spigset, O., Bramness, J.G., 2024. Methadone pharmacokinetics in opioid agonist treatment: Influencing factors and clinical implications. Basic Clin. Pharmacol. Toxicol. 134, 333–344. https://doi.org/10.1111/bcpt.13975

Chaturvedi, M., Kumar, M., Pathak, K., 2011. A review on mucoadhesive polymer used in nasal drug delivery system. J. Adv. Pharm. Technol. Res. 2, 215. https://doi.org/10.4103/2231-4040.90876

Chen, Y., Zhang, C., Huang, Y., Ma, Y., Song, Q., Chen, H., Jiang, G., Gao, X., 2024. Intranasal drug delivery: The interaction between nanoparticles and the nose-to-brain pathway. Adv. Drug Deliv. Rev. 207, 115196. https://doi.org/10.1016/j.addr.2024.115196

Chiang, C., 2003. Pharmacokinetics of the combination tablet of buprenorphine and naloxone. Drug Alcohol Depend. 70, S39–S47. https://doi.org/10.1016/S0376-8716(03)00058-9

Choudhury, M., Mathiazhagan, N., Reddy, J.S.R., 2024. Comparison of WHO Pain Ladder Management versus Severity-based Pain Management in Patients Presented with Acute Abdominal Pain Visiting Emergency Department. Apollo Med. 21, 153–8. https://doi.org/10.4103/am.am_116_23

Compton, P., Ling, W., Moody, D., Chiang, N., 2006. Pharmacokinetics, bioavailability and opioid effects of liquid versus tablet buprenorphine. Drug Alcohol Depend. 82, 25–31.

https://doi.org/10.1016/j.drugalcdep.2005.08.005

Cunha, S., Forbes, B., Sousa Lobo, J.M., Silva, A.C., 2021. Improving Drug Delivery for Alzheimer's Disease Through Nose-to-Brain Delivery Using Nanoemulsions, Nanostructured Lipid Carriers (NLC) and in situ Hydrogels. Int. J. Nanomedicine Volume 16, 4373–4390. https://doi.org/10.2147/IJN.S305851

Cunha, S., Swedrowska, M., Bellahnid, Y., Xu, Z., Sousa Lobo, J.M., Forbes, B., Silva, A.C., 2022. Thermosensitive in situ hydrogels of rivastigmine-loaded lipid-based nanosystems for nose-to-brain delivery: characterisation, biocompatibility, and drug deposition studies. Int. J. Pharm. 620, 121720. https://doi.org/10.1016/j.ijpharm.2022.121720

Danaei, M., Dehghankhold, M., Ataei, S., Hasanzadeh Davarani, F., Javanmard, R., Dokhani, A., Khorasani, S., Mozafari, M.R., 2018. Impact of Particle Size and Polydispersity Index on the Clinical Applications of Lipidic Nanocarrier Systems. Pharmaceutics 10, 57. https://doi.org/10.3390/pharmaceutics10020057

Danyuo, Y., Ani, C.J., Salifu, A.A., Obayemi, J.D., Dozie-Nwachukwu, S., Obanawu, V.O., Akpan, U.M., Odusanya, O.S., Abade-Abugre, M., McBagonluri, F., Soboyejo, W.O., 2019. Anomalous Release Kinetics of Prodigiosin from Poly-N-Isopropyl-Acrylamid based Hydrogels for The Treatment of Triple Negative Breast Cancer. Sci. Rep. 9, 3862. https://doi.org/10.1038/s41598-019-39578-4

Dash, T.K., Konkimalla, V.B., 2012. Poly-ϵ-caprolactone based formulations for drug delivery and tissue engineering: A review. J Control Release 158, 15–33. https://doi.org/10.1016/j.jconrel.2011.09.064

De Aquino, J.P., Parida, S., Sofuoglu, M., 2021. The Pharmacology of Buprenorphine Microinduction for Opioid Use Disorder. Clin. Drug Investig. 41, 425–436. https://doi.org/10.1007/s40261-021-01032-7

De Oliveira Junior, E.R., Nascimento, T.L., Salomão, M.A., Da Silva, A.C.G., Valadares, M.C., Lima, E.M., 2019. Increased Nose-to-Brain Delivery of Melatonin Mediated by Polycaprolactone Nanoparticles for the Treatment of Glioblastoma. Pharm. Res. 36, 131. https://doi.org/10.1007/s11095-019-2662-z

Deshmukh, K., Basheer Ahamed, M., Deshmukh, R.R., Khadheer Pasha, S.K., Bhagat, P.R., Chidambaram, K., 2017. Biopolymer Composites With High Dielectric Performance:

Interface Engineering, in: Biopolymer Composites in Electronics. Elsevier, pp. 27–128. https://doi.org/10.1016/B978-0-12-809261-3.00003-6

Dhowan, B., Lim, J., MacLean, M.D., Berman, A.G., Kim, M.K., Yang, Q., Linnes, J., Lee, C.H., Goergen, C.J., Lee, H., 2019. Simple minimally-invasive automatic antidote delivery device (A2D2) towards closed-loop reversal of opioid overdose. J Control Release 306, 130–137. https://doi.org/10.1016/j.jconrel.2019.05.041

Domnina, Yu.M., Suslov, V.V., Kedik, S.A., Volkova, P.O., 2021. Approaches to the Development of a Low-dose Naltrexone Preparation in the Form of a Nasal Spray (Review). Drug Dev. Regist. 10, 37–47. https://doi.org/10.33380/2305-2066-2021-10-1-37-47

Dorraj, G., Moghimi, H.R., 2015. Preparation of SLN-containing Thermoresponsive In-situ Forming Gel as a Controlled Nanoparticle Delivery System and Investigating its Rheological, Thermal and Erosion Behavior. Iran. J. Pharm. Res. 14, 347–58. https://pmc.ncbi.nlm.nih.gov/articles/PMC4403051/

Dunbar, J.L., Turncliff, R.Z., Dong, Q., Silverman, B.L., Ehrich, E.W., Lasseter, K.C., 2006. Single- and Multiple-Dose Pharmacokinetics of Long-acting Injectable Naltrexone. Alcohol. Clin. Exp. Res. 30, 480–490. https://doi.org/10.1111/j.1530-0277.2006.00052.x

Dürig, T., Karan, K., 2019. Binders in Wet Granulation, in: Handbook of Pharmaceutical Wet Granulation. Elsevier, pp. 317–349. https://doi.org/10.1016/B978-0-12-810460-6.00010-5

Ebrahimi, H.A., Javadzadeh, Y., Hamidi, M., Jalali, M.B., 2015. Repaglinide-loaded solid lipid nanoparticles: effect of using different surfactants/stabilizers on physicochemical properties of nanoparticles. DARU J. Pharm. Sci. 23, 46. https://doi.org/10.1186/s40199-015-0128-3

Edinoff, A.N., Nix, C.A., Reed, T.D., Bozner, E.M., Alvarez, M.R., Fuller, M.C., Anwar, F., Cornett, E.M., Kaye, A.M., Kaye, A.D., 2021. Pharmacologic and Clinical Considerations of Nalmefene, a Long Duration Opioid Antagonist, in Opioid Overdose. Psychiatry Int. 2, 365–378. https://doi.org/10.3390/psychiatryint2040028

El Taweel, M.M., Aboul-Einien, M.H., Kassem, M.A., Elkasabgy, N.A., 2021. Intranasal Zolmitriptan-Loaded Bilosomes with Extended Nasal Mucociliary Transit Time for

Direct Nose to Brain Delivery. Pharmaceutics 13, 1828. https://doi.org/10.3390/pharmaceutics13111828

Eleraky, N.E., Allam, A., Hassan, S.B., Omar, M.M., 2020. Nanomedicine Fight against Antibacterial Resistance: An Overview of the Recent Pharmaceutical Innovations. Pharmaceutics 12, 142. https://doi.org/10.3390/pharmaceutics12020142

Elkader, A., Sproule, B., 2005. Buprenorphine: Clinical Pharmacokinetics in the Treatment of Opioid Dependence. Clin. Pharmacokinet. 44, 661–680. https://doi.org/10.2165/00003088-200544070-00001

Fahmy, R.H., 2012. Statistical Approach for Assessing the Influence of Calcium Silicate and HPMC on the Formulation of Novel Alfuzosin Hydrochloride Mucoadhesive-Floating Beads as Gastroretentive Drug Delivery Systems. AAPS PharmSciTech 13, 990–1004. https://doi.org/10.1208/s12249-012-9823-2

Farah, S., Anderson, D.G., Langer, R., 2016. Physical and mechanical properties of PLA, and their functions in widespread applications — A comprehensive review. Adv. Drug Deliv. Rev. 107, 367–392. https://doi.org/10.1016/j.addr.2016.06.012

Fatouh, A.M., Elshafeey, A.H., Abdelbary, A., 2017. Agomelatine-based *in situ* gels for brain targeting via the nasal route: statistical optimization, *in vitro* , and *in vivo* evaluation. Drug Deliv. 24, 1077–1085. https://doi.org/10.1080/10717544.2017.1357148

Fayzullin, A., Bakulina, A., Mikaelyan, K., Shekhter, A., Guller, A., 2021. Implantable Drug Delivery Systems and Foreign Body Reaction: Traversing the Current Clinical Landscape. Bioengineering 8, 205. https://doi.org/10.3390/bioengineering8120205

Formica, M.L., Real, D.A., Picchio, M.L., Catlin, E., Donnelly, R.F., Paredes, A.J., 2022. On a highway to the brain: A review on nose-to-brain drug delivery using nanoparticles. Appl. Mater. Today 29, 101631. https://doi.org/10.1016/j.apmt.2022.101631

Galloway, G.P., Koch, M., Cello, R., Smith, D.E., 2005. Pharmacokinetics, safety, and tolerability of a depot formulation of naltrexone in alcoholics: an open-label trial. BMC Psychiatry 5, 18. https://doi.org/10.1186/1471-244X-5-18

Garg, A., 2024. In-situ gel: A smart carrier for drug delivery. Int. J. Pharm. 652, 123819. https://doi.org/10.1016/j.ijpharm.2024.123819

Ghosh, A., Majie, A., Karmakar, V., Chatterjee, K., Chakraborty, S., Pandey, M., Jain, N., Roy

Sarkar, S., Nair, A.B., Gorain, B., 2024. In-depth Mechanism, Challenges, and Opportunities of Delivering Therapeutics in Brain Using Intranasal Route. AAPS PharmSciTech 25, 96. https://doi.org/10.1208/s12249-024-02810-0

Giunchedi, P., Gavini, E., Bonferoni, M.C., 2020. Nose-to-Brain Delivery. Pharmaceutics 12, 138. https://doi.org/10.3390/pharmaceutics12020138

Goonoo, N., Bhaw-Luximon, A., Ujoodha, R., Jhugroo, A., Hulse, G.K., Jhurry, D., 2014. Naltrexone: A review of existing sustained drug delivery systems and emerging nano-based systems. J Control Release 183, 154–66. https://doi.org/10.1016/j.jconrel.2014.03.046

Govender, M., Indermun, S., Kumar, P., Choonara, Y.E., 2023. Potential Targeting Sites to the Brain Through Nasal Passage, in: Pathak, Y.V., Yadav, H.K.S. (Eds.), Nasal Drug Delivery: Formulations, Developments, Challenges, and Solutions. Springer International Publishing, Cham, pp. 83–99. https://doi.org/10.1007/978-3-031-23112-4_6

Govender, T., Choonara, Y., Kumar, P., Du Toit, L., Modi, G., Naidoo, D., Pillay, V., 2015. A Novel Melt-Dispersion Technique for Simplistic Preparation of Chlorpromazine-Loaded Polycaprolactone Nanocapsules. Polymers 7, 1145–1176. https://doi.org/10.3390/polym7061145

Guarnieri, M., Brayton, C., Tyler, B.M., 2018a. A Long-Term Study of a Lipid-Buprenorphine Implant in Rats. J. Vet. Med. 2018, 1–4. https://doi.org/10.1155/2018/2616152

Gude, S., Varun, A.B., 2024. Exploring innovative drug delivery systems for the targeted treatment and rehabilitation of individuals affected by narcotics and psychotropic substances: a multidisciplinary approach in pharmaceutics. Transl. Regul. Sci. 6, 2024–003. https://doi.org/10.33611/trs.2024-003

Guguta, C., van Eck, E.R.H., de Gelder, R., 2009. Structural Insight into the Dehydration and Hydration Behavior of Naltrexone and Naloxone Hydrochloride. Dehydration-Induced Expansion versus Contraction. Cryst. Growth Des. 9, 3384–3395. https://doi.org/10.1021/cg801051u

Gupta, M., Gowda, D., Kumar, T., Rosenholm, J., 2022. A Comprehensive Review of Patented Technologies to Fabricate Orodispersible Films: Proof of Patent Analysis (2000–2020). Pharmaceutics 14, 820. https://doi.org/10.3390/pharmaceutics14040820

Gupta, M.S., Kumar, T.P., Gowda, D.V., Rosenholm, J.M., 2021. Orodispersible films: Conception to quality by design. Adv. Drug Deliv. Rev. 178, 113983. https://doi.org/10.1016/j.addr.2021.113983

Gupta, R., Shah, N.D., Ross, J.S., 2016. The Rising Price of Naloxone — Risks to Efforts to Stem Overdose Deaths. N. Engl. J. Med. 375, 2213–2215. https://doi.org/10.1056/NEJMp1609578

Gupta, S.K., Kumar, S., 2019. An Overview on Intranasal Drug Delivery System: Recent Technique and its Contribution in Therapeutic Management. Curr. Res. Pharm. Sci. 9, 17–23. https://doi.org/10.24092/CRPS.2019.090201

Hagedorn, J.M., 2022. World Health Organization Analgesic Ladder, in: Banik, R.K. (Ed.), Anesthesiology In-Training Exam Review: Regional Anesthesia and Chronic Pain. Springer International Publishing, Cham, pp. 351–4. https://doi.org/10.1007/978-3-030-87266-3_67

Hanna, V., Senderovich, H., 2021. Methadone in Pain Management: A Systematic Review. J. Pain 22, 233–45. https://doi.org/10.1016/j.jpain.2020.04.004

Hasan, N., Imran, M., Kesharwani, P., Khanna, K., Karwasra, R., Sharma, N., Rawat, S., Sharma, D., Ahmad, F.J., Jain, G.K., Bhatnagar, A., Talegaonkar, S., 2021a. Intranasal delivery of Naloxone-loaded solid lipid nanoparticles as a promising simple and non-invasive approach for the management of opioid overdose. Int. J. Pharm. 599, 120428. https://doi.org/10.1016/j.ijpharm.2021.120428

Hassan, S.U., Khalid, I., Hussain, L., Barkat, K., Khan, I.U., 2022. Development and Evaluation of pH-Responsive Pluronic F 127 Co-Poly- (Acrylic Acid) Biodegradable Nanogels for Topical Delivery of Terbinafine HCL. Dose-Response 20, 15593258221095977. https://doi.org/10.1177/15593258221095977

Heidbreder, C., Fudala, P.J., Greenwald, M.K., 2023. History of the discovery, development, and FDA-approval of buprenorphine medications for the treatment of opioid use disorder. Drug Alcohol Depend. Rep. 6, 100133. https://doi.org/10.1016/j.dadr.2023.100133

Herlinger, K., Lingford-Hughes, A., 2022. Opioid use disorder and the brain: a clinical perspective. Addiction 117, 495–505. https://doi.org/10.1111/add.15636

Huanbutta, K., Puri, V., Sharma, A., Singh, I., Sriamornsak, P., Sangnim, T., 2024. Rise of

implantable drugs: A chronicle of breakthroughs in drug delivery systems. Saudi Pharm. J. 32, 102193. https://doi.org/10.1016/j.jsps.2024.102193

Huang, Qingqing, Chen, X., Yu, S., Gong, G., Shu, H., 2024. Research progress in brain-targeted nasal drug delivery. Front. Aging Neurosci. 15, 1341295. https://doi.org/10.3389/fnagi.2023.1341295

Huang, Qianqian, Chen, Y., Zhang, W., Xia, X., Li, H., Qin, M., Gao, H., 2024. Nanotechnology for enhanced nose-to-brain drug delivery in treating neurological diseases. J Control Release 366, 519–534. https://doi.org/10.1016/j.jconrel.2023.12.054

Hussain, A., Kimura, R., Chong-Heng, H., Kashihara, T., 1984. Nasal absorption of naloxone and buprenorphine in rats. Int. J. Pharm. 21, 233–237. https://doi.org/10.1016/0378-5173(84)90097-8

Iqbal, F.M., Ahmad, M., Tulain, U.R., 2017. Microwave Radiation Induced Synthesis of Hydroxypropyl Methylcellulose-Graft- (Polyvinylalcohal-Co-Acrylic Acid) Polymeric Network and its In Vitro Evaluation. Acta Pol. Pharm.-Drug Res. 74, 527–41. https://pubmed.ncbi.nlm.nih.gov/29624258/

Iravani, S., Varma, R.S., 2022. Advanced Drug Delivery Micro- and Nanosystems for Cardiovascular Diseases. Molecules 27, 5843. https://doi.org/10.3390/molecules27185843

Jeong, S.-H., Jang, J.-H., Lee, Y.-B., 2023. Drug delivery to the brain via the nasal route of administration: exploration of key targets and major consideration factors. J. Pharm. Investig. 53, 119–152. https://doi.org/10.1007/s40005-022-00589-5

Jeong, W.Y., Kwon, M., Choi, H.E., Kim, K.S., 2021. Recent advances in transdermal drug delivery systems: a review. Biomater. Res. 25, 24. https://doi.org/10.1186/s40824-021-00226-6

Jindal, A.B., Bhide, A.R., Salave, S., Rana, D., Benival, D., 2023. Long-acting parenteral drug delivery systems for the treatment of chronic diseases. Adv. Drug Deliv. Rev. 198, 114862. https://doi.org/10.1016/j.addr.2023.114862

Jones, C.M., Campopiano, M., Baldwin, G., McCance-Katz, E., 2015. National and State Treatment Need and Capacity for Opioid Agonist Medication-Assisted Treatment. Am. J. Public Health 105, e55–e63. https://doi.org/10.2105/AJPH.2015.302664

Jönsson, M., Mundin, G., Sumner, M., 2018. Pharmacokinetic and pharmaceutical properties of a novel buprenorphine/naloxone sublingual tablet for opioid substitution therapy versus conventional buprenorphine/naloxone sublingual tablet in healthy volunteers. Eur. J. Pharm. Sci. 122, 125–133. https://doi.org/10.1016/j.ejps.2018.06.024

Joshi, A.S., Patel, H.S., Belgamwar, V.S., Agrawal, A., Tekade, A.R., 2012. Solid lipid nanoparticles of ondansetron HCl for intranasal delivery: development, optimization and evaluation. J. Mater. Sci. Mater. Med. 23, 2163–2175. https://doi.org/10.1007/s10856-012-4702-7

Kakko, J., Alho, H., Baldacchino, A., Molina, R., Nava, F.A., Shaya, G., 2019. Craving in Opioid Use Disorder: From Neurobiology to Clinical Practice. Front. Psychiatry 10, 592. https://doi.org/10.3389/fpsyt.2019.00592

Kamali, H., Khodaverdi, E., Hadizadeh, F., 2018. Ring-opening polymerization of PLGA-PEG-PLGA triblock copolymer in supercritical carbon dioxide. J. Supercrit. Fluids 137, 9–15. https://doi.org/10.1016/j.supflu.2018.03.001

Kamali, H., Khodaverdi, E., Hadizadeh, F., Mohajeri, S.A., 2019. In-vitro, ex-vivo, and in-vivo evaluation of buprenorphine HCl release from an in situ forming gel of PLGA-PEG-PLGA using N-methyl-2-pyrrolidone as solvent. Mater. Sci. Eng. C 96, 561–575. https://doi.org/10.1016/j.msec.2018.11.058

Kapoor, D.N., Bhatia, A., Kaur, R., Sharma, R., Kaur, G., Dhawan, S., 2015. PLGA: a unique polymer for drug delivery. Ther. Deliv. 6, 41–58. https://doi.org/10.4155/tde.14.91

Kapoor, M., Cloyd, J.C., Siegel, R.A., 2016. A review of intranasal formulations for the treatment of seizure emergencies. J Control Release 237, 147–59. https://doi.org/10.1016/j.jconrel.2016.07.001

Karavelidis, V., Bikiaris, D., Avgoustakis, K., 2015. New thermosensitive nanoparticles prepared by biocompatible pegylated aliphatic polyester block copolymers for local cancer treatment. J. Pharm. Pharmacol. 67, 215–230. https://doi.org/10.1111/jphp.12337

Kariduraganavar, M.Y., Kittur, A.A., Kamble, R.R., 2014. Polymer Synthesis and Processing, in: Natural and Synthetic Biomedical Polymers. Elsevier, pp. 1–31. https://doi.org/10.1016/B978-0-12-396983-5.00001-6

Karolewicz, B., Górniak, A., Owczarek, A., Żurawska-Płaksej, E., Piwowar, A., Pluta, J., 2014.

Thermal, spectroscopic, and dissolution studies of ketoconazole–Pluronic F127 system. J. Therm. Anal. Calorim. 115, 2487–2493. https://doi.org/10.1007/s10973-014-3661-2

Karve, T., Dandekar, A., Agrahari, V., Melissa Peet, M., Banga, A.K., Doncel, G.F., 2024a. Long-acting transdermal drug delivery formulations: Current developments and innovative pharmaceutical approaches. Adv. Drug Deliv. Rev. 210, 115326. https://doi.org/10.1016/j.addr.2024.115326

Karve, T., Dandekar, A., Agrahari, V., Melissa Peet, M., Banga, A.K., Doncel, G.F., 2024b. Long-acting transdermal drug delivery formulations: Current developments and innovative pharmaceutical approaches. Adv. Drug Deliv. Rev. 210, 115326. https://doi.org/10.1016/j.addr.2024.115326

Kasina, V., Mownn, R.J., Bahal, R., Sartor, G.C., 2022. Nanoparticle delivery systems for substance use disorder. Neuropsychopharmacology 47, 1431–1439. https://doi.org/10.1038/s41386-022-01311-7

Kassick, A.J., Allen, H.N., Yerneni, S.S., Pary, F., Kovaliov, M., Cheng, C., Pravetoni, M., Tomycz, N.D., Whiting, D.M., Nelson, T.L., Feasel, M., Campbell, P.G., Kolber, B., Averick, S., 2019. Covalent Poly(lactic acid) Nanoparticles for the Sustained Delivery of Naloxone. ACS Appl. Bio Mater. 2, 3418–28. https://doi.org/10.1021/acsabm.9b00380

Kaur, I.P., Bhandari, R., Bhandari, S., Kakkar, V., 2008. Potential of solid lipid nanoparticles in brain targeting. J Control Release 127, 97–109. https://doi.org/10.1016/j.jconrel.2007.12.018

Kaur, P., 2018. Literature Review: Ring Opening Polymerization of Polylactide. J. Emerg. Technol. Innov. Res. 5, 471–89.

Kerman, I., Toppare, L., Yilmaz, F., Yagci, Y., 2005. Thiophene Ended ϵ -Caprolactone Conducting Copolymers and their Electrochromic Properties. J. Macromol. Sci. Part A 42, 509–520. https://doi.org/10.1081/MA-200054363

Khizar, S., Alrushaid, N., Alam Khan, F., Zine, N., Jaffrezic-Renault, N., Errachid, A., Elaissari, A., 2023. Nanocarriers based novel and effective drug delivery system. Int. J. Pharm. 632, 122570. https://doi.org/10.1016/j.ijpharm.2022.122570

Khodaverdi, E., Hadizadeh, F., Hoseini, N., Eisvand, F., Tayebi, M., Kamali, H., Oroojalian,

F., 2023. In-vitro and in-vivo evaluation of sustained-release buprenorphine using in-situ forming lipid-liquid crystal gels. Life Sci. 314, 121324. https://doi.org/10.1016/j.lfs.2022.121324

Kim, B.Y.S., Rutka, J.T., Chan, W.C.W., 2010. Nanomedicine. N. Engl. J. Med. 363, 2434–2443. https://doi.org/10.1056/NEJMra0912273

Kisku, A., Nishad, A., Agrawal, S., Paliwal, R., Datusalia, A.K., Gupta, G., Singh, S.K., Dua, K., Sulakhiya, K., 2024. Recent developments in intranasal drug delivery of nanomedicines for the treatment of neuropsychiatric disorders. Front. Med. 11, 1463976. https://doi.org/10.3389/fmed.2024.1463976

Kovaliov, M., Li, S., Korkmaz, E., Cohen-Karni, D., Tomycz, N., Ozdoganlar, O.B., Averick, S., 2017. Extended-release of opioids using fentanyl-based polymeric nanoparticles for enhanced pain management. RSC Adv 7, 47904–47912. https://doi.org/10.1039/C7RA08450A

Koyyalagunta, D., 2011. Opioid Analgesics, in: Specific Treatment Modalities for Pain and Symptom Management. Saunders, pp. 939–964.

Krupitsky, E., Blokhina, E., Zvartau, E., Woody, G., 2017. Antagonist Treatment for Opioid Dependence: Promise and Hurdles. Curr. Treat. Options Psychiatry 4, 221–230. https://doi.org/10.1007/s40501-017-0110-4

Krupitsky, E., Zvartau, E., Blokhina, E., Verbitskaya, E., Wahlgren, V., Tsoy-Podosenin, M., Bushara, N., Burakov, A., Masalov, D., Romanova, T., Tyurina, A., Palatkin, V., Slavina, T., Pecoraro, A., Woody, G.E., 2012. Randomized Trial of Long-Acting Sustained-Release Naltrexone Implant vs Oral Naltrexone or Placebo for Preventing Relapse to Opioid Dependence. Arch. Gen. Psychiatry 69, 973. https://doi.org/10.1001/archgenpsychiatry.2012.1a

Kunoe, N., Lobmaier, P., Vederhus, J.K., Hjerkinn, B., Hegstad, S., Gossop, M., Kristensen, Ø., Waal, H., 2009. Naltrexone implants after in-patient treatment for opioid dependence: randomised controlled trial. Br. J. Psychiatry 194, 541–546. https://doi.org/10.1192/bjp.bp.108.055319

Kurakula, M., Rao, G.S.N.K., 2020. Pharmaceutical assessment of polyvinylpyrrolidone (PVP): As excipient from conventional to controlled delivery systems with a spotlight on COVID-19 inhibition. J. Drug Deliv. Sci. Technol. 60, 102046.

https://doi.org/10.1016/j.jddst.2020.102046

Laffont, C.M., Gomeni, R., Heidbreder, C., Jones, J.P., Nasser, A.F., 2016. Population Pharmacokinetic Modeling After Repeated Administrations of RBP-6000, a New, Subcutaneously Injectable, Long-Acting, Sustained-Release Formulation of Buprenorphine, for the Treatment of Opioid Use Disorder. J. Clin. Pharmacol. 56, 806–815. https://doi.org/10.1002/jcph.665

Lambert, D.G., 2023. Opioids and opioid receptors; understanding pharmacological mechanisms as a key to therapeutic advances and mitigation of the misuse crisis. BJA Open 6, 100141. https://doi.org/10.1016/j.bjao.2023.100141

Lanier, R.K., Umbricht, A., Harrison, J.A., Nuwayser, E.S., Bigelow, G.E., 2008. Opioid detoxification via single 7-day application of a buprenorphine transdermal patch: an open-label evaluation. Psychopharmacology (Berl.) 198, 149–158. https://doi.org/10.1007/s00213-008-1105-z

Lanier, R.K., Umbricht, A., Harrison, J.A., Nuwayser, E.S., Bigelow, G.E., 2007. Evaluation of a transdermal buprenorphine formulation in opioid detoxification. Addiction 102, 1648–1656. https://doi.org/10.1111/j.1360-0443.2007.01944.x

Liechty, W.B., Kryscio, D.R., Slaughter, B.V., Peppas, N.A., 2010. Polymers for Drug Delivery Systems. Annu. Rev. Chem. Biomol. Eng. 1, 149–173. https://doi.org/10.1146/annurev-chembioeng-073009-100847

Likar, R., 2006. Transdermal buprenorphine in the management of persistent pain – safety aspects. Ther. Clin. Risk Manag. 2(1), 115–125.

Likar, R., Lorenz, V., Korak-Leiter, M., Kager, I., Sittl, R., 2007. Transdermal Buprenorphine Patches Applied in a 4-Day Regimen Versus a 3-Day Regimen: A Single-Site, Phase lll, Randomized, Open-Label, Crossover Comparison. Clin. Ther. 29, 1591–1606.

Ling, W., Casadonte, P., Bigelow, G., Kampman, K.M., Patkar, A., Bailey, G.L., Rosenthal, R.N., Beebe, K.L., 2010. Buprenorphine Implants for Treatment of Opioid Dependence: A Randomized Controlled Trial. JAMA 304, 1576. https://doi.org/10.1001/jama.2010.1427

Liu, Y., Bruce Sunderland, V., Liu, Y., George O'Neil, A., 2006. In Vitro and In Vivo Release of Naltrexone from Biodegradable Depot Systems. Drug Dev. Ind. Pharm. 32, 85–94. https://doi.org/10.1080/03639040500388466

Lofwall, M.R., Walsh, S.L., Nunes, E.V., Bailey, G.L., Sigmon, S.C., Kampman, K.M., Frost, M., Tiberg, F., Linden, M., Sheldon, B., Oosman, S., Peterson, S., Chen, M., Kim, S., 2018. Weekly and Monthly Subcutaneous Buprenorphine Depot Formulations vs Daily Sublingual Buprenorphine With Naloxone for Treatment of Opioid Use Disorder: A Randomized Clinical Trial. JAMA Intern. Med. 178, 764. https://doi.org/10.1001/jamainternmed.2018.1052

López-García, J., Lehocký, M., Humpolíček, P., Sáha, P., 2014. HaCaT Keratinocytes Response on Antimicrobial Atelocollagen Substrates: Extent of Cytotoxicity, Cell Viability and Proliferation. J. Funct. Biomater. 5, 43–57. https://doi.org/10.3390/jfb5020043

Lutfy, K., Cowan, A., 2004. Buprenorphine: A Unique Drug with Complex Pharmacology. Curr. Neuropharmacol. 2, 395–402. https://doi.org/10.2174/1570159043359477

Magill, E., Demartis, S., Gavini, E., Permana, A.D., Thakur, R.R.S., Adrianto, M.F., Waite, D., Glover, K., Picco, C.J., Korelidou, A., Detamornrat, U., Vora, L.K., Li, L., Anjani, Q.K., Donnelly, R.F., Domínguez-Robles, J., Larrañeta, E., 2023. Solid implantable devices for sustained drug delivery. Adv. Drug Deliv. Rev. 199, 114950. https://doi.org/10.1016/j.addr.2023.114950

Martins, P.P., Smyth, H.D.C., Cui, Z., 2019. Strategies to facilitate or block nose-to-brain drug delivery. Int. J. Pharm. 570, 118635. https://doi.org/10.1016/j.ijpharm.2019.118635

Masiuk, T., Kadakia, P., Wang, Z., 2016. Development of a physiologically relevant dripping analytical method using simulated nasal mucus for nasal spray formulation analysis. J. Pharm. Anal. 6, 283–291. https://doi.org/10.1016/j.jpha.2016.05.003

Mastropietro, D., Park, K., Omidian, H., 2017. 4.23 Polymers in Oral Drug Delivery, in: Comprehensive Biomaterials II. Elsevier, pp. 430–444. https://doi.org/10.1016/B978-0-12-803581-8.09291-2

McGuire, L.S., Slavin, K., 2020. Revisiting the WHO Analgesic Ladder for Surgical Management of Pain. AMA J. Ethics 22, E695-701. https://doi.org/10.1001/amajethics.2020.695

Mishra, V., Bansal, K.K., Verma, A., Yadav, N., Thakur, S., Sudhakar, K., Rosenholm, J.M., 2018. Solid Lipid Nanoparticles: Emerging Colloidal Nano Drug Delivery Systems. Pharmaceutics 10, 191. https://doi.org/10.3390/pharmaceutics10040191

Mohammadi, F., Shabani, A.M.H., Dadfarnia, S., Ansari, M., Asgharinezhad, A.A., 2020. Dispersive solid-phase extraction of buprenorphine from biological fluids using metal-organic frameworks and its determination by ultra-performance liquid chromatography. J. Sep. Sci. 43, 3045–3052. https://doi.org/10.1002/jssc.202000221

Mooney, L.J., Saxon, A., 2019. State-of-The-Art Treatment of Opioid Use Disorder, in: The Assessment and Treatment of Addiction. Elsevier, pp. 91–104. https://doi.org/10.1016/B978-0-323-54856-4.00006-7

Mundhey, D.A., Sapkal, N.P., Daud, A.S., 2016. Simultaneous Quantification of Buprenorphine HCl and Naloxone HCl by Vierordt's Method. Int. J. Pharm. Pharm. Sci. 8, 101–107. https://journals.innovareacademics.in/index.php/ijpps/article/view/8580

Naik, K., Du Toit, L.C., Ally, N., Choonara, Y.E., 2024. In vivo evaluation of a Nano-enabled therapeutic vitreous substitute for the precise delivery of triamcinolone to the posterior segment of the eye. Drug Deliv. Transl. Res. 14, 2668–2694. https://doi.org/10.1007/s13346-024-01566-1

Nanaki, S., Viziridou, A., Zamboulis, A., Kostoglou, M., Papageorgiou, G.Z., Bikiaris, D.N., 2020. New Biodegradable Poly(l-lactide)-Block-Poly(propylene adipate) Copolymer Microparticles for Long-Acting Injectables of Naltrexone Drug. Polymers 12, 852. https://doi.org/10.3390/polym12040852

Nasser, A.F., Greenwald, M.K., Vince, B., Fudala, P.J., Twumasi-Ankrah, P., Liu, Y., Jones, J., Heidbreder, C., 2016. Sustained-Release Buprenorphine (RBP-6000) Blocks the Effects of Opioid Challenge With Hydromorphone in Subjects With Opioid Use Disorder. J. Clin. Psychopharmacol. 36, 18–26. https://doi.org/10.1097/JCP.0000000000000434

Nasser, A.F., Heidbreder, C., Gomeni, R., Fudala, P.J., Zheng, B., Greenwald, M.K., 2014. A Population Pharmacokinetic and Pharmacodynamic Modelling Approach to Support the Clinical Development of RBP-6000, a New, Subcutaneously Injectable, Long-Acting, Sustained-Release Formulation of Buprenorphine, for the Treatment of Opioid Dependence. Clin. Pharmacokinet. 53, 813–824. https://doi.org/10.1007/s40262-014-0155-0

Nataraj, N., Rikard, S.M., Zhang, K., Jiang, X., Guy, G.P., Rice, K., Mattson, C.L., Gladden, R.M., Mustaquim, D.M., Illg, Z.N., Seth, P., Noonan, R.K., Losby, J.L., 2024. Public

Health Interventions and Overdose-Related Outcomes Among Persons With Opioid Use Disorder. JAMA Netw. Open 7, e244617. https://doi.org/10.1001/jamanetworkopen.2024.4617

Nath, R.P., Upton, R.A., Everhart, E.T., Cheung, P., Shwonek, P., Jones, R.T., Mendelson, J.E., 1999. Buprenorphine Pharmacokinetics: Relative Bioavailability of Sublingual Tablet and Liquid Formulations. J. Clin. Pharmacol. 39, 619–623. https://doi.org/10.1177/00912709922008236

Ndegwa et al., S., 2017. Injectable Extended-Release Naltrexone to Treat Opioid Use Disorder. CADTH Issues Emerg. Health Technol. 1–20.

Neves, A.R., 2015. Solid lipid nanoparticles as a vehicle for brain-targeted drug delivery: two new strategies of functionalization with apolipoprotein E. Nanotechnology 26, 495103. http://dx.doi.org/10.1088/0957-4484/26/49/495103

Neves, A.R., Queiroz, J.F., Weksler, B., Romero, I.A., Couraud, P.-O., Reis, S., 2015. Solid lipid nanoparticles as a vehicle for brain-targeted drug delivery: two new strategies of functionalization with apolipoprotein E. Nanotechnology 26, 495103. https://doi.org/10.1088/0957-4484/26/49/495103

Ng, W.S., Lee, C.S., Cheng, S.-F., Chuah, C.H., Wong, S.F., 2018. Biocompatible Polyurethane Scaffolds Prepared from Glycerol Monostearate-Derived Polyester Polyol. J. Polym. Environ. 26, 2881–2900. https://doi.org/10.1007/s10924-017-1175-2

Ngo, H.T.T., Arnold-Reed, D.E., Hansson, R.C., Tait, R.J., Hulse, G.K., 2008. Blood naltrexone levels over time following naltrexone implant. Prog. Neuropsychopharmacol. Biol. Psychiatry 32, 23–28. https://doi.org/10.1016/j.pnpbp.2007.06.007

Nichols, M.A., Riley, E.G., Chao, A.S., Sales, C.G., Miller, M.L., Curran, G.M., Ott, C.A., Snyder, M.E., Hudmon, K.S., 2023. Opioid Use Disorder Curricular Content in US-Based Doctor of Pharmacy Programs. Am. J. Pharm. Educ. 87, 100061. https://doi.org/10.1016/j.ajpe.2023.100061

Olsen, L., Christophersen, A.S., Frogopsahl, G., Waal, H., Morland, J., 2004. Plasma concentrations during naltrexone implant treatment of opiate-dependent patients. Br. J. Clin. Pharmacol. 58, 219–222. https://doi.org/10.1111/j.1365-2125.2004.02122.x

Omer, M.E., Halwani, M., Alenazi, R.M., Alharbi, O., Aljihani, S., Massadeh, S., Al Ghoribi, M.,

Al Aamery, M., Yassin, A.E., 2020. Novel Self-Assembled Polycaprolactone–Lipid Hybrid Nanoparticles Enhance the Antibacterial Activity of Ciprofloxacin. SLAS Technol. 25, 598–607. https://doi.org/10.1177/2472630320943126

Onugwu, A.L., Attama, A.A., Nnamani, P.O., Onugwu, S.O., Onuigbo, E.B., Khutoryanskiy, V.V., 2022. Development and optimization of solid lipid nanoparticles coated with chitosan and poly(2-ethyl-2-oxazoline) for ocular drug delivery of ciprofloxacin. J. Drug Deliv. Sci. Technol. 74, 103527. https://doi.org/10.1016/j.jddst.2022.103527

Paavola, A., Bernards, C.M., Rosenberg, P.H., 2016. Controlled release ibuprofen-poloxamer gel for epidural use – A pharmacokinetic study using microdialysis in pigs. Eur. J. Pharm. Biopharm. 108, 180–186. https://doi.org/10.1016/j.ejpb.2016.09.006

Packhaeuser, C.B., Schnieders, J., Oster, C.G., Kissel, T., 2004. In situ forming parenteral drug delivery systems: an overview. Eur. J. Pharm. Biopharm. 58, 445–455. https://doi.org/10.1016/j.ejpb.2004.03.003

Palmer, C.B., Meyrath, M., Canals, M., Kostenis, E., Chevigné, A., Szpakowska, M., 2022. Atypical opioid receptors: unconventional biology and therapeutic opportunities. Pharmacol. Ther. 233, 108014. https://doi.org/10.1016/j.pharmthera.2021.108014

Pandey, S.P., Shukla, T., Dhote, V.K., K. Mishra, D., Maheshwari, R., Tekade, R.K., 2019. Use of Polymers in Controlled Release of Active Agents, in: Basic Fundamentals of Drug Delivery. Elsevier, pp. 113–172. https://doi.org/10.1016/B978-0-12-817909-3.00004-2

Pandya, N.T., Jani, P., Vanza, J., Tandel, H., 2018. Solid lipid nanoparticles as an efficient drug delivery system of olmesartan medoxomil for the treatment of hypertension. Colloids Surf. B Biointerfaces 165, 37–44. https://doi.org/10.1016/j.colsurfb.2018.02.011

Papich, M.G., Narayan, R.J., 2022. Naloxone and nalmefene absorption delivered by hollow microneedles compared to intramuscular injection. Drug Deliv. Transl. Res. 12, 376–383. https://doi.org/10.1007/s13346-021-01096-0

Pardridge, W.M., 2012. Drug Transport across the Blood–Brain Barrier. J. Cereb. Blood Flow Metab. 32, 1959–1972. https://doi.org/10.1038/jcbfm.2012.126

Parhi, R., 2016. Development and optimization of pluronic® F127 and HPMC based thermosensitive gel for the skin delivery of metoprolol succinate. J. Drug Deliv. Sci.

Technol. 36, 23–33. https://doi.org/10.1016/j.jddst.2016.09.004

Patel, S.G., Bummer, P.M., 2017. Thermodynamics of aggregate formation between a non-ionic polymer and ionic surfactants: An isothermal titration calorimetric study. Int. J. Pharm. 516, 131–143. https://doi.org/10.1016/j.ijpharm.2016.10.053

Pathan, H., Williams, J., 2012. Basic opioid pharmacology: an update. Br. J. Pain 6, 11–6. https://doi.org/10.1177/2049463712438493

Paul, A.K., Smith, C.M., Rahmatullah, M., Nissapatorn, V., Wilairatana, P., Spetea, M., Gueven, N., Dietis, N., 2021. Opioid Analgesia and Opioid-Induced Adverse Effects: A Review. Pharmaceuticals 14, 1091. https://doi.org/10.1007/s11095-021-03069-x

Pawar, R., Pathan, A., Nagaraj, S., Kapare, H., Giram, P., Wavhale, R., 2023. Polycaprolactone and its derivatives for drug delivery. Polym. Adv. Technol. 34, 3296–3316. https://doi.org/10.1002/pat.6140

Plein, L.M., Rittner, H.L., 2018. Opioids and the immune system – friend or foe. Br. J. Pharmacol. 175, 2717–25. https://doi.org/10.1111/bph.13750

Raffa, R.B., Pergolizzi, J.V., 2014a. A modern analgesics pain ‘pyramid.’ J. Clin. Pharm. Ther. 39, 4–6. https://doi.org/10.1111/jcpt.12110

Rahmani, F., Ziyadi, H., Baghali, M., Luo, H., Ramakrishna, S., 2021. Electrospun PVP/PVA Nanofiber Mat as a Novel Potential Transdermal Drug-Delivery System for Buprenorphine: A Solution Needed for Pain Management. Appl. Sci. 11, 2779. https://doi.org/10.3390/app11062779

Ramenskaya, G.V., Shikh, E.V., Arzamastsev, A.P., Kukes, V.G., 2005. Pharmacokinetic Study of the New Domestic Hypodermic Form of Naltrexone: Prodetoxon Depot Tablets. Pharm. Chem. J. 39, 1–3. https://doi.org/10.1007/s11094-005-0066-3

Ramli, H., Zainal, N.F.A., Hess, M., Chan, C.H., 2022. Basic principle and good practices of rheology for polymers for teachers and beginners. Chem. Teach. Int. 4, 307–326. https://doi.org/10.1515/cti-2022-0010

Rani, N.S., Sannappa, J., Demappa, T., Mahadevaiah, 2015. Effects of CdCl2 concentration on the structural, thermal and ionic conductivity properties of HPMC polymer electrolyte films. Ionics 21, 133–140. https://doi.org/10.1007/s11581-014-1151-y

Rao, M., Agrawal, D.K., Shirsath, C., 2017. Thermoreversible mucoadhesive *in situ* nasal gel for treatment of Parkinson's disease. Drug Dev. Ind. Pharm. 43, 142–150. https://doi.org/10.1080/03639045.2016.1225754

Reddy, A.P., Parthiban, S., Vikneswari, A., Senthilkumar, G.P., 2014. A Modern Review on Solid Lipid Nanoparticles as Novel Controlled Drug Delivery System. Int. J. Res. Pharm. Nano Sci. 3, 313–25. https://doi.org/chrome-extension://efaidnbmnnnibpcajpcglclefindmkaj/http://www.ijrpns.com/article/A%20MODERN%20REVIEW%20ON%20SOLID%20LIPID%20NANOPARTICLES%20AS%20NOVEL%20CONTROLLED%20DRUG%20DELIVERY%20SYSTEM.pdf

Repka, M.A., Majumdar, S., Kumar Battu, S., Srirangam, R., Upadhye, S.B., 2008. Applications of hot-melt extrusion for drug delivery. Expert Opin. Drug Deliv. 5, 1357–1376. https://doi.org/10.1517/17425240802583421

Ritthidej, G.C., 2011. Nasal Delivery of Peptides and Proteins with Chitosan and Related Mucoadhesive Polymers, in: Peptide and Protein Delivery. Elsevier, pp. 47–68. https://doi.org/10.1016/B978-0-12-384935-9.10003-3

Rosenthal, R., Goradia, V., 2017. Advances in the delivery of buprenorphine for opioid dependence. Drug Des. Devel. Ther. 11, 2493–2505. https://doi.org/10.2147/DDDT.S72543

Rosenthal, R.N., 2019. Novel Formulations of Buprenorphine for Treatment of Opioid Use Disorder. FOCUS 17, 104–109. https://doi.org/10.1176/appi.focus.20180043

Rosenthal, R.N., Ling, W., Casadonte, P., Vocci, F., Bailey, G.L., Kampman, K., Patkar, A., Chavoustie, S., Blasey, C., Sigmon, S., Beebe, K.L., 2013. Buprenorphine implants for treatment of opioid dependence: randomized comparison to placebo and sublingual buprenorphine/naloxone: Buprenorphine implants for opioid dependence. Addiction 108, 2141–2149. https://doi.org/10.1111/add.12315

Saari, T.I., Strang, J., Dale, O., 2024. Clinical Pharmacokinetics and Pharmacodynamics of Naloxone. Clin. Pharmacokinet. 63, 397–422. https://doi.org/10.1007/s40262-024-01355-6

Saha, P., Verma, S., Das, P.S., 2017. Sublingual Drug Delivery: An Indication of Potential Alternative Route. Int. J. Curr. Pharm. Res. 9, 5. https://doi.org/10.22159/ijcpr.2017v9i6.23436

Salatin, S., Alami-Milani, M., Daneshgar, R., Jelvehgari, M., 2018. Box–Behnken experimental design for preparation and optimization of the intranasal gels of selegiline hydrochloride. Drug Dev. Ind. Pharm. 44, 1613–1621. https://doi.org/10.1080/03639045.2018.1483387

Salikolimi, K., Sudhakar, A.A., Ishida, Y., 2020. Functional Ionic Liquid Crystals. Langmuir 36, 11702–11731. https://doi.org/10.1021/acs.langmuir.0c01935

Satapathy, M.K., Yen, T.-L., Jan, J.-S., Tang, R.-D., Wang, J.-Y., Taliyan, R., Yang, C.-H., 2021. Solid Lipid Nanoparticles (SLNs): An Advanced Drug Delivery System Targeting Brain through BBB. Pharmaceutics 13, 1183. https://doi.org/10.3390/pharmaceutics13081183

Schmaljohann, D., 2006. Thermo- and pH-responsive polymers in drug delivery☆. Adv. Drug Deliv. Rev. 58, 1655–1670. https://doi.org/10.1016/j.addr.2006.09.020

Schmolka, I.R., 1972. Artificial skin. I. Preparation and properties of pluronic F-127 gels for treatment of burns. J. Biomed. Mater. Res. 6, 571–582. https://doi.org/10.1002/jbm.820060609

Schneider, C., Langer, R., Loveday, D., Hair, D., 2017. Applications of ethylene vinyl acetate copolymers (EVA) in drug delivery systems. J Control Release 262, 284–295. https://doi.org/10.1016/j.jconrel.2017.08.004

Schreiner, V., Detampel, P., Jirkof, P., Puchkov, M., Huwyler, J., 2021. Buprenorphine loaded PLGA microparticles: Characterization of a sustained-release formulation. J. Drug Deliv. Sci. Technol. 63, 102558. https://doi.org/10.1016/j.jddst.2021.102558

Schwarz, C., Mehnert, W., Lucks, J.S., Müller, R.H., 1994. Solid lipid nanoparticles (SLN) for controlled drug delivery. I. Production, characterization and sterilization. J Control Release 30, 83–96. https://doi.org/10.1016/0168-3659(94)90047-7

Shah, S., Shah, Dr.P., S.Patel, D., Patel, M., 2015. A Review on Extended Release Drug Delivery System and Multiparticulate System. World J. Pharm. Res. 4990, 724–747.

Sharifi, F., 2021. Engineering Quick- and Long-acting Naloxone Delivery Systems for Treating Opioid Overdose. Pharm Res 38, 1221–34. https://doi.org/10.1007/s11095-021-03069-x

Sharma, R., 2024. Recent advances in biopolymer-based mucoadhesive drug delivery systems for oral application. J. Drug Deliv. Sci. Technol. 91, 105227. https://doi.org/10.1016/j.jddst.2023.105227

Shi, Z., Hu, Y., Li, X., 2024. Polymer mechanochemistry in drug delivery: From controlled release to precise activation. J Control Release 365, 259–273. https://doi.org/10.1016/j.jconrel.2023.10.042

Sigmon, S.C., Moody, D.E., Nuwayser, E.S., Bigelow, G.E., 2006. An injection depot formulation of buprenorphine: extended biodelivery and effects. Addiction 101, 420–432. https://doi.org/10.1111/j.1360-0443.2006.01348.x

Sigmon, S.C., Wong, C.J., Chausmer, A.L., Liebson, I.A., Bigelow, G.E., 2004. Evaluation of an injection depot formulation of buprenorphine: placebo comparison. Addiction 99, 1439–1449. https://doi.org/10.1111/j.1360-0443.2004.00834.x

Silva, B.M.A., Borges, A.F., Silva, C., Coelho, J.F.J., Simões, S., 2015. Mucoadhesive oral films: The potential for unmet needs. Int. J. Pharm. 494, 537–551. https://doi.org/10.1016/j.ijpharm.2015.08.038

Sittl, R., 2003. Analgesic efficacy and tolerability of transdermal buprenorphine in patients with inadequately controlled chronic pain related to cancer and other disorders: A multicenter, randomized, double-blind, placebo-controlled trial. Clin. Ther. 25, 150–168. https://doi.org/10.1016/S0149-2918(03)90019-1

Skolnick, P., 2022. Treatment of overdose in the synthetic opioid era. Pharmacol. Ther. 233, 108019. https://doi.org/10.1016/j.pharmthera.2021.108019

Socías, M.E., Nolan, S., 2021. Can Extended-release Injectable Medications Help Curb United States and Canada's Opioid Overdose Epidemic? J. Addict. Med. 15, 15–17. https://doi.org/10.1097/ADM.0000000000000697

Sridhar, V., Wairkar, S., Gaud, R., Bajaj, A., Meshram, P., 2018. Brain targeted delivery of mucoadhesive thermosensitive nasal gel of selegiline hydrochloride for treatment of Parkinson's disease. J. Drug Target. 26, 150–161. https://doi.org/10.1080/1061186X.2017.1350858

Srivastava, A., Yadav, T., Sharma, S., Nayak, A., Akanksha Kumari, A., Mishra, N., 2016. Polymers in Drug Delivery. J. Biosci. Med. 04, 69–84. https://doi.org/10.4236/jbm.2016.41009

Strain, E.C., Moody, D.E., Stoller, K.B., Walsh, S.L., Bigelow, G.E., 2004. Relative bioavailability of different buprenorphine formulations under chronic dosing conditions. Drug Alcohol Depend. 74, 37–43. https://doi.org/10.1016/j.drugalcdep.2003.11.008

Strang, J., Volkow, N.D., Degenhardt, L., Hickman, M., Johnson, K., Koob, G.F., Marshall, B.D.L., Tyndall, M., Walsh, S.L., 2020. Opioid use disorder. Nat. Rev. Dis. Primer 6, 3. https://doi.org/10.1038/s41572-019-0137-5

Sullivan, J.G., Webster, L., 2015. Novel Buccal Film Formulation of Buprenorphine-Naloxone for the Maintenance Treatment of Opioid Dependence: A 12-Week Conversion Study. Clin. Ther. 37, 1064–1075. https://doi.org/10.1016/j.clinthera.2015.02.027

Sultana, A., Zare, M., Thomas, V., Kumar, T.S.S., Ramakrishna, S., 2022. Nano-based drug delivery systems: Conventional drug delivery routes, recent developments and future prospects. Med. Drug Discov. 15, 100134. https://doi.org/10.1016/j.medidd.2022.100134

Takalani, F., Kumar, P., Kondiah, P.P.D., Choonara, Y.E., 2024. Co-emulsified Alginate-Eudragit Nanoparticles: Potential Carriers for Localized and Time-defined Release of Tenofovir in the Female Genital Tract. AAPS PharmSciTech 25, 15. https://doi.org/10.1208/s12249-023-02723-4

Taylor, J.L., Samet, J.H., 2022. Opioid Use Disorder. Ann. Intern. Med. 175, 1–16. https://doi.org/10.7326/AITC202201180

Teleanu, R.I., Preda, M.D., Niculescu, A.-G., Vladâcenco, O., Radu, C.I., Grumezescu, A.M., Teleanu, D.M., 2022. Current Strategies to Enhance Delivery of Drugs across the Blood–Brain Barrier. Pharmaceutics 14, 987. https://doi.org/10.3390/pharmaceutics14050987

Tian, H., Lu, Z., Li, D., Hu, J., 2018. Preparation and characterization of citral-loaded solid lipid nanoparticles. Food Chem. 248, 78–85. https://doi.org/10.1016/j.foodchem.2017.11.091

Tiberg, F., Johnsson, M., 2011. Drug delivery applications of non-lamellar liquid crystalline phases and nanoparticles. J. Drug Deliv. Sci. Technol. 21, 101–109. https://doi.org/10.1016/S1773-2247(11)50009-7

Tiberg, F., Johnsson, M., Jankunec, M., Barauskas, J., 2012. Phase Behavior, Functions, and

Medical Applications of Soy Phosphatidylcholine and Diglyceride Lipid Compositions. Chem. Lett. 41, 1090–1092. https://doi.org/10.1246/cl.2012.1090

Tiihonen, J., Krupitsky, E., Verbitskaya, E., Blokhina, E., Mamontova, O., Föhr, J., Tuomola, P., Kuoppasalmi, K., Kiviniemi, V., Zwartau, E., 2012. Naltrexone Implant for the Treatment of Polydrug Dependence: A Randomized Controlled Trial. Am. J. Psychiatry 169, 531–536. https://doi.org/10.1176/appi.ajp.2011.11071121

Tijani, A., Dogra, P., Peláez, M.J., Wang, Z., Cristini, V., Puri, A., 2023. Mechanistic modeling-guided optimization of microneedle-based skin patch for rapid transdermal delivery of naloxone for opioid overdose treatment. Drug Deliv. Transl. Res. 13, 320–338. https://doi.org/10.1007/s13346-022-01202-w

Tijani, A.O., Garg, J., Frempong, D., Verana, G., Kaur, J., Joga, R., Sabanis, C.D., Kumar, S., Kumar, N., Puri, A., 2022. Sustained drug delivery strategies for treatment of common substance use disorders: Promises and challenges. J Control Release 348, 970–1003. https://doi.org/10.1016/j.jconrel.2022.06.034

Tiwari, G., Tiwari, R., Bannerjee, S., Bhati, L., Pandey, S., Pandey, P., Sriwastawa, B., 2012. Drug delivery systems: An updated review. Int. J. Pharm. Investig. 2, 2–11. https://doi.org/10.4103/2230-973X.96920

Tripathi, K., 2010. Opioid Analgesics and Antagonists, in: Essentials of Medical Pharmacology. Jaypee, New Delhi, pp. 453–68.

Ulery, B.D., Nair, L.S., Laurencin, C.T., 2011. Biomedical applications of biodegradable polymers. J. Polym. Sci. Part B Polym. Phys. 49, 832–864. https://doi.org/10.1002/polb.22259

Valentino, R.J., Volkow, N.D., 2018. Untangling the complexity of opioid receptor function. Neuropsychopharmacology 43, 2514–20. https://doi.org/10.1038/s41386-018-0225-3

Vargas-Schaffer, G., 2010. Is the WHO analgesic ladder still valid? Can. Fam. Physician 56, 514–7. https://pmc.ncbi.nlm.nih.gov/articles/PMC2902929/

Vergne-Salle, P., 2016. WHO Analgesic Ladder: Is It Appropriate for Joint Pain? From NSAIDS to Opioids. Int. Assoc. Study Pain 18. https://www.sbmfc.org.br/wp-content/uploads/2019/03/WHO-Analgesic-Ladder-Is-It-Appropriate-for-Joint-Pain-From-NSAIDS-to-Opioids.pdf

Vitore, J.G., Bharathi, K., Salave, S., Rana, D., Perla, A., Gupta, S., Shah, S., Pardhe, R., Chittemreddy, P., Kashid, S., Jadhav, R., Sharma, A., Patel, R., Jindal, A.B., Benival, D., 2023. Intranasal transmucosal drug delivery: An alternative approach to the parenteral route for medical emergencies. J. Drug Deliv. Sci. Technol. 83, 104421. https://doi.org/10.1016/j.jddst.2023.104421

Voronkov, M., Nikonov, G., Ataiants, J., Isakulyan, L., Stefanut, C., Cernea, M., Abernethy, J., 2022. Modifying naloxone to reverse fentanyl-induced overdose. Int. J. Pharm. 611, 121326. https://doi.org/10.1016/j.ijpharm.2021.121326

Walton, S.E., Krotulski, A.J., Glatfelter, G.C., Walther, D., Logan, B.K., Baumann, M.H., 2023. Plasma pharmacokinetics and pharmacodynamic effects of the 2-benzylbenzimidazole synthetic opioid, isotonitazene, in male rats. Psychopharmacology (Berl.) 240, 185–198. https://doi.org/10.1007/s00213-022-06292-5

Wang, M., Ma, X., Zong, S., Su, Y., Su, R., Zhang, H., Liu, Y., Wang, C., Li, Y., 2024. The prescription design and key properties of nasal gel for CNS drug delivery: A review. Eur. J. Pharm. Sci. 192, 106623. https://doi.org/10.1016/j.ejps.2023.106623

Wang, Y., Jiang, S., Wang, H., Bie, H., 2017. A mucoadhesive, thermoreversible in situ nasal gel of geniposide for neurodegenerative diseases. PLOS ONE 12, e0189478. https://doi.org/10.1371/journal.pone.0189478

Wiegand, T.J., Le Lait, M.-C., Bartelson, B.B., Dart, R.C., Green, J.L., 2016. Analysis of the Abuse and Diversion of the Buprenorphine Transdermal Delivery System. J. Pain 17, 745–752. https://doi.org/10.1016/j.jpain.2016.02.015

Wu, J., Wei, W., Wang, L.-Y., Su, Z.-G., Ma, G.-H., 2007. A thermosensitive hydrogel based on quaternized chitosan and poly(ethylene glycol) for nasal drug delivery system. Biomaterials 28, 2220–2232. https://doi.org/10.1016/j.biomaterials.2006.12.024

Xinchen, Y., Jing, T., Jiaoqiong, G., 2023. Lipid-based nanoparticles via nose-to-brain delivery: a mini review. Front. Cell Dev. Biol. 11, 1214450. https://doi.org/10.3389/fcell.2023.1214450

Yang, J., Bauer, B.A., Wahner-Roedler, D.L., Chon, T.Y., Xiao, L., 2020. The Modified WHO Analgesic Ladder: Is It Appropriate for Chronic Non-Cancer Pain? J. Pain Res. Volume 13, 411–7. https://doi.org/10.2147/JPR.S244173

Yasir, M., Chauhan, I., Zafar, A., Verma, M., Noorulla, K.M., Tura, A.J., Alruwaili, N.K., Haji, M.J., Puri, D., Gobena, W.G., Dalecha, D.D., Sara, U.V.S., Kumar, N., 2021. Buspirone loaded solid lipid nanoparticles for amplification of nose to brain efficacy: Formulation development, optimization by Box-Behnken design, in-vitro characterization and in-vivo biological evaluation. J. Drug Deliv. Sci. Technol. 61, 102164. https://doi.org/10.1016/j.jddst.2020.102164

Yasir, M., Sara, U.V.S., 2014. Solid lipid nanoparticles for nose to brain delivery of haloperidol: in vitro drug release and pharmacokinetics evaluation. Acta Pharm. Sin. B 4, 454–463. https://doi.org/10.1016/j.apsb.2014.10.005

Yeola, G.S., Darandale, S., Khire, A., Vavia, P.R., 2014. Fabrication and statistical optimization of a polysaccharide-based sublingual film of buprenorphine hydrochloride for breakthrough pain management: in vitro and in vivo performance. Drug Deliv. Transl. Res. 4, 116–125. https://doi.org/10.1007/s13346-013-0183-6

Young, K.H., Ehman, M., Reves, R., Maddox, B.L.P., Khan, A., Chorba, T.L., Jereb, J., 2016. Tuberculosis Contact Investigations — United States, 2003–2012. MMWR Morb. Mortal. Wkly. Rep. 64, 1369–1374. https://doi.org/10.15585/mmwr.mm6450a1

ANNEX A

ANIMAL RESEARCH ETHICS COMMITTEE
Registration number: AREC-101210-002

Date: 10/11/2023

Certificate reference: Waiver 10-11-2023-O
Category: O
Applicant: Sarjan Patel
Department: Department of Pharmacy and Pharmacology (WITS)
Tel: 011 717 2552; **Email**: 2618983@students.wits.ac.za

Re: Waiver from the Animal Ethics Research Committee of the University of the Witwatersrand

This letter is to confirm that Sarjan Patel (#2618983), Master's student in Pharmaceutics under the supervision of Prof. Yahya Choonara, Dr Mershen Govender and Dr Neil Butkov (Department of Pharmacy and Pharmacology), does not require full Animal Ethics Research Committee clearance to undertake the work titled ***"A thermo-responsive buprenorphine-naloxone solid lipid nanoparticle nasal spray for the treatment of opioid use disorder (OUD)"***.

Reason for waiver
The project is using nasal and blood brain barrier (BBB) membrane from of one sheep and one domestic pig *(sus scrofa domesticus*) already euthanized at WRAF.

Details of the study
The aim of the study is to develop a thermo-responsive gelling nasal spray containing solid lipid nanoparticles for the site-specific delivery of buprenorphine and naloxone to the brain for the treatment of OUD. Ex-vivo study will be conducted to determine the permeability of the nano-system and drug across the nasal and blood brain barrier (BBB) membrane of a euthanized sheep and pig as permeability is one of the several factors that affects the nose to brain drug delivery system.
Ex-vivo permeation studies will be conducted on sheep's and pig's nasal mucosa membrane using Franz diffusion cell. The obtained nasal mucosa and blood brain barrier (BBB) tissues from both the animals will be stored in the ice-cold phosphate buffer having pH 7.4. From the septum nasal mucosa and within the skull region BBB will be removed and immersed in ringer's solution immediately. Nasal mucosa will be mounted and stabilized in Franz diffusion cell assembly which will contain 10 mL phosphate buffer having pH 6.8 (simulating nasal fluid) in receptor compartment. After this, NLX-SLN and BUP-SLN equivalent to 4 mg naloxone (NLX) and 16 mg buprenorphine (BUP) will be re-dispersed in 2 mL phosphate buffer having pH 6.8 will be placed in donor compartment of capacity 3 mL having the surface area of 0.785 cm2. Later on, 1 mL of samples from donor compartment will be withdrawn at predetermine time intervals and to maintain the sink conditions equal volume of buffer will be added to receptor compartment. The concentration of NLX permeated from prepared NLX-SLN and BUP-SLN through nasal mucosa to the receptor compartment will be analyzed and measured by spectrophotometer at 280nm using UV spectrophotometer. Cumulative amount of drug permeated will be calculated using Eq. (1). The permeation

studies with the BBB will be carried out in the same way as with the nasal mucosa membrane but the phosphate buffer with pH 7.4 (simulating cerebrospinal fluid) will be used instead of pH 6.8.

Condition: The applicant should liaise with WRAF to obtain the tissue.

The individuals covered by the waiver are Sarjan Patel, Yahya Choonara, Mershen Govender and Neil Butkov (Department of Pharmacy and Pharmacology, WITS).

Please contact me should you require further information.

Yours sincerely

A/Prof Frederic Michel
Chair: Animal Research Ethics Committee
University of the Witwatersrand

ANNEX B

UNIVERSITY OF THE WITWATERSRAND, JOHANNESBURG	HUMAN RESEARCH ETHICS COMMITTEE (MEDICAL)

Office of the Deputy Vice-Chancellor (Research & Innovation)

TO: Mr S Patel
School: Therapeutic Sciences
Department: Pharmacy and Pharmacology
Division: WADDPRU
Medical School
University
E-mail: 2618983@students.wits.ac.za

CC: Supervisor: Professor YE Choonara <Yahya.Choonara@wits.ac.za>
and <HREC-Medical.ResearchOffice@wits.ac.za>

FROM: Mr Iain Burns
Human Research Ethics Committee (Medical)
Tel: 011 717 1252

E-mail: Iain.Burns@wits.ac.za

DATE: 05/04/2023

REF: *R14/49*

PROTOCOL NO: W-CBP-230405-03 (This is your ethics application study reference number. Please quote this reference number in all correspondence relating to this study)

PROJECT TITLE: *A thermo-responsive buprenorphine-naloxone solid lipid nanoparticle nasal spray for the treatment of opioid addiction*

Please find attached the Ethics Waiver Certificate for the above project. I hope it goes well and that an article in a recognized publication comes out of it. This will reflect well on your professional standing and contribute to the Government funding of the University.

MSWorks2000/Iain0007/ClearScanWaiver.wps

UNIVERSITY OF THE WITWATERSRAND, JOHANNESBURG	HUMAN RESEARCH ETHICS COMMITTEE (MEDICAL)

Office of the Deputy Vice-Chancellor (Research & Innovation)

05/04/2023

Ref: W-CBP-230405-03

TO WHOM IT MAY CONCERN

Waiver: This certifies that the following research does not require clearance from the Human Research Ethics Committee (Medical)

Investigator: Mr S Patel
Student No. (if appropriate): 2618983
Staff No. (if appropriate):

Supervisor: Professor YE Choonara

School: Therapeutic Sciences
Department: Pharmacy and Pharmacology
WADDPRU
Medical School
University

Project title: *A thermo-responsive buprenorphine-naloxone solid lipid nanoparticle nasal spray for the treatment of opioid addiction*

Reason: In vitro laboratory study
No human participants will be involved in the study

CB Penny

Dr CB Penny
Chairperson: Human Research Ethics Committee (Medical)

Research Office Secretariat:
Third Floor, Phillip Tobias Building, corner of St Andrews and York Roads, Parktown, Johannesburg 2193
Postal address: Private Bag 3, Wits 2050
Tel Nos: +27 (0)11 717 1234/1252/2656/2700
Office E-mail: HREC-Medical.ResearchOffice@wits.ac.za
Website:
https://www.wits.ac.za/research/researcher-support/research-ethics/ethics-committees/